COMPUTATION OF MAGNETOSTATIC FIELDS

P. Silvester

1. Mathematical Formulation of the Physical Problem.

Nearly all magnetostatic and quasi-static analyses presented to date have been based on scalar or vector potential formulations. These often appear in the forms

$$\text{div}\ \mu\ \text{grad}\ \phi = 0 \qquad (1)$$

$$\text{curl}\ \nu\ \text{curl}\ A = J \qquad (2)$$

Generally, these representations involving second order differential operators lead to simple discrete forms and favourable matrix properties (e.g. symmetry). In this form, the magnetic properties are easiest to represent as permeabilities or reluctivities. In contrast, the potentials may also be formulated in terms of integral equations; in that case, the magnetic properties are often easier to represent in terms of a magnetisation vector M, e.g.,

$$A = \frac{\mu_o}{4\pi} \int \left[\frac{J}{r} - \frac{4\pi\ M \times r}{r^3} \right] d\Omega \qquad (3)$$

Such formulations frequently lead to iterative methods of solution, since M is implicitly related to A. In consequence, wide use has been made of the integral forms in two sets of circumstances; the nonmagnetic case, in which M vanishes, and the nonlinear case, in which iterative methods must be employed in any event. The vector potential formulation is clearly less economic computationally, since three components must be considered. On the other hand, it is very difficult to treat distributed currents by the scalar potential technique, so that it is most useful where magnetic fields exterior to relatively thin conductors are to be calculated.

The differential equation formulations (1) and (2) require solving a three-dimensional operator equation of the form

$$D\ V = G \qquad (4)$$

where D is a differential operator and its associated boundary conditions, V is the variable sought, and G represents the given sources and boundary condition inhomogeneities. It is widely recognised that if G and D depend (in some coordinate system) only on two coordinate quantities, V does likewise, and the problem may be reduced to one in two dimensions. It is less well understood that an equivalent treatment is possible if G is quite general, but D depends on only two coordinate quantities. In such cases, V and G may be expanded in terms of suitable orthogonal functions, leading to replacement of the three-dimensional problem by a set of two-dimensional problems, which may be solved separately.

2. Discretisation of the Continuum Equations.

Two major discretisation methods have been widely employed: finite differences and finite elements. In the former, the solution is approximated at certain selected points in the region of interest, while in the latter, an approximation uniquely defined everywhere in the region is sought.

Finite difference methods tend to result in very large and very sparse systems of equations, for whose solution iterative methods have traditionally been employed. However, there exists good evidence that direct solution methods which take account of matrix sparsity are at least competitive with iteration techniques. Iteration methods suffer from two grave shortcomings in magnetostatics: their convergence is very slow, and there is no valid nonlinear theory to serve as a guide in choosing acceleration and stabilisa-

tion factors. The slowness of convergence is inherent in the interface conditions (large permeability ratios typically encountered, thus it is a result of the physical problem rather than of its mathematical treatment.

Finite element methods lend themselves well to the construction of Newton minimisation schemes, which do not suffer from the convergence troubles encountered by finite differences. They are geometrically flexible, allowing curved shapes to be modelled as well as rectilinear ones. The systems of algebraic equations to be solved are usually smaller and denser than with finite differences; thus sparsity-exploiting direct solvers are attractive, though some iterative techniques have been used as well (e.g., conjugate gradients). For integral equations, element functions need only possess C^0 continuity, and are thus relatively easy to construct (even though the resulting integrals are not always easy to evaluate) by Galerkin projections. For differential equation problems, C^1 continuity is required; suitable functions are easy to construct for the scalar case, but not for the vector case if restrictions are to be placed on the divergence of A.

3. Computational Considerations.

The mathematics of finite elements have now reached a level of development exceeding that of finite differences. Concurrently, practical algorithm development has been carried far by engineering analysts. Unfortunately, much less attention -- one might almost say none -- has been paid to establishing principles and standards of generally useful software. There are as many conventions and standards as programming groups, so that virtually every mathematical step has to be re-created by every programming group.

At present there exists no generally agreed language or terminology, oriented toward finite mathematics and computational solutions, for the description of magnetic field problems. This lack not only renders communication between programs incredibly difficult, it also leads to much fruitless discussion between analysts. Much valuable manpower and ingenuity is at present being wasted in the creation of input languages and data structures suitable only for specific, strongly restricted, analysis programs. In the future, effort needs to be directed to producing well-documented, generally useful software modules, and on which specific applications programs can be based. The ability to create these, however, presupposes agreement on the form of data structure for representing problems to be analysed.

Only rarely is the field solution itself of use to the analyst. Much more often, he seeks functionals of the field -- inductance values, generated voltages, lifting forces, power losses. The calculation of such quantities again requires the problem description, as well as the computed solution for the field, to be embedded in a data structure of standard form.

4. Conclusions.

Many good static field analysis programs now exist, particularly for two dimensional problems. Further work on nonlinear problems, especially in three dimensions and using integral equation formulations, may be anticipated. However, the greatest need at present is for standardisation of data bases so as to permit analysts to link together already existing program segments.

Discussion following paper:

(Fox, Oxford) (1) I would comment that the strongly implicit methods of Stone and corresponding factorization methods of people like Golub and Concus should be included in your list of methods. They seem to me to form a very satisfactory balance between iterative methods and direct methods, with more connection with the latter. I agree that direct methods have many attractions.

(2) It surely isn't true that Newton's method always converges from an arbitrary start? The method might be slow if you have to compute the Jacobian matrix all that often and although Newton has quadratic convergence, ie $e_{\nu+1} = ke_{\nu}^2$ (where e_{ν} is the error), this doesn't say that the number of significant figures is doubled at each stage. It is true for sufficiently small ν if k is not too big.

(Silvester, McGill) (1) I agree that semi-iterative (or semi-direct?) methods have many attractions, even though they are not widely used at present.

(2) For magnetostatics problems, where reluctivity and its first derivative are monotonic, the usual finite-element functionals are convex. Thus Newton's method converges. Unless really extreme saturation levels are encountered, starting Newton from a null solution (ie assuming the magnetic material to be linear) often yields potentials accurate to within a factor of two. In other words, one correct binary digit is usually achieved on the first or second Newton step. This starting point appears to be sufficiently near the solution to produce nearly quadratic convergence subsequently. Typically, 16 correct bits are obtained in the fifth or sixth iteration, if the maximum flux density in the problem is around 2.0 - 2.5 tesla.

(Jacobs, CERL) I am interested in the second method you described for treating problems in infinite regions which utilizes a linear operator for the imposed boundary condition at the artificially included finite boundary. Yet another method utilizes the inversion in a circle for two dimensions (on a sphere for three dimensions) of the outer part of the problem which extends to infinity. Thus one obtains two finite problems forming a discus or hyperdiscus matched on the common boundary. The resulting movement of rectangular coordinate nodal points (if used) to model such a curved boundary concords with your comments on the longer time spent on deriving the algebraic equations. With finite element methods one can also develop specific "infinite" elements which extend to infinity.

(Silvester) I quite agree. Inversion mappings have been used for various problems with good success; their main disadvantage I believe is a fussy and uneconomic program structure. Infinite finite elements (defined on an unbounded geometric region but bounded in energy) have been successfully used for various two-dimensional problems; they produce the desired boundary operator directly.

MAGNETOSTATIC FIELDS COMPUTED USING AN INTEGRAL EQUATION DERIVED FROM GREEN'S THEOREMS.

J Simkin and C W Trowbridge
Rutherford Laboratory, Chilton, Didcot, Oxon, OX11 0QX

ABSTRACT

A method of computing magnetostatic fields is described that is based on a numerical solution of the integral equation obtained from Green's Theorems. The magnetic scalar potential and its normal derivative on the surfaces of volumes are found by solving a set of linear equations. These are obtained from Green's Second Theorem and the continuity conditions at interfaces between volumes. Results from a two-dimensional computer program are presented and these show the method to be accurate and efficient.

1. INTRODUCTION

The present generation of computer programs for calculating magnetostatic fields in three dimensions are expensive to use and they will continue to be until new algorithms are developed. Changes in computer hardware, eg. parallel processors, may make it possible to obtain solutions more quickly, but, it is doubtful whether the amount of storage available will change significantly. In this paper the numerical solution of an integral equation derived from Green's Theorems is shown to have many advantages over existing integral equation methods.

Integral equation methods are now widely accepted and the Rutherford Laboratory program GFUN3D[1], which solves the integral equation for the volume distribution of induced magnetisation, has been successfully used for the design of many magnets. As an example of the accuracy of this program the measured and computed results for the homogeneity of an essentially two-dimensional C shaped dipole magnet are shown in Figure 1. This accuracy (better than 1 part in 10^4) was obtained by using 10 minutes of CPU time on an IBM 360/195, a cruder model capable of 1% accuracy would typically require 10 seconds CPU time. In the case of strongly three-dimensional magnets however, 60 minutes of CPU time are probably required for an accuracy better than 1%. Furthermore, for complex problems even when the magnetisation distribution has been computed, the time taken to compute fields at particular points is not trivial.

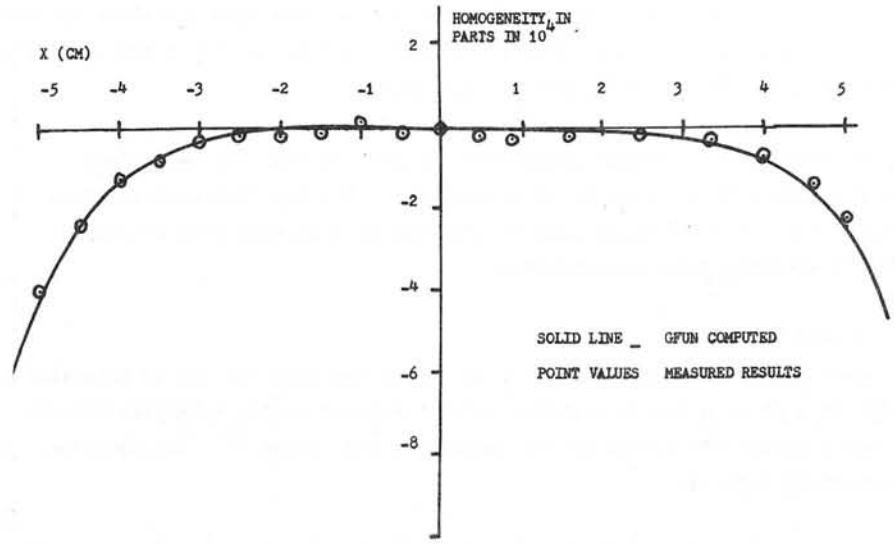

FIGURE 1 - MEASURED AND COMPUTED HOMOGENEITY OF THE FIELD PRODUCED BY A C-SHAPED MAGNET WITH SMALL POLE TIP SHIMS

Iselin[2] has proposed a scalar potential method that may prove to be more efficient than GFUN3D which uses the three component magnetisation. An alternative approach is the Boundary Integral Method, this method is based on the numerical solution of an integral equation for the magnetic scalar potential, derived from Green's Theorems. This approach has already been used for the solution of linear flow and elasticity problems.[3,4,5]

For linear problems, ie. constant permeability, it is only necessary to define the boundaries of regions with different permeability, together with a far field boundary condition - however the far field boundary can be expanded to infinity. A region may consist of several surfaces that do not touch or intersect and this fact together with the use of symmetry allows the calculation of fields with minimal effort. In an appendix an extension is discussed that will make it possible to include non-linear permeabilities.

To determine the magnetic field distribution in a region the magnetic scalar potential and its normal derivative to the boundary must be computed over the surface of the region. This is done numerically by sub-dividing the surface into small areas over which the potential and normal derivatives are assumed constant. The distribution is then found by solving a set of linear equations for the potential and its derivative.

A two-dimensional computer program was written to test the method and compare the accuracy with existing programs. Results from several tests are given. It is expected that this method will be even more attractive for three-dimensional calculations.

2. THEORY

Green's second theorem can be used to relate the magnetic scalar potential V(p) at a point p inside a volume to the magnetic scalar potential and its outward normal derivative on the surface of the volume.[6] The equation connecting them is:

$$V(p) = \frac{1}{4\pi} \int_{\text{volume}} \frac{1}{r} \nabla^2 V dV + \frac{1}{4\pi} \int_S \frac{1}{r} \frac{\partial V}{\partial n} ds - \frac{1}{4\pi} \int_S V \frac{\partial}{\partial n} \left(\frac{1}{r}\right) ds \qquad (1)$$

where r is the distance between the point p and an element of the volume or surface of the region. If the permeability of a region is constant then:

$$\nabla^2 V = 0$$

and therefore the first integral in equation (1) is zero. In Appendix 1 the use of a perturbation term based on the volume integral is shown as a possible means of extending the method to non-linear permeabilities.

If a surface is defined just inside the boundary of a volume and this surface is subdivided into small areas over which V and $\frac{\partial V}{\partial n}$ are constant then equation (1) becomes:

$$V(p) = \frac{1}{4\pi} \left[\sum_{j=1,m} \frac{dV_j}{\partial n_j} \int_{s_j} \frac{1}{r} ds_j - V_j \int_{s_j} \frac{\partial}{\partial n_j} \left(\frac{1}{r}\right) ds_j \right] \qquad (2)$$

where the surface is subdivided into m area elements. Equation (2) can also be used to express the potential of a point on this surface as a function of the potential and its outward normal derivative on each surface area element.

If the geometric factors relating to the potential and its derivative on every element of the surface are calculated for points at the centroid of every area element, then providing V or $\frac{\partial V}{\partial n}$ is known on every area element, the unknown values can be found by solving a set of exactly determined linear equations.

Of more interest is a problem consisting of regions with different permeability where there are interfaces between the regions. For example, consider a two-region problem, where region 1 has permeability μ_1 and region 2 has permeability μ_2. (This could correspond to region 1 being iron and region 2 air.) There must be some driving field, however this is at present of no account expect that a distribution of field H_v is assumed to be produced by a set of current carrying conductors. A surface is defined just inside each region and this surface is sub-divided into small elements with an exact correspondence between the elements across the interface between the regions.

Equation (2) then gives for each surface element:

$$V_j(R1) - \frac{1}{4\pi} \left(\sum_{i=1,n1} \frac{\partial V_i}{\partial n_i}^{(R1)} \int_{s_i} \frac{1}{r} ds_i - V_i(R1) \int_{s_i} \frac{\partial}{\partial n_i} \left(\frac{1}{r}\right) ds_i \right) = 0 \qquad (3)$$

$$V_k(R2) - \frac{1}{4\pi} \left(\sum_{i=1,n2} \frac{\partial V_i}{\partial n_2}^{(R2)} \int_{s_i} \frac{1}{r} ds_i - V_i(R2) \int_{s_i} \frac{\partial}{\partial n_i} \left(\frac{1}{r}\right) ds_i \right) = 0 \qquad (4)$$

where $V_j(R1)$ are the potentials in region 1 and $V_k(R2)$ are potentials in region 2. On the interface between the two regions V and $\frac{\partial V}{\partial n}$ on the surface elements are unknown in both regions. If V or $\frac{\partial V}{\partial n}$ is known on the surface elements that are not on the interface then the set of linear equations formed from (3) and (4) will still be under-determined. Two extra equations must be introduced for each interface element and these can be obtained from the interface continuity conditions. The equations are:

$$V_j(R1) = V_k(R2) \tag{5}$$

$$\mu_1\left(-\frac{\partial V_j(R1)}{\partial n_j} + H_{n_j}(R1)\right) = \mu_2\left(+\frac{\partial V_k(R2)}{\partial n_k} + H_{n_j}(R1)\right) \tag{6}$$

where $H_{n_j}(R1)$ is the outward normal component of the driving field on element j of region 1. The same ideas can be applied to problems consisting of any number of regions.

It is interesting at this stage to examine the set of equations generated to determine V and $\frac{\partial V}{\partial n}$ in a two region problem, where there is an interface between the regions. A pictorial representation of the equations is shown in Figure 2. There are n1 and n2 sides and m1 and m2 unknowns in region 1 and 2 respectively. The submatrix (1) is dense and is formed from the coefficients from equation (3) applied to the element of region 1. Similarly submatrix (4) comes from region 2. The submatrices (2) and (3) are sparse (two unknowns per row) and are generated from the interface conditions. The other areas contain zeros. If on the boundary surfaces where the potential or its derivative is known the value is zero then all the right-hand sides are zero except those corresponding to the normal $\bar{B}$ continuous boundary conditions.

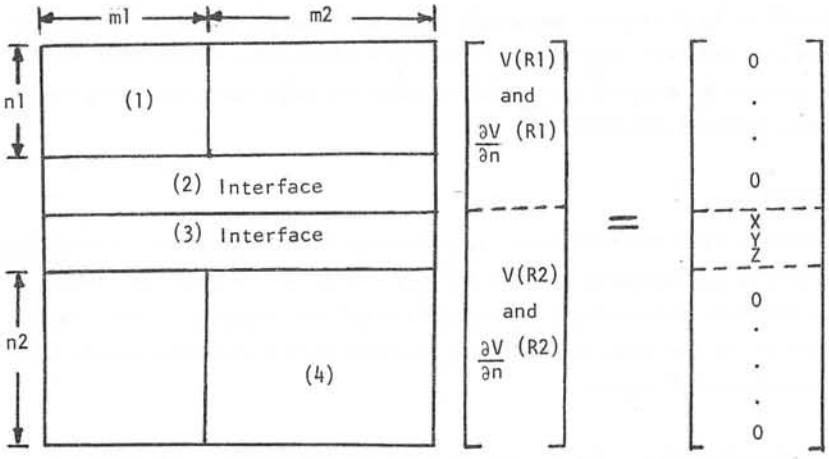

FIGURE 2 - A REPRESENTATION OF THE SET OF LINEAR EQUATIONS REQUIRED TO SOLVE FOR THE POTENTIAL AND ITS NORMAL DERIVATIVE IN A 2 REGION PROBLEM

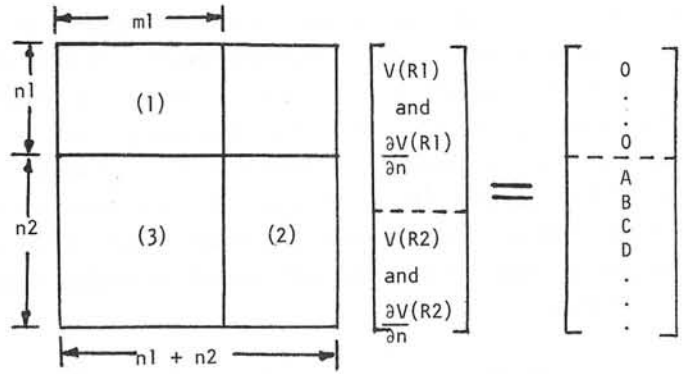

FIGURE 3 - SUBMATRICES (1) and (2) ARE DENSE, (3) IS SPARSE

In order to make the most efficient use of existing computer programs for solving linear equations the interface conditions can be used to replace unknowns on the interface in region 2 by the values in the equivalent elements in region 1. The order of the matrix can be reduced using this technique but at the expense of the loss of the blocking that previously existed. From a long term point of view it would be more efficient to use the blocked matrix and special factorising methods. Figure 3 shows the structure of the set of equations after order reduction has taken place. In the case of a problem only consisting of interfaces the order is reduced to half its previous size.

3. SYMMETRY

The number of unknowns in a problem can be reduced significantly when the geometry and its associated potential distribution possesses a known rotational or reflective symmetry. The two methods that can be employed to make use of this symmetry are shown pictorially in Figures 4 and 5. In Figure 4 a model of a dipole magnet is shown where the Dirichlet and Neumann boundary values have been used to imply the rest of the model. In Figure 5 the whole model is shown but, because the potentials in the 2nd, 3rd and 4th quadrants have an exact equivalence to those in the first quadrant, the potentials in the first quadrant are the only ones which must be computed explicitly.

The far field boundary shown in Figure 5 can be expanded to infinity because there are no boundary connections between it and the magnet; the far field boundary then has no effect on the problem whatsoever. This is obvious for real problems where the potential and its normal derivative to the far boundary can be defined as zero. It is not immediately clear in the two-dimensional infinite limit because the potential from a boundary side becomes infinite at large distances. However the divergence of the potential from a complete surface must be zero and therefore the contributions from all elements of a surface will cancel to produce zero potential at infinity.

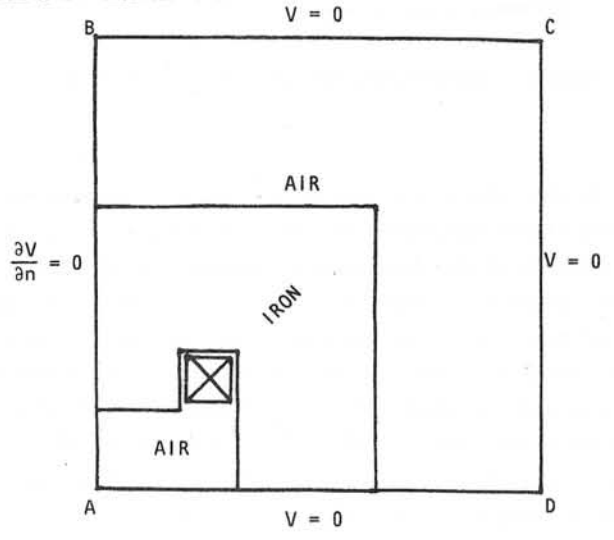

FIGURE 4 - BOUNDARY INTEGRAL METHOD MODEL USING NEUMANN AND DIRICHLET BOUNDARY VALUES

4. APPLICATIONS OF THE METHOD

A two-dimensional magnetostatic computer program was written to test the accuracy and efficiency of the method. The results for the program were very encouraging. In the program the fields from infinitely long conductors with polygonal cross section and curvilinear faces were computed using existing analytic expressions.[7] The boundaries between regions of different permeabilities were subdivided into plane faces over which the potential and its normal derivative were assumed to be constant. The expression for the potential and field from such faces are given in Appendix 2. The integrals can be evaluated for higher order basis

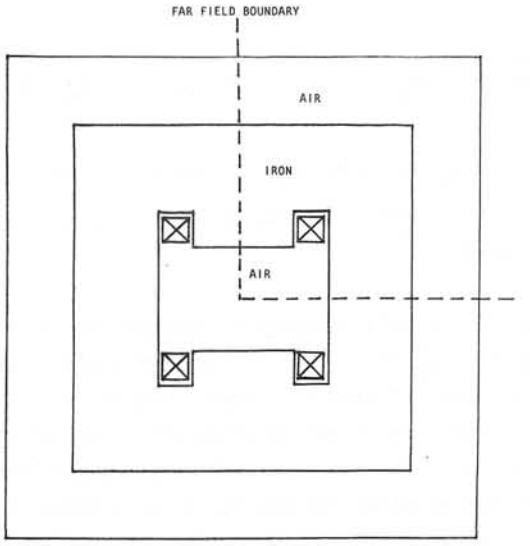

FIGURE 5 - BOUNDARY INTEGRAL METHOD MODEL USING EQUIVALENT ELEMENTS AND SYMMETRY - THE FAR FIELD BOUNDARY IS SHOWN BUT IT CAN BE AT INFINITY

functions but this leads to problems at external corners because the integrals have singular kernels. This problem can be solved but it was simply avoided in the present program by computing the potentials at the centroid of each element where the integral is well behaved. The program can be run interactively on the Rutherford Laboratory IBM 360/195 and in this version an elegant data input package was used for specifying the boundary data of polyhedra.[8]

5. RESULTS

The results from two test cases are included in this section; a comparison of analytic and computed results for the field in a hollow, infinitely long, constant permeability cylinder in a uniform external field; and a comparison of the GFUN and Boundary Integral Method computed fields for a two-dimensional C magnet.

(a) Hollow Cylinder. The fields in a hollow infinitely long constant permeability cylinder in a uniform field perpendicular to the axis of the cylinder were computed using the Boundary Integral Method. The inside radius of the cylinder was 5 cms and the outside radius 10 cms. The

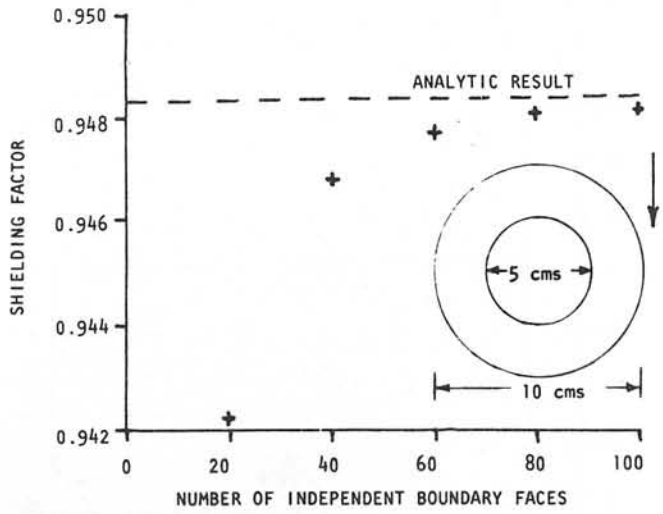

FIGURE 6 - SHIELDING FACTOR OF HOLLOW FERROMAGNETIC CYLINDER - INSIDE RADIUS 5 CMS, OUTSIDE RADIUS 10 CMS, PERMEABILITY 100 - AS A FUNCTION OF THE NUMBER OF INDEPENDENT BOUNDARY FACES IN THE MODEL.

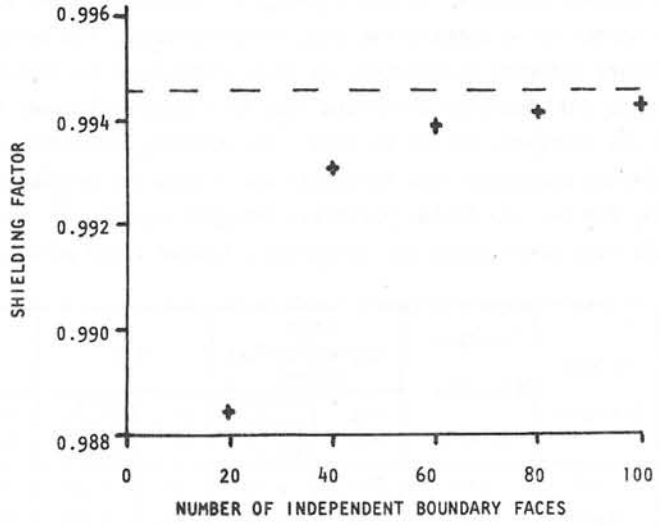

FIGURE 7 - SHIELDING FACTOR OF A HOLLOW FERROMAGNETIC CYLINDER - DIMENSIONS AS FIGURE 5, PERMEABILITY 1000 - AS A FUNCTION OF THE NUMBER OF INDEPENDENT BOUNDARY FACES.

cylinder was approximated by many-sided polyhedra and symmetry was used so that only potentials and derivatives in the first quadrant were computed explicitly. In Figures 6 and 7 the computed shielding factor of the cylinder is plotted as a function of the number of boundary faces for cylinders with relative permeabilities of 100 and 1000. The accuracy is very good, and most of the error is due to the polygonal approximation. The field in the hollow centre should be uniform and in the computed cases the homogeneity was always better than 2 in 10^4. An interesting point to note about the results is that the fields at points inside the cylinder were obtained as accurately as the shielding factor, this is not true in the GFUN program where eigenvalue solutions can be obtained.

(b) C-Shaped Dipole Magnet. The geometry of this magnet is shown in Figures 8 and 9, Figure 8 shows the GFUN model and Figure 9 the Boundary Integral Method model. The results in Figure 1 have shown that GFUN gives accuracies of the order of 0.01% for the homogeneity of this type of C magnet. GFUN was therefore used to compute the field homogeneity of the magnet shown in Figure 8 for steel with a relative permeability of 1000.0. In Figure 10 the GFUN results are compared to those obtained using the Boundary Integral Method (BIM) for several different models. Symmetry was used and therefore only the upper Y plane was computed explicitly. (In both these cases the far field boundary was at infinity.) The results for this case are again good. Figure 11 shows a computed map of lines of constant scalar potential for the 140 element BIM model.

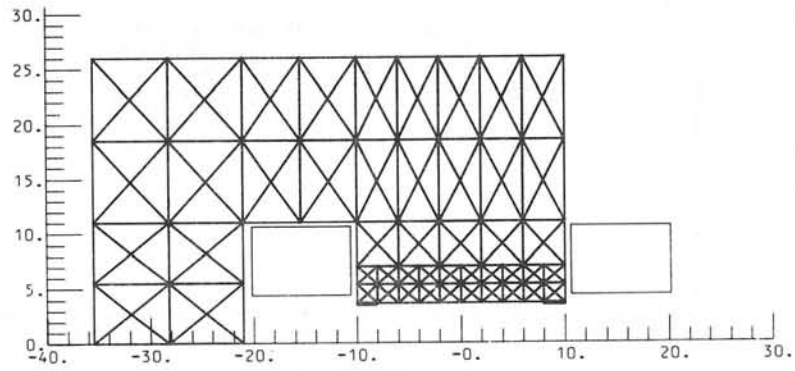

FIGURE 8 - GFUN MODEL OF A TWO-DIMENSIONAL C-MAGNET

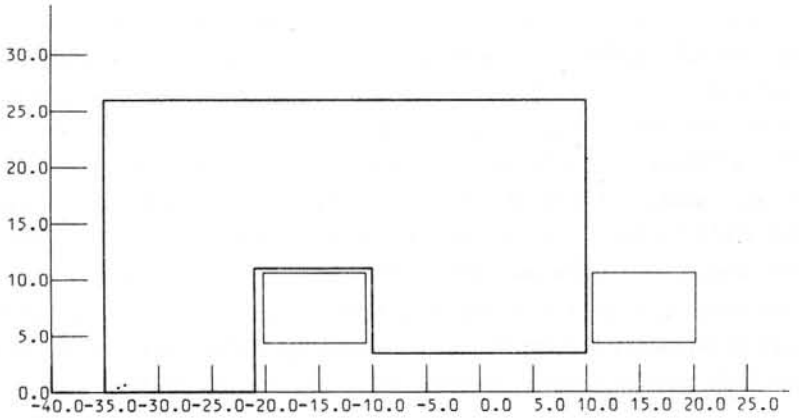

FIGURE 9 - BIM MODEL OF A TWO-DIMENSIONAL C-MAGNET

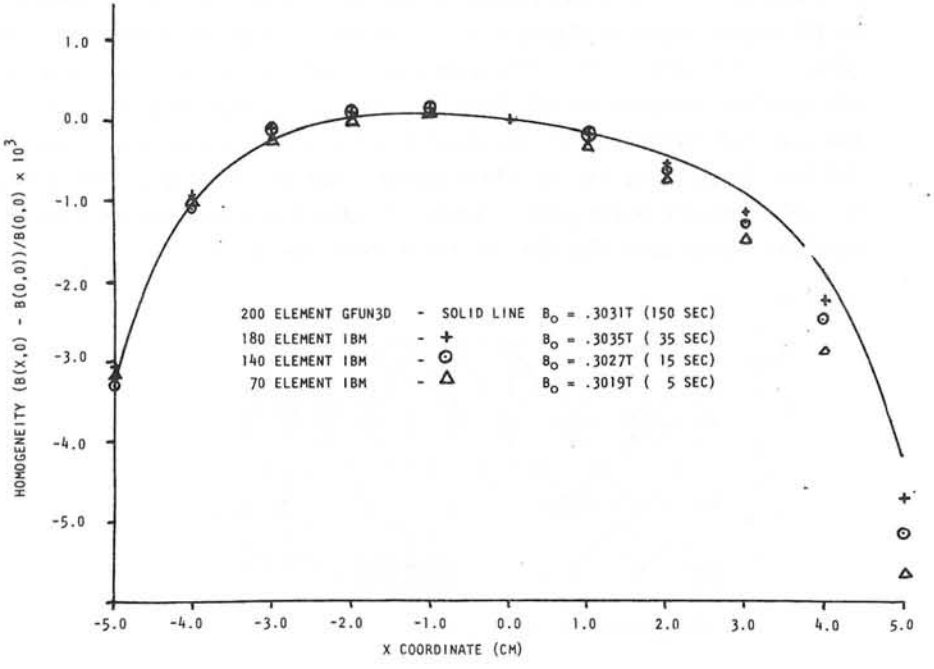

FIGURE 10 - COMPUTED HOMOGENEITY OF THE FIELD UNDER THE POLE TIP OF THE C MAGNET SHOWN IN FIGURE 8.

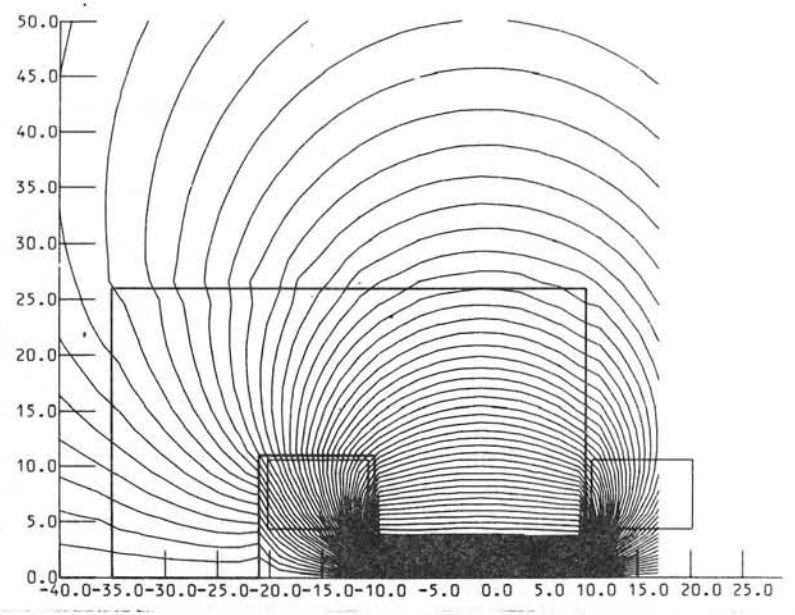

FIGURE 11 - A MAP OF THE COMPUTED MAGNETIC SCALAR POTENTIAL FOR A C-MAGNET

6. CONCLUSIONS

The results achieved for two-dimensional magnet problems are encouraging and appear to be competitive with other methods. The extension of the Boundary Integral Formulation to three dimensions is relatively straightforward and should in principle lead to a more efficienct algorithm than the one currently in use in GFUN. For example, the following table compares predicted computing time (seconds) for a range of problems, ie. for existing GFUN, BIM and the Scalar Potential Integral Equation[2] formulation. The table also gives times for computing a single field point.

Volume Elements	Surface Elements in BIM	GFUN Magnetisation Method		BIM		Scalar Int.Eq. Method	
		Int. Eq.	Single Field Point	Int. Eq.	Single Field Point	Int. Eq.	Single Field Point
216	216	114	2.16	12	0.36	4.2	2.16
343	294	450	3.43	30	0.49	18.0	3.43
512	384	1488	5.12	70	0.64	55.0	5.12
730	486	4320	7.30	133	0.80	162.0	7.30

It can be seen that, as the number of elements increases, BIM compares very favourably with the Scalar Integral Equation method both for the main solution and for fields at single points.

Since the existing program is restricted to constant permeability problems the best method for solving the non-linear problems must be established - the multi-region option outlined in Appendix 1 Section 2 will be tried first by modifying the existing two-dimensional program.

Finally, it should be emphasised that this method has a far wider range of applicability than magnetostatics; for example, solution of current flow potentials in association with eddy currents[8]; also it may be used to advantage in improving the efficiencies of programs already developed such as GFUN for computing the fields at single points.

7. ACKNOWLEDGEMENTS

The authors are indebted to the following Rutherford Laboratory staff: Dr D B Thomas, Head of Applied Physics Division for his encouragement throughout the work and to Mrs E Dawson for preparing the typescript.

8. REFERENCES

1. Armstrong, A G A M, Collie, C J, Diserens, N J, Newman, M J, Simkin, J and Trowbridge, C W. New Developments in the Magnet Design Computer Program GFUN. RL-75-066. Also in Proc. 5th Int. Conf. on Magnet Technology, Rome, 1975.

2. Iselin, Ch. A Scalar Integral Equation for Magnetostatic Fields. Proc. COMPUMAG Conf. on the Computation of Magnetic Fields, Oxford, April 1976.

3. Jawson, M A. Integral Equation Methods in Potential Theory I. Proc. Roy. Soc. A, 275 23-32, 1963.

4. Cruse, T A. Application of Boundary Integral Equation Method to 3D Stress Analysis. J. Computer and Structures, Vol.3, 509-527, Pergamon Press 1973.

5. Symm, G T. Potential Problems in Three Dimensions. Numerical Solution of Integral Equations, Chapter 24. Clarendon Press, Oxford 1974.

6. Smythe, W R. Static and Dynamic Electricity, page 53. McGraw Hill, 1968.

7. Collie, C J. A Program for Computing the Magnetic Fields of Two Dimensional Arrays of Conductors. RL-73-032.

8. Newman, M N. Application of Interactive Graphics Techniques to Magnet Design. Proc. COMPUMAG Conf. on the Computation of Magnetic Fields, Oxford, April 1976.

APPENDIX 1

EXTENSION OF THE GREEN'S THEOREM APPROACH TO NON-LINEAR MAGNETOSTATIC PROBLEMS.

There are two possible methods of extending the method to cover non-linear problems; the first involves using a perturbation term based on the volume integral in equation (1); the second would require the whole of an iron volume to be subdivided into separate volume elements on the surfaces of which the potential and its normal derivative are computed.

(1) Perturbation term method. The magnetic field H_T at a point can be divided into two parts - $\bar{H}_C$ due to currents and $\bar{H}_M$ due to the iron.

$$\bar{H}_T = \bar{H}_C + \bar{H}_M \tag{7}$$

Since:

$$\text{Div } \bar{B} = 0$$

Then:

$$\text{Div}(\mu\bar{H}_C + \mu\bar{H}_M) = 0 \tag{8}$$

(only isotropic materials are considered here)

From equation (8)

$$\mathrm{Div}(\mu\bar{H}_M) = (\nabla\mu).\ \bar{H}_M + \mu(\nabla.\bar{H}_M)$$

$$= (\nabla\mu).\ \bar{H}_M - \mu\nabla^2 V = -\ \mathrm{Div}(\mu\bar{H}_C)$$

Since:

$\mathrm{Div}(\mu H_c) = 0$ then:

$$\nabla^2 V = \frac{1}{\mu}\nabla\mu.\ \bar{H}_T \qquad (9)$$

Combining equations (2) and (9):

$$4\pi V(p) = \int_v \frac{1}{\mu}\ (\nabla\mu\ .H_T)\ \frac{dV}{r} + \int_s \frac{1}{r}\frac{\partial V}{\partial n}\,ds - \int_s V\frac{\partial}{\partial n}\left(\frac{1}{r}\right)ds \qquad (10)$$

This equation could be solved numerically by calculating the contributions of the volume integral when the solution for V and $\frac{\partial V}{\partial n}$ is known. Using a simple iterative scheme the values of V and $\frac{\partial V}{\partial n}$ could then be updated by resolving equations (3) and (4) with the volume integral contribution added to the right-hand sides and the continuity conditions modified.

(2) Volume subdividion method. The existing two-dimensional program can be used to evaluate this method. The ferromagnetic regions of a problem must be divided into small elements over which the change in permeability is small. The equations to be solved are unchanged but an iterative method must be used to converge the solutions for the permeabilities. This method has several advantages; the matrix to be solved is banded and sparse and has a similar structure to those obtained in finite element methods; a numerical calculation of the gradient of μ is not needed. It is hoped to try this second method if present improvements to integral equation methods do not fulfill their promise.[2]

APPENDIX 2

EXPRESSIONS FOR THE FIELD AND POTENTIAL FROM SINGLE AND DOUBLE LAYER SURFACE CHARGES ON INFINITELY LONG PLANE FACES OF FINITE WIDTH

A typical region consisting of many boundary faces is shown in Figure 12. All the expressions given below are for points in the local coordinate system of a boundary face - Figure 13. The faces are infinitely long and of the plane of the paper - in the Z direction:

(1) Potentials. The integrals to be evaluated are shown in equation (2). The potential at a point p(x,y) is:

$$V(p) = \frac{1}{4\pi}\left[V_j(2\theta) + 2\frac{\partial V_j}{\partial n}\,(x\ell n\ (r_1/r_2) + b\ell n(r_1 r_2) - 2b + y\theta)\right]$$

where 2b is the width of the face.

(2) Fields. The field at point p(x,y) is:

$$\bar{H} = -\ \mathrm{grad}\ V(p)$$

Therefore:

$$H_x = \frac{1}{2\pi}\left[V_j\ Y\left(\frac{1}{r_1^2} - \frac{1}{r_2^2}\right)\right.$$

$$\frac{\partial V_j}{\partial n}\left\{x\left(\frac{(x+b)}{r_1^2} - \frac{(x-b)}{r_2^2}\right) + \ell n(r\ /r\ ) + b\left(\frac{(x+b)}{r_1^2} - \frac{(x-b)}{r_2^2}\right)\right.$$

$$\left.\left. + \left(\frac{y^2}{r_1^2} - \frac{y^2}{r_2^2}\right)\right\}\right]$$

$$H_y = \frac{1}{2\pi}\left[V_j\left\{\frac{(x-b)}{r_2^2} - \frac{(x-b)}{r_1^2}\right\}\right.$$

$$\left. + \frac{\partial V_j}{\partial n}\left\{x\left(\frac{y}{r_1^2} - \frac{y}{r_2^2}\right) + b\left(\frac{y}{r_1^2} + \frac{y}{r_2^2}\right) + y\left(\frac{(x-b)}{r_2^2} - \frac{(x+b)}{r_1^2}\right) + \theta\right\}\right]$$

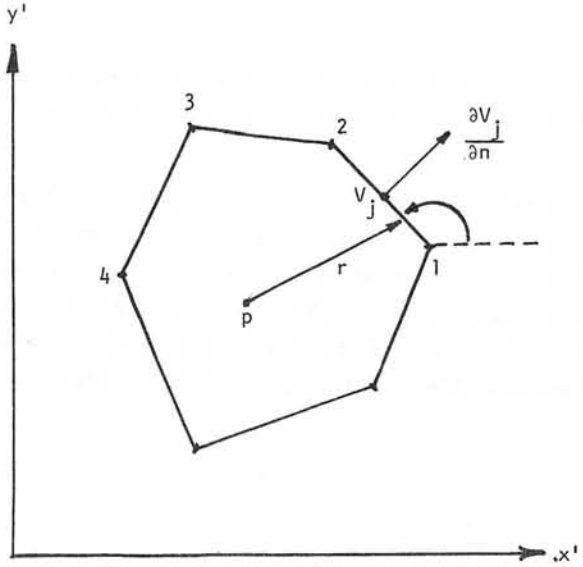

FIGURE 12 - GLOBAL COORDINATE SYSTEM.
A BOUNDARY SURFACE SUBDIVIDED INTO ELEMENTS

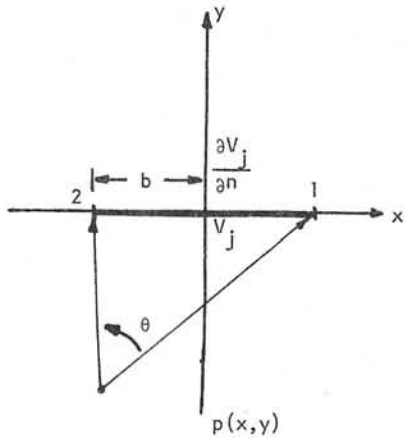

FIGURE 13 - LOCAL COORDINATE SYSTEM OF AN ELEMENT

Discussion following paper:

(Yeh, Oak Ridge) Please elaborate on the matching of the number of variables with the number of equations in your method.

(Simkin, Rutherford) If Neumann or Dirichlet boundary values are defined on every surface element the set of linear equations for the unknowns is exactly determined by the Green's theorem equations for every surface element. Where the potential and derivative are unknown on interfaces there must be an exact equivalence between elements forming surfaces on either side of the boundary. For each pair of equivalent elements two extra equations are obtained from continuity of V and B across the boundary. Thus for the pair of equivalent elements we have four unknowns and four equations - see the section of the paper on equation reduction.

(Rosten, CHAM Ltd) You mentioned the application of the IBM for computing the distribution of current within conductors. Would you elaborate this point.

(Simkin) The IBM can be used to compute the current flow at any position in the volume of a general 3-D variable cross section conductor. Having computed J, the conductor fields still need to be calculated using volume integration methods - see the paper by C J Collie on fields and potentials from hexahedra in the Proceedings.

(Rogers, Southampton) We have used an integral equation method based on Green's functions for each sub-region of the field. It has been successfully applied to the computation of functionals of the field (such as inductance) but we have found considerable errors in the local field at singular points. Do you have to take any special precautions to avoid this problem?

(Simkin) The fields and potentials are well behaved except at points close to areas of the surface where the potential or surface tangent changes discontinuously. At the moment the problem is avoided by displacing such points a very small distance. In future higher order basis functions will be used on our surface elements and it will be necessary to investigate methods of overcoming these weak singularities.

(Ohiwa, Cambridge) Could you give me some idea of the accuracy of the calculated field in terms of the number of mesh points, required storage and computer time.

(Simkin) The results included in the paper give some of the figures. Typically, for linear problems accuracies of the order of 1% can be obtained using 200K of storage and 6 seconds CPU time on an IBM 360/195. In solving the linear equations we have only used simple gaussian elimination and not made any use of the blocked and non-dense nature of the coefficient matrix. The method could be made more efficient.

A SCALAR INTEGRAL EQUATION FOR MAGNETOSTATIC FIELDS

Ch. Iselin
CERN, Geneva, Switzerland

Abstract

For the solution of magnetostatic field problems in three dimensions, integral equation methods have been used mainly because of the following advantages:

i) The unknown quantities need to be calculated in iron only, i.e. the domain of calculation is finite.

ii) The boundary conditions at infinity are taken care of automatically, and the magnetic field can be found correctly anywhere in space.

On the other hand, the following difficulties have been encountered with integral equation methods:

i) The number of unknowns is large; it must be found by inverting a full matrix.

ii) The condition number of the matrix to be inverted can be very large.

iii) The magnetic field is infinite on iron edges. This makes it impossible to use certain, otherwise convenient, approximations to the magnetic field.

In this paper we propose to solve the integral equation for the scalar potential in iron by Galerkin's method. It is believed that this avoids the last two of the above problems.

1. BASIC EQUATIONS

The magnetostatic field obeys the two Maxwell equations

$$\operatorname{div} \vec{B} = 0 \tag{1}$$

$$\operatorname{curl} \vec{H} = \vec{j} \ , \tag{2}$$

where

$\vec{B}$: magnetic flux density
$\vec{H}$: magnetic field strength
$\vec{j}$: current density.

Furthermore, $\vec{B}$ and $\vec{H}$ are related by the material equation

$$\vec{B} = \vec{B}(\vec{H}) \ . \tag{3}$$

We now introduce the magnetic field $\vec{H}_0$ of the coils alone, which obeys the equations

$$\operatorname{div} \vec{H}_0 = 0 \tag{4}$$

$$\operatorname{curl} \vec{H}_0 = \vec{j} \ . \tag{5}$$

The field $\vec{H}_0$ can be found by the law of Biot and Savart

$$4\pi \vec{H}_0 = \int_{\text{coils}} \frac{\vec{j} \times \vec{r}}{r^3} \, dV \ . \tag{6}$$

For any scalar potential ϕ the expression

$$\vec{H} = \vec{H}_0 + \operatorname{grad} \phi \tag{7}$$

fulfils eq. (2). Instead of using eq. (1), we can make use of the magnetization $\vec{M}$ of the iron

$$\vec{M} = \vec{B} - \mu_0 \vec{H} \ , \tag{8a}$$

or

$$\vec{M} = \vec{M}(\vec{H}_0 + \operatorname{grad} \phi) \ . \tag{8b}$$

Equation (8b) shows the functional dependence of $\vec{M}$ upon $\vec{H}$.

Equation (1) may then be replaced by

$$\mu_0 \operatorname{div} \operatorname{grad} \phi = - \operatorname{div} \vec{M} \ . \tag{9}$$

This has the solution

$$4\pi\mu_0\phi = - \int_{\text{iron}} \frac{\vec{M} \cdot \vec{r}}{r^3} \, dV \ . \tag{10}$$

It is clear that neither the potential ϕ nor the magnetization $\vec{M}$ is known at this stage. In this paper we are trying to give a method to find the scalar potential.

2. METHODS USED SO FAR

2.1 Halacsy's method

In the RENO computer program[1], the unknown is the scalar potential. It is found by the following procedure:

i) Insert the definition $\vec{B} = \mu\vec{H}$ into eq. (1).

$$\text{div } \vec{B} = \text{div } [\mu(H_0 + \text{grad } \phi)] = 0 \ . \tag{11}$$

ii) Combine eqs. (8) and (10) giving

$$4\pi\mu_0\phi = - \int_{\text{iron}} \frac{(\mu - \mu_0)(\vec{H}_0 + \text{grad } \phi) \cdot \vec{r}}{r^3} \, dV \ . \tag{12}$$

iii) Insert eq. (12) into eq. (11), yielding a rather complicated equation for ϕ.

iv) Solve the equation resulting from step (iii) numerically.

The equation for the scalar potential is solved using a regular rectangular grid. This imposes important restrictions on the iron geometry. The method is very difficult to adapt for anisotropic iron.

Note that both eqs. (11) and (12) uniquely determine the scalar potential, and that both have the same solution. This may be the reason why the method often breaks down, due to an attempt to invert a singular matrix.

2.2 Magnetisation method

To our knowledge, the first authors to use integral equation methods with success was Trowbridge et al.[2,3] The computer program GFUN solves the integral equation

$$\vec{H} = \vec{H}_0 - \frac{1}{4\pi\mu_0} \text{ grad } \int_{\text{iron}} \frac{\vec{M} \cdot \vec{r}}{r^3} \, dV \tag{13}$$

combined with the material equation

$$\vec{M} = \vec{M}(\vec{H}) \tag{14}$$

in terms of the magnetization $\vec{M}$ or of the total magnetic field strength $\vec{H}$. The method could easily be adapted for anisotropic iron. The GFUN program has been used with considerable success in several laboratories, but it still leaves some problems unsolved.

So far the program uses a piece-wise constant magnetization. The discontinuities of $\vec{M}$ on element boundaries can cause problems by allowing some non-physical solutions to be generated and by making difficult an accurate field calculation in the iron. One cannot use more sophisticated approximations for the magnetization, as long as they depend on values on iron edges, since on iron edges the fields are discontinuous.

Another disadvantage of this method is that its unknown is a vector and that the number of unknowns is higher by a factor of three compared with a method searching for the scalar potential.

3. THE PROPOSED METHOD

3.1 Basic idea

We note that the scalar potential ϕ introduced in eq. (7) must be finite in all space. We shall therefore try to solve eq. (10)

$$4\pi\mu_0\phi + \int_{\text{iron}} \frac{\vec{M} \cdot \vec{r}}{r^3} \, dV = 0 \tag{15}$$

together with the material equation

$$\vec{M} = \vec{M}(H_0 + \text{grad } \phi) \tag{16}$$

iteratively in terms of the scalar potential ϕ.

Assume that after k iterations we have found a guess $\phi^{(k)}$. The magnetization is then

$$\vec{M}^{(k)} = \vec{M}\left(\vec{H}_0 + \text{grad } \phi^{(k)}\right) \ . \tag{17}$$

Inserting $\phi^{(k)}$ and $\vec{M}^{(k)}$ into eq. (15) we have

$$4\pi\mu_0\phi^{(k)} + \int_{\text{iron}} \frac{\vec{r} \cdot \vec{M}^{(k)}}{r^3} \, dV = f^{(k)} \neq 0 \ . \tag{18}$$

The idea is now to find a linear integral equation for the k^{th} correction $\Delta\phi^{(k)}$ by linearizing in the neighbourhood of our last guess:

$$f^{(k+1)} \approx f^{(k)} + 4\pi\mu_0 \, \Delta\phi^{(k)} + \int_{\text{iron}} \frac{\vec{r} \cdot [P^{(k)} \text{ grad } \Delta\phi^{(k)}]}{r^3} \, dV = 0 \ . \tag{19}$$

Here $P^{(k)}$ is the (3 × 3) Jacobi matrix of partial derivatives of the components of $\vec{M}$ with respect to the components of $\vec{H}$.

3.2 Methods of solution

Let us now choose a suitable function space with the finite dimension N to approximate our scalar potential. In this space we define a base

$$\{\phi_n(x,y,z), \ N = 1, 2, 3, \ldots, N\} \ . \tag{20}$$

In terms of our base the k^{th} correction is approximated as

$$\Delta\phi^{(k)} \approx \sum_{n=1}^{N} c_n \phi_n(x,y,z) \ . \tag{21}$$

Further, we define the set of functions

$$\psi_n^{(k)} = \frac{\partial f^{(k+1)}}{\partial c_n} = 4\pi\mu_0\phi_n + \int_{\text{iron}} \frac{\vec{r} \cdot [P^{(k)} \ \text{grad} \ \phi_n]}{r^3} \, dV \ . \tag{22}$$

This allows us to write eq. (19) as

$$f^{(k)} + \sum_{n=1}^{N} c_n \psi_n^{(k)} = 0 \ . \tag{23}$$

We are left with a problem of linear algebra: that is to fit a function $f^{(k)}$ in the best possible way by a linear combination of (hopefully!) linearly independent functions $\psi_n^{(k)}$.

A solution to this fitting problem can be found by Galerkin's method. We define the inner product of two functions by

$$(u,v) = \int uv \, dV \ , \tag{24}$$

the integral being taken over the iron volume only, or over the whole space, whichever is more convenient for the functions concerned. We also select a linearly independent set of trial functions

$$\{t_m(x,y,z), \ m = 1, \ 2, \ 3, \ \ldots, \ N\} \ . \tag{25}$$

Then the relations

$$\left(t_m, \ f^{(k)}\right) + \sum_{n=1}^{N} c_n \left(t_m, \ \psi_n^{(k)}\right) = 0 \tag{26}$$

provide us with a system of N linear equations in the N unknowns c_n.

The simplest choice for the trial functions t_m is to use N Dirac functions. The scalar products in eq. (26) then simply mean evaluation in N different points, i.e. the correction is such that eq. (23) becomes true in these N points.

A solution of eq. (23) in the least-squares sense means minimization of

$$\left(f^{(k)}, \ f^{(k)}\right) = \text{minimum} \ . \tag{27}$$

The trial functions are then $t_m = \psi_m^{(k)}$. This choice must usually be ruled out, because the trial functions are non-zero in whole space, and the computational effort to evaluate the inner products is prohibitive.

A compromise would be to take $t_m = \phi_m$. Further investigations will be necessary to find out if this choice is worth the effort.

4. CHOICE OF BASE FUNCTIONS

4.1 Linear base functions

For a first trial of the method the base of functions was defined in a straightforward way. The iron was cut into small tetrahedra, allowing a rather general geometry. On each tetrahedron the potential was taken to be a linear function of position, defined by its values in the four vertices of the tetrahedron. The magnetic field and the magnetization were thus both constant throughout each tetrahedron, in a similar way to the GFUN program.

The trial functions t_m were taken to be Dirac functions centred on the tetrahedron vertices, i.e. eq. (23) was solved for the tetrahedron vertices. For simple problems, such as an iron cube in a homogeneous magnetic field, the results were rather encouraging. For more realistic problems, such as, for example, a race track coil surrounded by a cylindrical iron shell, the potential values were still approximately correct in the solution points, but very large oscillations of the potential appeared close to the iron surface. This was because the tangential component of the magnetic field should be nearly zero on the iron surface, which is only possible if the potential is allowed to vary to a higher degree than linear.

The use of linear base functions seems not to be appropriate if the number of calculation points is small. For a very fine subdivision of the iron it may possibly give reasonable results.

4.2 Quadratic base functions

For the second test, the same subdivision of the iron into tetrahedra was used. This time the potential was allowed to be a quadratic function of position, defined by its values in the vertices, plus the values in the midpoints of the tetrahedron edges. This made the magnetic field a linear function of position in each tetrahedron. The magnetization was assumed to vary linearly with position as well. Equation (23) was again solved in all points with unknown potential values.

The solution using quadratic base functions gave much better results than the approach using linear base functions. Even for a rather coarse subdivision of the iron, the results were comparable with results found using the GFUN program, but there is still a problem left. Since the magnetic fields were only coupled through the potential, when going from one tetrahedron to the next, they were not smooth on the interface. It remains to be investigated whether a different method of numeric differentiation of the potential gives better results. These investigations are under way.

4.3 Isoparametric base

Investigations are also under way on the use of an isoparametric representation as has been used in the finite element method[4]. This would permit one to use a very general geometry and still to have a smooth magnetic field all over the iron. Unfortunately, due to the lack of time, no numeric results can be presented yet.

REFERENCES

1) A.A. Halacsy, Three-dimensional analysis of magnetic fields with field-dependent permeability, Proc. 3rd Internat. Conf. on Magnet Technology, Hamburg, 1970 (DESY, Hamburg, 1972?), p. 113.

2) M.J. Newman, C.W. Trowbridge and L.R. Turner, GFUN: An interactive program as an aid to magnet design, Proc. 4th Internat. Conf. on Magnet Technology, Brookhaven, 1972 (U.S. Atomic Energy Commission, Washington, 1973), p. 617.

3) A.G.A.M. Armstrong, C.J. Collie, N.J. Diserens, M.J. Newman, J. Simkin and C.W. Trowbridge, New developments in the magnet design computer program GFUN3D, Proc. 5th Internat. Conf. on Magnet Technology, Rome, 1975 (Laboratori Nazionali del CNEN, Frascati, 1975), p. 168.

4) G. Strang and G.J. Fix, An analysis of the finite element method (Prentice Hall, Englewood Cliffs N.J., 1973).

Discussion following paper:

(Trowbridge, Rutherford) What set of basis functions did you chose and was the gain in efficiency expected with your method actually achieved?

(Iselin, CERN) I used three sets of base functions:

(1) tetrahedral elements with linear ϕ variation

(2) tetrahedral elements with quadratic ϕ variation

(3) 'isoparametric' (r, ϕ, θ) elements.

So far only case (3) gave acceptable results. The time for setting up the matrix is comparable to GFUN, but the time for one iteration is cut down to about 4%.

An account for the use of the FEM for magnetostatic problems

S.J. Polak, A. Wachters, A. de Beer

N.V. Philips' Gloeilampenfabrieken, ISA-DSA/SCA

Abstract

The FEM is considered for magnetostatic problems involving both soft isotropic and hard anisotropic materials in this article. Special attention is paid to existence and uniqueness aspects for these non-linear problems. For hard anisotropic materials a new model is introduced. The program package MAGGY contains this model and has been used to compare calculated with measured data.

1. Introduction

In the last ten years numerous calculations have been performed, using the FEM for the numerical approximation of solutions of magnetostatic problems. These are e.g. mentioned in [1] - [7]. In most descriptions no attention is paid to the validity of this use w.r.t. existence, uniqueness and convergence aspects. These do not trivially fit in the usual theory because magnetostatic problems are non-linear. Only in [2] a special approximation of the B-H curve is used for this purpose. Here the FEM is considered for a very general class of magnetostatic problems while paying special attention to the above-mentioned aspects. For hard anisotropic materials a new, simple and usable model is introduced. The model is available in the program package MAGGY. Results from computations with MAGGY are compared with measured data.

2. Basic notions

2.1. Suppose V an open simply connected region in R_3 or R_2 with closure $\overline{V}$, $\delta V=\overline{V}\backslash V$. On V we have the usual spaces L_2 and $\overset{\circ}{W}{}^1_2$ (see e.g. [9]). The space L_2 has the usual inner product and associated norm defined by

(2.1.1.) $$(f,g)_L=\int_V fg\ dv,\quad ||f||_L=(f,f)_L^{\frac{1}{2}}\ .$$

The space $\overset{\circ}{W}{}^1_2$ has inner product and norm

(2.1.2.) $$(f,g)_W=\int_V \text{grad } f.\text{grad } g\ dv,\quad ||f||_W=(f,f)_W^{\frac{1}{2}}$$

We will use P_k to denote some finite dimensional subspace of $\overset{\circ}{W}{}^1_2$.

2.2. For a magnetostatic problem on $V\subset R_3$ we have

(2.2.1.) $\text{curl } H = j$, H the magnetic field, j the current density;

(2.2.2.) $\text{div } B(H) = 0$, B the fluxdensity.

Suppose B an invertible vector function of H in the sequel. B is continously partially differentiable w.r.t. H. We note that $\int_V j^2\ dv<\infty$.

2.3. In this section 2.3. we consider the case where the problem is two-dimensional for symmetry reasons and in cartesian coordinates. We identify V with the accompanying region in R_2. Now j can have a component perpendicular to V only and thus is effectively a scalar function. A vector potential A is introduced with

(2.3.1.) $B = \text{curl } A$ on V, $A \equiv 0$ on δV

which represents condition (2.2.2.). Because j is perpendicular to V, A only needs to have one component, perpendicular to V. Therefore also A is effectively a scalar function. However where necessary A is to be interpreted as the appropriate vector.

Remark: in this case we have $|\text{curl } A| = |\text{grad } A|$ such that $A\equiv 0$ on δV is sufficient to give: $||\text{curl } A||_L=0 \Longleftrightarrow A=0$. Thus A is uniquely defined for a certain B. The equation (2.2.1.) then gives

(2.3.2.) $\text{curl } H\ (\text{curl } A) = j$ on V, $A\equiv 0$ on δV with $j\in L_2$.

The FEM is usually considered as the minimisation of the following energy integral:

$$(2.3.3.) \qquad E(A) = \int_V \int_0^{B=\mathrm{curl}\,A} H(b).db - 2jA \, dv$$

over some P_k. This is termed the energy formulation of the problem. The Galerkin formulation of (2.3.2.) is

$$(2.3.4.) \qquad \int_V H(\mathrm{curl}\,A).\ \mathrm{curl}\,f \, dv = \int_V j\,f\,dv \quad \text{for all } f \epsilon P_k$$

and f is interpreted as a vector perpendicular to V as usual. In §5 it is shown that these formulations are equivalent.

2.4. For a three dimensional problem (2.3.1.) does not uniquely define the vector potential. Thus we use a different approach. A "source field" H_c is established with

$$(2.4.1.) \qquad \mathrm{curl}\,H_c = j$$

This is e.g. done with Biot-Savart's law in vacuum. For the discussion of the FEM we assume this solution H_c with $H_c \epsilon L_2$ available. Then we use (2.2.2.) giving

$$(2.4.2.) \qquad \begin{aligned} \mathrm{div}\,B(H_c + \mathrm{grad}\,f) &= 0 \quad \text{on } V \\ f &\equiv 0 \quad \text{on } \delta V. \end{aligned}$$

The Galerkin formulation for this problem is

$$(2.4.3.) \qquad \int_V B(H_c + \mathrm{grad}\,f)\ \mathrm{grad}\,g \, dv = 0 \quad \text{for all } g \epsilon P_k.$$

3. B-H properties of various kinds of materials

3.1. Magnetic materials may be classified according to different criteria, either in the classes isotropic and anisotropic or in the classes of soft and hard. (see fig 1)

	soft	hard
isotropic		
anisotropic		

Fig.1. classes of magnetic materials

An isotropic material is characterised by the fact that a virginal sphere has no preferred direction. Other materials are anisotropic. Soft magnetic materials are characterised by the fact that no field in the material can exist if no external source for a magnetic field is present. Other materials are termed hard.
Here we will only discuss the B-H properties of materials belonging to the diagonal blocks of figure 1.

3.2. For soft isotropic materials the field dependence of the flux density is well-known:

$$(3.2.1.) \qquad B(H) = \mu(|H|)H,$$

where the magnetic permeability μ is a scalar, sothat B can be interpreted as a scalar function of H (B-H curve), which is differentiable and invertible.

3.3. For hard anisotropic materials the field dependence of the flux density may be formulated as follows:

$$(3.3.1.) \qquad B(H) = \mu(H)H + B_r,$$

where B_r is the remanence and $\mu(H)$ a tensor. In general $\mu(H)$ can not be obtained from available experimental data for such materials. However, for sintered hard anisotropic materials containing single domain particles one may take:

$$(3.3.2.) \qquad \mu(H) = \mu_0 \begin{bmatrix} \mu_{r//}(H_{//}) & 0 \\ 0 & \mu_{r\perp} \end{bmatrix}, \quad H_{//} = H.B_r/|B_r|$$

where $\mu_{//}$ can be obtained from the B-H curve and $\mu_{r\perp} \approx 1 + M_s^o/|H_A^o|$, in which M_s the saturation magnetic moment and $|H_A^o|$ the anisotropy field strength.
The approximation of μ(H) by e.g. (3.3.2.) is justified by experiments described in a paper of Zijlstra presented at this conference, and a model calculation described in the following sections.

3.4. The field dependence of the magnetic moment of a single domain particle can be obtained from a treatment similar to the one given by Stoner and Wohlfarth [18]. Since the anisotropy energy of a single domain particle is give to a first approximation by:

$$(3.4.1.) \qquad E_A = k \sin^2 \psi_i ,$$

where k is a parameter depending on the temperature, ψ_i is the angle between the magnetization vector M_i and the easy axis of the monocrystalline particle. In the presence of a magnetic field H, which makes an angle α_i with the easy axis, the equilibrium direction of M_i can be obtained from

$$(3.4.2.) \qquad \frac{\partial}{\partial \psi_i}(E_A - M_i.H) = 2k\cos\psi_i \sin\psi_i - |M_i||H|\sin(\alpha_i - \psi_i) = 0 ,$$

sothat as shown in figure 2 the magnetization is directed along the resultant of H and a hypothetical field $H_{A,i}$, the so-called anisotropy field of strength $2k\cos\psi_i/|M_i|$.

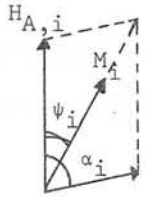

Fig. 2. Dependence of magnetic moment M_i of the magnetic field H and the anisotropy field $H_{A,i}$ for a single domain particle

If M_s is the spontaneous magnetisation per unit volume the magnetic moment M_i of a single domain particle per unit volume is:

$$(3.4.3.) \qquad M_i = M_s \frac{H + H_{A,i}}{|H + H_{A,i}|} \quad ; \quad |M_i| = M_s .$$

3.5. The magnetic moment M per unit volume in a point in the material may be considered as the sum of the magnetic moments per unit volume of the particles, each with a volume τ_i, in a small volume V surrounding the point sothat

$$(3.5.1.) \qquad M = \frac{1}{V} \sum_i M_i \tau_i = M_s \sum_i \frac{H + H_{A,i}}{|H + H_{A,i}|} \tau_i / V$$

If $\tau_i \ll V$ the summation may be replaced by integration. For spherical coordinates θ and ϕ and the probability density function $f(\theta,\phi)$ for the distribution of the direction of the particle magnetic moments

$$(3.5.2.) \qquad M(\bar{\alpha},|H|) = M_s \int_0^{2\pi} \int_0^{\pi} \frac{H + H_A(\theta,\phi)}{|H + H_A(\theta,\phi)|} f(\theta,\phi)\sin\theta d\theta d\phi /$$

$$\int_0^{2\pi} \int_0^{\pi} f(\theta,\phi)\sin\theta d\theta d\phi ,$$

where

$$(3.5.3.) \qquad |H_A(\theta,\phi)| = |H_A^o| \cos\phi(\theta,\phi) \quad , \quad |H_A^o| = 2k/M_s \quad ;$$

and due to (3.4.2.)

$$(3.5.4.) \qquad \cos\phi(\theta,\phi)\sin\phi(\theta,\phi) = \frac{|H|}{|H_A^o|} \sin(\alpha(\theta,\phi) - \psi(\theta,\phi)).$$

$\bar{\alpha}$ is the angle between H and the direction of the average of $H_A(\theta,\phi)$, which is the direction of the remanence.

3.6. For a uniform distribution:

$$(3.6.1.) \qquad f(\theta,\phi) = \begin{cases} 1 , & \text{for } 0 \le \theta \le \theta_0 \text{ and } 0 \le \phi \le 2\pi \\ 0 , & \text{for } \theta_0 \le \theta \le \pi \text{ and } 0 \le \phi \le 2\pi \end{cases}$$

the double integral of (3.5.2.) has been calculated by Gauss quadrature, after determination of the appropriate root of (3.5.4.), as function of H and $\bar{\alpha}$. Because of the appearance of Bloch walls for |H| smaller than 0.5 H_A^o a reversal field H_r was introduced (see paper of Zijlstra).
The results of the calculations show the following relations for the components of $M(\bar{\alpha},|H|)$ parallel and perpendicular to the direction of the remanence resp.

(3.6.2.) $M_{//}(\bar{\alpha},|H|) = M_{//}(\bar{\alpha}',|H'|)$ for $|H|\cos\bar{\alpha}=|H'|\cos\bar{\alpha}'$,

(3.6.3.) $M_{\perp}(\bar{\alpha},|H|) \simeq M_s|H|\sin\bar{\alpha}/(|H_A^\circ| + |H|\cos\bar{\alpha}), (\bar{\alpha},\theta_o<\frac{1}{4}\pi)$.

From these relations it follows that the magnetic susceptibility, defined by $M = \chi H + M_o$ is a tensor of following form:

$$\chi = \begin{bmatrix} \chi_{//}(|H|\cos\alpha) & 0 \\ 0 & M_s/(|H_A^\circ| + |H|\cos\bar{\alpha}) \end{bmatrix}$$

sothat $\mu_{r//} \equiv 1 + \chi_{//}(|H|\cos\alpha)$ can be obtained from the B-H curve if as argument the projection is taken along the direction of the remanence. For $\mu_{r\perp}$ can be taken $1 + M_s/(|H_A^\circ| + |H|\cos\bar{\alpha}) \simeq 1 + M_s/|H_A^\circ|$, since in practice $|H|<<|H_A^\circ|$ for the anisotropic materials of interest.

4. Basic inequalities

4.1. For notational ease we consider only 2 dimensional problems in this §. This is no restriction because the 3 dimensional extension is trivial here.
The models presented in §3 are of the following form:

(4.1.1.) $B = Z(H)H + B_r$

where $Z(H)$ is a matrix and B_r independant of H.
In the soft isotropic case $Z(H) = \mu(|H|)I$ where I is the identity matrix. For the hard anisotropic case we consider

(4.1.2.) $Z(H) = \begin{bmatrix} \mu_{//} & 0 \\ 0 & c \end{bmatrix}$, $\mu_{//}=\mu_0\mu_{r//}(H_{//}), c=\mu_0\mu_{r\perp}$

We note that there allways exists a $d<c$ such that

(4.1.3.) $0<d\leq\mu\leq d^{-1}$, $0<d\leq\frac{d|B|}{d|H|}\leq d^{-1}$ in the soft isotropic case and $0<d\leq\frac{dB_{//}}{dH_{//}}\leq d^{-1}$ for the hard anisotropic case.

The properties stated in the following lemma are used in §6.

Lemma (4.1.) If $\Delta H = H(B_2) - H(B_1)$
$\Delta B = B_2 - B_1$ then

(4.1.4.) $\Delta H.\Delta B \geq d^{-1}|\Delta B|^2$,

(4.1.5.) $\Delta H.\Delta B \geq d|\Delta H|^2$,

(4.1.6.) $|\Delta H|\leq 2d|\Delta B|$ and $|\Delta B|\leq 2d^{-1}|\Delta H|$

proof: We first consider the jacobian matrix $((\frac{\partial B}{\partial H}))$

In the soft isotropic case

(4.1.7.) $((\frac{\partial B}{\partial H})) = \mu(|H|)(I-\frac{1}{|H|^2}Z'(H)) + \frac{1}{|H|^2}\frac{d|B|}{d|H|}Z'(H)$

where $Z'(H) = \begin{bmatrix} H_x^2 & H_xH_y \\ H_xH_y & H_y^2 \end{bmatrix}$ is a semi-positive definite matrix. Also $I - Z'(H)/|H|^2$ is semi-positive definite, using (4.1.3.) we therefore have $|((\frac{\partial B}{\partial H}))| = \max_x((\frac{\partial B}{\partial H}))x.x/|x|^2 \geq d > 0$ or

(4.1.8.) $((\frac{\partial B}{\partial H}))\, x.x \geq d\,|x|^2$

From (4.1.7.) it also follows that

(4.1.9.) $|((\frac{\partial B}{\partial H}))| \leq \mu + \frac{d|B|}{d|H|} \leq 2\,d^{-1}$

In the hard anisotropic case we chose a coordinate system with $x//B_r$ and $y\perp B_r$. In this coordinate system we have

$$((\frac{\partial B}{\partial H})) = \begin{bmatrix} \frac{\partial B_{//}}{\partial H_{//}} & 0 \\ 0 & c \end{bmatrix}$$

where with (4.1.3.) we have again (4.1.8.) and (4.1.9.).

Using a Taylor development and $((\frac{\partial H}{\partial B})) = ((\frac{\partial B}{\partial H}))^{-1}$ we find (4.1.4.) - (4.1.6.)

5. Equivalence of the Galerkin and energy formulation in the two dimensional case.

5.1. For the proof of theorem (5.1.) we need the following equality on $V \subset R_3$

$$(5.1.1.) \qquad \int_V \text{curl } H.\ f\,dv = \int_V H.\text{curl } f\,dv + \int_{\delta V} (\Delta A \times H).n\ d\sigma$$

For the two dimensional case we can still use this formula by interpreting the vectors A, B and H as in (2.3.) and f//A. We assume the volume to have unit length perpendicular to $V \subset R_2$ and note that the contributions from top and bottom planes cancel.

5.2. The operator T is defined by

$$(5.2.1.) \qquad TA = \text{curl } H\ (\text{curl } A) - j$$

Theorem (5.1.)

$$(5.2.2.) \qquad E(A) \leq E(f) \quad \text{for all } f \in \mathring{W}_2^1 \iff$$

$$(5.2.3.) \qquad (TA,f)_L = 0 \quad \text{for all } f \in \mathring{W}_2^1$$

Proof: a. Suppose for a certain A and j we have (5.2.3.), then define

$$\Delta E = E(A) - E(f) = \int_V \int_{B-\Delta B}^{B} H(b).db - j.\Delta A\ dv$$

where $\Delta A = A - f$ and $\Delta B = \text{curl } \Delta A$.
We also have, using (5.1.1.) and $\Delta A = 0$ on δV that

$$\int_V j.\Delta A\ dv = \int_V H.\Delta B\ dv$$

Therefore

$$\Delta E = \int_V \int_{B-\Delta B}^{B} H(b).db - H(B).\Delta B\ dv$$

which with (4.1.8.) gives $\Delta E \leq 0$.

b. Now suppose $E(A) \leq E(f)$ for all $f \in \mathring{W}_2^1$. With (4.1.8.) we have

$$\int_{B-\Delta B}^{B} H(b).db \geq H(B-\Delta B).\Delta B$$

therefore

$$\int_V H(B-\Delta B).\Delta B - j.\Delta A\ dv = \int_V H(B).\Delta B - \Delta H.\Delta B - j.\Delta A\,dv \leq \Delta E \leq 0$$

where $\Delta H = H(B) - H(B-\Delta B)$ or using

$$\int_V H.\Delta B\ dv = \int \text{curl } H.\Delta A\ dv$$

we find

$$\int_V \Delta H.\Delta B - (\text{curl } H - j).\Delta A\ dv \geq 0$$

for all ΔA. Using a Taylor development for ΔH and taking ΔB small enough this implies

$$\int_V ((\frac{\partial H}{\partial B}))|\Delta B|^2 - (\text{curl } H - j).\Delta A\ dv \geq 0$$

we write $\Delta A = \varepsilon \Delta A'$ and see that we have, $\varepsilon^2 p + \varepsilon q \geq 0$ for all ε. Therefore $q \equiv 0$ or $(TA,f)_L = 0$

6. Existence, uniqueness and convergence

6.1. In this § the theory from §2 of [10] is applied for the magnetostatic problem. This theory is used in the following form

Theorem (6.1.)

Let T be a mapping from $\mathring{W}_2^1$ into L_2 satisfying

Q_1: there exists a $c_1 > 0$ such that

(6.1.1.) $(Tu - Tv, Z)_L \leq c_1 ||u-v||_W ||Z||_W$

for all u, v and $Z \epsilon \mathring{W}_2^1$ and

Q_2: there exists a c_2 such that

(6.1.2.) $(Tu - Tv, u-v)_L \geq c_2 ||u-v||_W^2$

for all u, $v \epsilon \mathring{W}_2^1$
then the problems

R : $(Tu,v)_L = 0$ for all $u \epsilon \mathring{W}_2^1$ and
R_k: $(Tu_k,v)_L = 0$ for all $u_k \epsilon P_k$ have unique solutions, and

(6.1.3.) $||u_k-u||_W \leq D \inf \{||z-u||_W | z \epsilon P_k\}$

for some fixed D>0

6.2. The problem posed in (2.3.) is considered here again. The operator T is defined by

$$TA = \text{curl } H(\text{curl } A) - j$$

Then

$$(TA_1-TA_2,A_3)_L = \int_V (H(\text{curl}A_1)-H(\text{curl}A_2)\text{curl}A_3 \, dv$$

and (4.1.6.) gives

$$|H(\text{curl}A_1)-H(\text{curl}A_2)| \leq 2d|\text{curl}(A_1-A_2)|$$

we find, using Schwartz inequality

$$(TA_1-TA_2,A_3)_L \leq ||A_1-A_2||_W ||A_3||_W$$

which is property Q_1.

$$(TA_1-TA_2,A_1-A_2)_L = \int_V (H(\text{curl}A_1)-H(\text{curl}A_2)). \text{curl}(A_1-A_2) \, dv$$

and (4.1.5.) gives

$$H(\text{curl}A_1)-H(\text{curl}A_2).\text{curl}(A_1-A_2) \geq d(\text{curl}(A_1-A_2))^2$$

which implies property Q_2.

6.3. In this section we consider the problem (2.4.). The operator T is defined by

$$Tf = \text{div } B(H_c + \text{grad } f)$$

As in section (6.2.) we may conclude that properties Q_1 and Q_2 are satisfied, this time using (4.1.4.) and (4.1.6.).

6.4. Thus for the problems posed in (2.3.) and (2.4.) we may apply theorem (6.1.). Convergence of approximate solutions depends on the spaces P_k. It follows from (6.1.3.) that, if $P_k \subset P_{k+1}$ and $\lim_{k\to\infty} P_k$ is dense in $\mathring{W}_2^1$ then $\lim_{k\to\infty} u_k = u$, see e.g. [11].

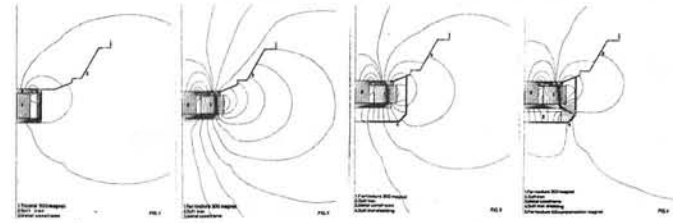

Fig. 3.

7. The program package MAGGY

7.1. The package MAGGY offers facilities for the approximation of 2-dimensional magnetostatic problems. These problems may be either in polar, cylindrical or cartesian coordinates. Calculations are performed using isoparametric bilinear quadrilaterals in either of these coordinates. The previous existence etc. considerations only apply in the cartesian case. The problem and algorithm information have to be given in a problem oriented language, MAGLAN.

The package contains an interpreter program which checks and expands the input and also generates part of the calculating program (e.g. dimension statements). Then a set of secondary programs is available for plotting, printing and the calculation of some secondary results. The package is completely written in Fortran. MAGGY2 is an open package in the sense that it is possible to give user chosen function names for most numbers in the input. The accompanying functions have to be given, immediately following the MAGLAN input.

7.2. The choice of elements in the FEM was done with ease of specification of the mesh as criterium rather then optimum flexibility. However structures of complicated nature have been analysed using MAGGY as can be seen in fig.3,5) In [3] an easy way of specifying a quadrilateral mesh can be found. Here an improved version is given.
A coarse quadrilateral mesh, topologically equivalent to a square mesh, has to be provided. An example is shown in fig. 4. The mesh is completed by the program with linear interpolation.

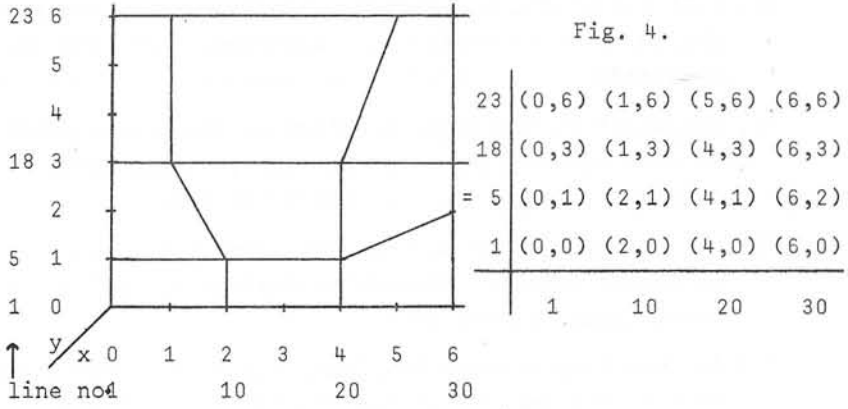

Fig. 4.

This mesh can be specified to the program by giving
x(1) = 4*0, x(10) = 2*2, 2*1, x(20) = 3*4, 5, x(30) = 4*6,
y(1) = 4*0, y(5) = 3*1, 2, y(18) = 4*3, y(23) = 4*6.

This **is all the mesh** information needed for MAGGY, is short and readable.

Fig. 5.

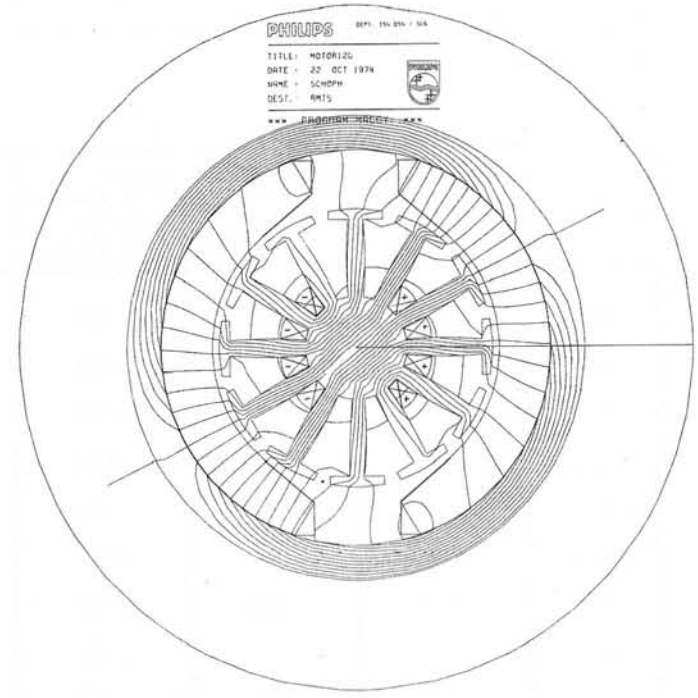

8. A comparison between computed an measured data

The flux, $A(z,R) \equiv 2\pi \int_0^R B(z,r) r \, dr$, in a cylindrical Ticonal 900 bar has been measured at a number of points in the axial direction, z. The flux also has been computed with MAGGY using the model for permanent magnets discussed in §3.
The results obtained for three different meshes are shown in Tabel 1, column two, three and four; $(z_1,r_2)/(z_2,r_2)$ indicates the total number of mesh lines in z- and r-direction within a region of $200*130mm^2$ surrounding the magnet, and the number of meshlines within the magnet of $44.875*10.875mm^2$ respectively.
The measured flux is shown in the last column of table 1. Except for the last two points near the pole of the magnet the results for the finest mesh agree with experiment to within 1%, and the difference is almost constant.

Table 1

Tinocal 900 bar with radius of 10.875mm and half length of 44.875. Flux measured through a cylinder with radius of 11mm is given in 10^{-3} Tesla.

z-coord	Flux calculated by MAGGY			Flux measured
	(11,11) /(5,4)	(21,19) /(9,6)	(43,37) /(19,12)	
0.0	.382	.393	.396	.392
2.5			.396	.392
5.0			.396	.392
7.5		.391	.395	.392
10.0			.394	.390
12.5			.392	.389
15.0	.374	.386	.390	.388
17.5			.387	.384
20.0		.380	.384	.380
22.5			.379	.375
25.0	.349	.368	.373	.369
27.5			.364	.360
30.0		.346	.353	.348
32.5			.337	.333
35.0	.284	.308	.317	.314
37.5			.290	.287
40.0		.245	.253	.249
42.5			.206	.195
44.875	.111	.124	.130	.120

Acknowledgement

We wish to thank mr. P.J. Schophuizen for the permission to publish fig.3,5 which stem from his use of MAGGY. We also wish to express our gratitude towards Dr. Zijlstra for his contributions in the development of the model presented in §3 and mr. Mimmel for the measurements shown in Tabel 1.

References

[1] C.Iselin, Some recent developments in computation of two dimensional fields in iron magnets, Third int. conf. on magnet technology, Hamburg, May 1970.

[2] R.Glowinski et A.Marocco, Analyse numerique du champ magnetique d'un alternateur par elements finis et surrelaxation ponctuelle nonlineaire, Computer methods in applied mechanics and engineering, vol3 no1 Jan.1974.

[3] E.Munro, B.A., Computer aided design methods in electron optics, Ph.D.Thesis, Cambridge University.

[4] P.Silvester and M.V.K.Chari, Analysis of a turbo alternator magnetic field by finite elements, IEEE, PAS 90, 1971, 454-464.

[5] P.Silvester and M.V.K.Chari, Finite element analysis of magnetically saturated D.C. machines, IEEE, PAS 90, 1971 2362-2372.

[6] A.M.Winslow, Numerical solution of the quasi-linear Poisson equation in a non-uniform triangle mesh, Journal of Comp. Phys. 2 (1967) 149-172.

[7] W.Kamminga, Finite element solutions for devices with permanent magnets. Journal of Physics D, Applied Physics Vol8, number 7, May 1975.

[8] Jerzyna Slomczynska. Nonlinear analysis of the magnetic flux in the magnetized magnet stabilised in air. IEEE, Vol MAG-10, No 4, December 1974.

[9] J.Neças. Les methodes directes en theorie des equations elliptiques, MASSON et CIE, 1967.

[10] P.G.Ciarlet, M.H.Schultz and R.S.Varga, Numerical methods of high order accuracy for nonlinear boundary value problems V, Numer. Math. 51-77 (1969).

[11] P.G.Ciarlet & P.A.Raviart, General Lagrange and Hermite interpolation in R^n with applications to finite element methods, 12 Arch. Rat. Mech. Anal. vol 46.

[12] G.Strang, G.J.Fix, An analysis of the finite element method, Prentice Hall Series in automatic computation, 1973.

[13] MAGGY2, user manual, Philips, UDV-DSA-SCA/AdB/SP/AW/75/022/jf.

[14] MAGGY2, example set, Philips, UDV-DSA-SCA/AdB/SP/AW/75/025/jf.

[15] S.J.Polak, MAGGY-A system for magnetic circuit computer aided design, Philips, ISCA-general 003, March 1974.

[16] S.J.Polak, Some aspects in developing MAGGY, Philips, ISCA MAC-CAD, December 1974.

[17] S.J.Polak, J.van Welij, Recent developments, Philips, ISCA MAG-CAD 1975, to appear.

[18] E.C.Stoner and E.P.Wohlfarth, Phil. Trans A240, 599-642, 1948.

[19] M.Bakker, P.W.Hemker, P.J. van der Houwen, S.J.Polak, M. van Veldhuizen, Colloquium discretiseringsmethoden, MC Syllabus 27, Mathematisch Centrum, Amsterdam 1976.

Discussion following paper:

(Becker, Texas) The issue of loss of accuracy in obtaining gradients of the finite element solution (by numerically differentiating the solution) is a serious one in the analysis of stress and flow problems as well as in the present context. Some techniques that have been used (with a mixed degree of success) includes:

(a) Use of higher order Lagrangian elements (usually isoparametric) with gradients calculated at appropriate interior points.

(b) Use of conjugate approximation or other projection methods (as in the work of Oden or of Wheeler).

(c) Use of mixed or mixed-hybrid models in which the gradients are solved directly.

Have you considered any of these techniques and, if so, how do you view their usefulness?

(Polak, Philips, Eindhoven) The problem mentioned is often encountered by us.

B values can be obtained by higher order Lagrange elements inside the elements.

If $\int H.ds$ has to be calculated over element boundaries I think that Hermite elements with interface conditions would be a good choice.

I am not sufficiently familiar with conjugate approximations and therefore cannot give an opinion on their value for this problem. Then of course in integral methods as in GFUN H is solved directly. However for larger problems the full matrix involved will compare unfavourably with the sparse FEM matrices.

As integral methods and GFUN are enjoying some prominence at this conference it is worthwhile clarifying this point.

For an nxn problem, the FEM with Choleski and simple elements used $\frac{1}{2}n^4$ operations. For the same problem the integral method would typically involve only $n^2/5$ unknowns which would require $1/3\ (1/5n^2)^3$ operations. The factor 5 chosen here is problem dependent but there is always an n for which the FEM becomes cheaper.

Therefore we can say that up to a certain magnitude integral methods should be good for calculating H directly and in general using FEM one has to use appropriate elements.

PHYSICAL BASIS OF THE VARIATIONAL METHOD FOR THE COMPUTATION OF MAGNETIC FIELD PROBLEMS

P. Hammond, Department of Electrical Engineering,
University of Southampton, England.

1. Introduction

The hallmark of good computational work is accuracy and attention to detail. The skilled worker who has these qualities in mind cannot easily take a detached view of the computation as a whole. In particular he is unlikely to question the need for the computation. Yet such questioning is essential if the physical concepts are to be disentangled from the algebraic and numerical techniques. Engineers who design such devices as transformers and rotating machines are used to thinking in terms of physical models. They use such terms as leakage flux and they represent the device by equivalent circuit parameters. To determine these parameters they need information about the magnetic field. Before the advent of computers this information was difficult to obtain and crude approximations had to be made. Now the opposite difficulty exists. Engineers are often swamped with information, which is not only useless in itself, but actually blocks the design process, because data-handling has become the over-riding difficulty. Under such circumstances the designer turns his back on computation and relies on intuition and experience, much as a physician may do when presented with a large array of chemical test results on a patient. This is of course a pity, but nevertheless it is a real problem. This paper is a plea for better co-operation between computer analysts and designers. It is a plea that the designer should explain to the analyst what information he needs and that the analyst should restrain his desire to show what the computer can do and concentrate instead on providing simple and elegant programs for particular needs. This does not necessarily mean that the big 'suite of programs' should be ignored, but it does mean that the analyst should seek to understand that the pressing need is for solutions to particular problems rather than for information which may be useful one day. Of course this is a big theme and cannot be dealt with in one paper. What can be done here is to illustrate the theme by a particular example. The example which has been chosen is the method of the calculus of variations which underlies the method of finite elements.

2. The variational method

The development of numerical methods for the solution of magnetic field problems has in general started from a consideration of the differential equations describing the field. These equations have been discretised and by this means a finite-difference mesh has been generated to replace the continuous field distribution. More recently the finite-element method has become popular, which is based on a definite integral or 'functional' of the field energy. Algebraically both methods may lead to similar computation schemes involving the solution of many simultaneous equations. If these equations are taken as the starting point of the computation the choice of method depends only on the past experience of the analyst and the characteristics of the digital computer available.

One might conclude that the physical content of the two methods would also be very similar, but a close examination shows that this is not so. Indeed, the differences can be put to good use in certain cases. Let us consider these differences. The finite-difference method starts with the differential relationships which relate the local field curvature, i.e. the divergence and curl, and the local time-variation of the field, to the local source density. In order to obtain the field in a region the numerical process scans the local source densities and then anchors the mesh to the boundary by imposing given boundary conditions. The finite-element method on the other hand depends on formulating an energy functional and finding its maximum or minimum by a variational technique. In this variational process the differential equation appears as the Euler-Lagrange equation of the functional. If the object of the method were to recover a known equation via an often unknown functional, this would be a strangely circuitous route. A physical interpretation of the functional is needed to make sense of the method.

To arrive at such an interpretation let us take the particular case of a Poissonian field. The functional is known to be $F = \iiint \phi \rho \, dv + \frac{1}{2} \iiint \phi \varepsilon \nabla^2 \phi \, dv$, where ϕ is a scalar potential and ρ is a source density. It is convenient to write this in 'inner product' notation

$$F = \langle \phi, \rho \rangle + \frac{1}{2} \langle \phi, \varepsilon \nabla^2 \phi \rangle$$

If ρ is taken as an assigned source density and ϕ as a variable, the first

variation of F is given by

$$\delta F = \langle \delta\phi, \rho \rangle + \langle \delta\phi, \varepsilon \nabla^2\phi \rangle .$$

Thus for zero first variation, we have $\varepsilon \nabla^2\phi + \rho = 0$, which is of course Poisson's equation. Thus the functional F is the required one. But where did it come from? Its stationary value is given by

$$F_s = \langle \phi, \rho \rangle - \frac{1}{2} \langle \phi, \rho \rangle = \frac{1}{2} \langle \phi, \rho \rangle ,$$

and this is the potential energy of a set of known sources ρ. The potential energy is the 'inter-action' of the sources in terms of the scalar potential ϕ, which in elementary field theory is defined as potential energy per unit source. It is therefore reasonable to start from the functional rather than from the field quantity itself, because the functional has physical significance in terms of energy.

But more remains to be said. Let us generalise the field equation $-\varepsilon \nabla^2\phi = \rho$ by adopting the operator notation $L\phi = \rho$. We then have

$$F = \langle \phi, \rho \rangle - \frac{1}{2} \langle \phi, L\phi \rangle$$

which can be recast into the form

$$F = \frac{1}{2} \langle \phi, \rho \rangle - \frac{1}{2} \langle \phi, L\phi - \rho \rangle .$$

The first term gives the potential energy and the second term introduces the constraint $L\phi = \rho$ by means of the familiar method of a Lagrange multiplier. The method, therefore, seeks the energy of the system of sources ρ subject to the operator equation of the field. Since the designer generally needs to know this energy rather than the field distribution, the method is well adapted to meet his needs. It should be noted that the functional is essentially a system parameter. It is of course possible to divide any system into smaller sub-systems, and if this is done the method is akin to the differential finite-difference method. But the functional can be of arbitrary size and does not need to be sub-divided.

3. The adjoint problem

The meaning and the possibilities inherent in the variational method become even clearer if a more general functional is considered. Let there be two sets of sources designated by ρ and ρ^a, and let their associated field quantities by ϕ and ϕ^a. Consider the mutual energy of the two sets of sources. This mutual energy is given by $\langle \phi, \rho^a \rangle = \langle \phi^a, \rho \rangle$. Consider the functional

$$F = \langle \phi, \rho^a \rangle - \langle \phi^a, L\phi - \rho \rangle$$

where ρ^a and ρ are the assigned known values of the sources. To find the stationary value of F we put

$$\delta F = 0 = \langle \delta\phi, \rho^a \rangle - \langle \delta\phi^a, L\phi - \rho \rangle - \langle \phi^a, L\delta\phi \rangle$$

If in the last term we transpose the operator L to another operator L^a, such that

$$\langle \phi^a, L\delta\phi \rangle = \langle L^a \phi^a, \delta\phi \rangle$$

we obtain the two conditions

$$L\phi = \rho \text{ and } L^a \phi^a = \rho^a .$$

The physical significance of this is clear. The first term of the expression

$$F = \langle \phi, \rho^a \rangle - \langle \phi^a, L\phi - \rho \rangle$$

gives the inter-action energy of the sources ρ and ρ^a. Hence the stationary value F_s determines this energy parameter. The parameter is subject to the two-fold condition that ϕ obeys $L\phi = \rho$ and ϕ^a obeys $L^a \phi^a = \rho^a$. The second system is called the adjoint system. The adjoint sources ρ^a are associated with their own field ϕ^a and an adjoint operator L^a. In many cases, such as Laplacian and Poissonian fields, $L = L^a$ and the operators are said to be self-adjoint. An important exception is the diffusion equation, which is not self-adjoint. If $\rho = \rho^a$ the stationary value of the functional F_s gives the self-energy of the system. Otherwise F_s gives the mutual energy of two systems.

On first meeting the adjoint field quantities one may regard them as a peculiarity of the variational method. More than that one may even decide that the appearance of the adjoint problem is a drawback of this method. Such a conclusion is very wide of the mark. The adjoint problem draws attention to the physical basis of field calculation methods in general and provides valuable guidance for the formulation of efficient computation schemes. To understand what is happening it is necessary to go back to the experimental basis of field theory.

Consider for instance the electrostatic field. The entire theory is built on the experimentally observed inter-action of electric charges. In the simplest case two charges act on each other and a mutual potential energy can be associated with the system formed by the two charges. The notion of an electric field only arises when the problem of inter-action is separated into two problems, in which one charge acts as a source for a field which then acts on the other charge. The field is no more or no

less than a useful mental construct which enables the problem to be separated into two stages.

It is therefore not surprising that information about a field distribution is of use to the designer only as far as it can be made to yield further information about such physical matters as force and energy. To put it very bluntly, the designer does not require the field map at all. This is at the root of much of the misunderstanding between computer analysts and designers, which is so common in industry. Of course we are overstating the difficulties, because to the experienced eye a field map does present useful information. Nevertheless it also contains much information which is not useful, namely the field distribution in a region free of matter. Moreover if the information is presented in numerical form, the problem of interpretation becomes well-nigh insoluble.

Since inter-action is the basis of both theory and practice in field problems, it is not surprising that the variational method draws attention to two field equations which have to be satisfied in order to determine the mutual energy for the equilibrium condition. Unless there is an adjoint source, there is no system. A single source by itself is an abstraction which has no counterpart in the physical world. The adjoint problem draws attention to the principle of reciprocity. The energy of a system is always a mutual relationship. Thus the self-energy, as for instance the self-inductance of a circuit is really a mutual energy of the parts of the circuit. The self-inductance is not a property of the material of the wire, but a property of the geometrical arrangement of the parts of the wire relative to each other. In the integration process the elements of the circuit fulfil the role of the adjoint sources as well as the original sources. The adjoint problem therefore coalesces with the original problem. If on the other hand mutual inductance is to be calculated each coil is the adjoint of the other.

4. The adjoint source as a probe of the field

The notion of mutual inductance leads to another important observation about field calculations. Suppose we regard the 'secondary' coil as a probe to be used in examining the field of a set of 'primary' coils. For every position of this probe there will be a mutual inductance between it and the primary coils. We can set up the energy functional as

$$F = \langle \underline{A}, \underline{J}^a \rangle - \langle \underline{A}^a, L\,\underline{A} - \underline{J} \rangle$$

where $\underline{J}$ are the primary current densities and $\underline{J}^a$ the current densities in the probe. $\underline{A}$ and $\underline{A}^a$ are the vector potentials due to these current densities and L is the operative $\frac{1}{\mu}\,\underline{\nabla} \times \underline{\nabla} \times$ which is also L^a. $\delta F = 0$ leads to $L\,\underline{A} = \underline{J}$ and $L^a\,\underline{A}^a = \underline{J}^a$. Suppose we require a map of the field parameter $\underline{A}$. In order to find $\underline{A}$ at a point, we need to shrink the probe to an infinitestimal current element. However, the probe must carry finite current in its infinitesimal cross-section, because if the current itself were to be infinitesimal there would be no measurable inter-action. Thus the current will have to have infinite density and can be represented by a Dirac δ function. Thus by requiring information about the local distribution of $\underline{A}$, we have decided that the probe must have the properties of a δ function. Similarly an electrostatic field map requires a probe which is a charge of infinite density and zero volume.

The inter-action energy can be written as either $\langle \underline{A}, \underline{J}^a \rangle$ or $\langle \underline{A}^a, \underline{J} \rangle$. The first form requires the use of the δ function probe and the second requires the use of the Green's function $\underline{A}^a$. This may be the better choice, but Green's function solutions tend to have slow convergence. The trouble is due to the stringent requirement to find the field at every point. All this information has to be paid for.

If the adjoint source is thought of as a probe designed to elicit information about the field, we notice at once how important it is that the designer should specify to the computer analyst what information he requires. If, for instance, the mutual inductance between two windings of a machine is required, the analyst can choose one of the windings as the 'probe'. Such a large probe will be insensitive to local field variations and this will reduce the computational effort. It would be wasteful to explore the field with a tiny probe and then derive the large-scale energy parameter.

5. An example of a self-inductance calculation

In problems of self-inductance the natural choice of probe is in terms of the assigned current density itself. We then obtain the energy in terms of the integral $\frac{1}{2}\langle \underline{A}, \underline{J} \rangle$. This integral may be insensitive to the actual distribution of $\underline{A}$ and it becomes possible to use a fairly rough approximation for $\underline{A}$ which will still give a close value for the energy and hence the inductance. As an example consider the internal inductance of a T-shaped conductor in a slot in highly-permeable iron as shown in the

figure.

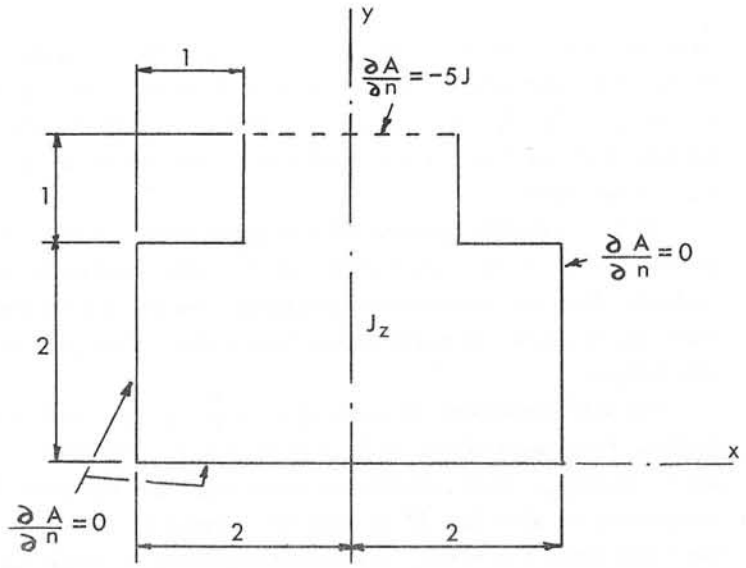

The slot is open at the top and we have assumed that the magnetic field is constant across the opening. There is a uniform current density $J_z = J$ across the section of the conductor, so that the total current is 10J. The iron is assumed to be infinitely permeable, so that the tangential H along the iron boundary is zero. Hence the tangential field across the opening of the slot is $H_x = -10J/2 = -5J$.

To calculate the internal inductance we have to isolate the conductor from the outide region. This can be done by assuming there to be a surface current across the opening of the slot which gives the correct magnetic field inside the slot and zero field outside. This means there is a current $I = H_x = -5J$ at the slot opening.

The internal inductance of such a conductor has been carefully investigated by various writers. Thus we have accurate values for purposes of comparison with the approximate values we shall derive by means of the variational method. In particular a paper[1] by Jones, Reed, Mullineux and Stoll gives a method from which we deduce that the internal inductance is $L = 0.570\ \mu_o$ H/m.

For the variational method we set up the usual functional

$$F = \frac{1}{2}\langle \underline{A}, \underline{J}\rangle + \frac{1}{2}\left|\underline{A}, \underline{I}\right| - \frac{1}{2}\langle \underline{A}, L\underline{A} - \underline{J}\rangle$$

where the second term describes the energy associated with the surface current at the slot opening. Thus

$$F = \langle \underline{A}, \underline{J}\rangle + \frac{1}{2}\left|\underline{A}, \underline{I}\right| - \frac{1}{2\mu_o}\langle \underline{A}, \underline{\nabla} \times \underline{\nabla} \times \underline{A}\rangle$$

$$= \langle \underline{A}, \underline{J}\rangle + \left|\underline{A}, \underline{I}\right| - \frac{1}{2\mu_o}\langle \underline{B}, \underline{B}\rangle$$

The first variation of F is given by

$$\delta F = \langle \delta\underline{A}, \underline{J}\rangle + \left|\delta\underline{A}, I\right| - \frac{1}{\mu}\langle \underline{B}, \delta\underline{B}\rangle = 0$$

We note that $A_x = A_y = 0$ and therefore $B_z = 0$. Also $B_x = \frac{\partial A_z}{\partial y}$ and $B_y = -\frac{\partial A_z}{\partial x}$.

To find an approximate value for the functional and therefore for the inductance we must choose appropriate functions for A_z. A constant value for A_z gives zero magnetic field and therefore does not contribute to the solution. We consider next $A_z = ax + by$. From symmetry a = 0, so that we have $A_z = by$. This implies that $B_y = 0$ and $B_x = b$ is a constant. Then

$$F = \langle by, J\rangle - \left|3b, 5J\right| - \frac{1}{2\mu_o}\langle b^2\rangle$$

$$= \int_0^2\int_{-2}^{+2} J\,b\,y\,dx\,dy + \int_2^3\int_{-1}^{+1} J\,b\,y\,dx\,dy - \int_{-1}^{+1} 15\,b\,J\,dx - \frac{5b^2}{\mu_o}$$

$$= 8\,J\,b + 5\,J\,b - 30\,J\,b - \frac{5b^2}{\mu_o}$$

$$= -17\,J\,b - \frac{5b^2}{\mu_o}$$

For $\delta F = 0$ we put $\frac{\partial F}{\partial b} = 0$, hence $-17J - \frac{10b}{\mu_o} = 0$ and $b = -1.7\mu_o J$

Substituting in F we obtain $F = 14.45\mu_o J^2$ and $L = 0.289\mu_o$, which should be compared with the accurate value $L = 0.570\mu_o$.

We have deliberately chosen a poor approximation in order to illustrate the method. It will have been noted that our choice of A_z implied a constant magnetic field everywhere in the conductor. Since we know that the field is zero at the bottom of the slot and that it has a finite value at the top, our choice is a poor one.

Let us consider an improved trial function $A_z = ay + by^2$, for which $B_x = a + 2by$. In the variational process we put $\frac{\partial F}{\partial a} = 0$ and $\frac{\partial F}{\partial b} = 0$ to obtain a and b. This gives $F = 24.25\mu_o J^2$ and $L = 0.485\mu_o$. This is

already within 15% of the correct value and may be sufficient for practical purposes. The power of the method is shown by the fact that a close approximation of the inductance has been obtained, although the field pattern is highly inaccurate. For instance at y = 0 we know that $B_x = 0$ but on approximation gives $B_x = a = 0.57\mu_o$ J. The reason for the power of the method lies in the fact that it has been designed to find the best value of the energy or the inductance and does not seek to find an accurate flux map. If the designer needs the inductance it is unnecessary and wasteful to find a field. Of course it is desirable to choose a reasonable trial function for the field, but the method is not very sensitive to the actual choice.

In this example we have used the variational method in exactly the same way as it is used in the method of finite elements. The only difference is that the shape of the conductor is somewhat unusual. Moreover most finite-element calculations use a linear relationship for the trial function. Clearly a linear relationship will give adequate closeness of fit over smaller regions. In any case finite-element solutions are not limited to linear representations of the potential. The difference between our method and that of the usual finite-element method does not lie in the mathematical technique, but in the approach to the problem. The finite-element method is generally used to obtain a field map and this, as has been mentioned before, implies a desire for information about the distribution of energy in a region. Our approach on the other hand is to regard the variational method as dealing with a system and seeking the energy of that system in an equilibrium condition.

6. Upper and lower bounds for the functional

One objection which could be raised to the method illustrated by the example of the T-shaped conductor is that the degree of approximation to the accurate solution is in general not known. This is a common failing in numerical methods and is similar to the uncertainty that exists in manufacturing processes. The correct choice of tolerances comes with experience. It is both expensive and useless to call for closer tolerances than those that are needed. But happily the variational method suffers less from uncertainty then many other methods. So far we have used only the equilibrium relationship which sets the first variation of the functional to zero. Further information can be obtained by considering the second variation. The sign of this variation determines whether the functional is a maximum or a minimum. Thus the functional $F = \langle \underline{A}, \underline{J} \rangle + \left| \underline{A}, \underline{J} \right| - \frac{1}{2\mu_o} \langle \underline{B}, \underline{B} \rangle$ is a maximum at its stationary value, because only the third term contributes to the second variation and its sign is negative.

It is a valuable property of the magnetostatic problem that a dual functional can be formulated which has the same stationary value but as a minimum. Thus the approximate functionals can be used to provide both a lower and an upper bound for the correct value. This greatly reduces the uncertainty.

The dual functional is given by $F' = \frac{\mu_o}{2} \langle \underline{H}, \underline{H} \rangle$. Reverting to our example, the simple choice of $H_y = 0$, $H_x = -\frac{5}{3} y$ J gives $F' = 32.41\mu_o J^2$ and $L' = 0.648\mu_o$. This provides an upper bound for the inductance. It is interesting to note that if we take the average of this upper bound and the lower bound $L = 0.485\mu_o$ previously obtained, we arrive at $L = 0.567\mu_o$ which is within ½% of the correct value. For a fuller discussion of dual upper and lower bounds the reader is referred to a paper 'The calculation of inductance and capacitance by means of dual energy principles' by the present author and Dr. J. Penman to be published shortly in the Proceedings of the Institution of Electrical Engineers.

7. Variational treatment of the diffusion equation

Finally it may be of interest to look at the treatment of diffusion problems by means of the variational method. Consider an assigned harmonic current distribution $\underline{J}e^{j\omega t}$. In order to obtain a functional independent of time we must choose an adjoint current which has a negative time variation. Thus $\underline{J}^* e^{-j\omega t}$ is a possible choice. $\underline{J}$ and J^* are complex conjugates. The vector potential and the adjoint vector potential are chosen similarly. The operator equation $L\underline{A} = \underline{J}$ is given by $\frac{1}{\mu} \underline{\nabla} \times \underline{\nabla} \times \underline{A} + j\omega\sigma\underline{A} = \underline{J}$ where σ is the conductivity and hence the operators are $L = \frac{1}{\mu} \underline{\nabla} \times \underline{\nabla} \times + j\omega\sigma$, and $L^a = \frac{1}{\mu} \underline{\nabla} \times \underline{\nabla} \times - j\omega\sigma$. The complex functional is given by $F = \langle \underline{A}, \underline{J}^* \rangle - \frac{1}{2} \langle \underline{A}^*, L\underline{A} \rangle$. This functional contains both the inductance and resistance. It is very interesting tha in this instance the adjoint quantities use a negative time. But of course this is exactly what is done by using the complex conjugate in phasor calculations. Once again the adjoint problem is an essential feature in the determination of the system parameters.

8. Conclusion

In this paper a plea has been made for a better understanding between computer analysts and designers of electrical machines. In particular it is urged that the designer often needs large-scale system parameters rather than the details of a field map. Variational methods are well-adapted to provide this information economically.

9. Reference

1. Jones, D.E., Mullineux, N., Reed, J.R., and Stoll, R.L. : 'Solid rectangular and T-shaped conductors in semi-closed slots', J. Engineering Mathematics 3, 2, 1969, pp.123-135.

Discussion following paper:

(Yeh, Oak Ridge) Could the variational bound approval be as useful when the quantity of interest is not the energy of interaction but some other quantity, eg the field in some region?

(Hammond, Southampton) The variational method seeks a functional, ie a quantity which can be described by a real or complex number. Thus the parameter of interest must be such a number if it is to be obtained by this method. If it is desired to find the field at a point, then this can be done by using a source which has strength unity and placing it at that point. The interaction energy is then equal to the field at the point. A scalar fiend can be found by a single functional, a vector field needs a vector probe and in general will need three functionals. The method is essentially an energy method, but this is not restrictive if it is realised that energy is what fields are all about.

(Popovic, Belgrade) I should like to agree with Prof Hammond that physical insight is often very important in making useful approximations for magnetic field problems. Frequently we are inclined to write a paper which should be entitled "A very general method for solving arbitrarily large problems with an application to a very small problem", when the small problem could be solved with a much simpler theory.

(Carpenter, Imperial College) The method gives a very neat way of deriving what appears to be a surprisingly accurate solution by simple approximations. But the accuracy depends on the upper and lower approximations being equally displaced from the exact solution. Is this a fortunate accident in the examples given, or can Prof Hammond obtain two solutions generally which are merely equally displaced?

(Hammond) I suspect that one needs to acquire experience with the method and I am still rather inexperienced. However, if the variable function is expressed as a polynomial then the order of the polynomial should probably be the same for the same physical quantity in both the upper and the lower bound. Thus in a linear magnetic material H and B should have the same type of approximation. It is also important to pay attention to the boundary conditions and use the same accuracy, or lack of it, in modelling the two functionals.

(Silvester, McGill) Would Prof Hammond care to indicate the extent of applicability of this theory to non-linear problems?

(Hammond) The method depends on the geometrical relationships of the field, ie on its curl and divergence. It is independent of the constitutive relationships. An analogous statement for networks says that Tellegen's theorem is independent of the linearity of the circuit elements. All that matters is that both Kirchhoff laws hold. If hysteresis is present, the problem would have to be specified by giving information about the initial state as well as the shape of the hysteresis loop.

(Jevons, Birmingham) A practical example of approaching the accurate solution from both sides and averaging the result, occurs in the use of resistance networks to determine circuit parameters of fields problems. Suppose a 'straight' analogue is made and the resistance measured, and then the dual made by interchanging equipotential and flow line boundaries and the resistance again measured. The average of the two measured values is very close to the accurate value for even very coarse meshes. One or two mesh refinements gives rapid convergence to the accurate value.

(Hammond) I have no first-hand experience of resistance analogues and am very greatful to Dr Jevons for confirming that the method works well in such an application.

(Reece, GEC) The machine designer would wish to know not only the self inductance of a tee-bar but also the AC resistance. Is it possible to use the method described in dissipative situations, and hence to obtain AC resistance?

(Hammond) Yes, the functional can be complex and embody both resistance and inductance. This is briefly treated in the last section of the paper. I do not think it is possible to obtain a doubly-bounded solution, however.

(Steel, CERL) Prof Hammond makes an important contribution to the conference in that he reminds us that we should always be aware of the questions which underlie the investigation of fields. This can be illustrated by one of many classical examples in the literature. I chose the determination of the maximum temperature of a thermally well insulated conductor carrying an electric current. If the non-linear relation between thermal and electric conductivities is taken into account then it has been shown by Raymond Holm that

(Steel, continued)

$$V^2 = 8 \int_{To}^{Tm} \rho \, \lambda \, dT$$

V is the potential across the conductor

Tm is the maximum temperature

To is the end temperature.

Note that for pure metals $\rho \lambda \propto T$ and the relation between Tm and V is algebraic and independent of the shape of the conductor!

(Hammond) The example cited by Mr Steel is new to me. It certainly reinforces Mr Steel's comments. It seems to me that the greatest challenge to a teacher is how to foster the gift of physical understanding with which some of his students are endowed.

SOME TECHNIQUES AND APPLICATIONS OF THE FINITE ELEMENT METHOD FOR SOLVING MAGNETIC FIELD PROBLEMS

Eric Munro

IBM Thomas J. Watson Research Center,
Yorktown Heights, New York 10598, U.S.A.

1. Introduction

The finite element method[1] provides a powerful numerical technique for solving magnetic field problems. The author's work in this field has been concerned mainly with using the method to calculate field distributions in magnetic electron lenses[2,3], and the computer programs developed for this purpose have recently been published[4]. In this paper, the principles of the method are summarized, the derivation of the finite element equations is explained, and techniques for solving the equations are discussed. Extensions of the method for handling the properties of materials with non-linear magnetization characteristics and permanent magnet materials are described. A technique for calculating the fields due to toroidal deflection coils inside rotationally-symmetric magnetic electron lenses is also presented. Each technique is illustrated by typical computed results, to show the wide range of applications of the method.

2. Principles of the finite element method

The partial differential equation of the boundary-value field problem is first replaced by a corresponding functional, whose minimization is equivalent to solving the original differential equation. The entire region inside the boundary is then divided into many small sub-regions called finite elements. These finite elements may be triangles, quadrilaterals or more complicated shapes. The potential distribution within each element is then approximated by some simple function of position, e.g. a first-order polynomial (first-order elements), a second-order polynomial (second-order elements), or a higher-order polynomial if extreme accuracy is required. Using this approximation, the potential distribution within each element is then expressed as a function of the potentials at mesh-points associated with the element. In this way, the contribution from each element to the overall value of the functional is expressed in terms of the mesh-point potentials. The requirement that the functional is to be minimized is then used to derive a set of algebraic equations, inter-relating the potentials at adjacent mesh-points. These equations are then solved to give the potential at each mesh-point.

3. Derivation of the finite element equations

The derivation of the finite element equations will be illustrated using the magnetic electron lens shown in Fig. 1 as an example. This lens consists of a magnetic circuit, polepieces and coil windings, which all have rotational symmetry about the axis XYZ. If the field distribution is required only in the polepiece region ABCD, this can be calculated using a scalar potential. If the fields are required throughout the entire magnetic circuit region EFGH which includes the coil windings, then a vector potential must be used. Each of these cases will be considered in turn.

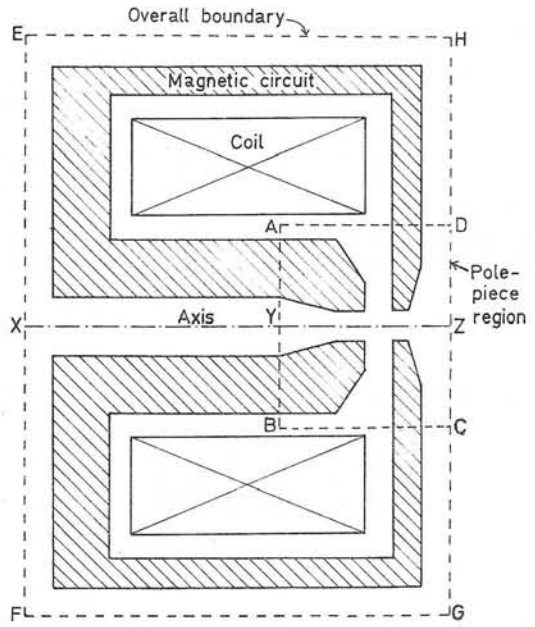

Fig. 1 Cross-section of a typical magnetic electron lens

3.1 Scalar potential formulation

The polepiece region ABCD contains no coil windings. The magnetic field strength $\underline{H}$ throughout this region can therefore be expressed as the gradient of a scalar potential V, i.e.

$$\underline{H} = \underline{\text{grad}}\ V \tag{1}$$

V satisfies the differential equation

$$\text{div}\ (\mu\ \underline{\text{grad}}\ V) = 0 \tag{2}$$

where μ is the permeability at any point. For linear problems, in which μ is assumed to be independent of $\underline{H}$, the solution of (2) subject to prescribed boundary conditions can be obtained by minimizing the functional

$$F = \iiint \tfrac{1}{2}\,\mu\ \underline{\text{grad}}\ V\ .\ \underline{\text{grad}}\ V\ \ dv \tag{3}$$

subject to the same boundary conditions. (A proof of this can be found in Ref. 2.) For the rotationally-symmetric lens of Fig. 1, (3) becomes

$$F = \iint \tfrac{1}{2}\,\mu \left[\left(\frac{\partial V}{\partial z}\right)^2 + \left(\frac{\partial V}{\partial r}\right)^2 \right] 2\pi r\ dz\ dr \tag{4}$$

The functional (4) must now be minimized numerically by the finite element method. To do this, the region to be analyzed is divided by a mesh into small quadrilateral regions (Fig. 2). The mesh lines are chosen to coincide with the polepiece profiles. A fine mesh is used where high accuracy is required; a coarser mesh is used elsewhere. Each quadrilateral is subdivided into two triangular finite elements. This subdivision is done in two separate ways (Fig. 3). A typical finite element is shown in Fig. 4. Let the potentials at the vertices be denoted by $V_i(z_i,r_i)$, $V_j(z_j,r_j)$ and $V_k(z_k,r_k)$. Since in our example we are using first-order finite elements, we make the approximation that the potential varies linearly over the element. With this approximation, the contribution ΔF from a single finite element to the value of the functional (4) is

$$\Delta F = \frac{\pi\mu r_0}{4a}\left[\left(\sum_{i=1}^{3} b_i V_i\right)^2 + \left(\sum_{i=1}^{3} c_i V_i\right)^2\right] \qquad (5)$$

where μ = permeability of element, r_o = value of r at centroid of element, a = area of element, $b_i=r_j-r_k$ and $c_i=z_k-z_j$. Differentiating (5) gives

$$\left[\frac{\partial \Delta F}{\partial V_i}\right] = \left[F_{ij}\right]\left[V_i\right] \qquad (6)$$

where

$$F_{ij} = \mu \frac{\pi r_0}{2a}(b_i b_j + c_i c_j) \qquad (7)$$

Using (7), a 3 x 3 matrix F_{ij} is calculated for every element of the mesh. Since F_{ij} is symmetric, only six coefficients need be stored for each matrix.

The matrices F_{ij} are now used to set up the finite element equations, by imposing the condition that the functional is to be minimized. To illustrate how this is done, let V_0 be the potential at a general mesh-point (see Fig. 3) and let V_1, V_2, ... , V_8 be the potentials at the eight adjacent mesh-points. The condition for minimizing the functional is

$$\frac{\partial F}{\partial V_0} = 0 \qquad (8)$$

Now, if V_0 is changed, keeping all the other potentials constant, then the corresponding change in the functional will be due only to the changes in the contributions from the twelve shaded elements E_1-E_{12} in Fig. 3. Thus from equation (8) we obtain

$$\left(\frac{\partial \Delta F}{\partial V_0}\right)_{E_1} + \left(\frac{\partial \Delta F}{\partial V_0}\right)_{E_2} + \ldots + \left(\frac{\partial \Delta F}{\partial V_0}\right)_{E_{12}} = 0 \qquad (9)$$

By substituting equation (6) for each of the elements E_1-E_{12} into equation (9), we obtain a nine-point finite element equation of the form

$$\sum_{m=0}^{8} P_m V_m = 0 \qquad (10)$$

where each coefficient P_m is the sum of appropriate terms of F_{ij}. In this way, a finite element equation is generated for every mesh-point which is not a boundary point. Points which lie on the symmetry axis YZ in Fig. 2 are treated as a special case, and at each of these points a six-point equation is obtained. The prescribed boundary potentials on the boundaries AY, AC and CZ (see Fig. 2) are then inserted into the equations. These equations are then solved, as described in Section 4, to give the potential

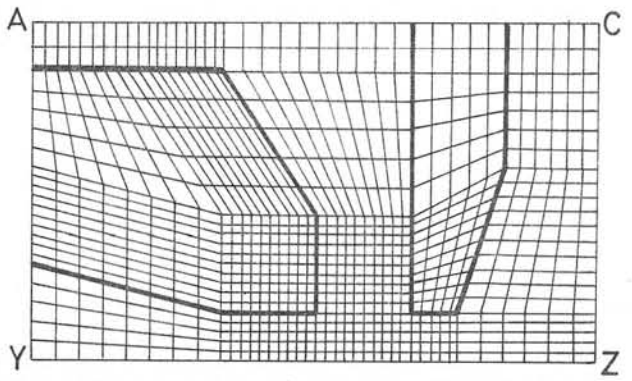

Fig. 2 Finite element mesh for calculating the scalar potential distribution in the polepiece region of the lens of Fig. 1

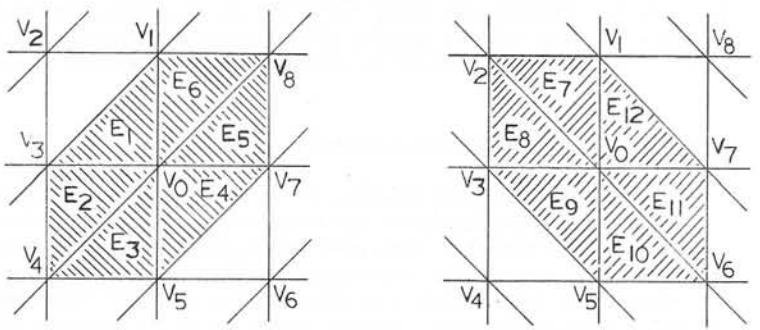

Fig. 3 Subdivision of the quadrilateral regions into triangular finite elements

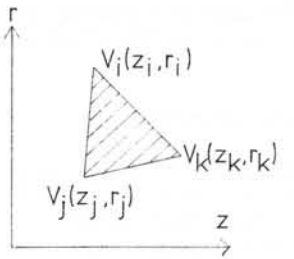

Fig. 4 A typical finite element for the scalar potential formulation

at each mesh-point. The scalar equipotentials can then be plotted out on a computer graph plotter, as shown in Fig. 5, and the field comonents at any point can be obtained by numerical differentiation of the computed mesh-point potentials.

A similar technique is used for calculating two-dimensional scalar potential distributions in planar (x,y) coordinate systems. In such cases, instead of using the functional (4), the following functional is used:

$$F = \iint \frac{1}{2}\mu \left[\left(\frac{\partial V}{\partial x}\right)^2 + \left(\frac{\partial V}{\partial y}\right)^2 \right] dx\, dy \qquad (11)$$

and equation (7) is replaced by

$$F_{ij} = \frac{\mu}{4a}(b_i b_j + c_i c_j) \qquad (12)$$

where μ = permeability of element, a = area of element, $b_i = y_j - y_k$ and $c_i = x_k - x_j$. In all other respects, the analysis of planar fields is identical to the analysis of rotationally-symmetric fields.

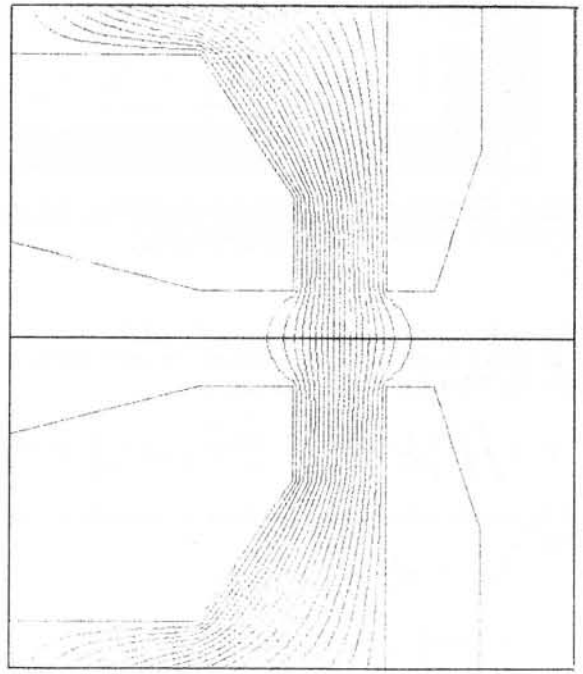

Fig. 5 Computed scalar equipotentials in the polepiece region of the lens of Fig. 1

3.2 Vector potential formulation

To calculate the field distribution throughout the the region EFGH in Fig. 1, which encloses the coil windings, a vector potential must be used, since a scalar potential cannot be used in regions containing currents. The vector potential $\underline{A}$ is defined such that the flux density $\underline{B}$ is the curl of $\underline{A}$, i.e.

$$\underline{B} = \underline{\text{curl}}\ \underline{A} \qquad (13)$$

$\underline{A}$ satisfies the differential equation

$$\underline{\text{curl}}\ \left(\frac{1}{\mu}\ \underline{\text{curl}}\ \underline{A}\right) = \underline{J} \qquad (14)$$

where μ = permeability and $\underline{J}$ = current density at any point. For linear problems, in which μ is assumed to be independent of $\underline{B}$, the solution of (14) subject to prescribed boundary conditions can be obtained by minimizing the functional

$$F = \iiint \left(\frac{1}{2\mu}\ \underline{\text{curl}}\ \underline{A} \cdot \underline{\text{curl}}\ \underline{A} - \underline{J}.\underline{A}\right) dv \qquad (15)$$

subject to the same boundary conditions. (A proof of this can be found in Ref. 2.) For the rotationally-symmetric lens of Fig. 1, (15) becomes

$$F = \iint \left\{ \frac{1}{2\mu} \left[\left(\frac{\partial A_\theta}{\partial z}\right)^2 + \left(\frac{\partial A_\theta}{\partial r} + \frac{A_\theta}{r}\right)^2 \right] - J_\theta A_\theta \right\} 2\pi r\, dz\, dr \qquad (16)$$

where J_θ and A_θ are the θ-components of $\underline{J}$ and $\underline{A}$ respectively. The functional (16) must now be minimized numerically by the finite element method. The procedure for doing this is analogous to that used in the scalar potential formulation. The region to be analysed is first divided into quadrilateral regions (Fig. 6). The mesh lines are chosen to coincide with the profiles of the magnetic circuit and coil windings. A fine mesh is

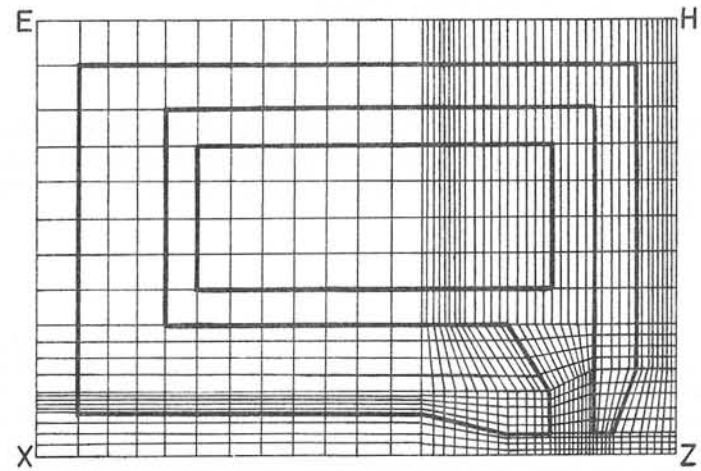

Fig. 6 Finite element mesh for calculating the vector potential distribution throughout the magnetic circuit and coil windings of the lens of Fig. 1

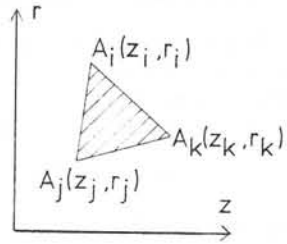

Fig. 7 A typical finite element for the vector potential formulation

used where high accuracy is required; a coarser mesh is used elsewhere. Each quadrilateral is subdivided into two triangular finite elements. This subdivision is done in two ways (Fig. 3). A typical finite element is shown in Fig. 7. Let the values of A_θ at the vertices of the element be denoted by $A_i(z_i,r_i)$, $A_j(z_j,r_j)$ and $A_k(z_k,r_k)$. Making the first-order finite element approximation, i.e. assuming that A_θ varies linearly over the element, we find that the contribution ΔF from a single element to the value of the functional (16) is

$$\Delta F = \frac{\pi r_0}{4\mu a}\left[\left(\sum_{i=1}^{3} b_i A_i\right)^2 + \left(\sum_{i=1}^{3} d_i A_i\right)^2\right] - \frac{2}{3} J_\theta \pi r_0 a \left(\sum_{i=1}^{3} A_i\right) \qquad (17)$$

where μ = permeability of element, r_o = value of r at centroid of element, a = area of element, $b_i=r_j-r_k$ and $d_i=z_k-z_i+2a/3r_o$. In obtaining (17) from (16), we have made the approximation that $\iint z^m r^n dz dr = z_o^m r_o^n a$, where (z_o,r_o) is the centroid of the element. This approximation is satisfactory provided that the elements are sufficiently small. Differentiating (17) gives

$$\left[\frac{\partial \Delta F}{\partial A_i}\right] = \left[F_{ij}\right]\left[A_i\right] + \left[G_i\right] \qquad (18)$$

where
$$F_{ij} = \frac{\pi r_0}{2\mu a}(b_i b_j + d_i d_j)$$

and
$$G_i = -\frac{2}{3} J_\theta \pi r_0 a \qquad (19)$$

Using (19), a 3 x 3 matrix F_{ij} and a value of G_i are calculated for each finite element. We then proceed to set up the finite element equations, using exactly the same reasoning as for the scalar potential formulation. In this case, each finite element equation has the general form

$$\sum_{m=0}^{8} P_m A_m = Q \qquad (20)$$

where each coefficient P_m is the sum of appropriate elements of F_{ij}, and Q is the sum of appropriate elements of G_i. The boundary conditions are that $A_\theta = 0$ on the outer boundaries EX, EH and HZ (see Fig. 6), and $A_\theta = 0$ on the axis XZ. These boundary conditions are inserted into the finite element equations. The equations are then solved, as described in Section 4, to give the vector potential A_θ at each mesh-point. The magnetic flux lines (lines of constant rA_θ) can then be plotted on a computer graph plotter, as shown in Fig. 8, and the flux density components at any point can be obtained by numerical differentiation of the computed mesh-point potentials.

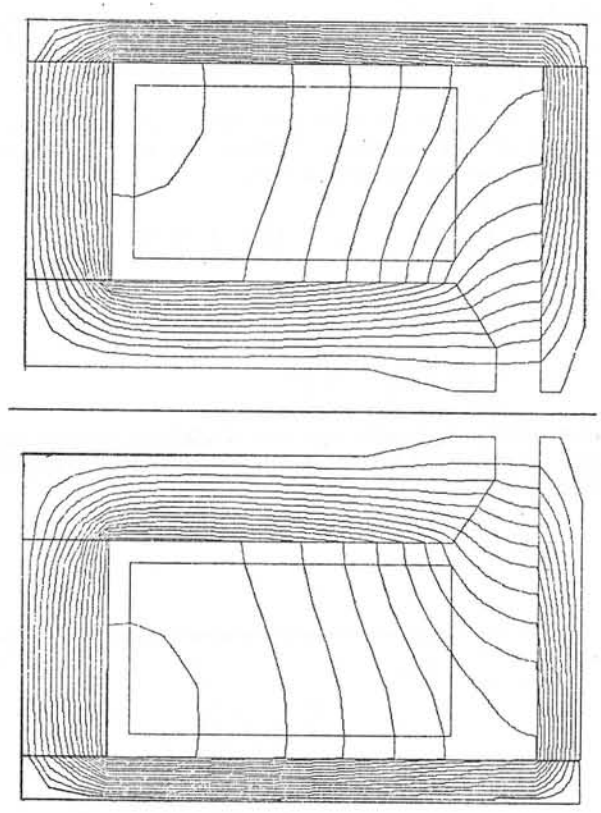

Fig. 8 Computed flux distribution throughout the magnetic circuit and coil windings of the lens of Fig. 1

An analogous technique is used for calculating two-dimensional vector potential distributions in planar (x,y) coordinate systems. In such cases, instead of using the functional (16), the following functional is used:

$$F = \iint \left\{ \frac{1}{2\mu}\left[\left(\frac{\partial A_z}{\partial x}\right)^2 + \left(\frac{\partial A_z}{\partial y}\right)^2\right] - J_z A_z \right\} dx\, dy \qquad (21)$$

where J_z and A_z are the z-components of J and A respectively; the expressions (19) are replaced by

$$F_{ij} = \frac{1}{4\mu a}(b_i b_j + c_i c_j)$$

and
$$G_i = -\frac{1}{3} J_z a \qquad (22)$$

where μ = permeability of element, a = area of element, $b_i=y_j-y_k$ and $c_i=x_k-x_j$; and the magnetic flux lines are lines of constant A_z. In all other respects, the calculation of vector potential distributions for planar fields is identical to that for rotationally-symmetric fields.

4. Methods for solving the finite element equations

Let there be I x J mesh-points in Fig. 2 or Fig. 6, and let them be numbered sequentially, column by column, as shown in Fig. 9. Then, if the finite element equations for each mesh-point are arranged in this same order, the matrix of coefficients will appear as shown in Fig. 10. This matrix contains nine non-zero diagonals, corresponding to the nine coefficients in each equation. This matrix will always be symmetric, because the constituent finite element matrices F_{ij} (see equation (7) or (12)) are themselves symmetric. Consequently, only five coefficients need be stored for the left-hand side of each equation. The equation for the $(i,j)^{th}$ mesh-point can therefore be written in the following form:

$$P_{i-1,j-1,5}\,V_{i-1,j-1} + P_{i,j-1,4}\,V_{i,j-1} + P_{i+1,j-1,3}\,V_{i+1,j-1}$$
$$+ P_{i-1,j,2}\,V_{i-1,j} + P_{i,j,1}\,V_{i,j} + P_{i,j,2}\,V_{i+1,j}$$
$$+ P_{i,j,3}\,V_{i-1,j+1} + P_{i,j,4}\,V_{i,j+1} + P_{i,j,5}\,V_{i+1,j+1} = Q_{i,j} \qquad (23)$$

The most straightforward way of solving these equations is by gaussian elimination and backward substitution, using a symmetric banded matrix subroutine[5]. This is the approach adopted by the author in his programs[4]. As the gaussian elimination proceeds, all the coefficients which lie between the outermost non-zero diagonals in Fig. 10 become filled with non-zeros. Since the matrix is symmetric, it is sufficient to store only the upper half of the band. Thus (I+2) coefficients must be stored per equation, or a total of (I+2)IJ coefficients for all the equations. Hence this method becomes very expensive on storage if large numbers of mesh-points are used. For example, the maximum mesh-size which the author has used with this method is 70 x 100 mesh-points. With each variable stored in double precision mode (8 bytes), approximately 4 megabytes of storage were required; this is feasible on a large computer, such as an IBM 370/168, with virtual storage capability[6]. Despite the expensive storage penalty, the gaussian elimination method has the great advantage that the solution is obtained directly, so that there are no questions of convergence or choice of iteration parameters to consider.

Polak[7] has greatly alleviated the storage problem for the gaussian elimination technique by storing most of the band matrix on a disc file, and only operating on a small block of the matrix in main storage at any given time.

For very large mesh-sizes, it may be preferable to use some iterative technique, such as successive over-relaxation[8], the alternating-direction implicit method[9], or approximate matrix factorization techniques, such as Stone's method[10] or Dupont, Kendall and Rachford's method[11]. With such techniques, the storage required is directly proportional to the number of mesh-points. The author has experimented with these techniques, and the general conclusion is that they work satisfactorily if suitable iteration parameters are chosen, but in all cases the convergence is slow and no rational basis has been found for choosing the iteration parameters in the case of complicated problems of practical importance. More study is required before the relative advantages of each method can be satisfactorily compared. The storage requirements and number of arithmetic operations for each method is summarized in Table 1.

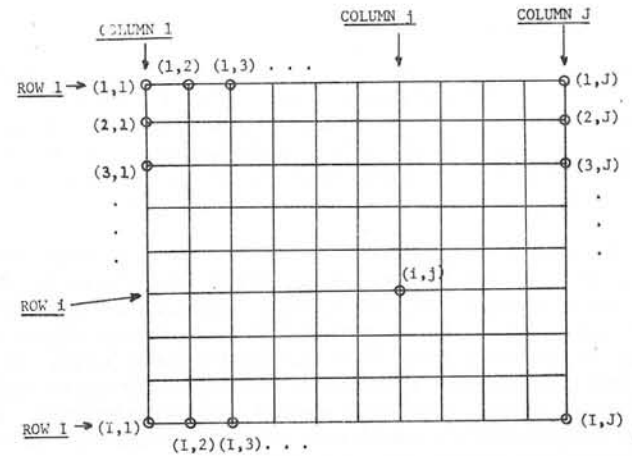

Fig. 9 Numbering of the I x J mesh-points column by column

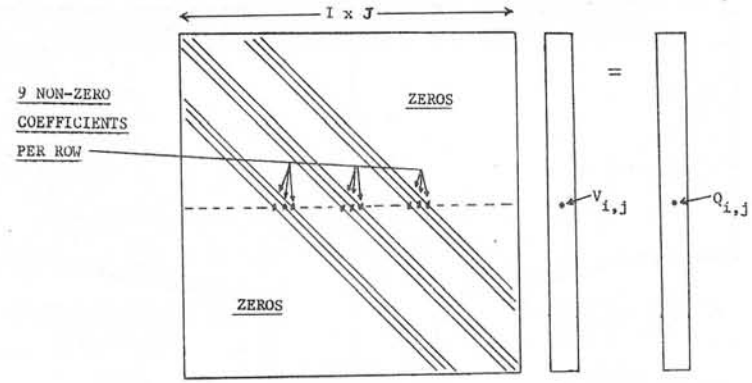

Fig. 10 The finite element equations written in matrix form

Method	No. of variables to be stored	No. of arithmetic operations required
Gaussian elimination	(I+3) IJ	$I^3 J$
Successive over-relaxation	6 IJ	19 IJN
Alternating-direction implicit method	7 IJ	20 IJN
Stone's method	14 IJ	40 IJN
Dupont, Kendall and Rachford's method	11 IJ	34 IJN

Table 1 Storage and time requirements for various methods of solving the equations (IxJ = no. of mesh-points; N = number of iterations)

5. Illustrative examples of computed flux distributions

A useful application of the vector potential formulation has been the analysis of electron lenses with superconducting polepieces[12]. Fig. 11 shows a typical example. The superconducting polepieces exclude magnetic flux (the Meissner effect), thus producing a very concentrated focusing field in the centre of the lens. The Meissner effect is simulated in the program simply by setting the relative permeability of the superconducting polepieces to a very small value, e.g. 10^{-6}.

The vector potential formulation has also proved particularly useful in analysing a type of electron lens called a 'snorkel lens', which was invented by Mulvey[13]. Fig. 12 shows a typical example, together with the computed flux distribution. A beam of electrons approaching the lens from the left is focused by the magnetic field in front of the 'snout' of the snorkel lens. Since the direct influence of the coil windings on the focusing field must be taken into account, such lenses could not be analysed by previous finite difference methods which used a scalar potential formulation. The properties of a range of such snorkel lenses have been calculated by the finite element method, and the results have been published in a recent paper[14].

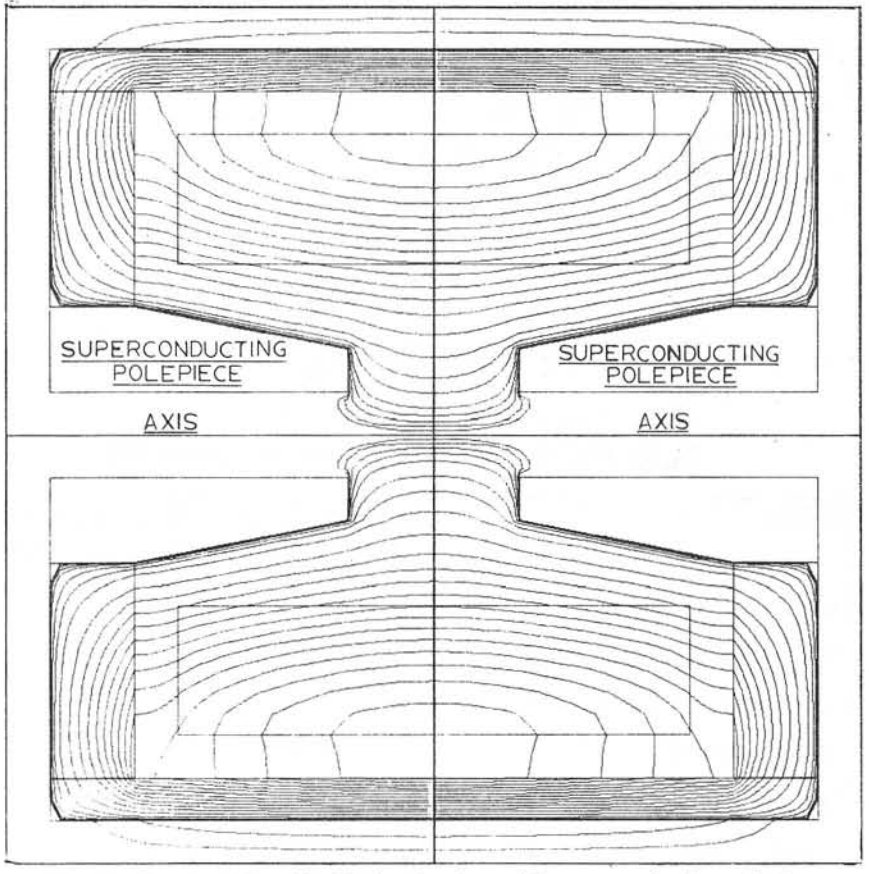

Fig. 11 Computed flux distribution in a lens with superconducting polepieces

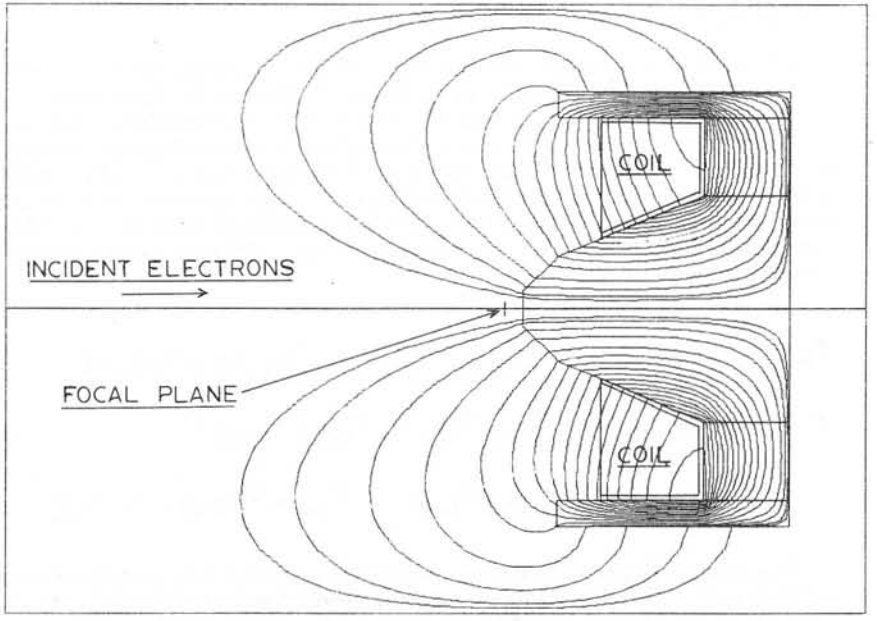

Fig. 12 Computed flux distribution for a snorkel lens

6. Solution of non-linear problems

The functionals (3) and (15) are valid only for linear problems, for which the permeability μ is assumed to be independent of the field strength H. In this section, the method is extended to solve field problems involving magnetic materials with non-linear magnetization characteristics, such as shown in Fig. 13. We define two quantities U_c and U (see Fig. 13) as follows:

$$U_c(H_1) = \int_0^{H_1} B\,dH = \text{complementary energy/unit volume}$$

$$U(B_1) = \int_0^{B_1} H\,dB = \text{stored energy/unit volume} \qquad (24)$$

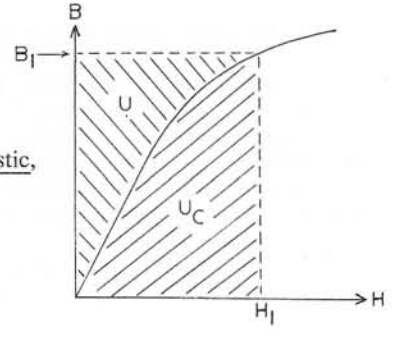

Fig. 13 A non-linear magnetization characteristic, showing the definitions of U and U_c

Then the appropriate functionals to be minimized for non-linear problems are as follows:

For scalar potential problems, the linear functional (3) is replaced by

$$F = \iiint U_c \, dv \tag{25}$$

and for vector potential problems, the linear functional (15) is replaced by

$$F = \iiint (U - \underline{J}.\underline{A}) \, dv \tag{26}$$

(A proof of the validity of these functionals can be found in Ref. 2.) Since the functionals (25) and (26) are non-linear, the resulting finite element equations are also non-linear. These equations have the general form

$$\frac{\partial F}{\partial V_i} = f_i(V_1, V_2, \ldots, V_n) = 0, \qquad i=1,n \tag{27}$$

where F is the value of the functional, V_i is the potential at the i^{th} mesh-point, f_i is a non-linear function of the mesh-point potentials and n is the number of finite element equations. These non-linear equations can be solved iteratively by Newton's method. To do this, an initial approximation to the solution is calculated using a constant permeability. Let this initial approximation be denoted by $[V_i^I]$. A set of residuals $[r_i]$ and a Jacobian matrix $[J_{ij}]$ are then calculated, whose general elements are defined as

$$r_i = f_i(V_1^I, V_2^I, \ldots, V_n^I) \tag{28}$$

$$J_{ij} = \frac{\partial f_i}{\partial V_j}(V_1^I, V_2^I, \ldots, V_n^I) \tag{29}$$

From equation (27), it follows that

$$r_i = \frac{\partial F}{\partial V_i}(V_1^I, V_2^I, \ldots, V_n^I) \tag{30}$$

$$J_{ij} = \frac{\partial^2 F}{\partial V_i \partial V_j}(V_1^I, V_2^I, \ldots, V_n^I) \tag{31}$$

To calculate r_i and J_{ij}, we invoke the fact that if V_i is changed, the resulting change in F is due solely to changes in the contributions ΔF to the functional from the twelve finite elements E_1-E_{12} in the neighbourhood of V_i (see Fig. 3). Thus from (30) and (31) we obtain

$$r_i = \left(\frac{\partial \Delta F}{\partial V_i}\right)_{E_1} + \left(\frac{\partial \Delta F}{\partial V_i}\right)_{E_2} + \ldots + \left(\frac{\partial \Delta F}{\partial V_i}\right)_{E_{12}} \tag{32}$$

$$J_{ij} = \left(\frac{\partial^2 \Delta F}{\partial V_i \partial V_j}\right)_{E_1} + \left(\frac{\partial^2 \Delta F}{\partial V_i \partial V_j}\right)_{E_2} + \ldots + \left(\frac{\partial^2 \Delta F}{\partial V_i \partial V_j}\right)_{E_{12}} \tag{33}$$

r_i and J_{ij} are calculated for each finite element equation using (32) and (33). The changes δV_i to be applied to the mesh-point potentials are then calculated by solving the matrix equation

$$[J_{ij}][\delta V_i] = -[r_i] \tag{34}$$

The matrix $[J_{ij}]$ has the same symmetric banded structure as the finite element coefficients, and so (34) can be solved using any of the methods discussed earlier. Having solved for $[\delta V_i]$, the new approximation to the potentials is given by

$$[V_i^{II}] = [V_i^I] + [\delta V_i] \tag{35}$$

$[V_i^{II}]$ is then used as the starting point for the next iteration. This cycle is repeated until all the residuals are negligibly small. The resulting potential distribution is the solution of the finite element equations (27). As an example, Fig. 14 shows the flux distribution in the lens of Fig. 1 at a very high excitation, computed using a non-linear magnetization characteristic. Comparison with the corresponding linear solution of Fig. 8 shows that the magnetic saturation at high excitations produces non-linear flux leakage in the back bore of the lens.

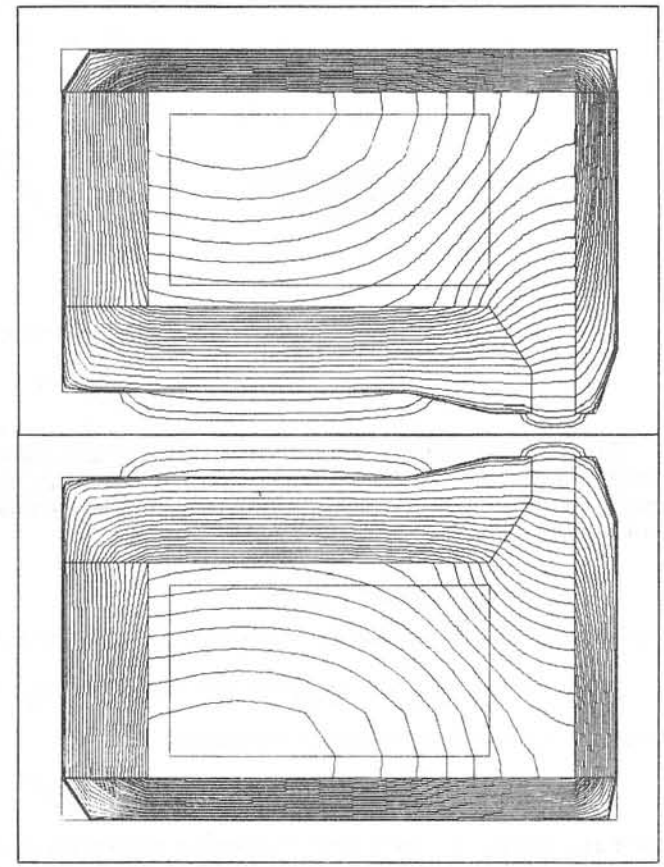

Fig. 14 Computed flux distribution for the lens of Fig. 1 under saturation conditions

7. Solution of problems involving permanent magnet materials

In Section 3, we described how to solve field problems involving magnetic materials with linear magnetization characteristics of the form

$$\underline{B} = \mu \underline{H} \tag{36}$$

where $\underline{B}$ = flux density, $\underline{H}$ = field strength and μ = permeability. In this section, we extend this method to the solution of problems involving permanent magnet materials with magnetization characteristics of the form

$$\underline{B} = \mu (\underline{H} + \underline{H}_c) \tag{37}$$

where $\underline{H}_c$ = 'coercive field strength', which is assumed to be a constant for the material. The type of magnetization characteristic corresponding to (37) is shown in Fig. 15.

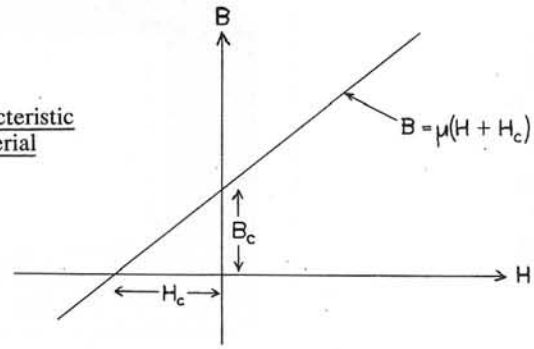

Fig. 15 Magnetization characteristic for a permanent magnet material

For the scalar potential formulation, we proceed in a manner analogous to that described in Section 3.1. The scalar potential V is still defined as in equation (1), but since $\underline{B}$ and $\underline{H}$ are now related by (37) instead of (36), the differential equation (2) must be replaced by

$$\text{div} \left[\mu \left(\underline{\text{grad}}\ V + \underline{H}_c \right) \right] = 0 \tag{38}$$

The functional whose minimization corresponds to the solution of (38) is

$$F = \iiint \tfrac{1}{2} \mu \left(\underline{\text{grad}}\ V + \underline{H}_c \right) \cdot \left(\underline{\text{grad}}\ V + \underline{H}_c \right) dv \tag{39}$$

For rotationally-symmetric systems, (39) becomes

$$F = \iint \tfrac{1}{2} \mu \left[\left(\frac{\partial V}{\partial z} + H_{cz} \right)^2 + \left(\frac{\partial V}{\partial r} + H_{cr} \right)^2 \right] 2\pi r \, dz \, dr \tag{40}$$

where H_{cz} and H_{cr} are the z and r components respectively of the coercive field $\underline{H}_c$. For a triangular finite element, the contribution ΔF to the value of the functional (40) is

$$\Delta F = \mu \pi r_0 a \left\{ \left[\frac{1}{2a} \left(\sum_{i=1}^{3} b_i V_i \right) + H_{zc} \right]^2 + \left[\frac{1}{2a} \left(\sum_{i=1}^{3} c_i V_i \right) + H_{rc} \right]^2 \right\} \tag{41}$$

where r_o, a, b_i and c_i are as defined for equation (5). Differentiating (41) gives

$$\left[\frac{\partial \Delta F}{\partial V_i} \right] = \left[F_{ij} \right] \left[V_i \right] + \left[G_i \right] \tag{42}$$

where

$$\left. \begin{aligned} F_{ij} &= \frac{\mu \pi r_0}{2a} \left(b_i b_j + c_i c_j \right) \\ \text{and} \quad G_i &= \mu \pi r_0 \left(b_i H_{zc} + c_i H_{rc} \right) \end{aligned} \right\} \tag{43}$$

The 3 x 3 matrix F_{ij} and the 3-component vector G_i are calculated using (43) for every finite element. The finite element equations are then set up using F_{ij} and G_i in exactly the same way as described in Section 3.1.

For permanent magnet problems in planar (x,y) coordinates, the expressions for F_{ij} and G_i corresponding to (43) are

$$\left. \begin{aligned} F_{ij} &= \frac{\mu}{4a} \left(b_i b_j + c_i c_j \right) \\ \text{and} \quad G_i &= \frac{\mu}{2} \left(b_i H_{xc} + c_i H_{yc} \right) \end{aligned} \right\} \tag{44}$$

where b_i and c_i are as defined for equation (12), and H_{xc} and H_{yc} are the x and y components of the coercive field $\underline{H}_c$.

For the vector potential formulation for permanent magnet materials, we rewrite (37) in the form

$$\underline{H} = \frac{1}{\mu} \left(\underline{B} - \underline{B}_c \right) \tag{45}$$

where $\underline{B}_c = \mu \underline{H}_c$ is the 'remanent flux density' (see Fig. 15). The vector potential $\underline{A}$ is still defined as in equation (13). However, since $\underline{B}$ and $\underline{H}$ are now related by (45), the differential equation (14) must be replaced by

$$\underline{\text{curl}} \left[\frac{1}{\mu} \left(\underline{\text{curl}}\ \underline{A} - \underline{B}_c \right) \right] = \underline{J} \tag{46}$$

The functional whose minimization corresponds to the solution of (46) is

$$F = \iiint \left[\frac{1}{2\mu} \left(\underline{\text{curl}}\ \underline{A} - \underline{B}_c \right) \cdot \left(\underline{\text{curl}}\ \underline{A} - \underline{B}_c \right) - \underline{J} . \underline{A} \right] dv \tag{47}$$

For rotationally-symmetric systems, (47) becomes

$$F = \iint \left\{ \frac{1}{2\mu} \left[\left(\frac{\partial A_\theta}{\partial z} + B_{cr} \right)^2 + \left(\frac{\partial A_\theta}{\partial r} + \frac{A_\theta}{r} - B_{cz} \right)^2 \right] - J_\theta A_\theta \right\} 2\pi r \, dz \, dr \tag{48}$$

where B_{cz} and B_{cr} are the z and r components of the remanent flux density $\underline{B}_c$. For a triangular finite element, the contribution ΔF to the value of the functional (48) is

$$\Delta F = \frac{\pi r_0 a}{\mu} \left\{ \left[\frac{1}{2a} \left(\sum_{i=1}^{3} b_i A_i \right) + B_{cr} \right]^2 + \left[\frac{1}{2a} \left(\sum_{i=1}^{3} d_i A_i \right) - B_{cz} \right]^2 \right\} - \frac{2}{3} \pi J_\theta r_0 a \left(\sum_{i=1}^{3} A_i \right) \tag{49}$$

where r_o, a, b_i and d_i are as defined for equation (17). Differentiating (49) gives

$$\left[\frac{\partial \Delta F}{\partial A_i} \right] = \left[F_{ij} \right] \left[A_i \right] + \left[G_i \right] \tag{50}$$

where

$$F_{ij} = \frac{\pi r_0}{2\mu a}(b_i b_j + d_i d_j)$$

and

$$G_i = \frac{\pi r_0}{\mu}(b_i B_{cr} - d_i B_{cz}) - \frac{2}{3} J_\theta \pi r_0 a \qquad (51)$$

The expressions (51) then replace the expressions (19) in the generation of the finite element equations.

For problems involving permanent magnet materials in planar (x,y) coordinates, the expressions corresponding to (51) are

$$F_{ij} = \frac{1}{4\mu a}(b_i b_j + c_i c_j)$$

$$G_i = \frac{1}{2\mu}(b_i B_{cy} - c_i B_{cx}) - \frac{1}{3} J_z a \qquad (52)$$

where b_i, c_i and J_z are as defined for equation (22), and B_{cx} and B_{cy} are the x and y components of the remanent flux density $\underline{B}_c$.

A typical application of this technique is shown in Figs. 16 and 17. It is a solution in planar (x,y) coordinates of a magnetic circuit containing an outer soft iron yoke of square cross-section, four tapered permanent magnets oriented so as to produce a quadrupole field, and four tapered soft iron polecaps. This might represent, for example, a permanent magnet quadrupole electron lens, or a permanent magnet four-pole stator for an electric motor. Fig. 16 shows the computed scalar potential distribution and Fig. 17 shows the computed vector potential distribution.

8. Calculation of the fields due to toroidal deflection coils inside rotationally-symmetric electron lenses

The concept of deflecting an electron beam by a toroidal deflection yoke located centrally inside a magnetic lens (Fig. 18) as a means of reducing the aberrations of an electron beam scanning system was first proposed by Pfeiffer[15]. In such systems, the rotationally-symmetric magnetic circuit of the lens has a significant influence on the deflection field. A method which has been devised for analysing such systems[16] will be summarized here. The current loading in the yoke is first expressed as a Fourier series of harmonic components, thus:

$$f(\theta) = (NI)_1 \sin\theta + (NI)_3 \sin 3\theta + (NI)_5 \sin 5\theta + \ldots \qquad (53)$$

where $(NI)_n$ represents the number of ampere-turns in the n^{th} harmonic. Then it can be proved that the field components due to the n^{th} harmonic of the current loading have the general form:

$$H_z = \frac{\partial\Phi}{\partial z}\cos n\theta \qquad H_r = \frac{\partial\Phi}{\partial r}\cos n\theta$$

$$H_\theta = -\frac{1}{n\mu}\left[\frac{\partial}{\partial r}\left(\mu r\frac{\partial\Phi}{\partial r}\right) + \frac{\partial}{\partial z}\left(\mu r\frac{\partial\Phi}{\partial z}\right)\right]\sin n\theta \qquad (54)$$

where Φ is a scalar function of z and r, and μ is the permeability at any point. $\Phi(z,r)$ satisfies the following differential equation:

$$\frac{\partial}{\partial r}\left(\mu r\frac{\partial\Phi}{\partial r}\right) - \frac{n^2\mu\Phi}{r} + \frac{\partial}{\partial z}\left(\mu r\frac{\partial\Phi}{\partial z}\right) = -\frac{n\mu\,(NI)_n\, g(r,z)}{r} \qquad (55)$$

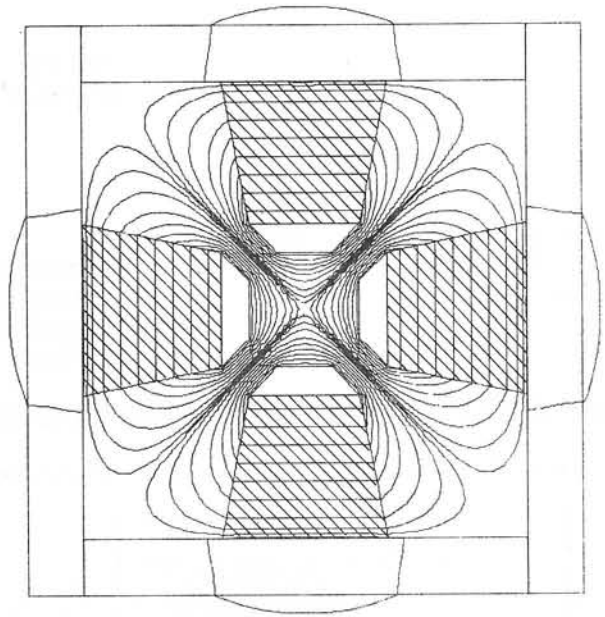

Fig. 16 Computed scalar potential distribution in a permanent magnet quadrupole lens (the permanent magnets are indicated by cross-hatching)

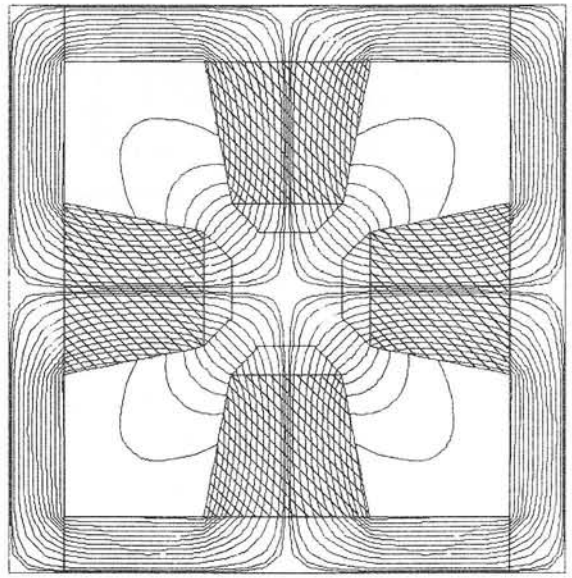

Fig. 17 Computed vector potential distribution in a permanent magnet quadrupole lens (the permanent magnets are indicated by cross-hatching)

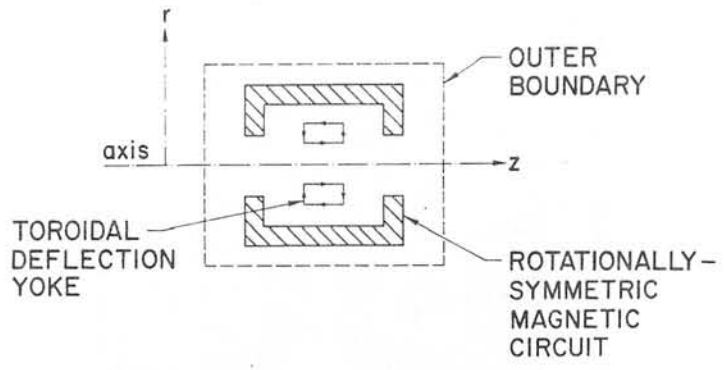

Fig. 18 A toroidal deflection coil inside a rotationally-symmetric magnetic electron lens

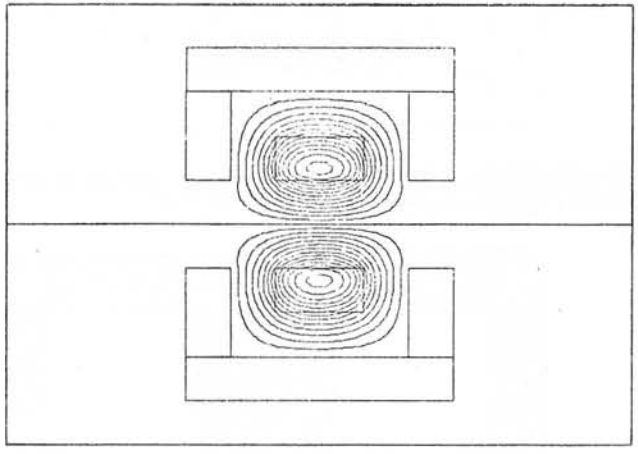

Fig. 19 Computed distribution of $\Phi(z,r)$ for a toroidal-coil-in-lens problem

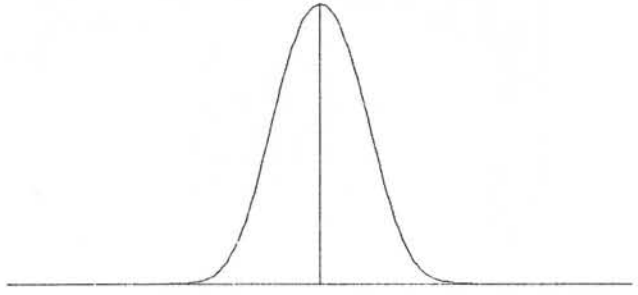

Fig. 20 Computed deflection field at the axis for the system shown in Fig. 19

where $g(z,r) = 1$ inside the cross-section of the deflection coil and $g(z,r) = 0$ outside the coil, and $\Phi(z,r) = 0$ on the outer boundary and also on the axis. The functional whose minimization corresponds to the solution of (55) is

$$F = \iint \left\{ \mu r \left[\left(\frac{\partial \Phi}{\partial r}\right)^2 + \left(\frac{n\Phi}{r}\right)^2 + \left(\frac{\partial \Phi}{\partial z}\right)^2 \right] - \frac{2n\mu\,(NI)_n\,\Phi g}{r} \right\} dr\,dz \qquad (56)$$

The functional (56) can then be minimized numerically using the finite element method to give the function $\Phi(z,r)$, and then the field components can be calculated using (54).

As an example, Fig. 19 shows the computed distribution of $\Phi(z,r)$ for the first harmonic ($n=1$) of a typical toroidal-yoke-in-lens problem, and Fig. 20 shows the corresponding computed transverse deflection field at the axis.

9. Conclusions

The principles of the finite element method and some of its applications in solving boundary-value static magnetic field problems have been described. The method can handle complicated magnetic circuit geometries, finite permeabilities, magnetic saturation effects and the properties of permanent magnet materials.

References

1. O.C. Zienkiewicz and Y.K. Cheung (1965), The Engineer, 220, 507-510.
2. E. Munro (1972), 'Computer-Aided Design Methods in Electron Optics', Ph.D. Thesis, Cambridge.
3. E. Munro (1973), 'Computer-Aided Design of Electron Lenses by the Finite Element Method', in 'Image Processing and Computer-Aided Design in Electron Optics', P.W. Hawkes, ed., Academic Press, London, 284-323.
4. E. Munro (1975), 'A Set of Computer Programs for Calculating the Properties of Electron Lenses', Cambridge University Engineering Department Report CUED/B-ELECT/TR 45 (1975).
5. IBM Publication GH20-0205-4, 'System/360 Scientific Subroutine Package' (1970), 137-142.
6. IBM Publication GC20-1800-1, 'IBM Virtual Machine Facility/370 Introduction' (1973), 10-11.
7. S.J. Polak (1974), Private Communication.
8. S.P. Frankel (1950), Math. Tables Aids Comput., 4, 65-75.
9. D.W. Peaceman and H.H. Rachford (1955), J. Soc. Indust. Appl. Math., 3, 28-41.
10. H.L. Stone (1968), SIAM J. Numer. Anal., 5, 530-558.
11. T. Dupont, R.P. Kendall and H.H. Rachford (1968), SIAM J. Numer. Anal., 5, 559-573.
12. I. Dietrich, H. Pfisterer and R. Weyl (1969), Z. angew. Phys., 28, 35-39.
13. T. Mulvey (1972), British Patent Application 40888/72, 'Improvements in or relating to magnetic lenses'.
14. E. Munro and O.C. Wells (1976), 'Some Comments on the Design of Magnetic Lenses for the Scanning Electron Microscope', Proc. 9th Annual Scanning Electron Microscope Symposium, IIT Research Institute, Chicago.
15. H.C. Pfeiffer (1974), Proc. 8th International Congress on Electron Microscopy, Canberra, Australia, 56-57.
16. E. Munro (1975), J. Vac. Sci. Technol., 12, 1146-1150.

Discussion following paper:

(Ohiwa, Cambridge) In the field of electron optics, the quantities required are the magnetic field and its derivatives with respect to Z rather than magnetic potential. Therefore, it is necessary to carry out numerical differentiation to obtain these quantities; losing sifnificance in doing so. How do you cope with this? Could you give me some idea of the accuracy of the calculated field in terms of the number of mesh points, required storage, and computer time?

(Munro, IBM, USA) I have carried out the numerical differentiation with respect to Z by using a cubic spline technique which ensures continuity of the first and second derivatives. For most applications, I generally have used a mesh of about 25 x 50 points, which generally enables the axial field distribution to be calculated to an accuracy of about 1%. For this mesh size, the storage required on an IBM 370/168 is approximately 250 kilobytes with all the variables stored in double precision mode, and the solution time is of the order of a few seconds. The maximum mesh size I have handled is about 80 x 100 points. In any given application, the accuracy of the results can be estimated by first solving the problem with a relatively coarse mesh, and then repeating the calculation with twice as many mesh points in each direction. In the latter case, the result will be about four times more accurate than in the former case, and this enables an estimate of the upper bound of the errors to be obtained.

(Diserens, Rutherford) When you calculate the fields from potentials do you apply any smoothing at this stage? How many points do you use in each field calculation?

(Munro) I have generally calculated the field distribution along the axis using a cubic spline technique which ensures continuity of the first and second derivatives. In this technique, I have not used any initial smoothing of the potential values at the mesh points. In the case of field components at internal mesh points, I have calculated the field components at the centroid of each quadrilateral region using the computed potential values at the four corners of the quadrilateral.

(Trowbridge, Rutherford) The calculation of magnetic lens aberrations requires the integral of the field to be calculated through the fringe field of the magnet - how did you ensure that the remote boundary in your computer model was sufficiently far away?

(Munro) No special techniques were used, however the position of the external boundary was varied to ensure that this effect could be made negligible.

(Jacobs, CERL) Dr Munro illustrates some interesting comparisons of various direct and iterative solution procedures. For the nine diagonal coefficient matrix with its special symmetric sparsity layout, the Strongly Implicit Procedure (Stone's method) would generally use a factorization into lower and upper triangular factors each with only five non-zero diagonals. Alternatively the factorization of the standard five diagonal matrix would be used in conjunction with a "modified" iterative scheme, where in essence, the other diagonal coefficients are relegated to the right hand side of the equation to add to the excitation source term. The important attribute of SIP is the marked lack of importance of accurate parameter selection. However, I believe the very special form of the matrix enables Gaussian elimination to be used with only very limited fill in. The method would eliminate the elements of the 1st column using the first row, then the elements of the (I + 1)st column using the (I + 1)st row; etc. The total number of operations is then proportional to IJ.

(Munro) I appreciate your comments on alternative implementations of Stone's method as it applies to nine-point equations, and I intend to try out both your suggestions, namely using triangular matrices with fine non-zero diagonals instead of four, and relegating the potentials at the corner nodes to the right-hand side of the equation. As regards your comments about the ability to perform Gaussian elimination of my banded matrix equation in a number of operations proportional to IJ, I do not think that this is possible, but I would very much like to hear a detailed algorithm for your proposed scheme, since if what you suggest is in fact possible, it would certainly represent a significant breakthrough in the direct solution of banded sparse matrix equations.

(Fox, Oxford) (1) I would like to ask if you used any special ordering in the equations for Gauss elimination. This is important, and for example the "optimal" ordering of F A George involves much less computer time and storage. (2) Following up Dr Jacob's remarks on the Stone method, it appears that the parameters are less important than the B matrix in LU = A + B, where L and U are your triangular matrices. It seems to be desirable, in current language, for A + B to have second-order comparability

(Fox, continued) with A, and I am not sure whether or not you looked into this. (3) You also mentioned a method by Dupont et al. They virtually put a parameter on the right-hand side of the equations, and Stone puts one on the left. I have heard of recent work in America in which somebody is trying to get the best of both worlds by putting parameters on both sides. I haven't seen the paper, but I could give you a reference.

(Munro) (1) I simply ordered the equations by numbering the mesh points sequentially column by column. I had believed that this ordering would result in the most efficient Gaussian elimination, because of its topological simplicity. However, if the method of George is more efficient, I will be very interested to incorporate it in my programs. (2) Up till now, my investigations of Stone's method have been somewhat limited and I am not sure whether the B matrix I have chosen ensures second-order comparability of (A + B) with A. I intend to investigate this as a result of your comment. (3) The method of Dupont et al does in fact allow for the possibility of variable iteration parameters on both sides of the equation. I will be interested to receive the reference on the recent paper published on this subject.

NUMERICAL MODELS OF THREE-DIMENSIONAL END WINDING ARRAYS

by

C.J. Carpenter* and D.H. Locke**

Abstract

The three-dimensional magnetic fields in machine end regions can be most conveniently solved in differential terms by computing a magnetic scalar potential. The complexity of the end winding shapes makes it difficult to translate the three components of the current density vector into suitable field sources in a simple and systematic way. For many purposes it is convenient to treat the field in travelling wave terms, and it is necessary to extract the fundamental and harmonic components of the sources. The paper examines the general problem of translating complex current distributions into equivalent sources for a numerical scalar potential computation. The method is applied to a turbogenerator end region and illustrated by field solutions.

Principle symbols

B	magnetic flux density	S	mesh coefficient matrix
F	network branch m.m.f	T	electric vector potential (eqn. 1)
H	magnetic field strength	w	separation direction
J	current density	∇	differential vector operator
m	harmonic number	μ	permeability
R_e	real part of complx quantity	Ω	magnetic scalar potential
r,θ,z	cylindrical coordinates	n,θ,t	local coordinate system (Fig. 1)
$\tilde{T}$	indicates phasor quantity	$\underline{T}$	indicates vector quantity

T', T'' T functions defined by equations 2 and 16 respectively

* Electrical Engineering Department, Imperial College, London, SW7 2BT

** C.A. Parsons and Co. Ltd., Heaton Works, Newcastle upon Tyne, NE6 2YL.

1 INTRODUCTION

The magnetic fields in the end regions of electrical machines are generated by winding end-connections of complex shape, and these give a three-dimensional flux pattern whose computation is of increasing importance in the design of turbogenerators and other large machines. The field in the vicinity of the windings can be predicted satisfactorily by numerical integration using current elements and simple image sources to model the nearest iron surface, and this method has long been used to obtain winding inductances and conductor forces. It is much less well suited, however, to the problem of predicting the fields and losses in the stator core, and in other materials exposed to the leakage field. Differential methods are then more conventient, preferably formulated in terms of a magnetic scalar potential[1,2], since this reduces the magneto-static problem to the calculation of a single function with simple and well-behaved boundary and interface conditions. Eddy currents are easily incorporated[2,3].

The use of a scalar function transfers attention from the problem of making three-dimensional field calculations to that of describing their sources. The current density vector $\underline{J}$ within the end windings has three components defined by the machine geometry. Each component varies in a complex manner, but not independently of the others. The extraction and translation of this data into a form suitable for a numerical model is tedious and prone to error. The sources can be expressed in terms of travelling waves, thus reducing the field computation from three dimensions to two, but this requires the extraction of the $\underline{J}$ components as a function of position in the end winding cross-section. The analysis can be carried out independently for many different sections through the winding, but this is often unnecessary.

It is shown in this paper that the practical problems of providing an economic description of the current density vector in an arbitrary winding configuration, and of translating these sources into a scalar potential computer program, are closely related. Although the principles of the field transformation from a solenoidal to a scalar potential form can be stated very simply in terms of a separation of field components[1,2], its practical application in a general purpose program, particularly one

with irregular elements, requires an operational and systematic formulation of the various ways in which the sources can be generated. The very flexibility of the method, and the range of choice in applying it, can be an embarrassment in preparing algorithms, and one objective is to combine this flexibility with the statement of precise computational instructions.

For present purposes it is assumed that the currents are all specified. The principles discussed are directly applicable to three-dimensional eddy current problems, and some aspects are examined in a companion paper[4]. The wider implications, however, require a more extensive treatment than can be given here.

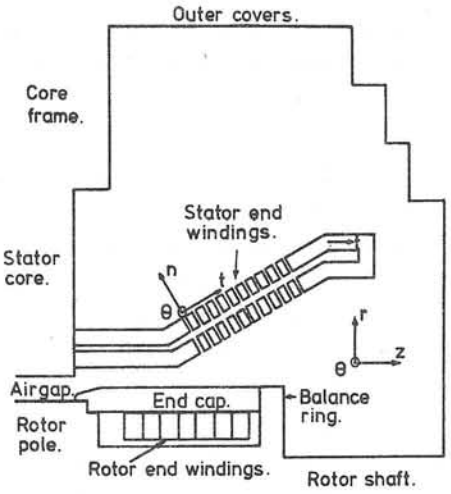

Figure 1. Turbogenerator end region.

2 CURRENT DISTRIBUTION AND DESCRIBING FUNCTION.

2.1 Machine geometry

The cross-sectional geometry of the machine, (Figure 1), including both stator and rotor end windings, may be assumed to be invariant with angular displacement θ, but the current distributions within the two widings vary with θ in different ways. The stator end winding is formed in a two-layer configuration in which all the coils usually, although not invariably, have the same shape. The rotor coils are confined to a single layer and form a concentric end winding, as illustrated in the developed view shown in Figure 2. The m.m.f. distribution produced by both windings varies approximately sinusoidally with θ in the airgap, but the variation in the end region depends on the actual coil shapes, and the separation of the two layers of the stator end winding. The problem is to translate this distribution of current carrying conductors into a numerical form in terms of some arbitrary distribution of nodes forming a rectangular, triangular or some other irregular two or three dimensional mesh.

2.2 Current describing function

The simplest describing function, $\underline{T}$, is one defined by:

$$\text{curl } \underline{T} = \underline{J} \qquad \ldots\ldots(1)$$

where $\underline{J}$ is the current density vector. $\underline{T}$ is an electric vector potential, or analogue of the magnetic vector potential $\underline{A}$ (defined by curl $\underline{A} = \underline{B}$), and, just as $\underline{A}$ provides a convenient flow function description in two-dimensional transverse magnetic field problems so the vector $\underline{T}$ can be used in a similar way by limiting it to a direction n normal to the plane in which the current flows. That is, everywhere in the end windings a local coordinate direction $\underline{n}$ is specified at right-angles to $\underline{J}$ and to the θ axis, and $\underline{T}$ is limited to the $\underline{n}$ direction (Figure 1). This condition, namely:

$$\underline{T}' \times \underline{n} = 0 \qquad \ldots\ldots(2)$$

defines a particular $\underline{T}$ function consisting of a single quantity T' from which the three components of $\underline{J}$ can be derived. For example, J_t and J_θ are given by:

$$J_t = -\frac{1}{r}\frac{\partial T'}{\partial \theta} \qquad \ldots\ldots(3a)$$

$$J_\theta = \frac{\partial T'}{\partial t} \qquad \ldots\ldots(3b)$$

with the coordinate sequence n, θ, t (Figure 1), and the components of the $\underline{J}$ vector derived in this way necessarily satisfy the current continuity condition:

$$div\ \underline{J} = 0$$

T' is constant outside the windings and here is assigned zero value.

The requirement imposed by equation 2 is possible since the divergence of $\underline{T}'$ is otherwise undefined. Taking the divergence of $\underline{T}' \times \underline{n}$:

$$\nabla . (\underline{T}' \times \underline{n}) = \underline{n} . (\nabla \times \underline{T}') - \underline{T}' . (\nabla \times \underline{n}) = 0$$

from equation 2. $\underline{T}' . (\nabla \times \underline{n})$ is zero, so that equation 1 and 2 together require that:

$$\underline{n} . \underline{J} = 0 \qquad \ldots\ldots(4)$$

a condition which $\underline{n}$ has been chosen to satisfy. The divergence of $\underline{T}'$ is zero in the conductor interior where the winding is flat, but is non-zero at any bends in the winding and also at the winding surface.

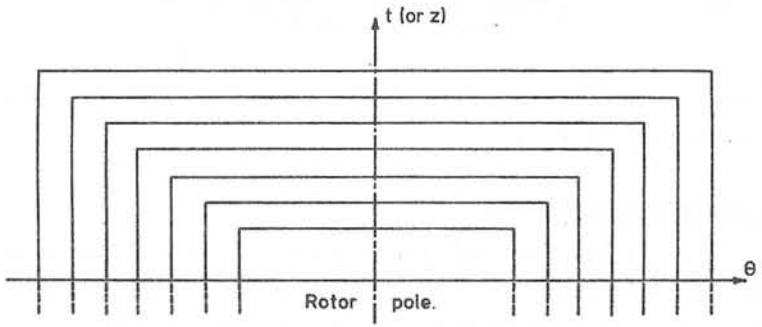

Figure 2. Rotor end winding drawing showing idealised conductor shapes and T'(θ,z) map. Contours of equal T' plotted for equal increments of T'.

2.3 Rotor end winding

A drawing of the rotor coil ends (Figure 2) can be interpreted as a map of lines of constant T' as a function of t (or z) and θ. This map is valid for all n (or r) values in the winding, and T' does not vary in time in a reference system moving with the rotor. In practice the variation of $T'(\theta, z)$ in both the θ and z directions is discontinuous in slope because of the coil insulation, but T' is everywhere defined.

A harmonic analysis of m.m.f. wave in the θ direction for different values of z gives the magnitude T'_m or the m th space harmonic:

$$T'_m(r, \theta, z) = R_e\left\{\hat{T}'_m(z) \exp(-jm\theta)\right\} \qquad m = 1, 3, 5 \quad \ldots\ldots(5)$$

where $R_e\{--\}$ denotes the real part. The harmonics give travelling waves when transformed to a stationary reference system. Because of the symmetry of the winding, the phase angle is not a function of z, and there are no even harmonics. The first seven terms of $T'_m(z)$, together with the major

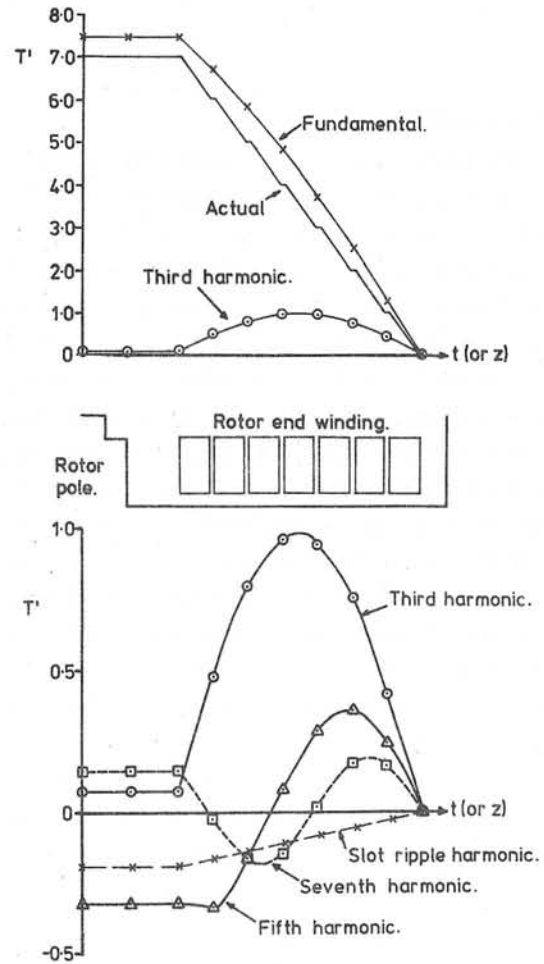

Figure 3. Rotor end winding harmonic analysis. T'(t) function and harmonics, $T'_m(t)$.

ripple harmonic (of slot frequency), are plotted in Figure 3 for a typical rotor end winding. The two current density components, J_z (or J_r) and J_θ are given by equation 3 and this shows that, at a given radius r, J_z is proportional to T' but phase shifted;

$$(\tilde{J}_z)_m = -jm\tilde{T}'_m/r \qquad .....(6)$$

where $\tilde{J}$ denotes a phasor. The T' and J_z diagrams are thus nearly interchangeable.

2.4 Stator end winding

The stator end winding is of more complex shape, but the n, t coordinate grid can be chosen arbitrarily since it provides only an intermediate step in the process of expressing T' as a function of r and z. The constant T' contours pass across the winding cross-section along the copper-insulation boundaries in the regions where J_θ is non-zero. This is in the sloping section (Figure 1) where the directions of the T' contours are defined by a rectangular n, t grid in which T' is independent of n. In other parts of the winding T' is constant. The $T'(t)$ values can be inserted from a knowledge of the $T'(\theta)$ function in the airgap (calculated from the airgap current distribution, using equation 3a), together with a diagram of the end winding coil shapes drawn in a typical θ, t surface (Figure 4). As in Figure 2, the coil shapes define the lines of constant T' in Figure 4, but the stator currents pulsate sinusoidally in time and the T' values are instantaneous when viewed from a stationary reference point. In general the actual coil shapes should be inserted in Figure 4, but a linearised winding outline such as that illustrated is sufficient for most purposes.

If the coils all have the same shape, so also have the constant T' contours, and $T'(t)$ varies only in phase. That is, the typical term of the Fourier series is now:

$$\tilde{T}'_m(r, \theta, z) = \hat{T}'_m \exp j\left(\phi_m(t) - m\theta\right) \qquad .....(7)$$

in which the magnitude $\hat{T}'_m$ is not a function of t, and is given by the Fourier coefficients computed in the airgap. The lines of constant phase ϕ are given by the coil shapes, $\theta(t)$, so that these shapes define $\phi_m(t)$. The function is approximately piece-wise linear with few segments as

Sinusoidally distributed winding currents.

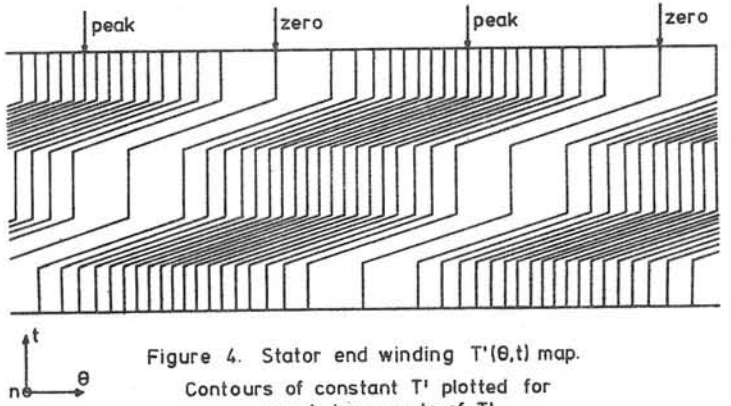

Figure 4. Stator end winding T'(θ,t) map. Contours of constant T' plotted for equal increments of T'.

indicated in Figure 4. Used in association with the n, t grid, it gives T'_m in terms of r and z.

3 SCALAR POTENTIAL SOURCES

One of the roles of the electric vector potential $\underline{T}$ is that of a current describing function for end widings of large cross-section. It extends to these the concept of m.m.f. distribution which is conventionally associated with current sheets, or with windings in air-gaps. T' is essentially the m.m.f. per unit thickness of the winding. But it also provides directly the transformation from the solenoidal field to a scalar potential equivalent. As the field $\underline{H}$ produced by the windings is given by:

$$curl\ \underline{H} = \underline{J} \qquad .....(8)$$

it follows from equation 1 that, for all T functions including T':

$$\underline{H} = \underline{T} - grad\ \Omega \qquad .....(9)$$

and the problem posed numerically is that of computing Ω. Since:

$$div\ \underline{B} = 0 \qquad .....(10)$$

the equation to be solved is:

$$\nabla.\left(\mu(\underline{T} - \nabla\Omega)\right) = 0 \qquad ....(11a)$$

Commonly T is non-zero only inside windings of non-magnetic material, which reduces equation 11a to:

$$\nabla^2\Omega = \nabla.\underline{T} \qquad ....(11b)$$

so that the equivalent magnetic poles, which are the sources of Ω, are generated by the divergence of $\underline{T}$.

One way to compute Ω is to find the equivalent pole distribution from $\underline{T}$, and model this in the usual way as a Poisson-type field source in finite element, or finite difference, terms. But this gives dome difficultly in formulation, and is liable to lead to unnecessary numerical errors, as $div\ \underline{T}$ is a discontinuous function confined largely to the surfaces of the windings, whereas the Poisson-type source function is usually assumed to be continuous over the elements in which it is non-zero.

An approach in terms of branch quantities provides a different method of deriving the node equations and a further insight into the nature and accuracy of the Ω model. It shows that, in two-dimensional problems in which a first-order finite element, or finite difference description is used, the accuracy is identical to that of a magnetic vector potential calculation on a network of similar size; more specifically, one which is the dual of that chosen for the Ω solution[5]. Since T can be regarded as a magnetic field component:

$$\int \underline{T} \cdot \underline{dl} = F_b \qquad .....(12)$$

is an m.m.f. which can be evaluated for each mesh branch b. It follows from equation 1 that the sum of the F_b quantities acting around any mesh is equal to the current enclosed, which is the current associated with the corresponding node in the dual network. Hence the branch flow quantities in the Ω model are the same as the corresponding branch potential differences in its dual, or magnetic vector potential equivalent[6] (provided that the problem is two-dimensional so that a simple dual can be derived).

Where F_b is zero, the network models the second term in equation 9 in the usual way and we obtain, either by finite element of finite difference methods, a set of nodal equations:

$$\{S\}\{\Omega\} = 0$$

in which the off-diagonal terms of the coefficient matrix $\{S\}$ represent the branch "conductance" values of the network[5], so that the equation for node p can be written

$$\sum_k S_{pk}(\Omega_p - \Omega_k) = 0$$

In regions where F_b is not zero, the effect of the additional m.m.fs. is to change the branch quantities, giving:

$$\sum_k S_{pk}(\Omega_p - \Omega_k) + \sum_k S_{pk}F_{pk} = 0 \qquad .....(13)$$

as the discreet form of equation 11. Calculating the sources of Ω requires the integration of T' along all the element edges, or lines joining adjacent nodes.

When using rectangular meshes, it is often inconvenient or impractical to choose them in such a way that the winding surfaces intersect the branches only at the network nodes. The branch-source method is then both the simplest and the most accurate way of deriving the source constant in the node equations. The result expresses the very simple requirement that, to define a scalar potential function, the current linkages with the network meshes must be replaced by F_b sources chosen so that their algebraic sum around every mesh is equal to the current linkage which is replaced. T' is one of any number of T functions defining a set of branch sources which will meet this condition. A general rule for defining the sources is to imagine that the current carrying conductors are separated from the network by tearing. As the current is withdrawn, we place in each intersected branch, an m.m.f. source F_b equal in magnitude to the current intersecting it. These sources are the network equivalent of dipoles, and a set of dipoles (of dipole moment T') defined in this way constitutes a magnetic shell equivalent of the winding[1,6]. When the windings are replaced by current sheets, F represents the magnitude of the potential discontinuity across a current sheet (a quantity which has previously[2] been denoted $\Delta\Omega$; however this notation is unsatisfactory when the current is spread out in a winding of finite thickness).

4 SOLUTION OF TURBOGENERATOR END REGION FIELD

Fundamental travelling wave solutions have been computed in cylindrical coordinates by the methods described in Sections 2 and 3. Equation 11 becomes:

$$\frac{1}{r}\frac{\partial}{\partial r}\left[\mu r\left(\frac{\partial \tilde{\Omega}}{\partial r} - \tilde{T}'_r\right)\right] + \frac{\partial}{\partial z}\left[\mu\left(\frac{\partial \tilde{\Omega}}{\partial z} - \tilde{T}'_z\right)\right] = \mu\frac{m^2}{r^2}\tilde{\Omega} \qquad .....(14)$$

since the sinusoidal variation of Ω with θ demands no variation in μ in this direction. The travelling-wave term on the right-hand side of

equation 14 can be treated as a source term in the usual way, and gives network branches to ground. The remainder can be expressed numerically in the manner described for equation 11.

The r, z plane mesh used for these solutions was square, with a node spacing equal to one half of the machine airgap length. Eddy current effects[4] have been omitted and all boundaries are assumed to be infinitely permeable except for the rotor end cap, which is non-magnetic (the effects of saturation in a magnetic and cap have been studied separately in a three-dimensional mesh). When the machine is on load the amplitudes, and relative angular positions, of the stator and rotor m.m.fs. vary with changing load, but by ignoring saturation the effect of each winding can be studied separately and the two load solutions combined linearly after appropriate scaling and angular displacement. The rotor end winding field is required in only one r, z plane since this winding generates a monophase flux pattern (equation 5), but the stator end winding field has both real and imaginary parts (equation 7). These three basic solutions are stored and combined as needed to give the field under any given operating conditions. Radial and axial flux densities are obtained directly from equation 9, whilst in the circumferential direction the flux density is given by:

$$B_\theta = j\mu\frac{\tilde{\Omega}}{r} \qquad \ldots\ldots(15)$$

Flux density components are commonly required for comparison with measurements, but since all three componetns are complex (requiring six field plots in all) there are difficulties in displaying them diagrammatically).

Figure 5 shows the Ω equipotentials plotted in the plane of peak winding m.m.f. (acting in the airgap) under short circuit conditions, when the two windings act nearly in opposition. The flux density maps which are reproduced in Figure 6 give the magnitudes of the three flux density phasors when the machine is operating at rated load with rated terminal voltage. These diagrams show contours of equal flux density, plotted without regard to phase angle. Comparisons of flux density calculations such as these with measurements will be reported elsewhere.

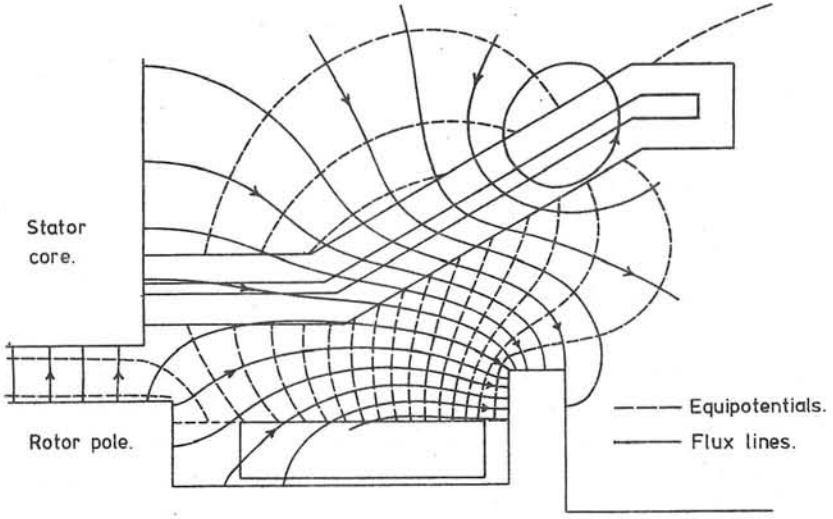

Figure 5. Short circuit rated current. End field in plane of maximum winding m.m.f.

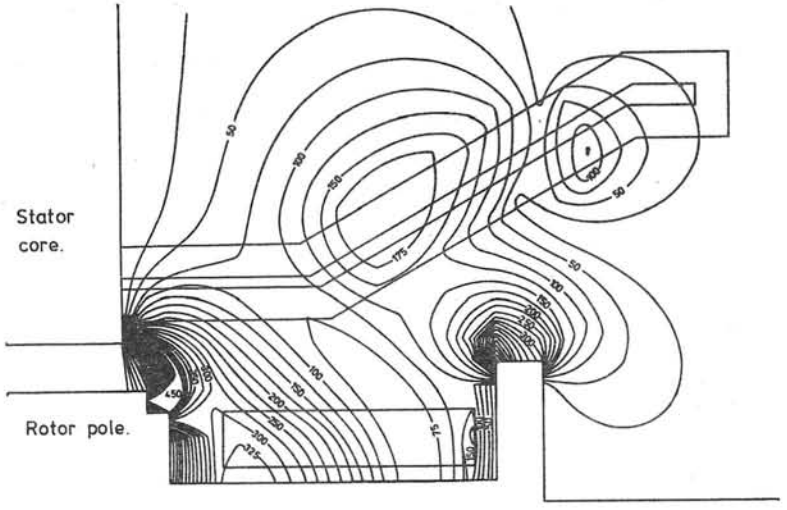

Figure 6a. Rated power 0·95p.f. lag. Peak radial flux density, $\hat{B}_r$.

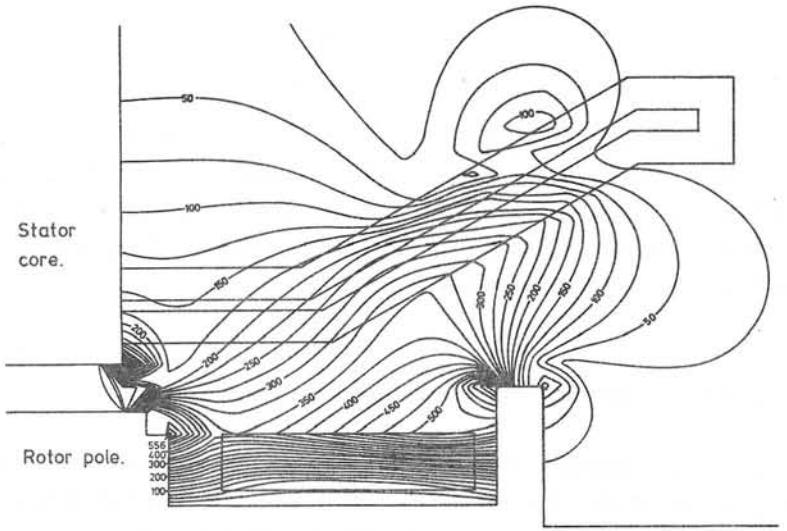

Figure 6b. Rated power 0·95 p.f. lag. Peak axial flux density, $\hat{B}_z$.

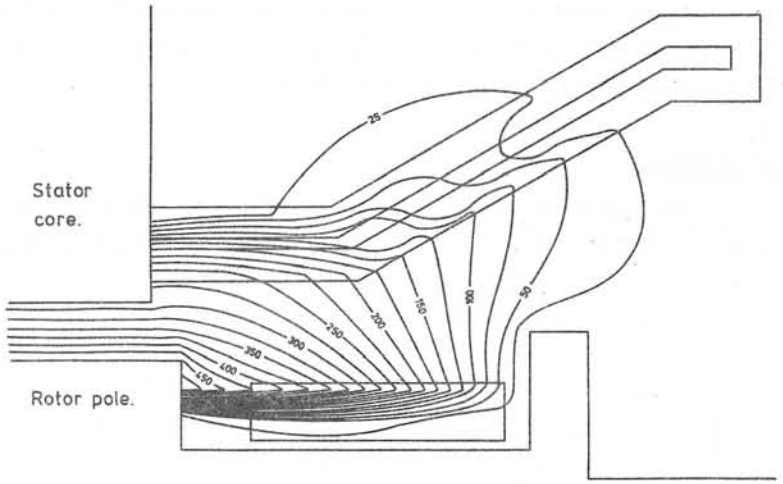

Figure 6c. Rated power 0·95 p.f. lag. Peak circumferential flux density, $\hat{B}_\theta$.

5 ALTERNATIVE SEPARATION METHODS

The $\underline{T}'$ vector has only one component in the local coordinate system, but its direction changes with position in the stator end winding. This complicates the computation of F, and the combination of $\underline{T}$ and *grad* Ω within the elements when $\underline{H}$ is required, particularly when using a triangular instead of a rectangular mesh. There are then some advantages in separating the two roles for $\underline{T}'$ using one $\underline{T}'$ as a current describing function and another, $\underline{T}''$, to provide input data for the field calculation. Various possibilities are currently being explored. By withdrawing the end winding current in a direction orientated relative to the r, z instead of the local n, t coordinates, $\underline{T}''$ can be given a constant direction. The current may, for example, be withdrawn in the $-z$ direction towards the stator. Alternatively it can be withdrawn in the $-r$ direction towards the axis, and then in the $-z$ direction through the airgap, giving some advantages in accuracy[1] since $\underline{T}''$ approximates to the required $\underline{H}$ field in the airgap. There are also various advantages in reducing the winding to an equivalent current sheet by first withdrawing the current inwards parallel to the $\underline{n}$, instead of the $\underline{t}$, direction in Figure 1. This replaces the distributed current by a simple scalar potential discontinuity, together with additional sources whose effect is small, so that the accuracy with which they have to be specified is much reduced. The current sheet approximation provides a convenient idealisation of the winding in several respects, and by carrying the withdrawal in the $\underline{n}$ direction further, the two layers can be reduced to a single current sheet as the major field source, together with additional sources whose effect is relatively localised.

These possibilities require a more general method of general method of generating $\underline{T}$ than that defined by equation 2. This is the only simple and convenient way of generating a describing function, but for other purposes the condition imposed by equation 4 is too restrictive. Because of the freedom of choice in the divergence of $\underline{T}$, any number of different functions can be defined to satisfy equation 1. The magnetic shell principle offers useful guidance, but it is not easily converted into an algorithm for constructing the scalar potential sources. The simplest way of providing for a more general orientation of the $\underline{T}$ vector is to define a direction $\underline{\omega}$

in which all the currents are withdrawn, using the tearing principle stated in section 3. The direction $\underline{w}$ can be aligned parallel to one coordinate axis; for example, choosing $\underline{w}$ in the z or θ direction generates the same $\underline{T}'$ function as before. One consequence of equation 2 is that $\underline{T}'$ can be obtained by withdrawal in any direction within the surface defined by the $\underline{n}$ vector. This property we now relinquish.

The withdrawal concept shows that there can be no component of $\underline{T}''$ in the withdrawal direction, as no network branch orientated in this direction is intersected or "torn" by any current. That is, having chosen the direction $\underline{w}$, we define $\underline{T}''$ so that:

$$\underline{T}'' \cdot \underline{w} = 0 \qquad \text{.....(16)}$$

This, coupled with equation 1, is both a possible and a sufficient definition of a set of branch sources (from equation 12) equivalent to the current linkages which they replace. Two consequences of the replacement of equation 2 by equation 16 is that $\underline{J}$ can have any arbitrary direction relative to $\underline{w}$, and $\underline{T}$ now has two components, whereas it was previously restricted to one in the local coordinate system. The modified definition is particularly important in three-dimensional eddy current problems in which the direction of the $\underline{J}$ vector is, in general, undefined, but here the treatment is restricted to magnostatic aspects.

From equations 1 and 16, it follows that:

$$\underline{J} \times \underline{w} = (\underline{w}.\nabla)\ \underline{T}'' \qquad \text{.....(17)}$$

and the T''_x and T''_y components can be constructed by dividing equation 17 by the magnitude of w and integrating:

$$T''_1 - T''_2 = \int_1^2 \underline{J} \times \underline{dw} \qquad \text{.....(18)}$$

Where J is zero T'' is constant, and is assigned zero value in the region 'upstream' of the winding, that is, before the displacement vector $\underline{w}$ intersects it: $\underline{T}''$, and hence F, are then completely defined. Equations 16, 17 and 18 express symbolically the possibility of defining any vector $\underline{T}$ to satisfy equation 1 by suppressing one component, leaving the other two defined independently of each other by one-dimensional integration. If $\underline{w}$ is chosen so that it is parallel to one of the coordinate axes (although not necessarily the same one throughout the withdrawal process), the F quantities are obtained directly in the branches of a rectangular network.

For example, if $\underline{w}$ is in the $-z$ direction in Figure 1, equation 3 is then replaced by:

$$J_r = \frac{\partial T''_\theta}{\partial z} \qquad \text{.....(19a)}$$

$$J_\theta = -\frac{\partial T''_r}{\partial z} \qquad \text{.....(19b)}$$

(from equation 17). The $\underline{T}''$ function for the rotor winding is the same as $\underline{T}'$, since J_r is zero, and when using a two-dimensional travelling wave description, $\underline{T}''$ due to the stator winding consists of only one component, T''_r, in the plane in which the solution is computed. T''_r depends on J_θ, which in turn, is given by equations 3 and 7:

$$J_\theta = -j\left(\frac{\partial \phi m}{\partial t}\right) T'_m \qquad \text{.....(20)}$$

where the $\phi(t)$ curve is the coil shape shown in Figure 5.

Only one component, T''_r is needed to compute F. The other, T''_θ, affects the $\underline{H}$ vector in the peripheral direction, and hence the travelling wave term on the right-hand side of equation 14. This becomes:

$$\mu \frac{1}{r} \frac{\partial H_\theta}{\partial \theta} = \mu\left(\frac{m^2 \tilde{}}{r^2}\Omega - j \frac{m\tilde{}}{r} T''_\theta\right) \qquad \text{.....(21)}$$

so that, in network terms, T''_θ is equivalent to generators connected in series with the branches to ground. The withdrawal in the $-z$ direction would normally be terminated at the stator lamination surface leaving a current sheet which is represented by a simple scalar potential discontinuity whose magnitude is everwhere specified.

6 CONCLUSIONS

It has been shown that the problem of describing a three-dimensional current distribution economically is closely allied to that of translating the field problem into magnetic scalar potential terms. The three components of the current density vector can be replaced by a single current describing function, T', which corresponds to a (scalar) current flow function when T' is appropriately defined. This extends to bulky windings the simple potential-jump concept associated with current sheets, and it assists the production of a numerical description of the current distribution from the actual winding geometry. The sources of the magnetic scalar potential, Ω, can be derived directly from T', but it is

sometimes more convenient to use for this purpose a less restrictive way of generating the $\underline{T}$ vector. Both methods can be stated concisely in vector terms, and hence translated into algorithms.

The method has been used to compute turbogenerator end fields, and is illustrated in these terms, but is applicable to all magnostatic problems in which the current distribution is specified. The replacement of T' by alternative T'' functions is, however, particularly appropriate to three dimensional eddy current problems in solids, where the direction of the current density vector is not specified, as distinct from laminated materials where $\underline{T}'$ is at right angles to the plane of the laminations[4].

Acknowledgements

The authors wish to thank both the Science Research Council and C.A. Parsons and Co. Ltd. for financial support, and the latter for permission to publish the computed results.

References

1 CARPENTER, C.J. Numerical solution of magnetic fields in the vicinity of current carrying conductors. Proc. IEE, 1967, 114 (11), pp1793-1800

2 CARPENTER, C.J. Computation of magnetic fields and eddy currents. 5th International Conference on Magnetic Technology. Rome, April 1975, pp 147-158

3 CARPENTER, C.J. and DJUROVIC, M. Three-dimensional numerical solution of eddy currents in thin plates, Proc. IEE, 1975, 122 (6) pp681-688

4 CARPENTER, C.J. and WYATT, E.A. Efficiency of numerical techniques for computing eddy currents in two and three dimensions. Compumag 1976.

5 CARPENTER, C.J. Finite element network models and their application to eddy-current problems. Proc. IEE, 1975, 122 (4), pp 455-462

6 CARPENTER, C.J. and RATTI, U. Comparison of scalar and vector potentials for the numerical solution of magnetic fields. L'Energia Elettrica, 1974, No. 4, pp 200-212.

Discussion following paper:

(Trowbridge, Rutherford Lab) Does the computer program based on your T junction method take into account iron?

Has the technique any advantages over other methods ie Biot Savart Law interpolation in the special case of conductor fields ?

(Carpenter, Imperial College) Yes, the results described include the effect of unsaturated iron surfaces, and we have made separate studies of saturation effects in highly saturated parts. Here a full three-dimensional mesh is necessary in place of the travelling-wave approximation, which depends on linearity. Usually T is zero inside the iron, but the only effect of removing this restriction is to add the T vector in equation 9 when calculating B from the B/H curve.

When there is no iron present then I think there is usually no advantage in any other method over the simple Biot-Savart (or Neumann) type of integration.

Occasionally a T vector can be easily constructed which is a close approximation to the required field, and the grad Ω term then represents a small correction. This has obvious advantages. Examples are given in reference 1 of the paper.

(Polak, NV Philips) Is there any comparison between calculated and measured data which gives an idea of the accuracy?

(Carpenter) Yes, we have made comparisons and we hope to publish these shortly. It is very difficult to summarise them in any brief statement because the results depend on the position at which B is measured, the component measured, and on the magnitude and phase angle of this load on the machine.

AN ANALYTICAL METHOD OF CALCULATING MAGNETIC FIELDS IN SLOTTED REGIONS

by

T.G. Phemister

C.A. Parsons and Co. Ltd., Newcastle upon Tyne

The magnetic field in slotted regions is defined by Fourier series with unknown coefficients. Continuity of the field at the top of the slots is used to set up infinite matrices relating the unknown coefficients to the boundary conditions. The infinite matrices are inverted analytically to give an explicit solution for the coefficients. The method is rapid and its theoretical accuracy is within the uncertainties in the manufacture of large generators.

1 Introduction

The origin of the work to be described was a requirement to calculate the three-dimensional magnetic field near the ends of large generators in more detail than existing computer programs permitted. The geometry of a generator is complicated, with its slotted structure and cooling ducts, and a program based on the straightforward application of finite difference or finite element methods demands too much computer time to be an ordinary design tool; the band-width of the resulting equations is uncomfortably large. If, however, a rapid method can be found for calculating the field in the slots and air-gap together, then an efficient scheme of iteration can be set up between the magnetic and non-magnetic regions.

The method to be described was designed for an iterative scheme in which, with normal flux density as the boundary condition for the magnetic regions, finite element methods were used to calculate surface magnetising forces for the next stage of iteration. The problem was, therefore, to calculate rapidly the magnetic field in the slots and air-gap when the surface magnetising forces were known on all boundaries. The method adopted was based on Fourier analysis. Systems of equations were set up for the Fourier coefficients and the matrix of left-hand sides was inverted analytically. The method is explained by applying it to the simplest problem in which its value is apparent; the problems in extending it to more complicated geometries are discussed afterwards.

2 Specification of problem

The simplest problem to which the method has been applied was a calculation of the two-dimensional magnetic field in the centre of a generator. To avoid obscuring the algebra by inessential detail, the following simplifications will be made.

(a) The generator is a perfect two-pole machine.

(b) The rotor is cylindrical and the currents in its windings are represented by a distribution of magnetic scalar potential on its surface.

(c) The fields are two-dimensional.

(d) The stator slots are rectangular.

(e) Curvature will be neglected at the top of the slots and a rectangular system of coordinates in each slot will be assumed compatible with polar coordinates in the air-gap.

(f) The air-gap length is greater than the width of the stator slots, the width of the tooth tips is not much less than the width of the slots, and the slots are deep with respect to their width.

None of these simplifications except (f) is necessary for the sucess of the method. A related method has been developed for geometries in which (f) does not hold.

The problem can be summarised as follows. A two-dimensional magnetic scalar potential is specified on the surface of a cylindrical rotor, on the stator tooth tips, and on all sides of the stator slots. Currents are specified in the stator slots. The magnetic field is to be calculated in the slots and air-gap.

3 Coordinate system

Polar coordinates r, θ will be used in the air-gap. The surface of the rotor is at $r = t$ and the stator tooth tips lie on $r = s$.

The centre of the stator slot numbered n lies on $\theta = c_n$ and the top

corners are at $r = s$, $\theta = c_n \pm d_n$. Rectangular coordinates x_n down the slot and y_n across the slot will be used. Thus, at the boundary between the slot and the air-gap, $x_n = 0$ and $y_n = s(\theta - c_n + d_n)$. The width of the slot is $w_n = 2sd_n$. There are N slots in a half circumference.

4 Schematic solution

The first step in solving the problem is to impose an arbitrary distribution of scalar potential on the boundaries between the slots and air-gap; the simplest is a linear variation between the corners of each slot. Unique solutions for the magnetic field can then be found in each slot separately and in the air gap separately. Since these regions are of a simple shape, the solutions can be obtained expeditiously by traditional methods. If these solutions are written as

$$\underline{H} = \underline{H}_n = \left(H_{xn},\ H_{yn}\right) \text{ in slot } n,$$

$$\text{and } \underline{H} = \underline{H}_g = \left(H_{gr},\ H_{g\theta}\right) \text{ in the air-gap,}$$

then the complete solution can be expressed as:

$$\underline{H} = \underline{H}_n - \nabla\Phi_n \text{ in slot } n$$

$$\text{and } \underline{H} = \underline{H}_g - \nabla\Phi_g \text{ in the air gap,}$$

$$\text{where } \Phi_n = \sum_{i=1,3}^{\infty} a_{ni} \sin\left(\frac{i\pi y_n}{w_n}\right) \exp\left(\frac{-i\pi x_n}{w_n}\right) + \sum_{j=2,4}^{\infty} b_{nj} \sin\left(\frac{j\pi y_n}{w_n}\right) \exp\left(\frac{-j\pi x_n}{w_n}\right)$$

$$\text{and } \Phi_g = \sum_{k=1}^{\infty} \frac{\left(\frac{r}{t}\right)^K - \left(\frac{t}{r}\right)^K}{\left(\frac{s}{t}\right)^K - \left(\frac{t}{s}\right)^K} \times \left[\sum_{n=1}^{N} \frac{2d_n}{\pi} \cos K\left(\theta - c_n\right) \sum_{i=1,3}^{\infty} a_{ni} Q_{nik} + \sum_{n=1}^{N} \frac{2d_n}{\pi} \sin K\left(\theta - c_n\right) \sum_{j=2,4}^{\infty} b_{nj} R_{njk}\right],$$

in which

$$K = 2k - 1,$$

$$Q_{nik} = \frac{-i\pi \cos K d_n}{d_n^2\left[K^2 - \frac{i^2\pi^2}{4d_n^2}\right]},$$

$$R_{njk} = \frac{j\pi \sin K d_n}{d_n^2\left[K^2 - \frac{j^2\pi^2}{4d_n^2}\right]}.$$

The limit is to be understood when the denominator is zero. The odd and even coefficients are treated separately because the terms to which they are attached behave differently.

A solution of this form satisfies all the boundary conditions except continuity for H_r between each slot and the air-gap. Fourier analysis of this remaining condition gives the equations required for calculating the unknown coefficients a_{ni} and b_{nj}. It will be found that $a_{ni} = O\left(i^{-5/3}\right)$ and $b_{nj} = O\left(j^{-5/3}\right)$. Using this, it is straightforward to prove that the order of summation in the series can be changed.

Up to this point, the method has been similar to work previously published, for example, by Midgley and Smethurst (1963) and Jones et al. (1969). As far as the writer is aware, however, what follows is new.

5 Explicit equations for the unknown coefficients

Equating the normal flux density across the top of each slot by Fourier analysis gives a set of equations which can be expressed in matrix form as:

$$\begin{bmatrix} E_{11} & F_{11} & E_{12} & F_{12} & \cdots & \cdots \\ G_{11} & H_{11} & G_{12} & H_{12} & \cdots & \cdots \\ E_{21} & F_{21} & E_{22} & F_{22} & \cdots & \cdots \\ G_{21} & H_{21} & G_{22} & H_{22} & \cdots & \cdots \\ \cdots & \cdots & \cdots & \cdots & \cdots & \cdots \\ \cdots & \cdots & \cdots & \cdots & \cdots & \cdots \end{bmatrix} \begin{bmatrix} \{a_{1p}\} \\ \{b_{1q}\} \\ \{a_{2p}\} \\ \{b_{2q}\} \\ \cdots \\ \cdots \end{bmatrix} = \begin{bmatrix} \{s_{1i}\} \\ \{t_{1j}\} \\ \{s_{2i}\} \\ \{t_{2j}\} \\ \cdots \\ \cdots \end{bmatrix}$$

where E_{nm}, F_{nm}, G_{nm}, H_{nm} ($n = 1, N$ and $m = 1, N$) are infinite square matrices, $\{a_{mp}\}$ and $\{b_{mq}\}$ are infinite column matrices of the unknown coefficients, and $\{s_{ni}\}$ and $\{t_{nj}\}$ are infinite column matrices which come from Fourier analysis of $H_{xn} - H_{gr}$ at the top of slot n.

If E_{nmip} is the i, p element of E_{nm}, then

$$E_{nmip} = \tfrac{1}{2}\delta_{nm}\,\delta_{ip} + \frac{2d_n d_m}{i\pi^2}\sum_{k=1}^{\infty} K\left(1 + P_k\right)\cos K\left(c_n - c_m\right) Q_{nik}\, Q_{mpk},$$

$$\text{where } P_k = \frac{2}{\left(\frac{s}{t}\right)^{2K} - 1}.$$

By expressing $Q_{nik}\, Q_{mpk}$ as three partial fractions, and by using their properties as Fourier coefficients, it may be shown that

$$\frac{2d_n d_m}{i\pi^2}\sum_{k=1}^{\infty} K\cos K\left(c_n - c_m\right) Q_{nik}\, Q_{mpk} =$$

$$\frac{-p}{2d_n d_m\left(\frac{i\pi}{2d_n}+\frac{p\pi}{2d_m}\right)}\sum_{k=1}^{\infty}\frac{\left[\begin{array}{l}\cos K\left(c_n - c_m + d_n + d_m\right) + \cos K\left(c_n - c_m - d_n - d_m\right) \\ + \cos K\left(c_n - c_m - d_n + d_m\right) + \cos K\left(c_n - c_m + d_n - d_m\right)\end{array}\right]}{\left(K + \frac{i\pi}{2d_n}\right)\left(K + \frac{p\pi}{2d_m}\right)}.$$

Uniform convergence ensures that this remains true in all cases, except $n = m$ and $i = p$ in which $\frac{1}{2}$ is added.

Phemister (1972) has shown that

$$\sum_{k=1}^{\infty}\frac{\cos Kx}{K + a} = \tfrac{1}{2}g(ax) - \tfrac{1}{2}g(a\pi - ax) + \frac{S(x)}{a^2} + 0\left(\frac{1}{a^4}\right),\quad 0 < x < \pi,$$

where $g(x)$ is the second generating function of the sine and cosine integrals and $|S(x)| < 0{\cdot}04$. Now $g(x) = \frac{1}{x^2} + 0\left(\frac{1}{x^4}\right)$ and so, if $n \neq m$ and the teeth are not greatly narrower than the slots, this part of E_{nmip} can be approximated as $\frac{constant}{i^2 p}$. The series with P_k, which is rapidly convergent, can also be so approximated, even when $n = m$. Thus the submatrices E_{nm} can be written approximately as

$$E_{nm} = \left\{\frac{e_{nm}}{i^2 p}\right\},\ n \neq m.$$

It can be shown similarly that, approximately,

$$F_{nm} = \left\{\frac{f_{nm}}{i^2 q}\right\} \text{ for all } n, m,$$

$$G_{nm} = \left\{\frac{g_{nm}}{j^2 p}\right\} \text{ for all } n, m,$$

$$\text{and } H_{nm} = \left\{\frac{h_{nm}}{j^2 q}\right\},\ n \neq m.$$

In the present application, F_{nm} and G_{nm} are, by symmetry, null matrices whenever $n = m$ but in general they can be expressed approximately in the forms given above even when $n = m$.

The submatrices E_{nn} and H_{nn} must be studied in more detail. With the extra $\frac{1}{2}$ that has been mentioned

$$E_{nnip} = \delta_{ip} - \frac{2p}{\pi d_n(i + p)}\sum_{k=1}^{\infty}\frac{1 + \cos 2Kd_n}{\left(K + \frac{i\pi}{2d_n}\right)\left(K + \frac{p\pi}{2d_n}\right)}$$

$$+ \frac{2p}{d_n^2}\sum_{k=1}^{\infty}\frac{KP_k\cos^2 Kd_n}{\left(K^2 - \frac{i^2\pi^2}{4d_n^2}\right)\left(K^2 - \frac{p^2\pi^2}{4d_n^2}\right)}.$$

Since P_k tends exponentially to zero and

$$\frac{\pi}{2d_n} >> 1,$$

the second series can be approximated by

$$\frac{1}{i^2 p} \times \frac{32 d_n^2}{\pi^4} \sum_{k=1}^{\infty} KP_k \cos^2 Kd_n.$$

The first series gives

$$\frac{-2p\left[ln\left(\frac{i}{p}\right) + g(p\pi) - g(i\pi)\right]}{\pi^2(i^2 - p^2)} + \frac{constant}{i^2 p} + negligible\ terms.$$

The formula $\lim_{x \to 0}\left(g(ix) - g(px)\right) = -ln\left(\frac{i}{p}\right)$ has been used in obtaining this and $g(x)$ has been expressed asymptotically when its argument is large.

Thus, if A is the matrix whose i, p element is

$$\delta_{ip} - \frac{2p}{\pi^2(i^2 - p^2)}\left[ln\left(\frac{i}{p}\right) + g(p\pi) - g(i\pi)\right],$$

the submatrix E_{nn} can be approximated as

$$A + \left(\frac{e_{nn}}{i^2 p}\right).$$

It may be shown that, if B is the matrix whose j, q element is

$$\delta_{jq} - \frac{2q}{\pi^2\left(j^2 - q^2\right)}\left[ln\left(\frac{j}{q}\right) - g(q\pi) + g(j\pi)\right],$$

the submatrix H_{nn} can be approximated as

$$B + \left(\frac{h_{nn}}{j^2 q}\right).$$

The matrices A and B are independent of the geometry and only the constants e_{nm} etc. are required to give an explicit formulation of the equations for the unknown coefficients. There is only a finite number of these coefficients and not many of them are needed, since they tend rapidly to zero as $|n - m|$ increases. The simplest way to calculate them is to set

$$e_{nm} = E_{nm11},$$
$$f_{nm} = 2F_{nm12},$$
$$g_{nm} = 4G_{nm21},$$
$$h_{nm} = 8H_{nm22},$$

with suitable modifications for e_{nn} and h_{nn}. By using asymptotic forms, this can be done rapidly.

The equations can then be expressed explicitly as

$$\left[diag\ \ (A,B,A,B,\ .....) + \begin{bmatrix} \left(\frac{e_{nm}}{i^2 p}\right) & \left(\frac{f_{nm}}{i^2 q}\right) \\ \left(\frac{g_{nm}}{j^2 p}\right) & \left(\frac{h_{nm}}{j^2 q}\right) \end{bmatrix}\right] \begin{bmatrix} \left(a_{mp}\right) \\ \left(b_{mq}\right) \end{bmatrix} = \begin{bmatrix} \left(\varepsilon_{ni}\right) \\ \left(t_{nj}\right) \end{bmatrix}.$$

6 Solution of the equations for the unknown coefficients

It has been shown by Phemister (1972) that an asymptotic form for the i, p element of A^{-1} when i and p are large is

$$\delta_{ip} + \frac{2p\left[\left(\frac{i}{p}\right)^{\frac{1}{3}} - \left(\frac{p}{i}\right)^{\frac{1}{3}}\right]}{\pi\sqrt{3}\ (i^2 - p^2)},$$

that B^{-1} has the same asymptotic form, and that A^{-1} and B^{-1} can be approximated by the matrices C and D, where the i, p element of C is

$$\delta_{ip} + \frac{2p\left[\left(\frac{i}{p}\right)^{\frac{1}{3}} - \left(\frac{p}{i}\right)^{\frac{1}{3}}\right]}{\pi\sqrt{3}\ (i^2 - p^2)} + \frac{0{\cdot}014718\ p}{(ip)^{\frac{5}{3}}} - \frac{0{\cdot}001893\ p}{(ip)^{\frac{7}{3}}}$$

and the j, q element of D is

$$\delta_{jq} + \frac{2q\left[\left(\frac{j}{q}\right)^{\frac{1}{3}} - \left(\frac{q}{j}\right)^{\frac{1}{3}}\right]}{\pi\sqrt{3}\ (j^2 - q^2)} - \frac{0{\cdot}032705\ q}{(jq)^{\frac{5}{3}}} + \frac{0{\cdot}014855\ q}{(jq)^{\frac{7}{3}}} .$$

The numerical constants were obtained by a least squares minimisation of the elements of $CA - I$ and $DB - I$, where I is the unit matrix.

The equations can be solved by expanding the reciprocal of the square matrix on the left hand side, to give, as the first two terms of the binomial series,

$$\begin{bmatrix} \{a_{ni}\} \\ \{b_{nj}\} \end{bmatrix} = \left\{ M - M \begin{bmatrix} \left\{\frac{e_{nm}}{i^2 p}\right\} & \left\{\frac{f_{nm}}{i^2 q}\right\} \\ \left\{\frac{g_{nm}}{j^2 p}\right\} & \left\{\frac{h_{nm}}{j^2 q}\right\} \end{bmatrix} M \right\} \begin{bmatrix} \{s_{mp}\} \\ \{t_{mq}\} \end{bmatrix}$$

where $M = diag\ (C,D,C,D,\ .....)$. Thus the unknown coefficients have been expressed explicitly in terms of known quantities.

The matrices A and B are those that arise in the problem of a single infinitely deep slot in a semi-infinite slab. The binomial expansion is the equivalent of solving first for each slot separately as if the stator bore were the only boundary and no other slots existed and afterwards correcting for the effect of other slots and other boundaries.

7 Types of a_{ni}, etc.

The solution that has been found is still expressed in terms of infinite matrices and would be difficult to handle as it stands. Phemister (1972) proposed, and Drumm (1973) confirmed, that the column matrices $\{s_{mp}\}$ and $\{t_{mq}\}$ could each be expressed to the required accuracy as the linear combination of four different types:

$$\left\{\frac{\ln p}{p^2}\right\},\ \left\{\frac{1}{p^2}\right\},\ \{\delta_{1p}\},\ \left\{\frac{1}{p^4}\right\},\ \text{and}\ \left\{\frac{\ln q}{q^2}\right\},\ \left\{\frac{1}{q^2}\right\},\ \{\delta_{2q}\},\ \left\{\frac{1}{q^4}\right\}.$$

It was established further that the products $C\{s_{mp}\}$ and $D\{t_{mq}\}$ could each be expressed to the required accuracy as a linear combination of four different types of column matrix:

$$\{i^{-\frac{5}{3}}\},\ \{i^{-\frac{7}{3}}\},\ \{\delta_{1i}\},\ \{\delta_{3i}\}\ \text{and}\ \{j^{-\frac{5}{3}}\},\ \{j^{-\frac{7}{3}}\},\ \{\delta_{2j}\},\ \{\delta_{4j}\}.$$

It follows that the products $C\left\{\frac{e_{nm}}{i^2 p}\right\}$ $C\{s_{mp}\}$ etc. can each be expressed as a linear combination of the same four odd or four even types of column matrix. Hence $\{a_{ni}\}$ and $\{b_{nj}\}$ can also be so expressed.

If all the algebra is performed on these types of infinite column matrix, then $\{s_{mp}\}$ and $\{t_{mq}\}$ can each be represented by a column matrix of only four elements, which are the parameters of the different types of infinite column matrix arising from $H_{xn} - H_{gx}$. Similarly, $\{a_{ni}\}$ and $\{b_{nj}\}$ can each be represented by a column matrix of four elements. C and D can be represented by 4×4 matrices whose elements are known absolutely and are independent of the problem. Similarly, any of the four products $C\left\{\frac{f_{nm}}{i^2 q}\right\}D$ etc. can be represented by the product of the appropriate scalar, f_{nm} etc., with one of four 4×4 matrices whose elements are known absolutely.

Thus, if $\{a^*_{nu}\}$ and $\{b^*_{nu}\}$, $u = 1,4$, $n = 1,N$, denote the four-element column matrices of parameters of the different types of $\{a_{ni}\}$ and $\{b_{nj}\}$, respectively, and if $\{s^*_{mv}\}$ and $\{t^*_{mv}\}$, $u = 1,4$, $m = 1,N$, denote the four-element column matrices of parameters of the different types of $\{s_{mp}\}$ and $\{t_{mq}\}$, respectively, then the solution can be expressed in the simple form:

$$\{a^*_{nu}\} = C^*\{s^*_{nv}\} - \sum_{m=1}^{N} e_{nm}\, E^*\{s^*_{mv}\} + f_{nm}\, F^*\{t^*_{mv}\},$$

$$\{b^*_{nu}\} = D^*\{t^*_{nv}\} - \sum_{m=1}^{N} g_{nm}\, G^*\{s^*_{mv}\} + h_{nm}\, H^*\{t^*_{mv}\},$$

where C^*, D^*, E^*, F^*, G^*, H^* are 4×4 matrices whose elements are known absolutely.

8 Calculation of the magnetic field

In the method which has been described, there are five steps in calculating the magnetic field.

(1) The constants e_{nm}, f_{nm}, g_{nm}, h_{nm} must be calculated. Since they depend only on the geometry, the calculation need be performed only once.

(2) For particular boundary conditions the fields $\underline{H}_n$ and $\underline{H}_g$ or the related vector potential must be calculated where required. The parameters, $\left\{s^*_{mv}\right\}$ and $\left\{t^*_{mv}\right\}$, of the types of $\left\{s_{mp}\right\}$ and $\left\{t_{mq}\right\}$ must also be found.

(3) The parameters, $\left\{a^*_{nu}\right\}$ and $\left\{b^*_{nu}\right\}$, of the types of $\left\{a_{ni}\right\}$ and $\left\{b_{nj}\right\}$ can then be calculated by, at worst, 80 N^2 multiplications in total. In practice only about 300 N multiplications are required because most interactions between slots are negligible.

(4) The magnetic field or the related vector potential must be calculated where required from $\left\{a^*_{nu}\right\}$ and $\left\{b^*_{nu}\right\}$.

(5) Local corrections must be made by numerical methods to allow for irregularities in the slots, such as wedge notches.

Step (4) needs further description. Within each slot, series such as

$$\sum_{i=1,3}^{\infty} \frac{z^i}{i^{\frac{2}{3}}}$$

appear, where z is complex and $|z| < 1$. On the stator bore series such as

$$\sum_{i=1,3}^{\infty} \frac{g(ix)}{i^{\frac{2}{3}}}$$

appear. Phemister (1972) and Drumm (1973) have established simple expressions for the functions defined by these series.

The time taken on an IBM 370/145 computer when the method was applied to a generator stator with 21 slots in a half circumference, was 2½ seconds (±0.02) for the initial calculations of Step (1) and 17 seconds (±0.12) for the calculations of Steps (2) to (5) inclusive.

9 Assessment of errors

The error in using C and D for A^{-1} and B^{-1} can be determined by calculating the elements of $CA - I$ and $DB - I$. The largest element of $CA - I$ is 0·0001816 in the 3, 3 position. Since the column matrix $\left\{s_{mp}\right\}$ which it multiplies behaves like $\frac{1}{p^2}$ for small values of p and is

$$O\left\{\frac{\ln p}{p^2}\right\}$$

for large p, this is roughly equivalent to an element one ninth as great in column 1. The greatest element in column 1 is 0·0000208 in row 5. The largest element in $DB - I$ is 0·0000475 in the 4, 6 position and the largest element in column 2 is 0·0000097 in row 6. The error in using C and D for A^{-1} and B^{-1} is, accordingly, much less than 10^{-4}.

The errors in replacing the matrices E_{nm} etc by $\left\{\frac{e_{nm}}{i^2 p}\right\}$ etc. and in stopping at the second term of the binomial series were investigated extensively by Drumm (1973). Within the range of air-gap lengths, slot widths, and tooth widths foreseeable on large generators, it was found that the worst error would be $2{\cdot}5 \times 10^{-4}$ and that the probable error was about 10^{-4}. The error in expressing the infinite column matrices as linear combinations of four types was similar.

The error in ignoring curvature at the top of the slots was difficult to estimate but was less than 10^{-3}. If this error proved troublesome in applications to smaller machines, it could be absorbed either by the local correction for the wedge notch or by a method discussed in Section 10.

There is an inconsistency in using expressions for the field which assume singularities of order $\frac{1}{3}$ at the corners of the teeth (corresponding to an infinitely permeable right-angle) when the boundary conditions arise from saturation and the angle is not exactly a right-angle. Taking the correct angle would make the order of the singularity about 0·328 and would certainly reduce it by less than 2%. The magnetic field tends to be rearranged to reduce saturation near the corners and magnetising forces of the order of 10^5 A/m exist only very near a corner. For right-angles of constant permeability the order of the singularity remains greater

than 0·3 in absolute value for relative permeabilities as low as 21. Moreover, the singularity cannot be allowed for exactly in the finite element solution in the teeth, since its nature is undefined. It seems almost certain for these reasons, though it has not been verified, that the error caused by the inconsistency is local to the corners and smaller than the error of the finite element solutions in the teeth.

To sum up, the errors in the method are almost certainly less than those in the accompanying finite element solutions and less than the uncertainties in the manufacture of the machines. For example, the rotor can sag by more than 3 mm between the main bearings in the longest generators.

10 Extensions of the method

Including the slots in the rotor is straightforward but the interactions between stator and rotor slots change as the rotor turns. There is no limitation to two-pole machines or to a cylindrical geometry.

Three-dimensional fields which vary exponentially or sinusoidally - most can be expressed as a linear combination of such fields - can be calculated in the same way by altering the constants e_{nm} etc.

Non-rectangular slots or compensation for curvature at the top of the slot can be treated either by local corrections or by incorporating a numerical solution within the slot in the general solution and so altering the constants e_{nm} etc.

For slots that are not deep or are insufficiently separated, a related method can be employed which has proved successful for calculating fields in the end regions of generators. This will be published as early as possible.

The method cannot be applied without further development to slots in which the wedge notches are so close to the corners that effectively they change the nature of the singularities.

11 Comparisons with measurements

Calculations by computer programs based on the method have been compared regularly with measurements on large generators. They have mostly agreed within experimental accuracy. For one machine, however, they differed by as much as 15% in the 5th harmonic on short circuit, a discrepancy which has never been explained.

12 Conclusion

A rapid and accurate method has been developed for calculating magnetic fields in slotted regions.

Acknowledgements

The work formed part of a collaborative programme of research by C.A. Parsons and Company Limited and the Central Electricity Generating Board. The writer wishes to thank C.A. Parsons for permission to publish, Mr. J.G. Steel of the CEGB for his encouragement, and Dr. M.J. Drumm, who prepared the method for the digital computer.

References

DRUMM, M.J. 1973, C.A. Parsons Working Paper.

JONES, D.E., MULLINEUX, N., REED, J.R. and STOLL, R.L. 1969, J. Eng. Maths., vol. 3, p123-135.

MIDGLEY, D. and SMETHURST, S.W. 1963, Proc. IEE., 110(8), p1465-1472.

PHEMISTER, T.G. 1972, C.A. Parsons Working Paper.

Discussion following paper:

(Fox, Oxford) There are numerical methods which solve problems in adjoining regions and then satisfy the conditions at the interface. They effectively work out a few columns of the inverse matrix corresponding to the finite difference operation, and these are analagous to the Green's function at relevant points of the boundary. Is there any relation between this numerical method and your analytical method?

(Phemister, Newcastle-upon-Tyne) There is a relation. The functions used here for correcting the first simple solutions are limits of sums of Green's functions, with the properties:

(1) They satisfy Laplace's equation everywhere except at the interface.

(2) They are continuous everywhere.

(3) They have defined discontinuities of their normal derivatives at the interface.

(4) Four of the functions are chosen in such a way that they account for the singularities of order $\pm$ 1/3 at each corner

The method is, therefore, the analytical counterpart of the numerical methods which Professor Fox describes, provided that the numerical method also accounts for the singularities.

(Moses, Wisconsin) Would the method of Schwarz-Christoffel transformations be applicable to field computation for slots?

(Phemister) Yes, in two-dimensional problems it can sometimes be used as an approximation. The author's experience, however, has been that field calculations from Schwarz-Christoffel transformations are cumbersome if the boundaries are neither equipotentials nor flux lines.

(Rogers, Southampton University) The singularities introduced by the corners of the slots do give rise to involved calculation if the local field is required. Very often in machine problems only an average field is necessary and in such cases the infinite matrices may be truncated drastically with very little loss in accuracy.

(Phemister) One result of the work that has been described is that singularities need not give rise to involved calculations. The seemingly difficult functions, defined by infinite series, have all been approximated in simple forms. Certainly truncation of the infinite set of equations is sometimes justified- in a calculation of the total magnetic energy, for example, the contribution of A_{ni} would be of order $i^{-10/3}$.

(Lindholm, Ampex Corp) The method appears similar to that of FAN used to analyze the field of a two-dimensional recording head with Fourier series. Although the potential is developed in a Fourier series, the magnetic field being the spatial derivative of the potential, is singular on the corners of the magnetic material. Consequently, the magnetic field on the corners cannot be represented by a finite Fourier series. The question is: how is this singularity treated in the present method?

(Phemister) The singularity is treated by using four infinite Fourier series for each slot; collectively they can account for the singularities of order $\pm$ 1/3 at each corner.

The calculation of forces and torques within numerical magnetic field calculation methods

K. Reichert, H. Freundl, W. Vogt
AG Brown Boveri
Baden/Switzerland

1) Forces and torques in magnetic fields

Magnetic fields give rise to localy varying force densities $\mathbf{f}$ in magnetizable and current carrying bodies and consequently to body forces $\mathbf{F}$ and torques $\mathbf{T}$:

$$\mathbf{F} = \int \mathbf{f} dV \quad (1) \qquad \mathbf{T} = \int \mathbf{r} \times \mathbf{f} dV \quad (2)$$

These actions are of great importance in all kinds of electromagnetic devices such as electrical machinery and magnetic levitation systems (Fig. 1). The more complex magnet fields in such equipment is nowadays computed by means of numerical methods as finite difference or element methods. It is therefore desirable to have available a simple method to compute forces $\mathbf{F}$ and torques $\mathbf{T}$ from discrete field-quantities obtained from these computations.

2) The general expression for the force density $\mathbf{f}$ [1,2,4]

There are several possibilities to derive expressions for the force density $\mathbf{f}$. Usually one starts from the power balance and then applies the principle of virtual displacement.

The power balance of a magnetic system (displacement current $\partial \mathbf{D}/\partial t = 0$; electric energy density $\int \mathbf{E} d\mathbf{D} = 0$) can be written in the form for rigid bodies:

$$\int \left\{ \operatorname{div} (\mathbf{E} \times \mathbf{H}) + \frac{d}{dt} \int_0^{\mathbf{B}} \mathbf{H} \cdot d\mathbf{B} + \mathbf{E} \cdot \mathbf{J} + \frac{d\mathbf{s}}{dt} \cdot \mathbf{f} \right\} dV = 0 \quad (3)$$

with: $\mathbf{E}$ = el. field strength, $\mathbf{H}$ = magn. field strength
$\mathbf{B}$ = magn. induction, $\mathbf{J}$ = current density

$\int_0^{\mathbf{B}} \mathbf{H} \cdot d\mathbf{B}$ = magn. energy density

$\mathbf{E} \cdot \mathbf{J}$ = joule power

$\frac{d\mathbf{s}}{dt} \cdot \mathbf{f}$ = mechanical power

$\operatorname{div} (\mathbf{E} \times \mathbf{H})$ = inflowing power

Using Maxwells equations:

$$\operatorname{rot} \mathbf{E} = -\frac{\partial \mathbf{B}}{\partial t} + \operatorname{rot} (\mathbf{v} \times \mathbf{B}) \quad (4) \qquad \operatorname{rot} \mathbf{H} = \mathbf{J} \quad (5)$$

We can transform:

$$\operatorname{div} (\mathbf{E} \times \mathbf{H}) = \mathbf{H} \cdot \operatorname{rot} \mathbf{E} - \mathbf{E} \cdot \operatorname{rot} \mathbf{H} = -\mathbf{H} \cdot \frac{\partial \mathbf{B}}{\partial t} - \mathbf{E} \cdot \mathbf{J} + \mathbf{H} \cdot \operatorname{rot} (\mathbf{v} \times \mathbf{B})$$

and get

$$\int \frac{d\mathbf{s}}{dt} \cdot \mathbf{f} dV = \int \left\{ \mathbf{H} \cdot \frac{\partial \mathbf{B}}{\partial t} - \frac{d}{dt} \int_0^{\mathbf{B}} \mathbf{H} \cdot d\mathbf{B} - \mathbf{H} \cdot \operatorname{rot} (\mathbf{v} \times \mathbf{B}) \right\} dV \quad (6)$$

In (6) the velocity $d\mathbf{s}/dt$ can be interpreted as a virtual velocity $\mathbf{v}$.

If the magnetic material is modeled by

$$\mathbf{B} = \mu \mathbf{H} + \mathbf{M}_p \quad (7)$$

the first two terms on the right-hand side of (6) can be transformed as follows:

$$\int \left\{ \mathbf{H} \cdot \frac{\partial \mathbf{B}}{\partial t} - \frac{d}{dt} \int_0^{\mathbf{B}} \mathbf{H} \cdot d\mathbf{B} \right\} dV = \int \left\{ \mathbf{H} \cdot \frac{\partial \mathbf{B}}{\partial t} - \frac{d}{dt} \left(\mathbf{H} \cdot \mathbf{B} - \int_0^{\mathbf{H}} \mathbf{B} \cdot d\mathbf{H} \right) \right\} dV =$$

$$= \int \int_0^{\mathbf{H}} \frac{\partial \mathbf{B}}{\partial t} \cdot d\mathbf{H} dV = \int \left\{ \int_0^{\mathbf{H}} \frac{\partial \mu}{\partial t} \mathbf{H} d\mathbf{H} + \frac{\partial \mathbf{M}_p}{\partial t} \cdot \mathbf{H} \right\} dV =$$

$$= -\int \mathbf{v} \cdot \left\{ \operatorname{rot} \mathbf{H} \times \mathbf{M}_p + \mathbf{H} \operatorname{div} \mathbf{M}_p + \int_0^{\mathbf{H}} \operatorname{grad} \mu \, \mathbf{H} d\mathbf{H} \right\} dV \quad (7)$$

with $\frac{\partial \mu}{\partial t} = - \mathbf{v} \cdot \operatorname{grad} \mu - \mu \operatorname{div} \mathbf{v}$

$$\frac{\partial \mathbf{Mp}}{\partial t} = \operatorname{rot} (\mathbf{v} \times \mathbf{Mp}) - \mathbf{v} \operatorname{div} \mathbf{Mp}$$

$$\int \mu \operatorname{div} \mathbf{v} \, dV = \oint \mu \, \mathbf{v} df = 0$$

$$\int \mathbf{H} \cdot \operatorname{rot} (\mathbf{v} \times \mathbf{Mp}) \, dV = \int \operatorname{div} (\mathbf{H} \times (\mathbf{v} \times \mathbf{Mp}) \, dV + \int (\mathbf{v} \times \mathbf{Mp}) \cdot \operatorname{rot} \mathbf{H} dV$$

$$= - \int \mathbf{v} \cdot (\operatorname{rot} \mathbf{H} \times \mathbf{Mp}) \, dV \quad (8)$$

The term $\mathbf{H} \cdot \operatorname{rot} (\mathbf{v} \times \mathbf{B})$ in (6) can be similarly transformed:

$$\int \mathbf{H} \cdot \operatorname{rot} (\mathbf{v} \times \mathbf{B}) \, dV = - \int \mathbf{v} \cdot (\operatorname{rot} \mathbf{H} \times \mathbf{B}) \, dV \quad (9)$$

Introducing (5) in (8) and (9), (8) in (7), (7) + (9) in (6) we get

$$\int \mathbf{v} \cdot \mathbf{f} dV = \int \mathbf{v} \cdot \left\{ \mathbf{J} \times (\mathbf{B} - \mathbf{Mp}) - \mathbf{H} \operatorname{div} \mathbf{Mp} - \int_0^H \operatorname{grad} \mu \, \mathbf{H} dH \right\} dV \quad (10)$$

and thus the expression for the force density f:

$$\mathbf{f} = \mathbf{J} \times (\mathbf{B} - \mathbf{Mp}) - \mathbf{H} \operatorname{div} \mathbf{Mp} - \int_0^H \operatorname{grad} \mu \, \mathbf{H} dH \quad (11)$$

by comparing the terms on both sides of (10).

The different terms in the force density (11) can be interpreted as follows:

- $\mathbf{J} \times \mathbf{B}$ is the force on a current carriing conductor in air
- $\mathbf{H} \operatorname{div} \mathbf{Mp}$ is the force on a permanent magnet ($J = 0$, $\operatorname{grad} \mu = 0$)
- $\int_0^H \operatorname{grad} \mu \, \mathbf{H} dH$ is the force in iron ($J = 0$, $Mp = 0$)

but in general it is not possible to so assign the terms of (11).

3) The calculation of forces $\mathbf{F}$ and torques $\mathbf{T}$ by means of surface integration [1..4]

The calculation of forces and torques by means of eg. (1) and (2) using (11) in numerical field calculations is inadvisable and inefficient because:

- Eq. (1) and (2) require volume integration
- in non linear cases (μ = f (H or B)) the magnetic history should be known, otherwise (10) can not be evaluated i.e. several field calculations.

The solution to this problems is

- calculation of $\mathbf{F}$ and $\mathbf{T}$ by means of surface integration
- surface integration in μ = const (air).

The volume integrals (1) and (2) can be transformed into surface integrals as the integration of a surface stress p over an arbitrary surface enclosing the body (Fig. 2) should result in the same forces and torques as the volume integration over the body using the force density f (11). i.e.:

$$\mathbf{F} = \int_V \mathbf{f} \, dV = \oint_A \mathbf{p} \, dA \quad (12)$$

$$\mathbf{T} = \int_V \mathbf{r} \times \mathbf{f} \, dV = \oint_A \mathbf{r} \times \mathbf{p} \, dA \quad (13)$$

By defining the tensor ϕ : $\mathbf{f} = \operatorname{div} \phi$ the volume integral can be converted into a surface integral using gauss integral formulae. This results in:

$$\mathbf{p} = \mathbf{H} (\mathbf{n} \cdot \mu \mathbf{H}) - \mathbf{n} \int_0^H \mu \, \mathbf{H} dH \quad (14)$$

with $\mathbf{n}$ the unit outward vector normal to the surface A. If the integration surface A is outside the material the expression for the surface stress $\mathbf{p}$ (14) can be simplified to:

$$\mathbf{p} = \mu_o (\mathbf{n} \cdot \mathbf{H})\,\mathbf{H} - \frac{1}{2}\mu_o H^2 \mathbf{n} = \frac{1}{\mu_o}(\mathbf{n} \cdot \mathbf{B})\,\mathbf{B} - \frac{1}{2\mu_o} B^2 \mathbf{n} \qquad (15)$$

It is interesting to note that in eq. (15) the non linear character of the body which is enclosed by the surface A is not directly expressed.

Eq. (15) together with (12) or (13) is best suited to the calculation of forces and torques of discrete field values resulting from numerical field calculations because

- only surface integration is required
- in nonlinear cases (μ = f (B or H)) one field calculation is sufficient if the integration surface A is in air.
- Any integration surface A will result in the same force if the body is fully enclosed.

However this method also has some limitations:

- The result is always a total force F or torque T acting on a simple connected body.
- Fictive air gaps are not allowed if they are disturbing the field.
- The method does not provide information over the body stress as eq. (11).
- The body has to be rigid.

4) The calculation of forces $\mathbf{F}$ and torques $\mathbf{T}$ within numerical field calculations

4.1 Procedure in general

The calculation of a body force $\mathbf{F}$ or torque $\mathbf{T}$ by means of eq. (12), (13) and (15) is straightforward.

- Calculate discrete values of potentials (vector- or skalarpotential $\mathbf{A}$, φ) or other descriptive field quantities, by means of finite difference, finite element or other numerical techniques using a grid or element distribution.
- Define the integration surface A around the body. Any A should result in the same force and torque as long as the body is enclosed. Therefore simplified integration surfaces A can be chosen (Fig.2,3). The surface A should pass through the centers of the elements.
- Calculate the magnetic field strength $\mathbf{H}_i$ or the induction $\mathbf{B}_i$ in the elements i crossed by A.
- Calculate the surface stress $\mathbf{p}_i$ (15) in the element$_i$.
- Calculate the force $\mathbf{F}$ and the torque $\mathbf{T}$:

$$\mathbf{F} = \sum \Delta \mathbf{F}_i = \sum_{i=1}^{N} \mathbf{p}_i \Delta A_i \qquad (16) \qquad \mathbf{T} = \sum \Delta \mathbf{T}_i = \sum_{i=1}^{N} \mathbf{r}_i \times \mathbf{p}_i \Delta A_i \qquad (17)$$

4.2 Procedure for some typical elements

a) Two-dimensional rectangular element: $\mathbf{p} = (p^x, p^{y'})$

With the vectorpotentials A_{ik}, $A_{i,\,k+1}$, $A_{i+1,\,k}$, $A_{i+1,\,k+1}$ in the corners of the rectangular element (Fig. 4), one calculates the components of the induction:

$$B^x_{i,k} = \frac{A_{i,\,k+1} + A_{i+1,\,k} - A_{i,\,k} - A_{i+1,\,k}}{2\,h_k}$$

$$B^y_{i,k} = \frac{A_{i,k+1} + A_{i,k} - A_{i+1,k+1} - A_{i+1,k}}{2\,h_i}$$

If the integration surface A has the direction of the x-axis, we have $\mathbf{n} = e_y$

$$p^{xy}_{i,k} = \frac{1}{\mu_0} B^x_{i,k} \cdot B^y_{i,k} \; ; \quad p^{yy}_{i,k} = \frac{1}{2\mu_0} (B^{y2}_{i,k} - B^{x2}_{i,k})$$

$$\Delta F^{xy}_{i,k} = \ell \cdot p^x_{i,k} \cdot h_i \; ; \; \Delta F^{yy}_{i,k} = \ell \cdot p^y_{i,k} \cdot h_i$$

ℓ is the length perpendicular to the xy plane.

For $\mathbf{n} = e_x$ we get:

$$p^{xx}_{i,k} = \frac{1}{2\mu_0} (B^{x2}_{i,k} - B^{y2}_{i,k}) = - p^{yy}_{i,k} \qquad (18)$$

$$p^{yx}_{i,k} = \frac{1}{\mu_0} B^x_{i,k} B^y_{ik} = p^{xy}_{i,k} \qquad (19)$$

$$\Delta F^{xx}_{i,k} = \ell \cdot p^{xx}_{ik} h_k \; ; \quad \Delta F^{yx}_{i,k} = \ell \cdot p^{yx}_{i,k} \cdot h_k$$

b) Two-dimensional triangular element: $\mathbf{p} = (p^x, p^y)$ (Fig. 5)
The path of integration can be:
1-s-2, 1-s-3, 2-s-3 or any others.

In a first-order element the induction B is constant and given by:

$$B^x = \frac{\partial A}{\partial y} = \frac{1}{2F} \sum_{i=k,n,m} c_i A_i \; ; \quad B^y = \frac{\partial A}{\partial x} = \frac{1}{2F} \sum_{i=k,n,m} b_i A_i$$

with $b_k = y_m - y_n$; $c_k = x_n - x_m$

$b_m = y_n - y_k$; $c_m = x_k - x_n$

$b_n = y_k - y_m$; $c_n = x_m - x_k$

F = Fläche Δ

The normal vector to the integration path 1-s is:

$$\mathbf{n}_{1s} = \frac{\mathbf{i}(y_n - \frac{y_m + y_k}{2}) - \mathbf{j}(x_n - \frac{x_m + x_k}{2})}{\sqrt{(x_n - \frac{x_m + x_k}{2})^2 + (y_n - \frac{y_m + y_k}{2})^2}}$$

or $n_{1s} = \mathbf{i}\, n^x_{1s} + \mathbf{j}\, n^y_{1s}$

The contribution ΔF_{1s} of the integration path 1-s to the force F is therefore:

$$\mathbf{F}_{1s} = \frac{\ell \cdot \ell_{1s}}{u_0} (n^x_{1s} B^x + n^y_{1s} B^y)(\mathbf{i}B^x + \mathbf{j}B^y) - \frac{1}{2}(B^{x2} + B^{y2}) \cdot (\mathbf{i}n^x_{1s} + \mathbf{j}n^y_{1s})$$

with $\ell_{1s} = \frac{1}{3}\sqrt{(x_n - \frac{x_m + x_k}{2})^2 + (y_n - \frac{y_m + y_k}{2})^2}$

Similar expressions can be derived for the contributions of 2-s and 3-s.

c) Complex field quantities
If the variation of the field is quasistationary sinosoidal, the situation can best be described by complex quantities:

$$B^x = \mathrm{Re}\, \underline{B}^x e^{j\omega t} \qquad (20)$$

Where $\underline{B}^x$ is complex: $= B^x e^{j\varphi_x}$. Introducing this in eq. (18) we receive for the components of $p_{i,k}$

$$p^{xx}_{i,k} = \frac{1}{2\mu_0} (\mathrm{Re}\ \underline{B}^x e^{j\omega t} \cdot \mathrm{Re}\ \underline{B}^x e^{j\omega t} - \mathrm{Re}\ \underline{B}^y e^{j\omega t}\ \mathrm{Re}\ \underline{B}^y e^{j\omega t}) \quad (21)$$

$$p^{yx}_{i,k} = \frac{1}{\mu_0}\ \mathrm{Re}\ \underline{B}^x e^{j\omega t} \cdot \mathrm{Re}\ \underline{B}^y e^{j\omega t} \quad (22)$$

with $n = e_x + e_y$

If Z_1 and Z_2 are to complex numbers we have the relationship:

$$\mathrm{Re}\ (Z_1)\ \mathrm{Re}\ (Z_2) = \frac{1}{2}\ \mathrm{Re}\ (Z_1 \cdot Z_2 + Z_1 \cdot Z_2^*)$$

* means conjugate complex.

Using this relation we receive for $p^{xy}_{i,k}$:

$$p^{yx}_{i,k} = \frac{1}{2\mu_0} B^x B^y \left\{\cos\ (2\omega t + \varphi_x + \varphi_y) + \cos\ (\varphi_x - \varphi_y)\right\}$$

This means that the method is also applicable to sinosoidal fields, if we use a complex potential $\underline{A}$:

$$A = \mathrm{Re}\underline{A}e^{j\omega t}$$

with $\underline{A} = AR + j\,AI$ we can calculate:

$$B^x_{i,k} = \frac{1}{2h_k} \sqrt{(AR_{i,k+1} + AR_{i+1,k} - AR_{i,k} - AR_{i+1,k})^2 + (AI_{i,k+1} + AI_{i+1,k} - AI_{i,k} - AI_{i+1,k})^2}$$

and $B^y_{i,k}$ in the same way if we have a rectangular grid.

5) Application

A system of subroutines has been written to compute forces and torques from discrete field quantities based on a certain element type. The method has been applied to a number of magnetic field and eddycurrent problems.

Fig. 6 shows an example, the magnetic field in a cross-section of a magnetic levitation system. The main problem was there the calculation of the forces F^x and F^y between the rail and the magnet especially for different off-set positions x/b because in this design the magnet is also supposed to keep the train in the middle of the rail. Using a rectangular grid, the vector potential approach and the finite element method the discrete field distribution was calculated considering saturation in the iron. From these quantities the forces F^x and F^y were derived by means of surface integration. The results (Fig. 7) did agree very well with measurements.

Literature:

[1] Diesselhorst, H. : Magnetische Felder und Kräfte J.A. Barth-Verlag, Leipzig, 1939

[2] Stratton, J.A. : Electromagnetic Theory

[3] Carpenter, C.J. : Surface integration methods of calculating forces on magnetic iron parts Proc. I.E.E. 106C (1960)

[4] Kamerbeek E.M.H. : On the theoretical and experimental determination of electromagnetic torques in electrical machines Philips. Res. Rept. Suppl. 1970, No.4

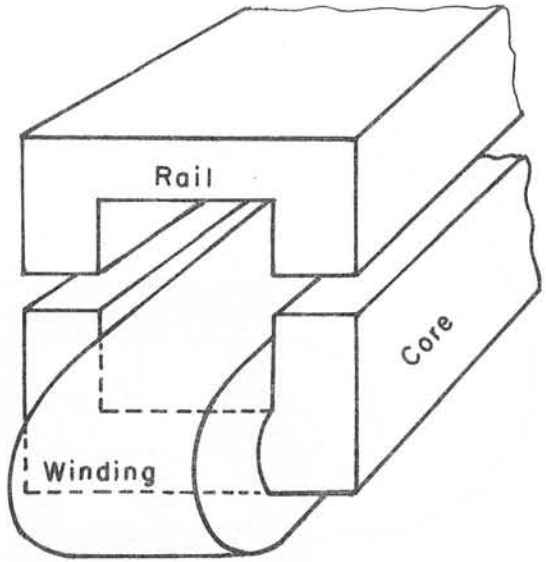

Fig.1 : Magnetic levitation system

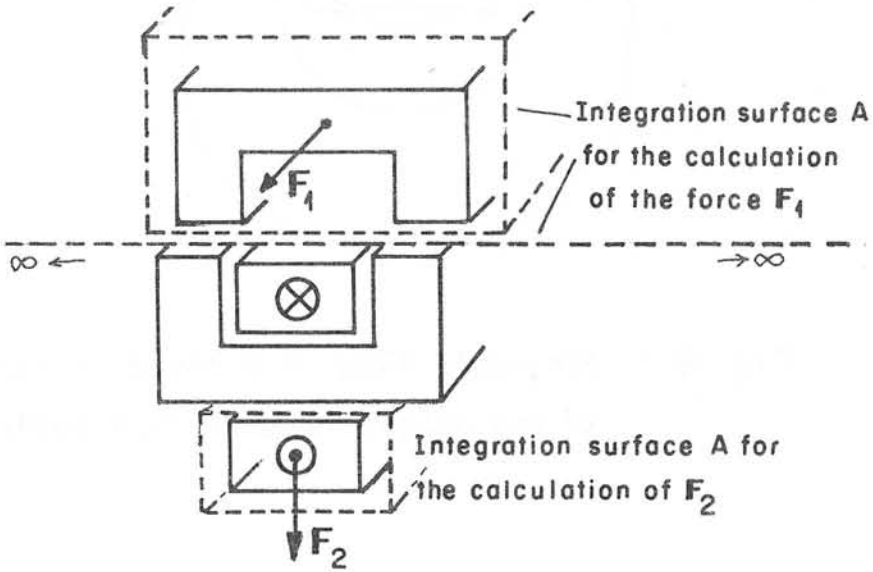

Fig. 2 : Definition of the surface integration

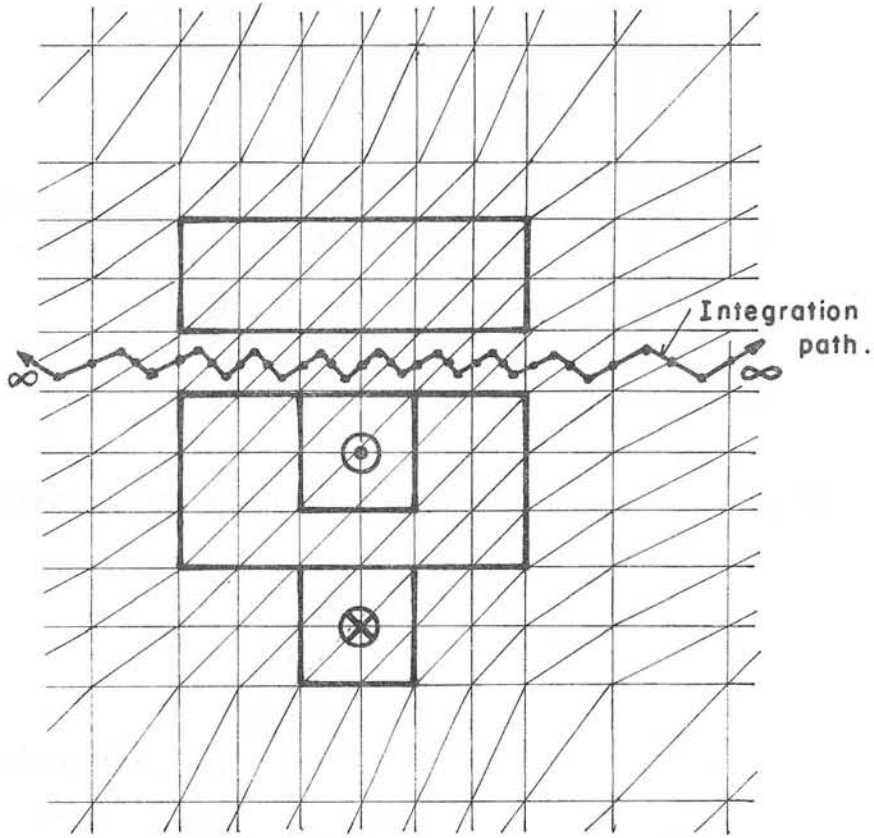

Fig. 3 : Finite element grid, integration path for force calculation by surface integration.

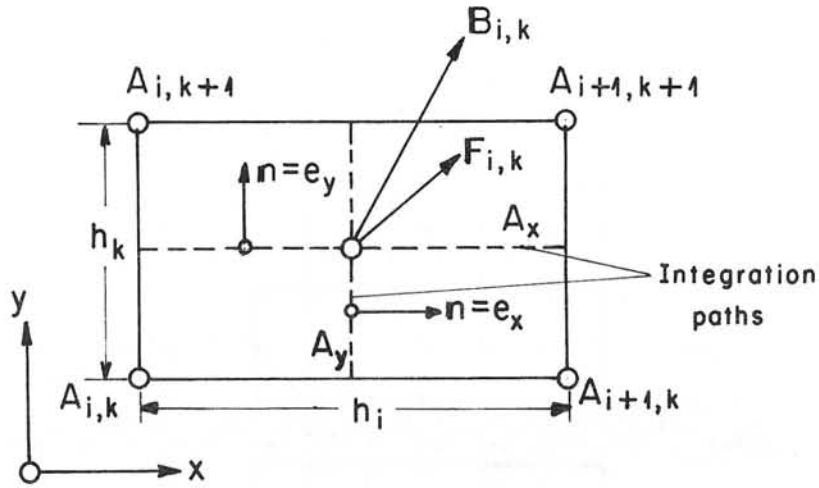

Fig. 4 : Two-dimensional rectangular element

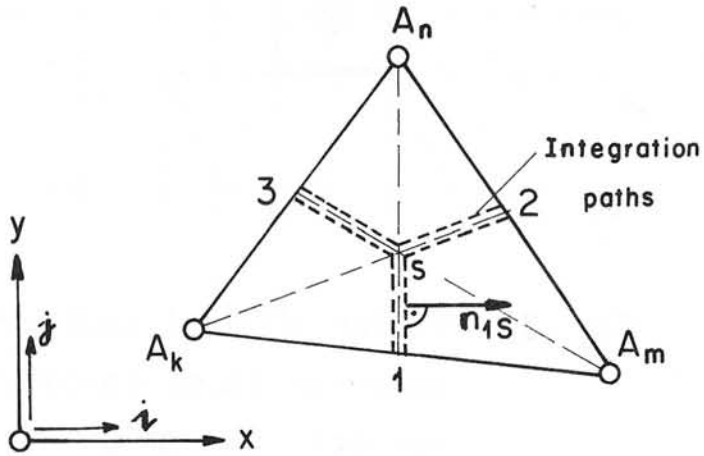

Fig. 5 : Two-dimensional triangular element

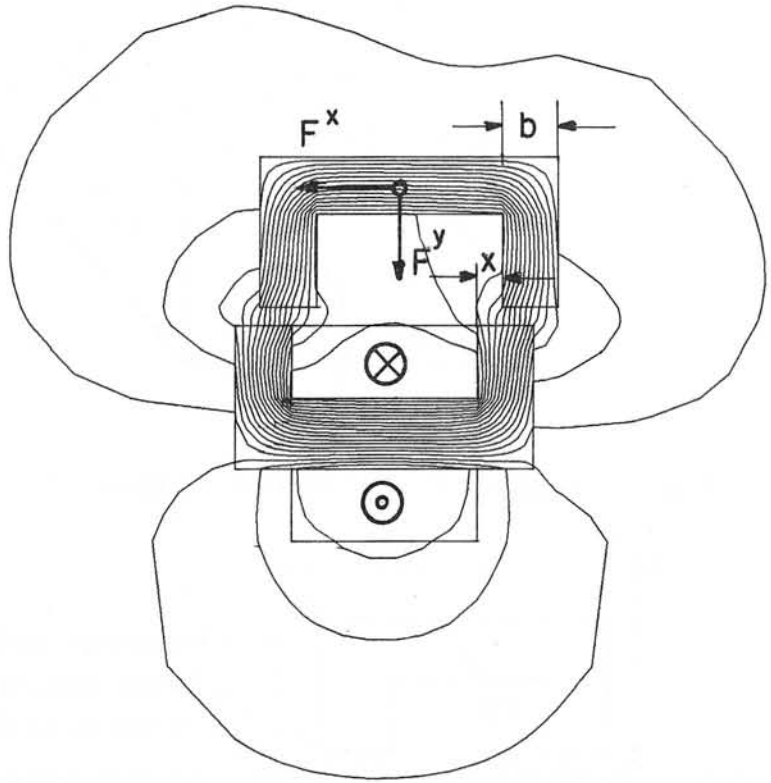

Fig. 6 : Magnetic field in a cross-section of the magnetic levitation system

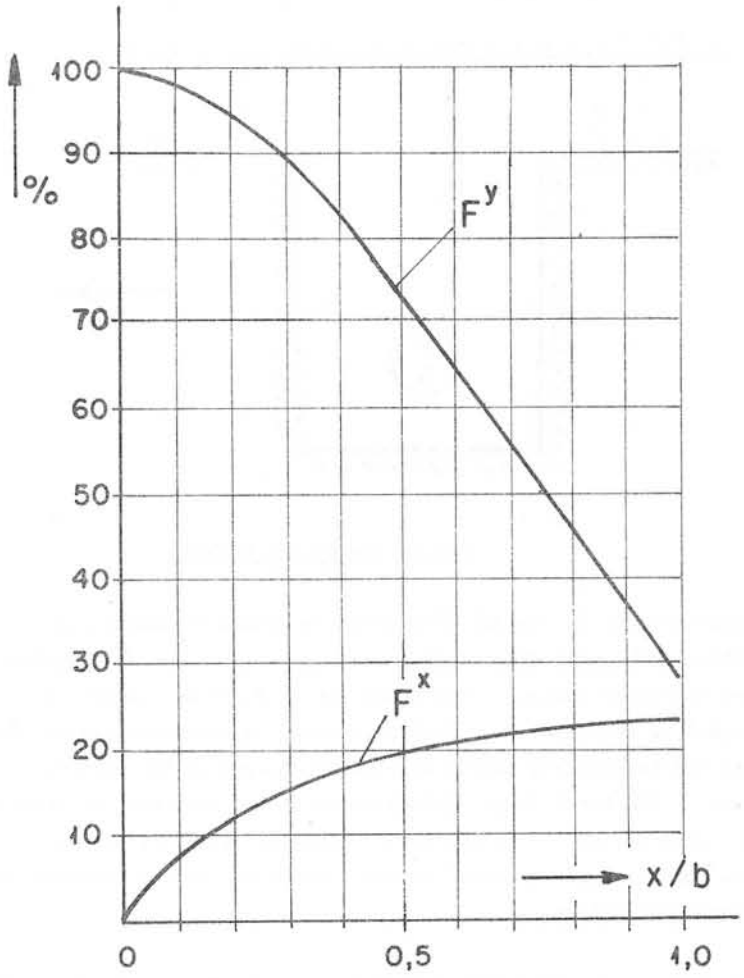

Fig. 7 : Force F^x and F^y in the magnetic levitation system versus displacement x/b

Discussions following paper:

(Hammond, Southampton Univ) Dr Reichart has drawn attention to the simplification which results from drawing the surface for his stress calculation in air. Does he think that useful information can be obtained by drawing a surface in iron or does he think that this is not possible in principle?

(Reichert/Freundl) In general the introduction of an artifical airgap is not allowed whilst using the surface integration method because it may change the original field distribution and thus the total force. But if the modification of the field by the airgap is small or has considerable influence on the force this trick can be used.

(Carpenter, Imperial College) May I first elaborate a little further the question of force distribution? The energy argument leads to forces acting on the iron surfaces - surface tractions - tending to pull the surface layer off the material behind, and the physical significance of these forces is very doubtful. The same argument applied to electric forces on dielectric fluids leads to negative hydrostatic pressures. The energy argument presupposes continuous media, whereas in attempting to separate "magnet" from "mechanical" forces inside the material we are driven to examine its physical - i.e. Dipole - structure. It is not difficult to show that, using an idealised model, Dr Reichert's equations give the forces on half-dipoles, and that we obtain a wholly different force distribution if we consider whole dipoles (whether using energy arguments or otherwise). The problem of defining any force distribution which has any real physical significance is fundamental since the "magnetic" forces are a part of the particle interactions which determine the mechanical properties of the material, so that inside the iron the distinction between "magnetic" and "mechanical" forces tends to become meaningless. We need an operational definition of "stress", which is not a quantity which is directly observable. If we observe strain, then magnetostriction assumes a key role. In my own investigations (both in 1960* and since) I have found that, once we agree on an opera-

*Carpenter, C J "Surface Integral Methods of Calculating Forces on Magnetised Iorn Parts" Proc. IEE 106C 1960.

tional definition, all methods lead to the same result. Moreover, if we define "Stress" in any looser way, then I have found that, where the stresses are large enough to be of importance in engineering applications (i.e. near failure) then the differences which we obtain by using different models are too small to be experimentally significant.

I suggest that simple energy arguments can be misleading in these contexts and that deriving the Maxwell stress equations this way can imply unnecessary limitations, because of problems associated with energy loss in eddy currents and hysteresis. I am sure Dr Reichert will agree that surface integration will always give the force on whatever is enclosed by the surface, whether the energy is conserved or not.

Dr Reichert referred to the need to make air gaps around the part of the interest as a limitation of the method. I regard it, on the contrary, as an asset. If the force which we compute is to be observable (and therefore meaningful) we must be able to separate the part from the rest of the device. In practice we always have air gaps, however, small they may be, and the method draws attention to any peculiarities, such as domain effects which may be associated with iron surfaces (nearly) in contact with each other.

My final point concerns the shape of the surfaces which we choose to integrate over. These do not have to conform with the iron surfaces, and there are sometimes substantial advantages to be gained by choosing other shapes, particularly when calculating "sideways" forces, as in Dr Reichert's two C-cores. The possibilities can be illustrated most clearly by tracing a simplified example. The sideways force on a slot carrying a current (Fig A) can be shown, usually by energy arguments, to be the same as if the conductor where placed in the gap and the slot filled in. This is difficult to show by an integration surface which passes straight through the gap or by one which follows the slot surface. But, the integration surface shown in Fig A gives the force by inspection:

$$F = \tfrac{1}{2} g \, (H_1^2 - H_2^2) = I \, \frac{H_1 + H_2}{2} \quad N/m$$

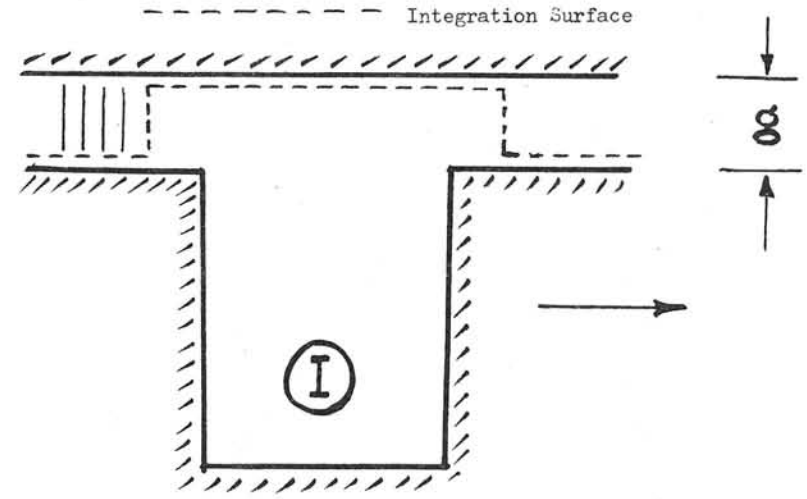

Fig A Conductor in Slot

(Reichert/Freundl) Our eq (11) gives the force density in an infinitestimal volume element dV. Therefore we cannot distinguish between different forces. The situation is different if one is interested in the force on a finite volume. A permanent magnet for example can be modelled either by surface charges or by Ampere's currents. The total force in both cases is the same but the stress inside is different. Therefore, we agree that the distinction between magnetic and mechanical forces inside is "model depending" and therefore meaningless.

(Perin, Cern) 1. Does your method assume that all the magnetic flux which crosses the integration surface passes through the ferro-magnetic body?

2. How close has the surface in air to be to the body?

(Reichert) 1. No, any field situation can be handled.

2. The path of integration has to in air, it has to be closed but it can be arbitrary within this limit. The resulting force is independent

of the path of integration but can depend on the accuracy of the discrete field quantities as calculated by the FE-method.

(Chevalley, Cern) Have you ever looked at the contributions of the differcult terms in the equation?

In a particular case I found that the integral $\int$ grad μ HdH is small ($\sim$ 3%) and could be ignored.

(Reichert) The contribution of the different terms in the volume element force equation is problem dependent. Therefore a general answer cannot be given to the answer. In an electric machine for example the term F x μH is only important if the conductor is exposed to the field H (open slot).

(Armstrong, Rutherford) How do you deal with the singularity at the corners of the surface of integration?

Your general method is given in J Strattan, Electromagnetic Theory (McGraw Hill 1941).

(Reichert) In a FE solution a singularity does not show up unless the element size is not zero. The result is always a finite magnetic field distribution in the grid, even at the corners. With reference to your statement there are a number of textbooks which are describing the method in general, but to my knowledge up to now nobody has mentioned the application of the method within the FE - or FD - method.

CALCULATION OF THE MAGNETIC SYSTEM ELEMENTS OF THE ISOCHRONOUS CYCLOTRON BY THE GRID METHOD

Yu.G.Alenitsky, S.B.Vorozhtsov, N.L.Zaplatin

Laboratory of Nuclear Problems
Joint Institute for Nuclear Research, Dubna, USSR

I. Introduction

The calculation of magnetic fields by the grid method in systems containing ferromagnetic and current elements allows one to analyse the effect of iron saturation and magnetic flux distribution when induction is varied in a wide range. By using the available programmes for calculating the two-dimensional configuration, ref. /1,2,3,4,5/, one can obtain good quantitative results. By separating the cross section for calculations from the whole three-dimensional configuration and choosing for it some realistic boundary conditions one can obtain the results coinciding with the experiment to an accuracy of (1÷5)%.

II. Short Description of the Programme

The TRIMA programme system, a modified version of the TRIMD /2/ programme which in its turn had been written basing on ref. /1/, has been developed at the Laboratory of Nuclear Problems, JINR.

The programme solves the nonlinear differential equation of elliptical type in private derivatives presented in the finite-difference form. The equation is as follows:

For the Cartesian system of coordinates (x,y)

$$\frac{\partial}{\partial x}\left[\frac{1}{\mu}\frac{\partial u(x,y)}{\partial x}\right]+\frac{\partial}{\partial y}\left[\frac{1}{\mu}\frac{\partial u(x,y)}{\partial y}\right]=-0{,}4\pi J(x,y)$$

For the cylindrical system of coordinates (r,z)

$$\frac{\partial}{\partial z}\left[\frac{1}{\mu r}\frac{\partial}{\partial z}[r\cdot u(r,z)]\right]+\frac{\partial}{\partial r}\left[\frac{1}{\mu r}\frac{\partial}{\partial r}[r\cdot u(r,z)]\right]=-0{,}4\pi J(r,z)$$

where U is the vector potential of the magnetic field (G × cm), $\mu=\mu(B)$ is the permiability of ferromagnetic, J is current density (a/cm^2), U and J are the normal planes (x,y) or (r,z).

Fig. 1 shows the diagrams of possible boundary conditions The Dirichlet zero boundary condition is set at all boundaries (fig.1-A) in usual cases. If the axis y=0 is the symmetry axis, the Neumann zero condition is set at this boundary. For the cylindrical system of coordinates with $r \to 0$ the vector potential is found from the condition $rU(r,z) = a(z)\times r^2$ which results from the fact that at the r=0 axis the field is an even function.

The TRIMA programme approximates the $\mu(B^2)$ dependence by the analytic expression proposed in /6/. As a result of the optimization of the programme part, the time consuption for calculations is reduced about 4 times, the number of grid points was increased up to 1600 (without using the external computer memory). The programme has been written for the BESM-6 computer.

III. Calculation of the Magnetic System Elements

As has been shown in ref. /7/, the amplitude of the magnetic field variation of spiral shims is fairly well described by the infinite system of rectilinear ferromagnetic bars. To choose preliminary the azimuthal width and the height of the spiral shims of the "F" facility some experiments have been performed by using 4 pairs of rectilinear bars /8/.

A similar mathematic modelling may be performed by using the computer programme. Fig. 2 shows the experimental lay out with ferromagnetic bars in the electromagnet gap and the calculation region shown by the dashed line. The results of calculations are presented as a function of $B_1 = F(B)$, where

$$B_1 = 0.5 \,/\, B(0,0) - B(X_{max},0) \,/\,,$$

$$B = 0.5 \,/\, B(0,0) + B(X_{max},0) \,/\,.$$

For the programme calculation of the configuration of this type a scheme of boundary conditions is envisaged, which is shown in fig. 1.B.

The left and right boundaries of the calculation region are set by $U(0,y) = const_1$, $U(x_{max},y) = const_2$ which indicates the absence of the flux going through these boundaries. At the y = 0 boundary the Neumann zero condition is possible, when y = 0 is the symmetry axis or the Dirichlet zero condition. For $y = y_{max}$ the Neumann zero condition or the Dirichlet condition is possible $U(x, y_{max}) = f(x)$.

The calculation of our rectilinear bars was made for the following boundary conditions:

$$U(0,y) = 0,\quad U(x_{max},y) = B_o \times x_{max},\quad \frac{\partial U(x,y)}{\partial y}\Big/_{y=0} = 0$$

at the $y = y_{max}$ boundary the following two boundary conditions were set:

$$U(x, y_{max}) = B_o \times x,\quad \frac{\partial U(x,y)}{\partial y}\Big/_{y=y_{max}} = 0$$

In this case the calculation results remained the same. This may be explained by the fact that the upper boundary is located sufficiently far so that no redistribution of the magnetic flux at the pole caused by bars located in the electromagnet gap, at the upper boundary of the calculation region occurs.

The calculation shows fairly well the state of ferromagnetic elements and the redistribution of the μ magnetic permiability and the magnetic fluxes when the field level is changed. Fig. 3 shows the flux distribution for run I (fig.2) at the average induction level in the gap (1.0T, 1.3T, 1.6T). As the calculations show, with the average level of the induction B = 1.3T, the rectilinear bar approaches saturation, the induction inside the bar is B=(2.0-2.1)T. For the calculation of $B_1(B)$ (800 mesh points, five induction levels) twelve minutes of the BESM-6 computer time are required.

The comparison of calculation and experimental dependences (fig.2) shows that the curves are identical.

The difference of the value $2B_1$ obtained by calculation from that obtained experimentally is (1-3)% and may be explained by the finiteness of ferromagnetic bars used in the experiment, by the decrease of the field in the flat gap of the electromagnet and the discrepancy of the $\mu(B)$ properties of the applied ferromagnetic and calculation approximation.

An example of the calculation of the electromagnet pole edge is shown in fig. 4. The mesh of 1500 points is used, the BESM-6 computer time is about 10 minutes. The boundary conditions differ from those used above only at the upper boundary which is distributed into two parts (fig. 1-C).

1) $x < x_k$ is the constant flux,

2) $x > x_k$ is the flux determined by the potential of the magnetic dipole.

As is seen from Fig.4, in the radial region of the $r < r_k$, where r_k is the radius of the electromagnet pole, the difference of calculations from the curve obtained experimentally by using the electromagnet (Ø1200mm) does not exceed 0.5%. However, the great divergence of the experiment and calculation curves for $r > r_k$ is seen. This means that the boundary potential given as a dipole potential differs from real conditions at the electromagnet.

It is necessary to mention that when using the boundary conditions of this type, it is desirable to fulfil the following correlations:

$$Z_{max} \geq 2\, h_M,\quad r_{max} \geq 1.2\, r_k\ .$$

When developing the magnet system for the U-120M isochronous cyclotron it is important to select such a configuration of spiral shims which could provide the minimum relative changing of the magnetic fields when varying the induction level.

As has been shown in ref. [9], one may achieve this for the central region of the magnetic system by varying the angular width of spiral shims and using the axial grooves in them.

The general schematic view of the cross section along

the spiral axis line of the U-120M magnetic system is shown in fig. 5, the dashed line shows the calculation region. The boundary conditions are given as shown in fig.1-B.

The results of calculations for the shims with grooves and without them at two limit induction levels are shown in figs. 6,7[10]. Comparing figs. 6-C and 6-D, one may see the essential increase of the horizontal component of the flux at the low induction level, which results in field increase in the median plane at small radii (fig. 8-A).

As is seen from figs. 6-A and 6-C, the vertical grooves reduce the fraction of the flux hitting the centre from large radii at low induction.

Thus, in the case of shims with grooves (figs.6-A,B) one observes less essential change of the pattern of magnetic flux distribution with increasing the induction level.

Figs. 7-C and 7-D show the distributions of magnetic permiability for shims without grooves. With B = 1.0 T (Fig.7-C) a sharp increase of permiability is observed with decreasing the radius. The gradient is $d\mu/dr=-250\ cm^{-1}$ with r =7 cm, therefore, the magnetic flux lines are directed to the centre. At large induction levels B = 2.2 T(fig. 7-D) the shim is saturated, and μ at a larger shim section does not exceed 10 and nearly uniform distribution of permiability is observed. In this case the gradient $d\mu/dr=-2.0cm^{-1}$ over the larger part of the central shim region. Consequently, the horizontal component of the flux is reduced which results in field increasing at small radii.

A similar μ distribution at the same induction levels for shims with grooves are shown in figs. 7-A and 7-B.Comparing fig.7-C and 7-A relating to low induction one observes the following:

1)the distributions μ, at the pole are of similar kind,

2)the central part and the shim teeth are not saturated, axial grooves in the shims prevent the passage of the horizontal component in the teeth region. Such unsaturated teeth promote the uniform passage of the flux through the shim and pole contact region. This is proved by the reduction of the pole permiability in the regions opposite the teeth and the increase of the pole permiability over the grooves (the reflection effect).

3. The general state of the shim section under the grooves is described by a lower average value of the permiability $\mu = 15$ at the same excitation level which impedes the defelction of the magnetic flux lines in the horizontal direction.

4. The radial gradients μ of the shims under the grooves are considerably smaller than those in the shims without grooves.

With large induction levels (fig. 7-B) the shim teeth are saturated approximately equally with the lower part of the shim. Horizontal fluxes similar to the case with shims without grooves are impeded. Special attention should be paid to the region of larger μ in the shim body directly under the grooves as well as a more noticeable effect of reflecting the teeth at the pole.

The calculational distribution of magnetic field intensity in the median plane for the case under consideration are shown in fig. 8-A. The curves are matched in pairs at the field level for r = 16 cm. For the shim with grooves (curves 3 and 4) the field difference in the radial range of 3-10 cm is reduced about 300 Oe, and the field peak due to the horizontal component of the flux disappears.

Fig. 8-B shows the experimental values of the field peak for configurations and exciation levels under consideration. The comparison with calculational data shows the coincidence of the dependences. However, in the range of r= (30-35) cm noticeable distortions are observed which are caused by artificial conditions of flux absence through the right-hand side boundary taken in the calculation scheme.

In conclusion it is worth mentioning that the given calculations do not claim for complete quantitative

description of 3-dimensional structure of the magnetic system and are just a model for clearing out the physical phenomenon in this part of the magnetic system. The calculation model makes it possible to determine the variations of magnetic field intensity and the redistribution of μ in iron when varying the shim geometry.

The calculations of the chosen parts of the magnetic system performed by using the TRIMA programme do not consume much computer time. Hence, this method can be extensively used when modelling complicated magnetic systems. Despite the fact that the accuracy of calculations (1÷5)% is much poorer than that for field shaping (0.02%) required for accelerators, such calculations are the only method permitting the analysis of the magnetic state of ferromagnetic when varying its configuration and the level of the external magnetizing field.

References

1. A.M.Winslow, J.Computer Phys., V 1, No.2(1966) pp.149-172.
2. S.B.Vorozhtsov, L.T.Zakamskaya, N.L.Zaplatin. JINR Communication P9-5013, Dubna, 1970.
3. M.T.Diserens, RMEL/R, 171(1969).
4. John S.Colonias. "Partical Accelerator Design. Computer Program". Academic Press, New-York and London, 1974.
5. Y.T.Puzynovich. NIIEFA Preprint B-0178, Leningrad, 1973.
6. Y.S.Derendyaev, B.A.Klenin. JINR Communication, P-11-6579, Dubna, 1972.
7. V.P.Dmitrievsky, et al. JINR Communication, 1431, Dubna, 1960.
8. S.B.Vorozhtsov, N.I.Dyakov, N.L.Zaplatin, JINR Communication, 9-4517, Dubna, 1969.
9. Y.G.Alenitsky, N.L.Zaplatin, A.A.Kropin, N.A.Morozov. Proc. III Working Meeting on the U-120M Isochronous Cyclotron, Czeske Budejovic, CSSR, 14-18 May, 1973. JINR Communication P9-7339, Dubna, 1973.
10. Y.G.Alenitsky, S.B.Vorozhtsov, N.L.Zaplatin, JINR Commucation P9-7412, Dubna, 1973.

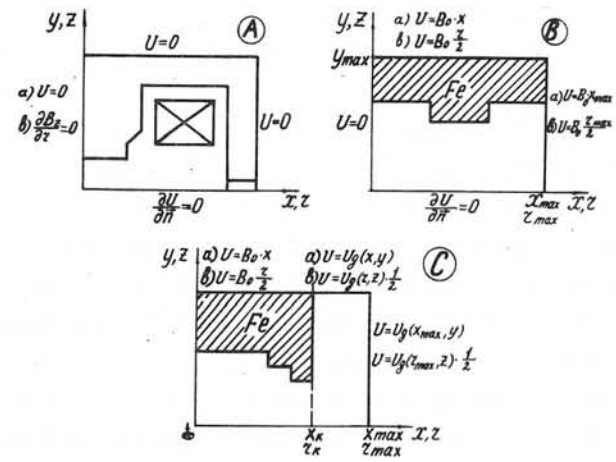

Fig. 1

1) Boundary conditions: a) Cartesian system of coordinates b) cylindrical system of coordinates.

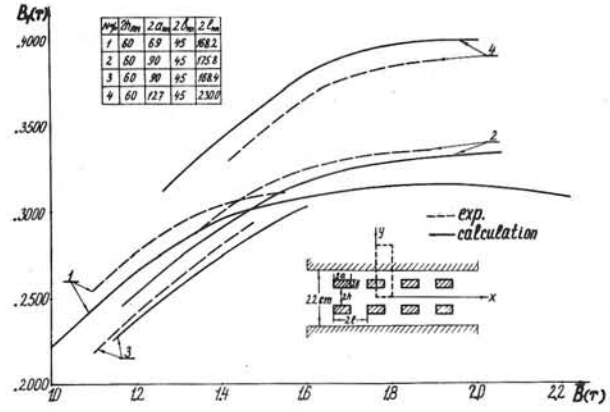

Fig. 2 .

Experimental procedure and the calculation of the rectilinear bar system. The dependences $B_1(B)$.

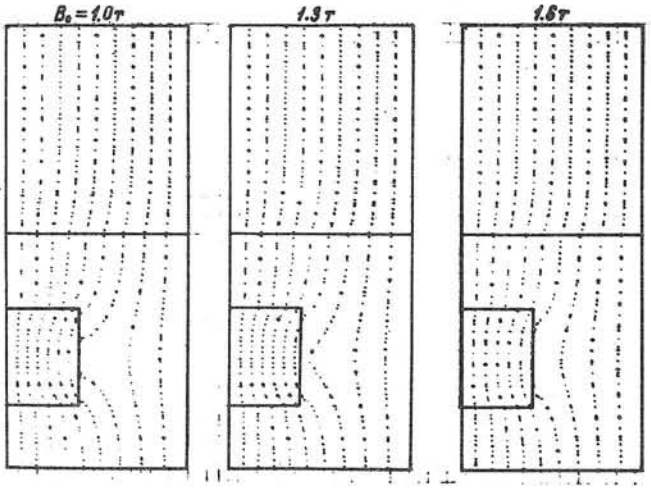

Fig. 3

Distribution of magnetic flux lines for the following levels: B = 1.0 T, 1.3 T, 1.6 T

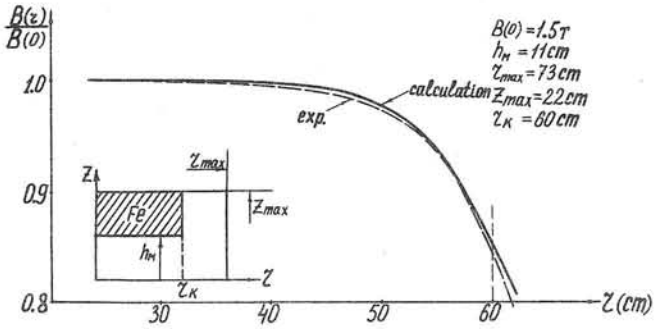

Fig. 4

Electromagnetic pole edge, the calculation procedure and the obtained characteristics of $B(r)/B_o$.

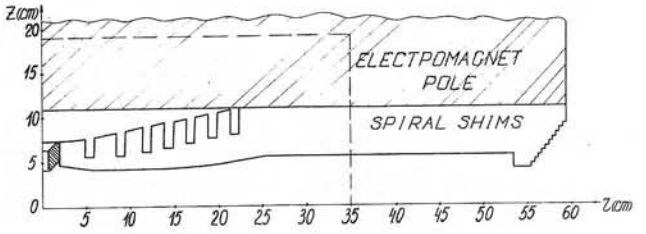

Fig. 5

Cross section of the U-120M magnetic system, the dashed line is the calculation region.

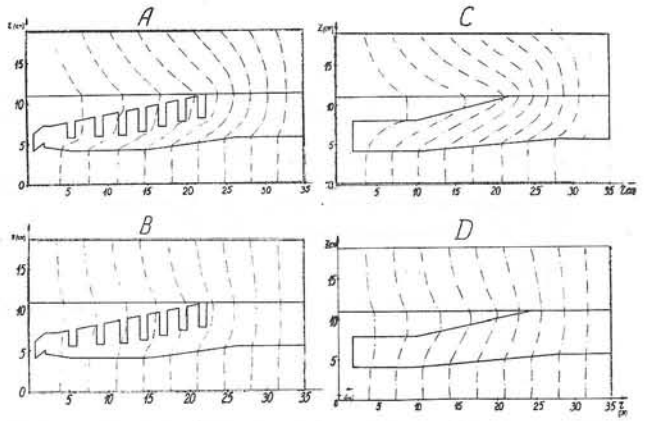

Fig. 6

The distribution of the magnetic flux lines

A, C - B_o = 1.0 T

B, D - B_o = 2.27 T

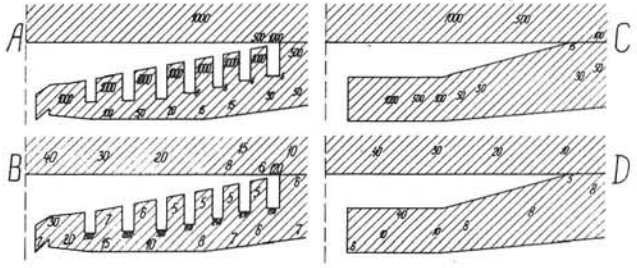

Fig. 7

Distribution of magnetic permiability

A, C - B_o = 1.0 T
B, D - B_o = 2.27 T

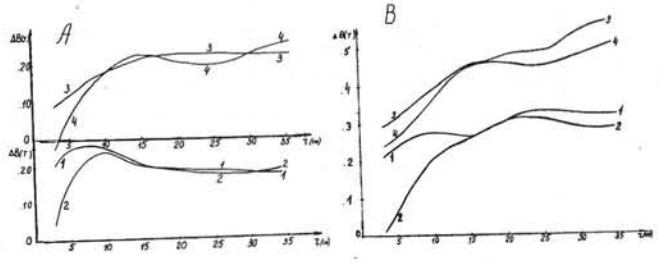

Fig. 8

Magnetic field intensity in the median plane

A- calculation , B -measured magnetic field in the hill

1,2 - shims without grooves

3,4 - shims with grooves

1,3 - B_o = 1.0 T

2,4 - B_o = 2.27 T.

ON THE COMPUTATION OF THREE-DIMENSIONAL MAGNETOSTATIC FIELDS BY THE INTEGRAL EQUATION METHOD

V.Ts.Banchev, S.B.Vorozhtsov

Joint Institute for Nuclear Research, Dubna, USSR

The integral equation method for the computation of 3-dimensional magnetostatic fields in the presence of iron has been mostly developed during the last years [1-3]. In this paper the polyhedron of an arbitrary form is suggested to be used as a region with uniform magnetization. Two numerical methods for the solution of the resulting system of simultaneous nonlinear algebraic equations were tried.

Dividing a magnetic body into polyhedral regions with a constant magnetization vector in each one, the problem of finding the magnetic field intensity inside the magnet iron is reduced to the solution of the following set of simultaneous nonlinear algebraic equations (the Gaussian system of units).

$$\mu_a H_a - \frac{1}{4\pi}\sum_{q=1}^{N}(\mu_q - 1)\sum_{\chi=x,y,z} H_{\chi q} f_{\xi\chi}(D\xi_{aq_1}, D\xi_{aq_2}, \ldots, D\xi_{aq_M}) = H_{\xi ca}, \quad (1)$$

where $\xi = x, y, z$, $a = 1, 2, \ldots, N$,

$$\mu_a = \mu_a\left(\sqrt{\sum_{\xi} H^2_{\xi a}}\right) \quad (2)$$

is the known permeability curve of the specific magnetic material, $D\xi_{aqi} = \xi_a - \xi_{qi}$, $i = 1, 2, \ldots, M$,
i denotes the vertex number of the "q" polyhedron,
a denotes the number of the polyhedron for the central point of which equation (1) is written, N is the total number of polyhedrons, $f_{\xi\chi}$ is the demagnetization coefficients or the field strength component H_ξ in the "a" polyhedron produced by the magnetization component $M_\chi = 1.0$ of the "q" polyhedron. The procedure for the calculation of $f_{\xi\chi}$ has been described in ref. [4].

$H_{\xi ca}$ is the magnetic field of the magnet excitation coil at the "a" polyhedron centroid in the absence of the magnet iron. The method for the $H_{\xi ca}$ computation for a coil of an arbitrary 3-dimensional configuration has been given in ref. [5].

$H_{\xi a}$, $H_{\chi q}$ are the known field intensity components at the polyhedron centroids. Their total number is 3N. The nonlinearity of system (1) is due to the nonlinear dependence in (2).

In order to reduce the number of equations and unknowns in the cases, when the magnet configuration has planes of symmetry in a properly chosen coordinate system, set (1) is written only for the polyhedrons in the first octant. For the calculation of the contribution to the second term and the right-hand side in (1) from the remaining part of the magnet, situated in the other octants, it is convenient to express the coordinates, the field components and the current densities in these octants by the corresponding quantities in the first octant. If there is only one plane of symmetry (fig.1a) this is achieved by means of the transformations

$$\vec{X}_{1\xi} = I_\chi \cdot \vec{X}_0, \quad (3)$$

$$\vec{H}_{1\xi} = N_\xi \cdot I_\chi \cdot \vec{H}_0, \quad (4)$$

$$\vec{j}_{1\xi} = -N_\xi \cdot I_\chi \cdot \vec{j}_0, \quad (5)$$

where $\vec{x}_0 = \begin{pmatrix} x \\ y \\ z \end{pmatrix}$ is the radius vector of a point in the first octant, $\vec{X}_{1\xi}$ is the radius vector of the point reflected in the coordinate plane, which is normal to the ξ axis,

$$I_\chi = \begin{pmatrix} 1-2\delta_{x\xi} & 0 & 0 \\ 0 & 1-2\delta_{y\xi} & 0 \\ 0 & 0 & 1-2\delta_{z\xi} \end{pmatrix}, \quad (6)$$

where

$$\delta_{\chi\xi} = \begin{cases} 0, & \chi \neq \xi \\ 1, & \chi = \xi \end{cases}, \quad (7)$$

$$N_\xi = \begin{cases} 1 \text{ in the case of reflection of the field vector in the specified plane,} \\ -1 \text{ in the case of antisymmetry,} \end{cases} \quad (8)$$

$\vec{j}$ is the current density vector. The sign of reflection in the current transformation is opposite to the sign of field reflection according to

$$\vec{H} = 4\pi/C \cdot \mathrm{rot}\, j \quad (9)$$

Reflection in two coordinate planes is characterized by the following transformations:

$$\vec{X}_{2\xi} = I_{xx} \cdot \vec{X}_0 , \quad (10)$$

$$\vec{H}_{2\xi} = N_\xi \cdot N_{\xi 1} \cdot I_{xx} \cdot \vec{H}_0 , \quad (11)$$

$$\vec{j}_{2\xi} = N_\xi \cdot N_{\xi 1} \cdot I_{xx} \cdot \vec{j}_0 , \quad (12)$$

where ξ_1 is obtained from ξ by cyclic permutation according to the following rule

$$x \rightarrow z \rightarrow y \rightarrow x ,$$

$$I_{xx} = \begin{pmatrix} (1-2\delta_{x\xi})(1-2\delta_{y\xi}) & 0 & 0 \\ 0 & (1-2\delta_{y\xi})(1-2\delta_{z\xi}) & 0 \\ 0 & 0 & (1-2\delta_{z\xi})(1-2\delta_{x\xi}) \end{pmatrix} \quad (13)$$

In this case the reflection in the specified planes of symmetry is carried out at first according to (3)-(5) and then according to (10)-(12) (fig.1b).

For the reflection in all coordinate planes we have

$$\vec{X}_{3\xi} = I_{xxx} \cdot X_0 , \quad (14)$$

$$\vec{H}_{3\xi} = N_x \cdot N_y \cdot N_z \cdot I_{xxx} \cdot \vec{H}_0 , \quad (15)$$

$$\vec{j}_{3\xi} = -N_x \cdot N_y \cdot N_z \cdot I_{xxx} \cdot \vec{j}_0 , \quad (16)$$

where

$$I_{xxx} = (1-2\delta_{x\xi})(1-2\delta_{y\xi})(1-2\delta_{z\xi}) . \quad (17)$$

The reflection is carried out successively according to (3)-(5) and (10)-(12) in all coordinate planes and according to (14)-(16) in any, but only one symmetry plane (fig. 1c).

Some remarks on the numerical solution of the system of nonlinear equations (1) will be made now. The strong nonlinearity and the great number of the unknowns, in general, make the problem of finding a solution to system (1) a difficult task even when using powerful computers. Therefore, the choice of a suitable numerical method with fast convergence which requires small storage and allows comparatively crude initial approximations, is of great importance. In this connection the method of conjugate gradients (Klessig-Polak's algorithm[6]) and a modification of the Gauss-Newton method, the so-called autoregularized Gauss-Newton iterative process (ARP-F), implemented in the REGN subroutine[7], were tried. Both methods are computationally stable. The method of conjugate gradients requires smaller storage (of the order of the number of unknowns, i.e. about 3N) than the Gauss-Newton process, which requires storage of the order of $9N^2$ (note that by the method of conjugate gradients the sum of residuals of equations (1) was minimized). But the second method converges faster than the first one. Moreover, the automatic choice of the regularization parameter, depending on the behaviour of iterative process criteria, is an advantage of the second method as well. The demagnetization coefficients $f_{\xi_a x}$ and the right-hand side $H_{\xi ca}$ were calculated in advance and were kept in the external memory of the CDC-6400 computer. The solution was considered to be found when

$$\max_i |\varepsilon_i| \leq 10^{-9} \text{ and } \sum_{i=1}^{3N} \varepsilon_i^2 \leq 10^{-19} , \quad (18)$$

where ε_i are the residuals of equations (1).

The numerical experiments showed that the method of conjugate gradients converges much more slowly and requires greater computer time than the autoregularized Gauss-Newton process. This has led to the conclusion that

that its application for the solution of system (1) is inexpedient, though it requires smaller storage than the Gauss-Newton method. Besides, for the solution of (1), when the number of the unknowns is great, the autoregularized Gauss-Newton iterative process can be modified with the help, e.g., of the method described in ref. /8/, for the inversion of large matrices with the use of the external memory.

Finally, mention that in some particular cases, e.g., when iron is saturated, system (1) can be solved by the method of successive approximations, which does not require large storage (as to the conditions of its application, see ref. /9/).

Here are the results of some numerical experiments, carried out with the use of the REGN subroutone (an autoregularized Gauss-Newton process). As a test problem, a pair of ring-shaped shims, placed in a uniform external magnetic field with the following components $H_x = 0$, $H_y = 0$, $H_z = 12050.7$ Oe, was chosen. A part of this system situated in the first octant was divided into 4 polyhedrons, as shown in fig. 2. The calculation was made by taking into account the field symmetry with respect to the planes XOZ, YOZ and its antisymmetry with regard to the XOY plane. The right-hand side of set (1) multiplied by 0.1 was used as an initial approximation. The solution of (1) for this problem was obtained in 7 iterations for 9 seconds CDC-6400 computing time. As a verification the same configuration was calculated by the difference method implemeted in the POISSON program /10/ in the cylindrical coordinate system with the boundary conditions shown in fig. 2. In the absence of the ring-shaped shims these boundary conditions produce a uniform field having the components $H_x = 0$, $H_y = 0$, $H_z = 12050.7$ Oe.

In both calculations the distributions of the fields at $z = 0$, reduced to the same external field level, coincide everywhere, except the region of $10\ \text{cm} < r < 13\ \text{cm}$ with an accuracy of 1% from the contribution of the shims to the field. The difference in the results near the boundary ($A_r = \text{const.}$) is due to the calculation error in the POISSON program which arises from the artificial localization of the field by the boundary conditions. Magnetization inside the shims computed by the difference method varied within the limits $4\pi M_z = 14.0\text{-}16.6$ kGauss. By the integral equation method it was found to be $4\pi M_z \approx 14.3$ kGauss. This is a satisfactory coincidence keeping in mind the small number of polyhedrons. The results were additionally checked by computing the field of a pair of ring-shaped shims, whose magnetization was $4\pi M_x = 0$, $4\pi M_y = 0$, $4\pi M_z = 14.3$ kGauss by the method described in ref. /11/. The result obtained nearly coincides with that of the calculation by the integral equation method.

A serious test for the developed system of programs was the computation of a real C-shaped magnet, the configuration of one quarter of which is shown in fig. 3. The first octant of the magnet was divided into 48 polyhedrons with constant magnetization, as shown in fig. 3. Most of the elements of the division were situated near the working gap of the magnet at $z = 0$. The initial approximation was $H_{\xi a} = 0.001$ Oe, $\xi = x, y, z$, $a = 1, 2, \ldots, N$. The calculation of this problem required about 6 hours of the CDC-6400 computing time and about 200 iterations. The results of the computation of the magnetic field in the $z = 0$ plane along the mid-line of the magnet pole $x = 0$ is given in fig. 4, in comparison with the experimental curve for the same Ampere-turns Iw = 11985. As is evident from the figure, the field dependence on "y" has wavy behaviour in accordance with the structure of the magnet pole division into polyhedrons. In order to obtain the computed field close to the experimental one, the gap between the magnet poles being so small and the magnetization distribution inside the magnet iron being strongly non-uniform, it is necessary, apparently, to increase the

number of elements, into which the pole is divided, approximately twice. However, as it follows from the experience gained during the calculation of the magnet divided into 48 polyhedrons such a problem cannot be solved with the use of the CDC-6400 computer because of the central memory and computing time limitations. Its solution requires the use of a computer of CDC-7600 type. In fact, it turns out that with the help of the created system of programmes 3-dimensional configurations with a comparatively large working region, free of iron (e.g., magnets of bubble chambers), can be calculated using the CDC-6400 computer.

The authors are pleased to thank E.P.Zhidkov and N.L.Zaplatin for their continous interest and encouragement during the preparation of this work. The authors are also indebted to T.N.Dudareva for her help in carrying out the calculations and designing the results.

References

1. A.G.A.Armstrong, C.J.Collie et al., Proc. 5th Int.Conf. on Mag.Techn.,Frascati, 1975.
2. O.V.Tozoni, "CALCULATION OF 3-DIMENSIONAL ELECTROMAGNETIC FIELDS","Technica"Publishing House, Kiev, 1974.
3. N.J.Newman, C.W.Trowbridge, L.R.Turner. Proc. 4th Int. Conf. on Mag.Tech., Brookhaven, 1972.
4. M.Odyniec, S.B.Vorozhtsov, JINR Communcation E9-8811, 1975.
5. A.A.Halacsy, Univ. of Nevada, Reno, Engineering Rep. No.40, 1970.
6. E.Polak, "NUMERICAL METHODS OF OPTIMIZATION", "Mir" Publishing House, 1974, p.351.
7. L.Aleksandrov, JINR preprint P9-7259, Dubna, 1973.
8. L.Fox. An Introduction to Numerical Linear Algebra. Oxford University Press, 1965.
9. A.U.Luccio. University of Maryland, Technical Report No. 74-104, 1974.
10. K.Halbach, R.Holsinger, S.Magyary. Proceedings of the 5th Int. Conf. on Magnet Technology, Frascati, 1975.
11. V.I.Danilov, N.L.Zaplatin et al. Preprint P-702, JINR, Dubna, 1961.

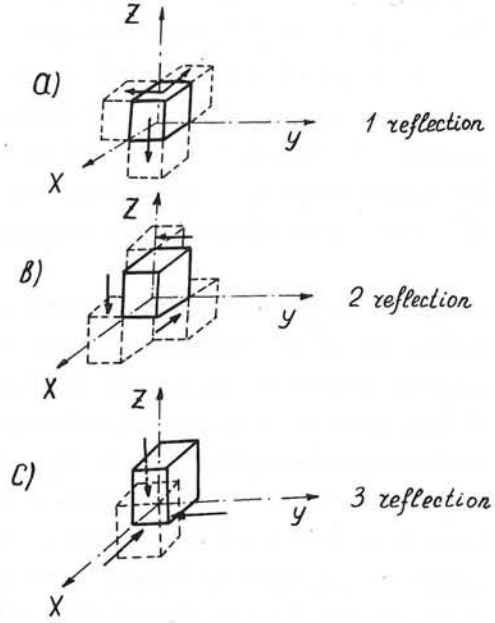

Fig.1. Magnet symmetry.

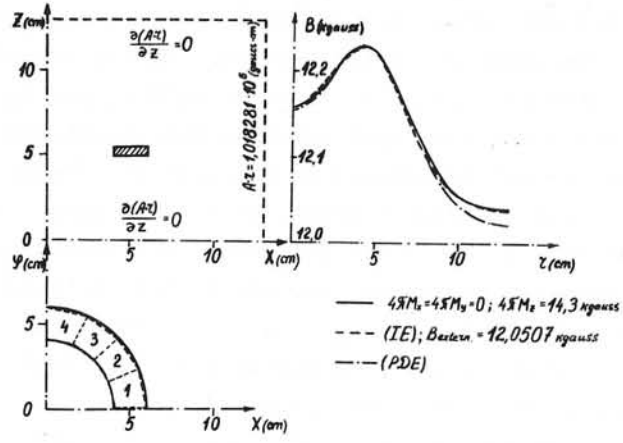

Fig. 2. Test problem .

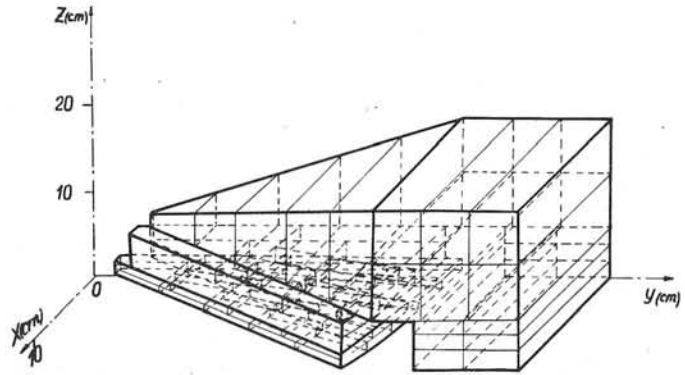

Fig. 3. C-shaped magnet .

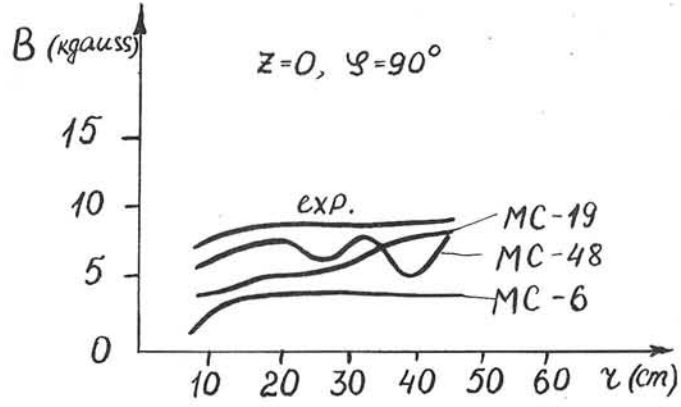

Fig.4. Results of calculations of the C-shaped magnet .

MAGNETIC FIELDS AND POTENTIALS OF LINEARLY VARYING CURRENT OR MAGNETISATION IN A PLANE BOUNDED REGION

C J Collie
Rutherford Laboratory, Chilton, Didcot, Oxon, OX11 0QX

ABSTRACT

In magnetic field problems solutions are obtained using the integral equation method by discretising the material and by assuming the functional form of the source (current or magnetisation) in each element.

The assumptions made here are that the source density is a linear function of the coordinates and that the elementary volume has plane sides (that is either a polyhedron or its limiting cases of plane polygon and infinite prism). The potentials and field are then expressed as a summation over the faces, edges and corners of the elements involving only elementary functions, and all the coefficients are tabulated.

It is also shown that the same technique is applicable to integral boundary method problems making the same assumptions.

1. INTRODUCTION

1.1 Task. The task of this paper is to calculate the effect of current or magnetisation sources at a point in terms of the density of the sources: which is the central task in solving magnetic field problems by integral equation methods. This cannot be done explicitly in general so simplifying assumptions must be made. Those used here are:

(a) The material is divided into elements with plane sides. In the general case treated in paragraphs 2-3, 5-7, this is a polyhedron. The special cases of a plane polygon, eg. a current sheet, and an infinite prism are examined in paragraphs 4 and 8 respectively.

(b) The source density is a linear function of the coordinates. This includes constant density as a special case and the method could be extended to higher order polynomials. In paragraph 7 the parameters of the linear function are assumed to be the values of the source at the corners, elsewhere this is immaterial.

1.2 Notation. This is exemplified in Figure 1.2.1, which shows a typical face and edge of the elementary volume. The field point x has Cartesian coordinates x_i (i = 1, 2, 3) and a typical source point x' has coordinates x'_i. Most of the analysis is performed in terms of the relative coordinate $U_i = x'_i - x_i$. The summation convention is used throughout. Thus for example:

$(\nabla \times \underline{A})_i = \varepsilon_{ijk} \frac{\partial A_k}{\partial x_j}$, with ε_{ijk} the totally antisymmetric form.

$r = (U_i U_i)^{\frac{1}{2}}$ = distance between x and x'

$R = (U_i U_i)^{\frac{1}{2}}$ (i = 1, 2) used in paragraph 8.

(ξ, η, ζ) are the coordinates in a rotated frame with the ζ axis normal to a face and the η axis perpendicular to an edge. The differentials of volume, surface normal, and 2-dimensional edge normal are denoted by dV, dS_i, dL_i. Other symbols are defined as they are introduced.

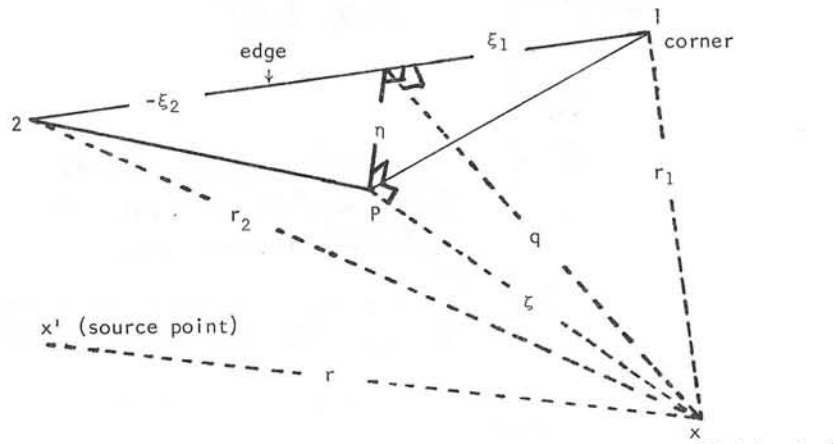

FIGURE 1.2.1 - THE VOLUME ELEMENT

2. FORMULATION OF POTENTIALS AND FIELDS IN 3 DIMENSIONS

The integral forms for relating current and magnetisation to potential and field may be found in (1) or (5) e.g. In SI units they are:

Vector potential due to current:

$$A_i(x) = \frac{\mu_o}{4\pi} \int J_i(x') \{\frac{1}{r}\} \, dV \qquad (2.1)$$

Field due to current:

$$B_i(x) = \varepsilon_{ijk} \frac{\partial A_k}{\partial x_j} = \varepsilon_{ijk} \frac{\mu_o}{4\pi} \int J_k(x') \{\frac{U_j}{r^3}\} dV \qquad (2.2$$

Magnetic scalar potential due to magnetisation:

$$U(x) = \frac{-1}{4\pi} \int M_i(x') \{\frac{U_i}{r^3}\} dV \qquad (2.3)$$

Vector potential due to magnetisation:

$$A_i(x) = \frac{-\mu_o}{4\pi} \int \varepsilon_{ijk} M_j(x') \{\frac{U_k}{r^3}\} dV \qquad (2.4)$$

Field due to magnetisation:

$$B_i(x) = \varepsilon_{ijk} \frac{\partial A_k}{\partial X_j}(x) = -\mu_o \frac{\partial U(x)}{\partial x_i}$$

$$= \frac{\mu_o}{4\pi} \int M_j(x') \{\frac{3U_iU_j}{r^5} - \frac{\delta ij}{r^3}\} \, dV \qquad (2.5)$$

Evaluation of these integrals is to be carried out for the volume described in paragraph 1 for the case when the sources J_i and M_i are linear functions of x'. Since $U_i = x'_i - x_i$ the sources are therefore also linear functions of U. The integrals needed are thus just the terms in braces in (2.1) - (2.5), and U_m multiplied by these terms.

3. REDUCTION OF VOLUME TO SURFACE INTEGRALS

All the integrals which are shown to be needed in paragraph 2 can be obtained by successive differentiation of the source point - field point distance r. To avoid confusion with the components of some vector r_i we denote this by R and indicate differentiation with respect to U_i by a subscript. That is R_{ij} means $\partial^2 R/\partial U_i \partial U_j$. We then obtain the following scheme:

$R = r = (U_iU_i)^{\frac{1}{2}}$

Differentials of R

General Forms	Contractions
$R_i = \frac{U_i}{r}$	
$R_{ij} = \frac{-U_iU_j}{r^3} + \frac{\delta_{ij}}{r}$	$R_{ii} = \frac{2}{r}$
$R_{ijk} = \frac{3U_iU_jU_k}{r^5} - \frac{\delta_{ij}U_k}{r^3} - \frac{\delta_{jk}U_i}{r^3} - \frac{\delta_{ki}U_j}{r^3}$	$R_{ijj} = -\frac{2U_i}{r^3}$
$R_{ijkk} = 2\{\frac{3U_iU_j}{r^5} - \frac{\delta_{ij}}{r^3}\}$	$R_{iijj} = -8\pi\,\delta(\underline{r})$

TABLE 3.1 - DIFFERENTIALS OF r. ($\delta(\underline{r})$ IN THE THREE-DIMENSIONAL DIRAC δ FUNCTION)

Since all the integrands of paragraph 2 are either entries in Table 3.1 or combinations of them, and all the entries are differentials of the line above, their integrals are immediately expressible as integrals over the surface. R_{ij} is given as an example to explain the method and notation, and the results for all of them are tabulated in Table 3.2:

$$\int R_{ij} \, dV = \int \partial/\partial U_j \, (R_i) \, dV = \int R_i dS_j = \int (U_i/r) \, dS_j \qquad (3.2)$$

Since the surface consists of plane faces, the direction of dS_j is constant over each face. Introducing new axes so that the new U_3 axis is parallel to dS_i, (that is along the outward normal) the face will have the equation $U_3 = \zeta$, where ζ is the distance from the field point to the face (see Figure 1.2.1). The rotation is carried out using the rotation matrix a_{ij} defined so that the relation between the new (starred) axes and the old is:

$$U_i^* = a_{ji}U_j \; ; \; U_i = a_{ij}U_j^* , \; a_{ik}a_{jk} = a_{ki}a_{kj} = \delta_{ij} \qquad (3.3)$$

Then (3.2) gives:

$$\int R_{ij}\, dV = \sum_{faces} \int (1/r) a_{im} U_m^* \, a_{j3}\, dS \qquad (3.4)$$

Where $dS_3 = dS$ and a_{j3} are the direction cosines of the outward normal to the face. A two-dimensional vector $V_i = [U_1^*, U_2^*]$ is introduced and $U_3^* = \zeta$. (3.4) then becomes:

$$\int R_{ij}\, dV = \sum_{faces} \int a_{j3} \left(a_{i3} \frac{\zeta}{r} + a_{ip} \frac{V_p}{r}\right) dS \qquad (3.5)$$

(p = 1,2 only)

Note that $a_{ip} V_p = (U_i - a_{i3}\zeta)$ and is invariant under rotations about the U_3^* axis, which leave a_{j3} unchanged. a_{ip} is therefore a two-dimensional vector. In Table 3.2 the integrands of the other R's are similarly decomposed into ζ and V_p parts.

Term	Integrand of dS for face with normal along a_{j_3}
R_i	$a_{i3}\, r$
R_{ij}	$a_{i3}(a_{j3} \frac{\zeta}{r} + a_{jp} \frac{V_p}{r})$
R_{ii}	$\frac{\zeta}{r}$
R_{ijk}	$a_{i3}(-a_{j3}a_{k3} \frac{\zeta^2}{r^3} - \zeta a_{j3}\zeta a_{kp} \frac{V_p}{r^3} - a_{k3}\zeta a_{jq} \frac{V_q}{r^3} - a_{jp}a_{kq} \frac{V_p V_q}{r^3} + \frac{\delta_{jk}}{r})$
R_{ijj}	$a_{i3}(\frac{2}{r})$
R_{ijkk}	$a_{i3}\,(-2a_{j3} \frac{\zeta}{r^3} - 2a_{jp} \frac{V_p}{r^3})$
R_{iijj}	$-2 \frac{\zeta}{r^3}$ (integrates to - 2 x solid angle subtended by the face)

TABLE 3.6 - FIRST INTEGRALS OF THE DIFFERENTIALS OF R

The entries in this table are not unique since it is only over a closed surface that the integral theorem:

$$\int \frac{\partial \phi}{\partial U_i}\, dV = \int \phi\, dS_i$$

can be applied. Thus the entry for R_{ij} is not symmetrical, and it would even be possible to write perversely:

$$\int R_{ijj}\, dV = \int \frac{\partial}{\partial U_j} R_{ij} = \int \left(- \frac{U_i U_j}{r^3} + \frac{\delta_{ij}}{r} \right) dS_j$$

$$= \int \left(- \zeta a_{ip} \frac{V_p}{r^3} + a_{i3}\left(-\frac{\zeta^2}{r^3} + \frac{1}{r}\right)\right) dS$$

instead of:

$$\int R_{ijj}\, dV = \frac{\partial}{\partial U_i} R_{jj}\, dV = \int \frac{2}{r}\, dS_i = \int a_{i3} \left(\frac{2}{r}\right) dS$$

The forms chosen are the simplest ones.

4. SURFACE INTEGRALS IN THREE DIMENSIONS

The expressions (3.6) may arise without immediately deriving from integration of (2.1) - (2.5). Thus in solving problems by Green's theorem methods the starting point will be Green's second theorem:

$$4\pi\phi(x) = - \int \nabla^2 \phi \; \frac{1}{r}\, dV + \int \frac{1}{r} \frac{\partial \phi(x')}{\partial x'_i}\, dS_i + \int \phi(x') \frac{U_i}{r^3}\, dS_i \qquad (4.1)$$

relating the value of the potential $\phi(x)$ to its value and normal gradient on the surface of the volume. For linear problems the first right-hand side term is zero. The solution of the simplified equation so obtained may be attempted by approximating the surface by a set of plane facets and assuming constant or linearly varying behaviour for ϕ and $\partial\phi/\partial x'_i$ on each facet. When this is done all the required integrals occur in (3.6).

Another case is the idealization called a current sheet. A surface current density K_i, has potentials and fields corresponding to (2.1) - (2.2):

$$A_i = \frac{\mu_o}{4\pi} \int K_i(x') \left\{\frac{1}{r}\right\} dS \qquad (4.2)$$

$$B_i = \varepsilon_{ijk} \frac{\partial A_k}{\partial x_j} = \varepsilon_{ijk} \frac{\mu_o}{4\pi} \int K_k(x') \frac{U_j}{r^3} dS \qquad (4.3)$$

Again, on the assumption of linear variation for K_i. all the integrals are in (3.6). A magnetostatics program based on (4.1) is described in[2] and the eddy current program of [3] includes current sheets.

5. REDUCTION OF SURFACE TO LINE INTEGRALS

The integrals of (3.6) may be integrated further by an extension of the technique of paragraph 3. Corresponding to R we now need two generating functions denoted by M and Q and defined in (5.1)

$M = r^3/9 + \zeta^2 r/3 - \frac{1}{3}\|\zeta\|^3 \log(\zeta + \|\zeta\|)$; $r = (V_i V_i + \zeta^2)^{\frac{1}{2}}$
$M_i = r\,V_i/3 + \zeta^2\,V_i/3r - \|\zeta\|^3\,V_i/3r\,(r + \|\zeta\|)$
$Q = \|\zeta\| \log(r + \|\zeta\|)$
$Q_i = \frac{\|\zeta\|\,V_i}{r(r + \|\zeta\|)}$ (Definitions of M and Q)
$M_{ii} = r \equiv P$ (Definition of P)
$P_i = \frac{V_i}{r}$
$P_{ij} = -\frac{V_i V_j}{r^3} + \frac{\delta_{ij}}{r}$
$P_{ii} = \frac{\zeta^2}{r^3} + \frac{1}{r}$ $\qquad$ $Q_{ii} = \frac{\zeta^2}{r^3}$
$(P_{ii} - Q_{ii}) = \frac{1}{r} \equiv T$ (Definition of T)
$T_i = -\frac{V_i}{r^3}$

TABLE 5.1 - DIFFERENTIALS OF M AND Q

Every entry in (3.6) can be expressed as a combination of those in (5.1), so they can all be integrated. P_{ij} is given as an example:

$$\int P_{ij}\,dS = \int \partial P_i/\partial V_j dS = \int P_i\,dL_j = \int V_i/r\,dL_j \qquad (5.2)$$

Since the boundaries of the face are the edges of the polyhedron, the direction of dL_j is constant for each edge. If a_{ij} is chosen so that the V_2 axis is along the outward normal to edge, then the equation of the edge is $V_2 = \eta$ with $\eta = a_{j2}U_j$, a constant. Call this new rotation matrix b_{ij}; it is a particular a_{ij} which is completely determined while a_{ij} fixed only the 3-axis in the transformed system. For convenience c_{ij} is introduced to connect a_{ij} and b_{ij}:

$$U_i^{**} = b_{ij}U_j = c_{ki}U_k^{*} = c_{ki}a_{jk}U_j$$

with

$$U_3^{**} = U_3^{*} = \zeta,\ U_2^{**} = \eta;\ c_{k3} = c_{3k} = \delta_{3k} \qquad (5.3)$$

Of course only b_{ij}, the fully determined form, can occur in the results. Note that there is a b_{ij} for every edge in every face. (5.2) to (5.3) give:

$$\int P_{ij}dS = \sum_{\text{edges}} \int c_{ik} \frac{V_k^{*}}{r} c_j\ dw = \sum_{\text{edges}} \int \left(c_{i1}\frac{w}{r} + c_{i2}\frac{\eta}{r}\right) c_{j2}\ dw \qquad (5.4)$$

where $w = V_1^{*} = b_{i1}U_i$ is the remaining variable. The w axis is along the edge and the perpendicular from field point to the edge has w = 0 (see Figure 1.2.1).

The tables which follow give firstly the separation into η and w parts for the entries in (5.1), secondly the expressions for the first integrals of R in terms of the differentials of M and Q, and thirdly the second integrals of R.

Integrand	Integral for edge normal to b_{i_2}
M_{ii}	$\eta \frac{r}{3} + \frac{\zeta^2\eta}{3} - \frac{\lvert\zeta\rvert^3\eta}{3r(r+\lvert\zeta\rvert)}$
P_i	$c_{i_2} r$
P_{ij}	$c_{i_2} (c_{j_2} \frac{\eta}{r} + c_{j_1} \frac{w}{r})$
P_{ii}	$\frac{\eta}{r}$
Q_{ii}	$\frac{\lvert\zeta\rvert \eta}{r(r+\lvert\zeta\rvert)}$
T	$\frac{\eta}{r} - \frac{\lvert\zeta\rvert \eta}{r(r+\lvert\zeta\rvert)}$
T_i	$c_{i_2} \frac{1}{r}$

TABLE 5.5 - INTEGRALS OF M AND Q DIFFERENTIALS

Integrand	Integral
R_i	$a_{i3} M_{pp}$
R_{ij}	$a_{i_3} (a_{j_3\tau} T + a_{jp} P_p)$
R_{ii}	ζT
R_{ijk}	$a_{i_3}(a_{j_3}a_{k_3}(2T-P_{pp}) + (a_{j_3}a_{kp}+a_{k_3}a_{jp})\zeta T_p + a_{jp}a_{kq}P_{pq}$
R_{ijj}	$a_{i\,3}(2T)$
R_{ijkk}	$a_{i_3}(-2a_{j_3} \frac{Q_{pp}}{\zeta} + 2a_{jp}T_p)$
R_{iijj}	$-2 \frac{Q_{pp}}{\zeta}$

TABLE 5.6 - FIRST INTEGRALS IN M Q FORM

TERM	INTEGRAND OF dw FOR EDGE NORMAL TO b_{j2}
R_i	$b_{i_3}(\eta\frac{r}{3} + \zeta^2 \frac{\eta}{3r} - \frac{\lvert\zeta\rvert^3\eta}{r(r+\lvert\zeta\rvert)})$
R_{ij}	$b_{i_3}(b_{j_3}\zeta(\frac{\eta}{r} - \frac{\lvert\zeta\rvert\eta}{r(r+\lvert\zeta\rvert)}) + b_{j_2}r)$
R_{ii}	$\zeta(\frac{\eta}{r} - \frac{\lvert\zeta\rvert\eta}{r(r+\lvert\zeta\rvert)}$
R_{ijk}	$b_{i_3}(b_{j_3}b_{k_3}(\frac{\eta}{r} - \frac{2\lvert\zeta\rvert\eta}{r(r+\lvert\zeta\rvert)} + (b_{j_3}b_{k_2}+b_{k_3}b_{j_2})\frac{\zeta}{r} + b_{j_2}(b_{k_2}\frac{\eta}{r}+b_{k_1}\frac{w}{r}))$
R_{ijj}	$b_{i_3}(\frac{2\eta}{r} - \frac{2\lvert\zeta\rvert\eta}{r(r+\lvert\zeta\rvert)}$
R_{ijkk}	$b_{i_3}(-2b_{j_3}\frac{\lvert\zeta\rvert}{\zeta}\frac{\eta}{r(r+\lvert\zeta\rvert)} + 2b_{j_2}\frac{1}{r})$
R_{iijj}	$-2\frac{\lvert\zeta\rvert}{\zeta}\frac{\eta}{r(r+\lvert\zeta\rvert)}$

TABLE 5.7 - SECOND INTEGRALS OF THE DIFFERENTIALS OF R

6. FORM OF RESULTS

6.1 Third Integration. To complete the derivation of closed expressions for integrals of all the required forms it is necessary to give the definite integrals of the 4 functions appearing in (5.7) or (5.5) and to show that the original symmetries are restored when the sums over the edges and faces are performed.

Taking the integrals first we have simply:

$$\int_{\zeta_2}^{\zeta_1} r\, dw = \frac{(r_1 + r_2)}{4\ell}\left((r_1 - r_2) + \ell^2\right) + \frac{q^2}{2}\log\left(\frac{(r_1 + r_2 + \ell)}{(r_1 + r_2 - \ell)}\right)$$

$$\int_{\zeta_2}^{\zeta_1} \frac{dw}{r} = \log\left(\frac{r_1 + r_2 + \ell}{r_1 + r_2 - \ell}\right)$$

$$\int_{\zeta_2}^{\zeta_1} \frac{w}{r}\, dr = r_1 - r_2 \qquad (6.1.1)$$

$$\int_{\zeta_2}^{\zeta_1} \frac{\eta}{r(r + |\zeta|)} = 2\left[\tan^{-1}\frac{\xi_1}{(r_1 + |\zeta|)}\,\frac{\eta}{(r_1 + q)} - \tan^{-1}\frac{\xi_2}{(r_2 + |\zeta|)}\,\frac{\eta}{(r_2 + q)}\right]$$

Where ξ_1, ξ_2 are the w coordinates of the end points of the edge, $\ell = \xi_1 - \xi_2$ is the length of the edge, and $q = (\zeta^2 + \eta^2)^{\frac{1}{2}}$ is the distance of the field point from the line. (See Figure 1.2.1). The last expression in (6.1) is $|\zeta|/\zeta$ x the solid angle subtended by the area P12 in Figure 1.2.1. Note that the log term in (6.1.1) is unbounded on the edge. R_{ijkk} and T_i are the only forms containing this term without a protecting factor.

6.2 Restoring Symmetry. The only apparently unsymmetric form in (5.5) is P_{ij} which is:

$$\int P_{ij}\, dS = \sum_{\text{edges}} \int c_{i_2}\left(c_{j_2}\frac{\eta}{r} + c_{j_1}\frac{w}{r}\right) dw$$

Only the second term in this is unsymmetrical. Its value by (6.1.1) is $c_{i_2}c_{j_1}(r_1 - r_2)$. The same value of r as r_1 occurs in the adjacent side of the face (see Figure 6.2.1) as r_2'. So each corner coordinate occurs in a combination like:

$$c_{i_2}c_{j_1} - c'_{i_2}c'_{j_1} \qquad (6.2.1)$$

Now c_{ij} rotates simply in the plane of the face. So (6.2.1) is of the form:

$$\begin{bmatrix} -\sin\theta\cos\theta & -\sin^2\theta & 0 \\ \cos^2\theta & \sin\theta\cos & 0 \\ 0 & 0 & 1 \end{bmatrix} - \begin{bmatrix} -\sin\theta'\cos\theta' & \sin^2\theta' & 0 \\ \cos^2\theta' & \sin\theta'\cos\theta' & 0 \\ 0 & 0 & 1 \end{bmatrix}$$

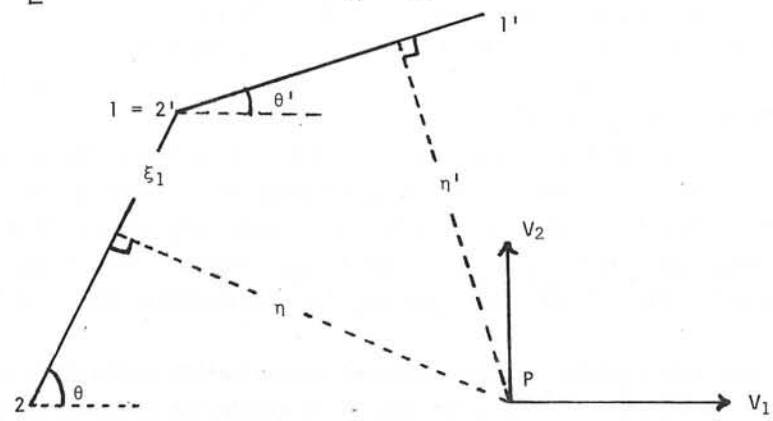

FIGURE 6.2.1 - RELATION BETWEEN ADJACENT c_{ij}

which is symmetrical on interchange of 1 and 2. The same argument shows the symmetry in jk of the last term of R_{ijk} in (5.7), since the b_{ij} for different edges in the same face are different c_{ij} multiplied by the same a_{ij}.

A different argument is required to restore the symmetry in i,j of the terms in (5.7). Thus the last term in R_{ij} is by (6.1.1).

$$\sum_{\text{faces}}\ \sum_{\text{edges}} \log\left(\frac{r_1 + r_2 + \ell}{r_1 + r_2 - \ell}\right) b_{i_3}\, b_{j_2} \qquad (6.2.2)$$

The same log term will thus occur twice for each edge, with the $b_{i_3}b_{j_2}$ for the two faces which join along the edge. Now the b_{j_2} in this case are not independent: since b_{j_3} is normal to the face, the edge $b_{j_1} = -b'_{j_1}$ must be parallel to $(\underline{b}_{j_3} \wedge \underline{b}'_{j_3})$, and b_{j_2} is $(\underline{b}_{j_3} \wedge \underline{b}_{j_1})$. Carrying out the vector products gives:

$$b_{i_3}b_{j_2} + b'_{i_3}b'_{j_2} = \frac{b_{i_3}b'_{j_3} + b_{j_3}b'_{i_3} - (b_{k_3}b'_{k_3})(b_{i_3}b_{j_3} + b'_{i_3}b'_{j_3})}{(1 - (b_{k_3}b_{k_3})^2)^{\frac{1}{2}}} \qquad (6.2.3)$$

which is symmetrical in i and j. The only remaining case is the symmetry between i and k of R_{ijk}. It has been shown to be symmetrical in j and k when the summation is carried out over all the edges on a face, by the argument of (6.2.1), and in i and j by that of (6.2.2) when both contributions to an edge are summed, from which it follows that it must be symmetrical in i and k when the whole summation is complete.

7. SINGULARITIES IN THE RESULTS

The integrals of (6.1.1) contain a solid angle term, which is discontinuous on the surface, and a log term which is unbounded on the edges of the volume. Inspection of (5.7) shows that these terms only occur without a protecting factor in R_{ijkk} and its trace R_{iikk}, which derive from the magnetisation field (2.5), and these only from the constant term in $M_j(x')$.

This means that a method based on constant magnetisation within each volume element, such as GFUN[4] can obtain the field within the iron only by an indirect averaging process, analogous to the Lorentz averaging by which H_i is derived from B_i within material, as described for example in[5]. Since a linear dependence for $M_j(x')$ also contains a constant term it might appear that the same is true for this case, but in fact these singularities and discontinuities can cancel out on internal edges and boundaries.

To see this it is necessary to look more fully at the linear magnetisation supposition. While any polyhedron can be used as element in the constant magnetisation case, the linear magnetisation case is likely to be used only with a tetrahedral element, the 4 corner values of magnetisation being just sufficient to determine the 4 parameters of the linear function $a_o + a_i x_i'$. Thus on defining $x_o' \equiv 1$, the supposition of linear magnetisation within the element amounts to saying that for some constants $N_{\alpha\beta}$

$$M_i(x') = M\alpha_i \, N_{\alpha\beta} x'_\beta \qquad (\alpha,\beta \text{ summed from 0-3}) \tag{7.1}$$

with $M\alpha_i = M_i(x\alpha)$; its value at the α^{th} corner. Setting $x' = x\gamma$ in (7.1)

$$M\gamma_i = M\alpha_i \, N_{\alpha\beta} x\gamma_\beta$$

$$\therefore \; N_{\alpha\beta} \, x\gamma_\beta = \delta\alpha\gamma \tag{7.2}$$

Substitute (7.1) into (2.5) and obtain:

$$B_i(x') = \frac{\mu_o}{4\pi} \int M\alpha_j \, N_{\alpha\beta} \, (U_\beta + x_\beta) \left(\frac{3U_i U_j}{r^5} - \frac{\delta_{ij}}{r^3}\right) dV \tag{7.3}$$

where $U_o' = 0$, $x_o = 1$.

The coefficient of $\int R_{ijkk} \, dV$ (see (3.7)) in B_i is therefore:

$$\frac{\mu_o}{8\pi} M\alpha_j \, N_{\alpha\beta} x_\beta \equiv W(x) \quad \text{(definition of W)} \tag{7.4}$$

Imagine the field point x approaching the corner $x\gamma$, that is $x_\beta = x\gamma_\beta + \varepsilon_\beta$ ($\varepsilon_o = 0$), where ε is an infinitesimal vector. Then by (7.2):

$$W(x\gamma + \varepsilon) = \frac{\mu_o}{8\pi} (M\gamma_j + M\alpha_j \, N_{\alpha\beta} \, \varepsilon_\beta) \tag{7.5}$$

Referring now to (5.7), consider the contributions to the field of the common face of 2 adjacent elements. The b_{j_3} are along the outward normal and thus simply change sign and the solid angle also changes sign. The b_{j_2} are equal since they are the outward normal to the edge, and the log term is the same for the two elements. The $M\gamma$ contribution in (7.5) will thus exactly cancel, and the contributions from other corners are $0(\varepsilon)$.

Now imagine x approaching not a corner but an edge. That is $x_\beta = (px\gamma_\beta + qx\delta_\beta + \varepsilon_\beta)$ with $p + q = 1$. Then similarly to (7.5) we have:

$$W(px\gamma + qx\delta + \varepsilon) = \frac{\mu_o}{8\pi} (pM\gamma_j + qM\delta_j + M\alpha_j N_{\alpha\beta} \, \varepsilon_\beta) \tag{7.6}$$

Again, considering adjacent elements, it is only the common corners which make finite contributions to W, and these exactly cancel. Similarly the field is continuous on crossing a face.

So the only troublesome points are on external corners and edges where physically iron will be saturated. Some special procedure must be adopted to deal with these, such as radiusing the corners or placing the nodes of

the mesh a little inside the material boundaries. Elsewhere the linear magnetisation supposition should provide directly values for the field within the iron and as (5.7) shows, requires the evaluation of exactly the same transendental functions, and no others, as constant magnetisation. A given mesh will generally contain fewer nodes than elements, so it should also be economical.

8. THE TWO DIMENSIONAL LIMIT

8.1 Formulation in two dimensions. A case of considerable practical interest, because set ups which approximate to it allow considerable computational savings, occurs when there is no variation of any quantity in one direction, so that the volume of interest becomes an infinite prism. The form the results obtained take in this case is not immediately apparent because such systems only approximate to reality when they are balanced. Without this restraint (2.1) diverges.

It is easier to start again with the relationships which connect sources, and fields in this case. They are[1], with subscripts indicating 2 vectors throughout.

Vector potential due to current:

$$A_i(x) = -\frac{\mu_o}{2\pi} \int j_i(x') \log R/a \, dS \qquad (8.1.1)$$

Field due to current:

$$B(x) = \varepsilon_{ij} \frac{\partial A_j}{\partial x_i} = \frac{\mu_o}{2\pi} \varepsilon_{ij} \int j_i(x') \frac{U_i}{R^2} \, dS \qquad (8.1.2)$$

(There is also the case when j_3 exists, but exactly the same integrals occur, so it is omitted.)

Magnetic Scalar potential due to magnetisation:

$$U(x) = \frac{-1}{2\pi} \int M_i(x') \frac{U_i}{R} \, dS \qquad (8.1.3)$$

Vector Potential due to magnetisation:

$$A(x) = -\frac{\mu_o}{2\pi} \int \varepsilon_{ij} \frac{M(x')}{R^2} U_j \, dS \qquad (8.1.4)$$

Field due to magnetisation:

$$B_i(x) = \varepsilon_{ij} \frac{\partial A(x)}{\partial x_j} = -\mu_o \frac{\partial U(x)}{\partial x_i} = \frac{\mu_o}{2\pi} \int M_j(x') \left(\frac{2U_iU_j}{R^4} - \frac{\varepsilon_{ij}}{R^2}\right) dS \qquad (8.1.5)$$

In which the constant a in (8.1.1) is quite arbitrary and is the trace of the fact that only balanced systems are meaningful, when it will cancel. The evaluations are to be carried out for $j_i(x')$ and $M_i(x')$ linear functions of x', or U. The area of integration is tne polygon of Figure 8.1.1, with the prism extending to ± infinity in the x_3 direction.

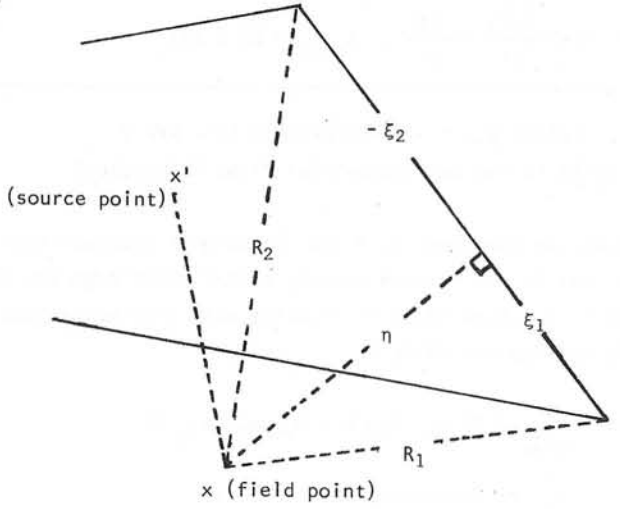

FIGURE 8.1.1 - REGION OF INTEGRATION FOR THE TWO-DIMENSIONAL LIMIT

8.2 Reduction of surface to line integrals. Analagously to the treatment of paragraph 3, all the required integrands can be derived in differentials of R^2 and $R^2 \log R$, according to the scheme of (8.2.1), setting the arbitrary constant a to 1.

$X = R^2 \log R, \quad Y = R^2$ (Definition of X and Y)
$X_i = 2U_i \log R + U_i \qquad Y_i = 2U_i$
$X_{ij} = 2\frac{U_iU_j}{R^2} + \delta_{ij}(1 + 2\log R), \; X_{ii} = 4 + 4\log R, \; Y_{ii} = 4$
$X_{ijk} = 2(-2\frac{U_iU_jU_k}{R^4} + \delta_{ij}\frac{U_k}{R^2} + \delta_{jk}\frac{U_i}{R^2} + \delta_{ki}\frac{U_j}{R^2})$
$X_{ijj} = 4\frac{U_i}{R^2}$
$X_{ijkk} = 4(-2\frac{U_iU_j}{R^4} + \frac{ij}{R^2}), \; X_{iijj} = 8\pi\delta(\underline{R})$

TABLE 8.2.1 - DIFFERENTIALS OF X AND Y
($\delta(\underline{R})$ is the two dimensional Dirac δ function)

Again analagously to paragraph 3, a two dimensional rotation matrix is introduced so that in the rotated system, a particular edge has the equation $U_2 = \eta$ = a constant. Then (3.3) still holds with sums understood as from 1 to 2 and the analogue of (3.4) is

$$\int X_{ij}\, dS = \sum_{\text{edge}} \int (2U_m^* \log R + U_m^*)\, a_{im}\, a_{j2}\, dL \qquad (8.2.2)$$

Introducing $V = U_1^*$, this becomes, since $dL = dL_1$

$$\int X_{ij}\, dS = \sum_{\text{edges}} \int a_{j2}\,(a_{i2}\,(2\eta \log R + \eta) + a_{i1}(2V \log R + V)\, dV \qquad (8.2.3)$$

Carrying out a similar procedure for each item in (8.2.7) gives Table 8.2.4, choosing the simplest of the non unique forms as in (3.6)

Term	
X_i	$a_{i2}\,(\eta^2 \log R + V^2 \log R)$
Y_i	$a_{i2}\,(\eta^2 + V^2)$
X_{ij}	$a_{i2}\,(a_{j2}\,(2\eta \log R + \eta) + a_{j1}\,(2V \log R + V))$
X_{ii}	$2\eta \log R + \eta$
Y_{ii}	2η
X_{ijk}	$a_{i2}\,(2a_{j2}a_{k2}\frac{\eta^2}{R^2} + 2a_{j2}a_{k1}\frac{\eta V}{R^2} + 2a_{k2}a_{j1}\frac{\eta V}{R^2} + 2a_{j1}a_{k1}\frac{V^2}{R^2} + \delta_{jk}(1 + 2\log R))$
X_{ijj}	$a_{i2}\,(4 + 4\log R)$
X_{ijkk}	$a_{i2}\,(4a_{j2}\frac{\eta}{R^2} + 4a_{j1}\frac{V}{R^2})$
X_{iijj}	$4\eta/R^2$

TABLE 8.2.4 - FIRST INTEGRALS OF THE DIFFERENTIALS OF X AND Y

The singular and discontinuous forms arising in (8.2.4) are:

$$\int_{\zeta_2}^{\zeta_1} \frac{V}{R^2} = \log R_1/R_2 \text{ and } \int_{\zeta_2}^{\zeta_1} \frac{\eta}{R^2} = \frac{|\eta|}{\eta} \times |\text{angle subtended by edge}| \qquad (8.2.5)$$

which can be shown to give rise to continuous fields internally for linear magnetisation in the same way as in paragraph 7.

9. REFERENCES

1. W R Smythe. Static and Dynamic Electricity
McGraw Hill 1968.

2. J Simkin, C W Trowbridge. Magnetostatic fields computed using an integral equation derived from Green's Theorems.
(These Proceedings)

3. C S Biddlecombe, C J Collie, J Simkin, C W Trowbridge. The Integral Equation Method Applied to Eddy Currents. (These Proceedings)

4. A G A M Armstrong, C J Collie, N J Diserens, M J Newman, J Simkin, C W Trowbridge. New Developments in the Magnet Design Computer Program GFUN. RL-75-066 and Proc. 5th Int. Conf. on Magnet Technology, Frascati, Rome, 1975.

5. F N H Robinson. Macroscopic Electromagnetism. Permagon Press 1973.

Non-divergent Vector Finite Elements for Magnetic Field Calculations

Z. J. Csendes

General Electric Company
Schenectady, New York 12345

Abstract

In this paper, a novel set of two and three-dimensional approximation functions are derived which satisfy the condition that their divergence equals zero. These functions are useful for approximating operator equations involving non-divergent magnetic field quantities. The application of these functions to two-dimensional finite element analysis is presented and the procedure is illustrated with the two-component vector magnetic field solution of a stranded, slot-embedded conductor.

1. Introduction

A large number of magnetic field problems are formulated in terms of non-divergent vector field quantities. Often the most convenient representation of these quantities is in terms of an operator equation in which the non-divergent nature of the field is not specified. For example, in three-dimensional magnetostatic problems, the vector potential must independently satisfy both a vector Poisson equation and the Coulomb gauge, and in magnetic field induction calculations [1,2], the current distribution must separately satisfy both a vector integral equation and a zero-divergence condition. For this reason, the numerical solution of vector magnetic field problems has remained limited to a few isolated cases [3,4], and most numerical work in magnetic field analysis has involved only the direct solution of one-component field quantities.

In this paper, a complete set of interpolatory polynomial vectors are derived which satisfy the condition that their divergence equals zero in a rectangular region. These polynomials form a natural set of approximating functions for non-divergent magnetic field quantities and eliminate the difficulty of imposing the zero-divergence condition on a numerical solution. Coupled with solution techniques derived from the finite element method, these polynomials constitute a powerful method of solving many two and three-dimensional magnetic field problems.

The remainder of this paper is divided into three main parts. Section 2 contains the definition and the derivation of interpolating non-divergent vector polynomials as well as a brief examination of some of their properties; Section 3 presents the application of these polynomials to the finite element method; and Section 4 describes the numerical solution of the two-component magnetic field distribution in a stranded, slot-embedded conductor.

2. Non-divergent Polynomial Vectors

2.1 Definition

The finite element analysis of a two-component non-divergent vector field requires the evaluation of polynomial vectors of the form

$$\bar{\alpha}_{ij}(x,y) = p_{ij}(x,y)\ \bar{I}_x + q_{ij}(x,y)\ \bar{I}_y \qquad (1)$$

in which $p_{ij}(x,y)$ and $q_{ij}(x,y)$ are polynomials of minimal order satisfying the following properties:

(i) $p_{ij}(x,y)$ and $q_{ij}(x,y)$ are product separable, i.e., it is possible to write $p_{ij}(x,y)$ and $q_{ij}(x,y)$ in the form

$$p_{ij}(x,y) = X_i(x)\ Y_j(y) \qquad (2)$$

$$q_{ij}(x,y) = -W_i(x)\ Z_j(y) \qquad (3)$$

(ii) The functions $p_{ij}(x,y)$ and $q_{ij}(x,y)$ interpolate on an m by n grid of points (a_i,b_j):

$$p_{ij}(a_k,b_\ell) = \delta_{ij}^{k\ell} \qquad i,k = 1,\ldots,m \quad j,\ell = 1,\ldots,n \qquad (4)$$

$$q_{ij}(a_k,b_\ell) = 0$$

It is assumed throughout that $a_i \neq a_j$ and that $b_i \neq b_j$ if $i \neq j$.

(iii) The vector $\bar{\alpha}_{ij}(x,y)$ has zero divergence

$$\nabla \cdot \bar{\alpha}_{ij}(x,y) = 0 \qquad (5)$$

2.2 Admissible Forms

Conditions (i) and (iii) may be combined to yield the following equations

$$\frac{\partial X_i(x)}{\partial x} = \lambda W_i(x) \qquad (6)$$

$$\frac{\partial Z_j(y)}{\partial y} = \lambda Y_j(y) \qquad (7)$$

Equations (6) and (7) provide the divergence condition in terms of the functions $X(x)$, $Y(y)$, $W(x)$ and $Z(y)$. Since the relative magnitudes of X and Y and of W and Z are arbitrary, without loss of generality it is possible to set $\lambda = 1$.

Since $p_{ij}(x,y)$ and $q_{ij}(x,y)$ are polynomials, the functions $X_i(x)$ and $Z_j(y)$ may be represented as

$$X_i(x) = \sum_{k=0}^{M} \alpha_k^i \, x^k \qquad (8)$$

$$Z_j(y) = \sum_{k=0}^{N} \beta_k^j \, y^k \qquad (9)$$

where M and N are the orders of $X_i(x)$ and of $Z_i(y)$, respectively, and the coefficients α_k^i and β_k^i are to be determined. According to equations (6) and (7) the functions $W_i(x)$ and $Y_j(y)$ are polynomials of order one less than the polynomials $X_i(k)$ and $Z_j(y)$, respectively.

The interpolation conditions (ii) may be stated in terms of the functions $X_i(x)$, $Y_j(y)$, $W_i(x)$ and $Z_j(y)$ by substituting (2) and (3) into (4). This gives

$$\begin{aligned} X_i(a_k) &= \delta_{ik} \\ Y_j(b_\ell) &= \delta_{j\ell} \\ W_i(a_k) &= 0 \\ Z_j(b_\ell) &= 0 \end{aligned} \qquad (10)$$

These equations imply, respectively, that (a) the points $x = a_k$, $k=1,\ldots,i-1,i+1,\ldots,m$ are the roots of the polynomial $X_i(x)$; (b) the points $y = b_k$, $k=1,\ldots,j-1,j+1,\ldots,n$ are roots of the polynomial $Y_j(y)$; (c) the points $x = a_k$, $k-1,\ldots,m$ are roots of $W_i(x)$; and that (d) the points $y = b_k$, $k-1,\ldots,n$ are roots of $Z_j(y)$. Thus there are M+m+1 free parameters x_k in $X_i(x)$ and M+m+1 free parameters w_k in $W_i(x)$. Equating the derivative of $X_i(x)$ to $W_i(x)$ results in M-1 equations in 2M-2m unknowns. (The value of $\alpha_M^i \, \beta_N^j$ is set in the normalization $p_{ij}(a_i,b_j)=1$). A unique solution of this system is therefore possible if and only if

$$M = 2m-1 \qquad (11)$$

A similar reasoning with $Y_j(y)$ and $Z_j(y)$ implies that

$$N = 2n-1 \qquad (12)$$

2.3 Explicit Representation

Evaluating the derivative of $X_i(x)$ at the points $x=a_p$ and setting the result equal to $W_i(a_p)$ leads to the equations

$$X_i(x) = \alpha_m^i (x-x_i) \, A_i(x) \qquad (13)$$

$$W_i(x) = \alpha_m^i \, A_i(x) + (x-x_i) A_i'(x) \qquad (14)$$

where $A_i'(x)$ is the derivative of $A_i(x)$ and

$$A_i'(x) = \prod_{\substack{k=1 \\ k\neq i}}^{m} (x-a_k)^2 \qquad (15)$$

$$x_i = a_i + \frac{A_i(a_i)}{A_i'(a_i)} \qquad (16)$$

In the same way, it follows that

$$Z_j(y) = \beta_N^j (y-b_j)\ B_j(y) \tag{17}$$

$$Y_j(y) = \beta_N^j\ B_j(y) + (y-b_j)\ B_j'(y) \tag{18}$$

where

$$B_j(y) = \prod_{\substack{k=1 \\ k\neq l}}^{n} (y-b_k)^2 \tag{19}$$

One final condition needs to be imposed on the polynomials. This is the condition that

$$p_{ij}(a_i,b_j) = 1 \tag{20}$$

Evaluating the expressions $X_i(a_i)$ and $Y_j(b_j)$ and substituting into (20) gives

$$\alpha_M^i\ \beta_N^j = \frac{A_i'(a_i)}{A_i^2(a_i)B_j(b_j)} \tag{21}$$

One possible set of solutions of this equation is

$$\alpha_M^i = \frac{A_i'(a_i)}{A_i^2(a_i)}$$

$$\beta_N^j = \frac{1}{B_j(b_j)} \tag{22}$$

2.4 Further Properties

One of the most interesting properties of non-divergent vector interpolation polynomials is their relationship to Gaussian quadrature formulas. Since the polynomial $X_i(x)$ is of order 2m-1, it can be integrated exactly by the quadrature formula

$$\int w(x)X_i(x)dx = \prod_{l=1}^{m} X_i(a_l)C_l^m \tag{23}$$

where $w(x)$ is a weighting function and the C_l^m are quadrature weights with a degree of precision 2m-1. Taking the points a_i to coincide with the nodes a_l used in the quadrature, (23) reduces to

$$\int w(x)X_i(x)dx = C_i^m \tag{24}$$

A similar reasoning with $Y_j(y)$, $W_i(x)$ and $Z_j(y)$ gives

$$\int w(y)Y_j(y)dy = C_j^n$$

$$\int w(x)W_i(x)dx = 0 \tag{25}$$

$$\int w(y)Z_i(y)dy = 0$$

Thus, there obtains the following remarkable result: the application of a Gaussian quadrature formula to a two-dimensional scalar field is equivalent to approximating the scalar field with one component of a two-component non-divergent polynomial vector field, the integral of the second component of which is zero.

In three dimensions, non-divergent vector interpolation polynomials are obtained by taking

$$\bar{\gamma}_{ijk}(x,y,z) = X_i(x)\ Y_i(y)\ Y_k(z)\ \bar{I}_x + W_i(x)\left[X_j(y) - Z_j(y)\right]Y_k(z)\bar{I}_y - W_i(x)W_j(y)Z_k(z)\bar{I}_z \tag{26}$$

Furthermore, in the cylinderical coordinate system, the following three-component vector is both interpolatory and non-divergent

$$\bar{\gamma}_{ijk}(r,z,\theta) = \frac{1}{r}\ X_i(r)\ Y_j(z)\ Y_k(\theta)\bar{I}_r + \frac{1}{r}\ W_i(r)\left[X_j(z)-Z_j(z)\right]Y_k(\theta)\bar{I}_z - W_i(r)W_j(z)Z_k(\theta)\bar{I}_\theta \tag{27}$$

3. Vector Finite Element Formulation

3.1 Variational Expression

In a number of magnetic field problems, a two-component vector field $\bar{V}$

$$\bar{V} = \begin{bmatrix} V_x \\ V_y \end{bmatrix} \tag{28}$$

must be both non-divergent

$$\frac{\partial V_x}{\partial x} + \frac{\partial V_y}{\partial y} = 0 \tag{29}$$

and satisfy the operator equation

$$(\mathcal{L} + \lambda)\bar{V} = \bar{F} \tag{30}$$

where λ is a constant, $\bar{F}$ is a two-component forcing function and $\mathcal{L}$ is the operator

$$\mathcal{L} = \begin{bmatrix} \nabla^2 & 0 \\ 0 & \nabla^2 \end{bmatrix} \tag{31}$$

It is well known that an energy functional corresponding to the operator equation (30) is given by [5]

$$\mathcal{F}(\bar{V}) = \int \bar{V}^T(\mathcal{L}+\lambda)\bar{V}d\Omega - 2\int \bar{V}^T\bar{F}\, d\Omega \tag{32}$$

where Ω is the region of integration. Applying Green's first identity to equation (32) results in

$$\mathcal{F}(\bar{V}) = -\int (G\bar{V})^T(G\bar{V})d\Omega + \lambda \int \bar{V}^T\bar{V}d\Omega - 2\int \bar{V}^T\bar{F}\, d\Omega \tag{33}$$

where G is the matrix

$$G = \begin{bmatrix} \partial/\partial_x & 0 \\ \partial/\partial_y & 0 \\ 0 & \partial/\partial_x \\ 0 & \partial/\partial_y \end{bmatrix} \tag{34}$$

Consequently, an approximate solution of the operator equation (30) subject to the divergence condition (29) may be obtained by extremizing the functional $\mathcal{F}(\bar{V})$ in equation (33) in the space of non-divergent two-component vectors $\bar{V}$.

3.2 Non-divergent Basis Functions

An arbitrary, non-divergent two-component vector $\bar{V}$ may be approximated in a rectangular region by the vector

$$\bar{V}(x,y) = \sum_{i=1}^{m}\sum_{j=1}^{n} K_{ij}\bar{\alpha}_{ij}(x,y) + \sum_{i=1}^{m}\sum_{j=1}^{n} L_{ij}\bar{\beta}_{ij}(x,y) \tag{35}$$

where K_{ij} and L_{ij} are arbitrary coefficients and $\bar{\alpha}_{ij}(x,y)$ and $\bar{\beta}_{ij}(x,y)$ are the vectors

$$\bar{\alpha}_{ij}(x,y) = \begin{bmatrix} P_{ij}(x,y) \\ q_{ij}(x,y) \end{bmatrix} \tag{36}$$

$$\bar{\beta}_{ij}(x,y) = \begin{bmatrix} q_{ji}(x,y) \\ P_{ji}(x,y) \end{bmatrix} \tag{37}$$

Substituting equation (35) into equation (33), differentiating $\mathcal{F}(\bar{V})$ with respect to K_{rs} and setting the result equal to zero yields

$$-\sum_{i=1}^{m}\sum_{j=1}^{n} K_{ij}\int\{\frac{\partial p_{ij}}{\partial x}\frac{\partial p_{rs}}{\partial x} + \frac{\partial p_{ij}}{\partial y}\frac{\partial p_{rs}}{\partial y} + \frac{\partial q_{ij}}{\partial x}\frac{\partial q_{rs}}{\partial x} + \frac{\partial q_{ij}}{\partial y}\frac{\partial q_{rs}}{\partial y}\}d\Omega$$

$$+ \lambda \sum_{i=1}^{m}\sum_{j=1}^{n} K_{ij}\int\{p_{ij}\,p_{rs} + q_{ij}\,q_{rs}\}d\Omega \tag{38}$$

$$= \sum_{i=1}^{m}\sum_{j=1}^{n} F_{x_{ij}}\int\{p_{ij}\,p_{rs} + q_{ij}\,q_{rs}\}d\Omega$$

where $F_{x_{ij}}$ are the coefficients of the x-component of $\bar{F}$. A similar equation is obtained for L_{ij}.

3.3 Vector Notation

Introducing the vector notation

$$\tilde{X}(x) = [X_1(x) \quad X_2(x) \quad \ldots \quad X_m(x)]$$

$$K = \begin{bmatrix} K_{11} & \cdots & K_{1n} \\ \vdots & & \vdots \\ K_{m1} & \cdots & K_{mn} \end{bmatrix} \tag{39}$$

equation (38) may be written in the matrix form

$$-2\, I_{WW}\, K\, J_{YY}^T - I_{XX}\, K\, J_{UU}^T - I_{VV}\, K\, J_{ZZ}^T + \lambda\,(I_{XX}\, K\, J_{YY}^T + I_{WW}\, K\, J_{ZZ}^T) = I_{XX}\, F_x\, J_{YY}^T + I_{WW}\, F_x\, J_{ZZ}^T \tag{40}$$

where I_{AA} and J_{AA} are the integrals

$$I_{AA} = \int \tilde{A}^T(x)\, \tilde{A}(x)\,dx \qquad J_{AA} = \int \tilde{A}^T(y)\, \tilde{A}(y)\,dy \tag{41}$$

and $\tilde{U}(y)$ and $\tilde{V}(x)$ are the vectors

$$\tilde{U}(y) = \frac{\partial \tilde{Y}(y)}{\partial y} \qquad \tilde{V}(x) = \frac{\partial \tilde{W}(x)}{\partial x} \tag{42}$$

Finally, applying the vec operation to both sides of equation (40) gives (vec $M = [M_1^T \ldots M_n^T]^T$ where M_i is the $i^{\underline{th}}$ column of a matrix M)

$$-(2\, J_{YY} \textcircled{X} I_{WW} + J_{UU} \textcircled{X} I_{XX} + J_{ZZ} \textcircled{X} I_{VV})\,\text{vec } K + \lambda\,(J_{YY} \textcircled{X} I_{XX} + J_{ZZ} \textcircled{X} I_{WW})\,\text{vec } K = (J_{YY} \textcircled{X} I_{XX} + J_{ZZ} \textcircled{X} I_{WW})\,\text{vec } F_x \tag{43}$$

where $\textcircled{X}$ denotes the Kronecker product $A \textcircled{X} B = (a_{ij} B)$ [6].

A very similar development differentiating $\mathcal{G}(\bar{V})$ with respect to the coefficients L_{rs} results in the equation

$$-(2\, J_{WW} \textcircled{X} I_{YY} + J_{VV} \textcircled{X} I_{ZZ} + J_{XX} \textcircled{X} I_{UU})\,\text{vec } L + \lambda\,(J_{WW} \textcircled{X} I_{ZZ} + J_{XX} \textcircled{X} I_{YY})\,\text{vec } L = (J_{WW} \textcircled{X} I_{ZZ} + J_{XX} \textcircled{X} I_{YY})\,\text{vec } F_y \tag{44}$$

Equations (43) and (44) provide two uncoupled matrix equations to be solved for the unknown coefficients K_{ij} and L_{ij}.

4. Application to Slot-Embedded Conductors

4.1 Discretization

Figure 1(a) provides a descriptive picture of a slot-embedded conductor including the adjacent air-gap region, indicating the locations of the conducting strands and the regions of insulation. A finite element discretization corresponding to this conductor using rectangular elements is presented in Figure 1(b). This Figure also presents the boundary conditions which need to be satisfied by the magnetic field components B_x and B_y.

Assuming that there are no source currents, the magnetic field in a slot-embedded conductor satisfies equations (29) and (30) with $\bar{V} = \bar{B}$, $\bar{F} = 0$ and $\lambda = -j\omega\mu\sigma$ in the conducting regions, $\lambda = 0$ in the non-conducting regions. Consequently, the analysis in the previous sections may be applied directly to solve the slot-embedded conductor problem in Figure 1.

The lowest order non-divergent polynomial vectors occur by taking m=n=2 in equation (4). In this case, letting the interpolation nodes correspond to the corners of the rectangle $-a \le x \le a$, $-b \le y \le b$, the interpolation polynomials become

$$\begin{aligned} X_1(x) &= X_2(-x) = (x-a)^2\,(x+2a)/4a^3 \\ Y_1(y) &= Y_2(-y) = (y-b)(3y+b)/4b^2 \\ W_1(x) &= W_2(-x) = 3(x-a)\,(x+a)/4a^3 \\ Z_1(y) &= Z_2(-y) = (y+b)(y-b)^2/4b^2 \\ V_1(x) &= V_2(-x) = 3x/2a^3 \\ U_1(y) &= U_2(-y) = (3y-b)/2b^2 \end{aligned} \tag{45}$$

Using these polynomials, the integrals I_{AA} and J_{AA} in equations (43) and (44) are easily evaluated; the numerical values obtained are presented in Table 1.

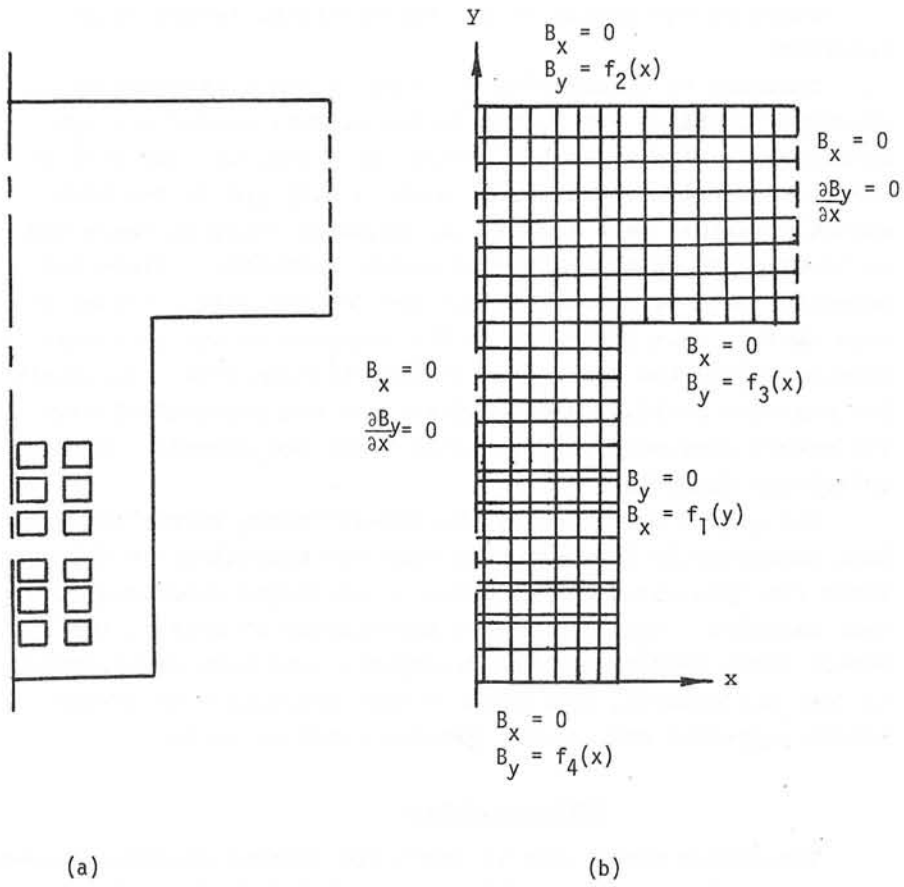

Figure 1. (a) Typical slot-embedded conductor geometry showing the conducting strands, the liquid cooling ducts and the adjacent airgap.

(b) Rectangular finite element subdivision of the slot-embedded conductor geometry in (a) and a description of the boundary conditions satisfied by the magnetic field.

Table 1. Numerical values of the matrices I_{AA} (or of J_{AA} with a replaced by b) evaluated using the interpolation polynomials in equation (45). The matrices are symmetric with $I_{AA}(2,1) = I_{AA}(1,2)$ and $I_{AA}(2,2) = I_{AA}(1,1)$.

A	$I_{AA}(1,1)$	$I_{AA}(1,2)$
X	26a/35	9a/35
Y	4a/15	-a/15
W	3/5a	3/5a
Z	$8a^3/105$	$6a^3/105$
V	$3/2a^3$	$-3/2a^3$
U	2/a	-1/a

4.2 Solution

For the purposes of the present investigation, a computer program was written to assemble and solve equations (43) and (44) for the x and y components of the magnetic field for the problem in Figure 1. The program accepts as data the slot width and the slot depth, the airgap thickness and the tooth spacing, as well as the locations of the conducting strands.

Taking the boundary condition forcing functions to be of the form

$$\begin{aligned} f_1(y) &= C_1 x + C_2 \\ f_2(x) &= -1.0 \\ f_3(x) &= -0.37 \\ f_4(x) &= -0.10 \end{aligned} \qquad (46)$$

where C_1 and C_2 are constants, the magnetic field distribution in Figure 2 results. In this Figure, lines of equal magnetic flux magnitude have been plotted, since this plot is easier to comprehend than separate plots of the x and y components of the complex-valued magnetic field.

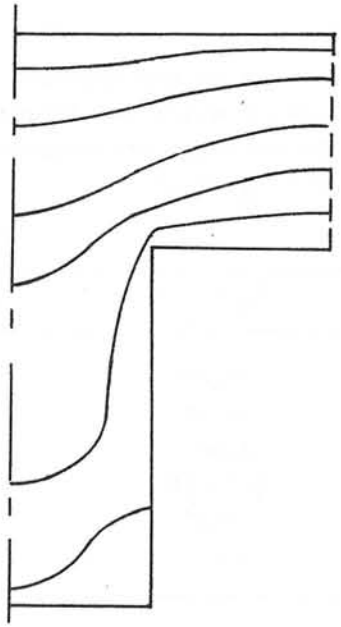

Figure 2. A plot of the equi-magnitude lines of the magnetic field for the problem in Figure 1.

5. Conclusions

A finite element method has been developed for the solution of magnetic field problems involving non-divergent vector field quantities. The method is based on the use of non-divergent vector approximation polynomials, which are derived in this paper. Although the finite element formulation presented is specifically designed to solve two-component vector field problems, extension to three-component vector fields is straight-forward since three-component non-divergent polynomials may be obtained from the two-component non-divergent polynomials, as shown in Section 2.4.

As a simple illustration of the application of the vector finite element method, a two-component vector solution of the magnetic field in a slot-embedded conductor is presented in this paper. Although the procedure employed treats the x and y-components of the magnetic field independently, non-divergence of the solution vector is assured by the choice of the non-divergent vector basis functions.

Compared to alternative analyses of the slot-embedded conductor problem, the vector finite element method has two advantages. First of all, in both the classicial analysis of the slot-embedded conductor problem [7,8,9] and in the more recent numerical work [10,11] the magnetic field is described in terms of an axially directed vector potential. Since the magnetic field is defined as the curl of the vector potential, this implies that the error in the computer vector potential is exaggerated by the process of differentiation used to obtain the magnetic field. This limitation is not encountered with the method presented in this paper since the magnetic field is solved for directly.

The second advantage of the non-divergent vector formulation presented in this paper is that the approximation functions are "pre-screened" in order to eliminate undesired divergent behavior. The alternative possibility of solving the vector field problem and the divergence condition simultaneously (as, for example, described in [4]) presents much larger matrix equations and, hence, greater computer costs.

Acknowledgement

The author would like to thank the General Electric Company for permission to publish this paper and M.V.K. Chari for discussions about the slot-embedded conductor problem.

References

1. Z.J. Csendes, A. Gopinath and P. Silvester, "Generalized matrix inverse techniques for local approximations of operator equations", in The Mathematics of Finite Elements and Applications, J.R. Whiteman (ed.), London: Academic Press, pp. 189-199, 1973.

2. A. Gopinath and P. Silvester, "Calculation of inductance of finite-length strips and its variation with frequency", IEEE Trans. Microwave Theory Tech., vol. MTT-21, pp. 380-386, 1973.

3. S. Sackett, "Solution of the magnetostatics problem in three space dimensions", Proceedings of the Second Conference on Analysis of Magnetic Fields, University of Nevada, Reno, Nevada, pp. 67-75, 1969.

4. H. Okuda, T. Kawamura and M. Nishi, "Finite element solution of magnetic field and eddy current problems in the end zone of turbine generators", IEEE Power Engineering Society Winter Meeting, Paper A 76 141-2, New York, 1976.

5. I. Stakgold, Boundary Value Problems of Mathematical Physics, New York: MacMillan, 1968.

6. C.R. Rao and S.K. Mitra, Generalized Inverse of Matrices and its Applications, New York: John Wiley, 1971.

7. L.V. Bewley, Two-dimensional Fields in Electrical Engineering, New York: Dover, 1963.

8. J. Lammeraner and M. Stafl, Eddy Currents, London: Iliffe Books, 1966.

9. R.L. Stoll, The Analysis of Eddy Currents, Oxford: Clarendon Press, 1974.

10. P. Silvester, "Dynamic resistance and inductance of slot-embedded conductors", IEEE Trans. Power Apparatus and Systems, vol. PAS-87, pp. 250-256, 1968.

11. A. Konrad, J.L. Conlomb, J.C. Sabonnadiere, and P. Silvester, "Finite element analysis of steady state skin effect in a slot-embedded conductor", IEEE Power Engineering Society Winter Meeting, New York, 1976.

A GENERALIZED FINITE DIFFERENCE METHOD FOR THE COMPUTATION OF ELECTRIC AND MAGNETIC FIELDS

by G.B. Denegri, G. Molinari, A. Viviani
Electrical Engineering Department, University of Genoa
Viale Causa 13, 16145 Genoa, Italy

1. Abstract

A generalized form of the finite difference method is proposed to solve boundary value problems of the elliptic type, such as stationary magnetic or electric field problems.

The new method allows us to use grid forms of the type usually adopted by the finite-elements method.

In such a grid, the internal elliptic equations and the boundary and interface conditions can be discretized by expressing the potential V by a Taylor series expansion stopped at the N-order terms around any gridpoint. The particular procedure used produces an algebraic system which is better conditioned with respect to the ones typical of traditional finite-difference problems, and is very similar to those common to the finite-elements method. The new method eliminates completely the difficulties usually presented by the finite-difference method in the treatment of boundary and interface conditions. A comparison with the finite-elements method can give various results, because both methods present various implementation forms. However, the proposed method seems to warrant higher precision, especially when interface conditions are involved.

2. Introduction

At the present time, as far as the numerical solution of field problems is concerned, the finite-elements method is generally considered more powerful than the finite-difference one. This is essentially due to the fact that the finite-elements method allows us to introduce a non-ordered set of gridpoints; on the contrary, the finite-difference method requires a set of gridpoints arranged at the intersections of two or three orthogonal sheaves of straight lines. Almost any other advantage of the finite-elements method depends on this fact. It allows us to optimize the gridpoints distribution on the basis of the geometry of the problem. Besides, it eliminates the cumbersome interpolation procedures required by the finite-difference method at the boundary and interface conditions, which cause difficulties in inverting the algebraic system obtained by the discretization, owing to the increase in the matrix band amplitude.

The introduction of curvilinear grids into the finite-difference method[1,2] reduces the difficulties in adapting the grid to the problem, though the interpolation procedures at the boundary and interface conditions are still necessary.

As a consequence, the finite-elements grid structure remains more versatile, especially when complicated boundary shapes are concerned.

However, the finite-difference method turns out to be inadequate especially because it is applied in a restrictive version, which wastes some of the method's features.

A generalized form of the finite-difference method is presented here, which can be considered on the same level as the finite-elements one, and can be more suitable to particular problems.

For the sake of simplicity, the generalized procedure is described in the case of bidimensional problems requiring only scalar potentials. Its extension to tridimensional problems is an easy matter.

3. The definition of the problem

Let us consider a boundary value problem defined at any continuity point of a set D in the x-y-plane by a second order linear partial differential equation of the elliptic type, given in the form:

$$a_{20}\frac{\partial^2 V}{\partial x^2} + a_{02}\frac{\partial^2 V}{\partial y^2} + a_{11}\frac{\partial^2 V}{\partial x \partial y} + a_{10}\frac{\partial V}{\partial x} + a_{01}\frac{\partial V}{\partial y} + a_{00}V = f_0 \qquad (3.1)$$

where a_{20}, ... , a_{00} and f_0 are constant or given functions of x, y. On the boundary of the set D, the following general conditions are imposed:

$$b_1 V + b_2\frac{\partial V}{\partial n} = f_1 \qquad (3.2)$$

where b_1, b_2 and f_1 are constant or given functions of x, y, and n is the inward normal to the boundary. The set D can be divided into partial subsets D_i. On their interfaces, the following conditions hold:

$$V_j = V_k + f_2 \tag{3.3}$$

$$c_j \frac{\partial V_j}{\partial n_j} + c_k \frac{\partial V_k}{\partial n_k} = f_3 \tag{3.4}$$

where j and k are subscripts referring to regions D_j and D_k; c_j, c_k, f_2, f_3 are constant or given functions of x, y, and n_j, n_k are the inward normals to the boundaries of D_j and D_k.

4. The discretization of the partial differential problem

The generalization of the finite-difference method proposed requires the introduction of a grid of the type used in the finite elements procedure (Fig. 1).

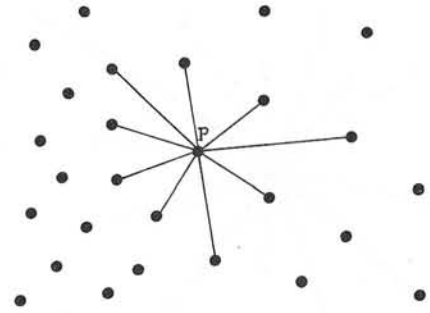

Fig. 1 - M-point star around an internal gridpoint P (case with N=3, M=9)

At any internal gridpoint P, the potential V can be expressed by a Taylor series expansion, stopped at the N-order terms, of the form:

$$V = \sum_{0}^{N} n \sum_{l+m=n} \frac{1}{l!m!} \left.\frac{\partial^n V}{\partial x^l \partial y^m}\right|_P (x - x_P)^l (y - y_P)^m \tag{4.1}$$

Then, the potential must be computed at M=(N+1)(N+2)/2-1 gridpoints around P, generally at the M gridpoints nearest to P (Fig. 1). At the gridpoints P_i (i=1,M), we have:

$$V_{Pi} - V_P = \sum_{1}^{N} n \sum_{l+m=n} \frac{1}{l!m!} \left.\frac{\partial^n V}{\partial x^l \partial y^m}\right|_P (x_{Pi} - x_P)^l (y_{Pi} - y_P)^m \tag{4.2}$$

Eqs. (4.2) form a system of M equations in the M unknowns $\left[\partial^n V/(\partial x^l \partial y^m)\right]\Big|_P$. This system can be solved and gives the M potential derivatives as functions of the potential values at the M gridpoints around P

$$\left.\frac{\partial^n V}{\partial x^l \partial y^m}\right|_P = \sum_{1}^{M} i \; A_{lmi} (V_{Pi} - V_P) \tag{4.3}$$

Then, eq. (3.1) can be discretized by using eqs. (4.3). Substitution into eq. (3.1) gives an algebraic equation of the form:

$$V_P = \sum_{1}^{M} i \; B_i V_{Pi} + B_0 \tag{4.4}$$

where

$$B_i = \frac{\sum_{1}^{2} n \sum_{l+m=n} a_{lm} A_{lmi}}{\sum_{1}^{2} n \sum_{l+m=n} a_{lm} \sum_{1}^{M} i \; A_{lmi} - a_{00}} \tag{4.5}$$

$$B_0 = - \frac{f_0}{\sum_{1}^{2} n \sum_{l+m=n} a_{lm} \sum_{1}^{M} i \; A_{lmi} - a_{00}} \tag{4.6}$$

The coefficients A_{lm} are functions of the coordinates of the gridpoints x_{Pi}, y_{Pi}, x_P, y_P, and consequently the coefficients B_i and B_o can be computed as functions of the above coordinates and of the values of a_{lm} and f_o at P.

5. The discretization of the boundary conditions

The boundary conditions of the type (3.2) can be imposed provided that a suitable number of gridpoints are arranged on the boundary lines (Fig. 2). The discretization procedure, which must be applied to any boundary gridpoint where $b_2 \neq 0$, is similar to the one described in the previous Section.

By means of the expansion (4.1) applied to a boundary gridpoint P, we can compute the potential at M-1 gridpoints P_i (i=1,M-1) around P, ge-

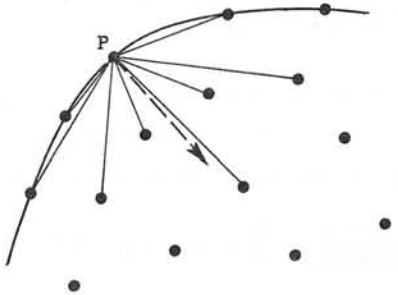

Fig. 2 - (M-1)-point star around a boundary gridpoint P (case with N=3,M=9).

nerally at the M-1 gridpoints nearest to P (Fig. 2). This procedure gives M-1 equations of the type (4.2). A system of M equations is obtained by introducing the following expression of the normal potential derivative:

$$\left.\frac{\partial V}{\partial n}\right|_P = \left.\frac{\partial V}{\partial x}\right|_P \left.\frac{\partial x}{\partial n}\right|_P + \left.\frac{\partial V}{\partial y}\right|_P \left.\frac{\partial y}{\partial n}\right|_P = \left.\frac{\partial V}{\partial x}\right|_P n_x + \left.\frac{\partial V}{\partial y}\right|_P n_y \qquad (5.1)$$

where $\bar{n}=(n_x,n_y)$ is the unit vector normal to the boundary at P (Fig. 2). The inversion of the system made up of eqs. (4.2) and (5.1) gives the M potential derivatives as functions of both the potential values at the M-1 gridpoints around P and the normal derivative:

$$\left.\frac{\partial^n V}{\partial x^l \partial y^m}\right|_P = \sum_1^{M-1} i \; A_{lmi}(V_{Pi} - V_P) + A'_{lmM}\left.\frac{\partial V}{\partial n}\right|_P \qquad (5.2)$$

The substitution of eq. (3.2) into eq. (5.2) gives:

$$\left.\frac{\partial^n V}{\partial x^l \partial y^m}\right|_P = \sum_1^{M-1} i \; A_{lmi}(V_{Pi} - V_P) + A_{lmM}\left(\frac{f_1}{b_1} - V_P\right) \qquad (5.3)$$

with

$$A_{lmM} = A'_{lmM}\frac{b_1}{b_2} \qquad (5.4)$$

Finally, the substitution of eqs. (5.3) into eq. (3.1) gives an algebraic equation of the form:

$$V_P = \sum_1^{M-1} i \; B_i V_{Pi} + B_0 \qquad (5.5)$$

where the coefficients B_i (i=1,M-1) are defined by relations of the form (4.5), whereas B_0 is given by:

$$B_0 = \frac{\sum_1^2 n \sum_{l+m=n} a_{lm}A_{lmM}\frac{f_1}{b_1} - f_0}{\sum_1^2 n \sum_{l+m=n} a_{lm}\sum_1^M i A_{lmi} - a_{00}} \qquad (5.6)$$

The above coefficients are functions of the coordinates of the gridpoints and of the values a_{lm}, f_0, f_1, b_1 and b_2 at P.

When $b_2=0$, the condition (3.2) reduces to a Dirichlet boundary condition, which can be directly introduced into the system.

6. The discretization of the interface conditions

The interface conditions (3.3), (3.4) must be imposed by introducing a suitable number of gridpoints on any interface line (Fig. 3). Due to eq. (3.3), which introduces a discontinuity into the potential, any interface

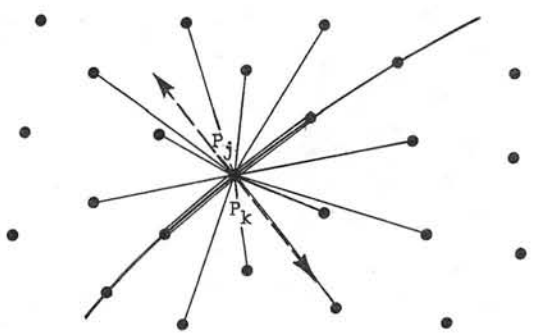

Fig. 3 - 2(M-1)-point star around an interface gridpoint P (case with N=3, M=9).

gridpoint P must be replaced by two separate gridpoints P_j and P_k, belonging to the two regions D_j and D_k separated by the interface line. The discretization procedure, which must be applied to any couple of interface gridpoints, follows directly from the one described in the previous Section.

By means of the expansion (4.1) applied to an interface gridpoint P_j (or P_k), we can compute the potential at M-1 gridpoints P_{ij} (or P_{ik}) (i=1, M-1) around P_j (or P_k), generally at the M-1 gridpoints nearest to P_j (or

P_k), all belonging to D_j (or D_k). A system of M equations is obtained by means of M-1 equations of the type (4.2) and of one equation of the type (5.1), obtained by suitably defining the normal derivative as function of the unit vector $\bar{n}_j=(n_{xj},n_{yj})$ or $\bar{n}_k=(n_{xk},n_{yk})$ normal to the boundary at P_j (or P_k) (see Fig. 3). The inversion of the system gives the M potential derivatives in D_j (or D_k) in a form similar to the one of eqs. (5.2). Then, the substitution of these equations into eq. (3.1) gives two equations of the form:

$$\left.\frac{\partial V_j}{\partial n_j}\right|_{P_j} = \sum_1^{M-1} i\ C_{ij}(V_{Pij} - V_{Pj}) + C_{Mj}V_{Pj} + C_{Oj} \qquad (6.1)$$

$$\left.\frac{\partial V_k}{\partial n_k}\right|_{P_k} = \sum_1^{M-1} i\ C_{ik}(V_{Pik} - V_{Pk}) + C_{Mk}V_{Pk} + C_{Ok} \qquad (6.2)$$

where, with reference to eqs. (5.2), it is, for j:

$$C_{ij} = -\frac{\sum_1^2 n \sum_{l+m=n} a_{lmj}A_{lmij}}{\sum_1^2 n \sum_{l+m=n} a_{lmj}A'_{lmMj}} \qquad (6.3)$$

$$C_{Mj} = -\frac{a_{00j}}{\sum_1^2 n \sum_{l+m=n} a_{lmj}A'_{lmMj}} \qquad (6.4)$$

$$C_{Oj} = \frac{f_{0j}}{\sum_1^2 n \sum_{l+m=n} a_{lmj}A'_{lmMj}} \qquad (6.5)$$

and analogously for k.

The substitution of eqs. (6.1), (6.2) into eqs. (3.3), (3.4) gives the algebraic equations:

$$V_{Pj} = \sum_1^{M-1} i\ B_{ij}V_{Pij} + \sum_1^{M-1} i\ B_{ik}V_{Pik} + B_O \qquad (6.6)$$

$$V_{Pk} = V_{Pj} - f_2 \qquad (6.7)$$

where:

$$B_{ij} = \frac{c_jC_{ij}}{c_j \sum_1^{M-1} i\ C_{ij} + c_k \sum_1^{M-1} i\ C_{ik} - c_jC_{Mj} - c_kC_{Mk}} \qquad (6.8)$$

$$B_{ik} = \frac{c_kC_{ik}}{c_j \sum_1^{M-1} i\ C_{ij} + c_k \sum_1^{M-1} i\ C_{ik} - c_jC_{Mj} - c_kC_{Mk}} \qquad (6.9)$$

$$B_O = \frac{c_jC_{Oj} + c_kC_{Ok} + c_k \sum_1^{M-1} i\ C_{ik}f_2 - c_kC_{Mk}f_2 - f_3}{c_j \sum_1^{M-1} i\ C_{ij} + c_k \sum_1^{M-1} i\ C_{ik} - c_jC_{Mj} - c_kC_{Mk}} \qquad (6.10)$$

The above coefficients are functions of the coordinates of the grid-points, of the values of a_{lm} and f_0 at P_j and P_k, of c_j at P_j, of c_k at P_k, and of f_2 and f_3 at P_j (or P_k, which is the same).

7. General features of the proposed method

On the whole, the algebraic equations (4.4),(5.5),(6.6) and (6.7) form an algebraic system of the type:

$$[B][V] = [F] \qquad (7.1)$$

whose solution can be found by various methods, depending on the properties of matrix [B]. Such properties are quite various, depending on the shape of the grid used; however, they generally seem very similar to those resulting from the finite-elements applications. The large number of implementation forms make difficult a general comparison between the new method and the most commonly used ones.

Once the solution of the system (7.1) has been obtained by direct or iterative methods, the new finite-difference scheme is particularly suitable to evaluate the field everywhere in the space. The potential and the field components at a given point Q can be computed by using the Taylor series expansion (4.1) and its derivatives relevant to the gridpoint P nearest to Q. The partial derivatives present in that series can now be evaluated as functions of the potential of the gridpoints near P by means of eqs. (4.3),(5.3), and so on.

The above potential and field computation procedure, which is valid for points not belonging to the grid, presents the same degree of approximation as that typical of the discretization procedure, and is particularly suitable to compute field values near a boundary or interface line, which

can be of notable interest and are usually computed with some difficulties.

8. Some remarks on the grid form

The method proposed can be implemented in various forms, depending on the grid chosen for the discretization.

The simplest form can be obtained in the case of a Taylor series expansion (4.1) stopped at the second order terms (N=2, M=5). In this case, the internal equations (4.4) involve five gridpoints P_i, in addition to the central one, P (Fig. 4). The boundary equations (5.5) involve four gridpoints (Fig. 5), and the interface equations (6.6) involve eight gridpoints

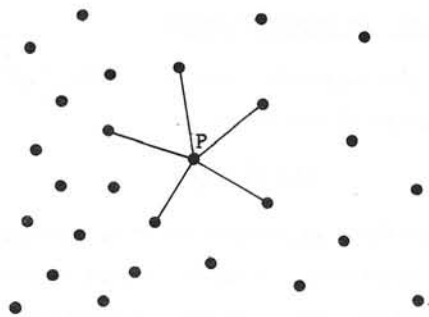

Fig. 4 - 5-point star around an internal gridpoint P (case with N=2,M=5).

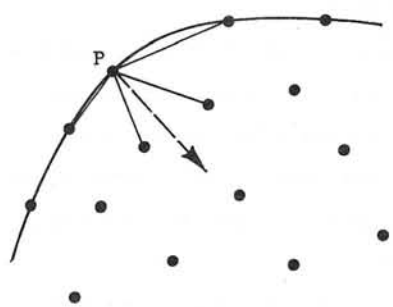

Fig. 5 - 4-point star around a boundary gridpoint P (case with N=2,M=5)

(Fig. 6). However, if f_2 is zero in eq. (6.7), only six gridpoints are necessary instead of eight. In this implementation form, if four gridpoints are placed on two orthogonal straight lines passing through the central

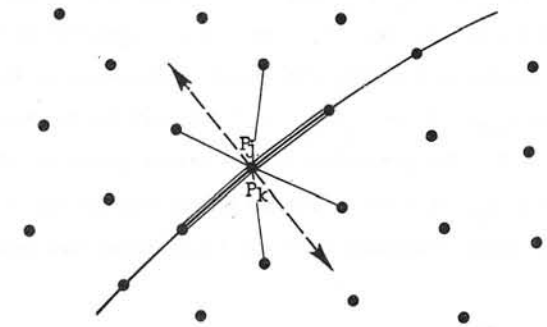

Fig. 6 - 8-point star around an interface gridpoint P (case with N=2,M=5).

gridpoint P, the equation (4.4) degenerates into the form typical of the traditional finite-difference method, and the coefficient of the fifth gridpoint tends to zero. It must be noted that the difference between the discontinuity equations and the internal ones is much smaller than in traditional finite-difference methods, where the equations involving normal derivatives are derived from interpolation procedures which need many gridpoints, for instance, six in the boundary equations, and twelve in the interface ones, precision being equal.

An application of the new method can be limited to the introduction of the boundary and interface conditions involving normal derivatives. In this case, the internal equations remain unchanged with respect to the traditional finite-difference ones, and the new method is used only to simplify the discontinuity conditions.

Less simple forms of the method involve a Taylor series expansion stopped at higher order terms. This choice yields higher precision of the results with a smaller gridpoints number. For instance, it is possible to take into account second, third and fourth order terms in the expansion by taking N=4 and M=14. Then, the internal equations involve 14 gridpoints, the boundary ones 13, and the interface ones 26; the difference between the equations increases notably.

9. A comparison with traditional numerical methods

The new method proposed presents such a variety of implementation forms that a comparison with previous methods should now be untimely. However, we can outline the problem as follows.

With respect to traditional finite-difference schemes, the new method seems to be much more powerful. It coincides with the traditional method only in its simplest form (N=2) applied to a Cartesian grid, and only in the internal equations. The discontinuity equations are already simpler, and allow us to reduce notably the iteration number required for convergence by overrelaxation iterative methods, owing to a reduction in the band amplitude of the matrix B .

The differences between the proposed method and the finite-elements one are not easily definable: both methods may be applied in many different ways, so that their comparison depends essentially on the particular implementation used.

Both methods introduce an approximate expansion of the potential in the grid. Probably, the finite-elements method can use a larger number of different approximating functions. However, in the authors' opinion, the new finite-difference method can generally warrant higher precision of the results. This assertion is first based on the complete form of the Taylor series expansion, stopped at the N-order terms, which is used in the method, and then on the high precision with which the boundary and interface conditions are locally imposed.

Besides, the new finite difference method seems to simplify the implementation for various differential problems, and for various degrees of approximations. Finally, it seems to allow us a very simple and accurate procedure of potential and field evaluation at points not belonging to the grid.

Anyhow, most of the drawbacks of the finite-difference procedure with respect to the finite-elements one seem to have been eliminated.

10. Examples

The implementation of the new method proposed is presently under way. As an example, in the following we shall apply our method to a simple case where a comparison with a theoretical solution is possible.

The problem is one of computing the magnetic field produced by a rectilinear wire of circular cross section carrying a time-constant current I.

The problem can be solved by the introduction of a vector potential A with only the axial component A_z different from zero.

To obtain a comparison with a finite-elements solution of the same problem, we resort to a computation, carried out by means of first order triangular elements, which is available in the literature[3]. Indeed, to facilitate the comparison, we have used the same gridpoints also for our finite-difference application. The grid used is shown in Fig. 7, where we have indicated, at any gridpoint, the composition of the relevant star by means of segments directed towards the gridpoints involved in the discretized equation. We have used a second order discretization (N=2, M=5),

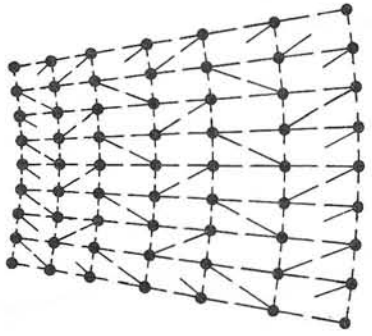

Fig. 7 - An example of field computation by the method proposed. The gridpoints coincide in both the finite-elements and the finite-difference computation.

which is the most consistent with the finite-elements solution considered.

The boundary conditions imposed have been $A_z=100$ on the internal circle of Fig. 7, $A_z=0$ on the external one, and $\partial A_z/\partial n=0$ on the two radii which delimitate the definition set of the problem.

In Fig. 8, we show the relative errors on the potential obtained by

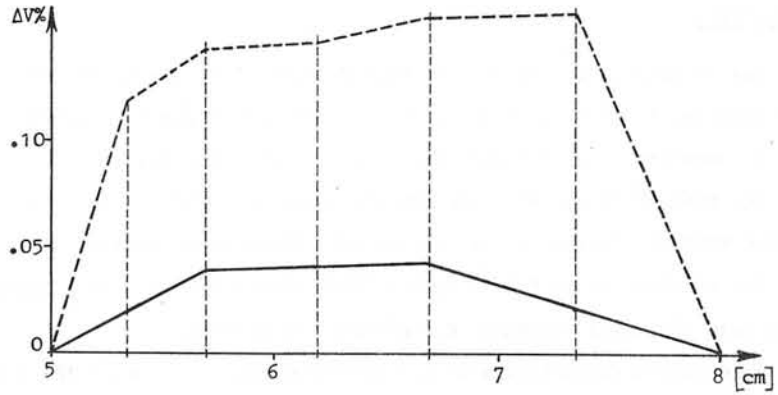

Fig. 8 - Comparison between the absolute value of the relative errors on the potential for the problem of Fig. 7.
Continuous curve: finite-difference solution.
Dashed curve: finite-elements solution[3].

the method proposed (continuous curve) and the ones of the finite-elements solution (dashed curve). They are relevant to the gridpoints placed on the symmetry axis of the problem (horizontal axis in Fig. 7).

Analogous results, relating to the magnetic field on the same symmetry axis, are plotted in Fig. 9.

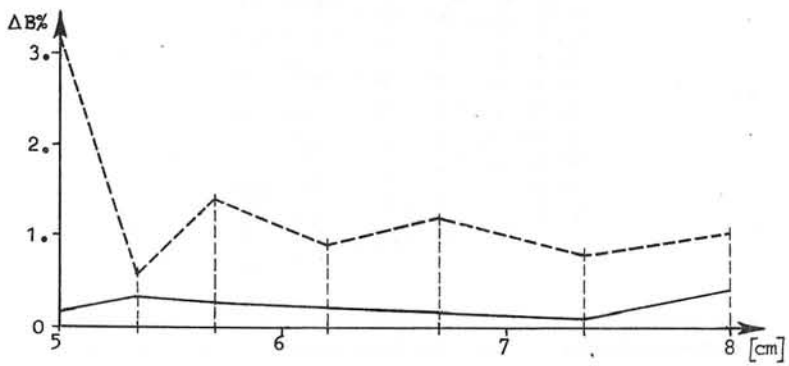

Fig. 9 - Comparison between the absolute value of the relative errors on the magnetic field for the problem of Fig. 7.
Continuous curve: finite-difference solution.
Dashed curve: finite-elements solution[3].

As we can see, the new method gives satisfactory results in the example presented above. They exhibit a non-negligible improvement with respect to the ones obtained by the finite-elements method, especially as far as the field is concerned.

Other examples carried out by the authors have also provided good results. In particular, the new method lends itself to grid optimization, and in this connection the present authors have already obtained very satisfactory results, which are described elsewhere[4].

11. Conclusions

The introduction of a finite-elements grid form in the finite-difference procedure seems particularly useful to blend the best features of the two methods and to obtain a new powerful field computation procedure.

This has been accomplished by means of a discretization procedure, which has allowed us to use irregular grids and to obtain various orders of approximation, depending on the truncation errors in the series expansion of the potential around any gridpoint.

The new method exhibits too many implementation ways to allow an immediate, conclusive description of its features. However, the results obtained seem to show that the old disadvantages of the finite-difference procedure with respect to the finite-elements one have been eliminated. Indeed, some advantages should be obtained, such as higher precision of the results, an easier implementation procedure, and a better flexibility in adapting the method to various problems and to various computation requirements, especially when derivatives of the potential are necessary. It is too early to give a positive statement of the qualities of the new method. However, there are indications that the good results obtained so far may be confirmed in the future.

12. Acknowledgment

The authors acknowledge the financial support of the Gruppo Macchine Elettriche of CNR (Electric Machinery Research Group of the Italian Research Council).

13. References

1. L. Ceriturioni and A. Viviani: "Contribution to numerical computation of Laplacian fields". Proc, IEE. Vol. 122, 1975, p. 1327.

2. G.B. Denegri, G. Molinari and A. Viviani: “A program for electric field computation using a finite-difference method with curvilinear grid”, 1975 International High Voltage Symposium, Zurich, Vol. 1, p. 6.

3. M. Fanelli: "Il metodo degli elementi finiti: possibilita di applicazione a problemi di interesse degli elettrotecnici", L’Elettrotecnica, Vol. 62, 1975. p. 513.

4. B. Delfino, G.B. Denegri, G. Molinari,.A. Viviani: “A contribution to high precision numerical computation of Laplacian fields", to be presented at the International Conference on Numerical Methods in Electrical and Magnetic Field Problems, Santa Margherita (Italy), May-June 1976.

FINITE ELEMENT APPROXIMATION AND ITERATIVE METHODS OF SOLUTION FOR 2-D NON-LINEAR MAGNETOSTATIC PROBLEMS

R. Glowinski - A. Marrocco
Univ. PARIS VI - IRIA/LABORIA

I. INTRODUCTION

The numerical analysis of the magnetic field in a tetrapolar alternator is presented here. The actual problem is a tridimensional one, but in this paper we study only the middle cross-section of the machine and the problem is reduced to a two-dimensional one. (see fig.1). The approximation is made by the technique of finite elements (conformal P_1 finite element). For the engineer this choice corresponds to the following approximation : in the iron (stator or rotor), the magnetic permeability will be constant over each element. The numerical solution of the resulting algebraic (non-linear) system is carried out by different methods (linearization, Newton-Raphson, point over-relaxation method, penalty-duality).

II. STATEMENT OF THE PROBLEM

The Maxwell's equations (for magnetostatic) are the following

$$\nabla\times\vec{H} = \vec{j} \qquad (2.1)$$

$$\vec{B} = \mu\vec{H} \qquad (2.2)$$

$$\nabla\cdot\vec{B} = 0 \qquad (2.3)$$

where

. $\vec{H}$ is the magnetizing force (or magnetic field intensity),

. $\vec{j}$ is the current density vector and (2.1) is the Maxwell-Ampere relation,

. $\vec{B}$ is the flux density (or magnetic induction) and μ is the magnetic permeability (scalar function for isotropic material)

Equation (2.2) gives the relation between magnetizing force $\vec{H}$ and flux density $\vec{B}$. This relation is linear in air where we have $\mu=\mu_o=4\pi\ 10^{-7}$ MKSA, but it becomes non linear in iron because the magnetic permeability is a function of $|\vec{H}|$ (or a function of $|\vec{B}|$). This dependence of μ versus $\vec{H}$ or $\vec{B}$ can be extracted from caracteristic curves - see fig. 2 and 3 - (the hysteresis effect is not considered). With (2.3) it is classical (see Durand (1)) to introduce the potential vector A such that

$$\vec{B} = \nabla\times\vec{A} \qquad (2.4)$$

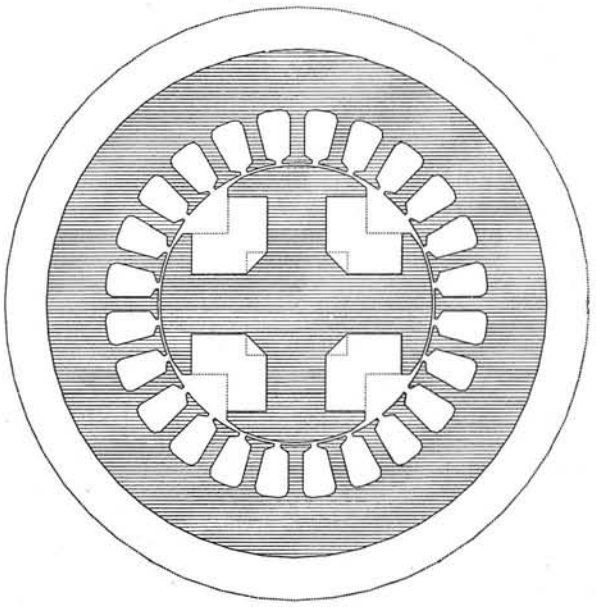

Figure 1
Tetrapolar alternator

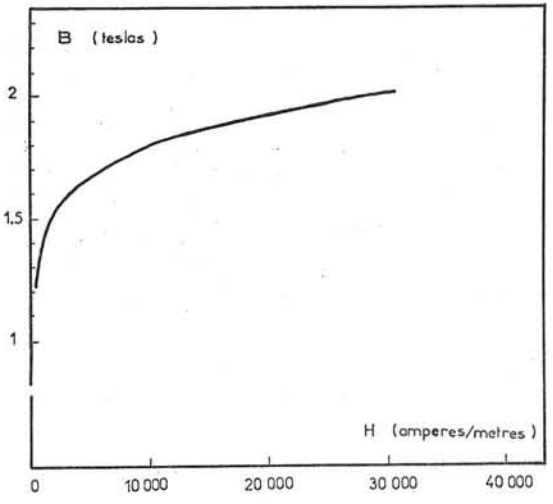

Figure 2
Stator B-H characteristic

With this relation,(2.1), (2.2), (2.3) is reduced in :

$$\nabla\times(\nu\nabla\times\vec{A}) = \vec{j} \qquad (2.5)$$

where ν is the magnetic reluctivity ($\nu=\frac{1}{\mu}$).

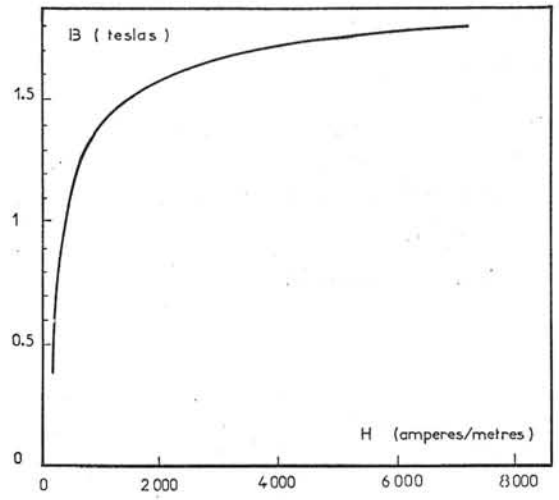

Figure 3

Rotor B-H characteristic

In our 2.D problem the potential vector $\vec{A}$ and current density $\vec{j}$ have a particular structure

$$\vec{A} = (0,0,A_3)$$
$$j = (0,0,j_3)$$

where A_3 and j_3 depend only of x_1, x_2.
In this case (2.5) may be written in the following way.

$$-\sum_{i=1}^{2} \frac{\partial}{\partial x_i} \left(\nu \frac{\partial A_3}{\partial x_i}\right) = j_3 \quad \text{or} \quad -\nabla\cdot(\nu\nabla\cdot A_3) = j_3, \qquad (2.6)$$

(2.6) is the partial differential equation we have to study. This equation (2.6) (or 2.5) is theoretically given for the whole space. In practice we take a bounded domain Ω and the potential vector must satisfy suitable properties on the boundary. See fig. 1 for the domain considered.

There is an air-region in the outside of the stator and on its boundary we take $A_3 = 0$. The physical meaning of this condition is : all flux lines are in the domain shown on fig. 1 (there is no magnetic phenomenon outside Ω). The numerical results show that this condition $A_3 = 0$ could be prescribed in fact on the stator boundary.

From a theoretical point of view, we study the problem in the domain Ω with homogeneous Dirichlet condition ; for computations it will be sufficient to take only a quarter of circle.

III. MATHEMATICAL MODEL

III.1. Partial differential equations

The domain Ω is a disk in $\mathbb{R}^2$, and we denote by Γ the boundary of Ω. The magnetic field determination is equivalent to the solution of the partial differential equation

$$\left.\begin{aligned} &-\frac{\partial}{\partial x_1}\left(\nu(x,A)\frac{\partial A}{\partial x_1}\right) - \frac{\partial}{\partial x_2}\left(\nu(x,A)\frac{\partial A}{\partial x_2}\right) = j \quad \text{in } \Omega \\ &A|_\Gamma = 0, \end{aligned}\right\} \qquad (3.1)$$

where A is a function of x_1, x_2. The reluctivity ν is a function of the space variable $x = \{x_1, x_2\}$ and also of the function $|\vec{B}|$ in the iron. In 2.D we have $|\vec{B}| = |\nabla \times \vec{A}| = |\nabla\cdot \vec{A}|$ if $\vec{A} = (0,0,A)$, so that ν is also a function of A.

If we factorize the reluctivity ν by

$$\nu = \nu_o \nu_r$$

where $\nu_o = \frac{1}{\mu_o} = \frac{1}{4\pi 10^{-7}}$ MKSA is the reluctivity of air and ν_r is the relative reluctivity with respect to air, in iron ν_r is a non linear function of $|\vec{B}|$; it is more convenient to express ν_r as a function of $|\vec{B}|^2 = |\text{grad } A|^2$ and we can write (3.1) as

$$\left.\begin{aligned} &-\frac{\partial}{\partial x_1}\left(\nu_r(x,|\text{grad } A|^2)\frac{\partial A}{\partial x_1}\right) - \frac{\partial}{\partial x_2}\left(\nu_r(x,|\text{grad } A|^2)\frac{\partial A}{\partial x_2}\right) = \mu_o j \text{ in } \Omega \\ &A|_\Gamma = 0 \end{aligned}\right\} \qquad (3.2)$$

III.2. Energy functional

Solving (3.2) is equivalent to the minimization in a suitable space of the magnetic energy given by

$$\mathcal{F}(A) = \int_\Omega \left[\int_0^{|\vec{B}|} \nu_r(x,b)\, b\,db\right] dx - \int_\Omega \mu_o\, j\cdot A\, dx \qquad (3.3)$$

where $|\vec{B}| = |\nabla \times \vec{A}|$, $\vec{A} = (0,0,A)$ (see for instance CHARI-SILVESTER (2)). The Euler equation of the optimisation problem gives equation (3.2). With our choice of ν_r, if we denote by ψ the function such that :

$$\left.\begin{aligned} &\frac{\partial \psi}{\partial |\vec{B}|^2}(x,|\vec{B}|^2) = \nu_r(x,|\vec{B}|^2) \\ &\psi(x,o) = 0, \end{aligned}\right\} \qquad (3.4)$$

then the energy functional becomes

$$\mathcal{F}(A) = \frac{1}{2}\int_\Omega \psi(x, |\text{grad } A|^2)dx - \int_\Omega \mu_o j.A \, dx \qquad (3.5)$$

III.3. Reluctivity approximation

Let us take the B-H characteristics of stator and rotor. We assume that these curves are single-valued (no hysteresis effect). We take points from these characteristic curves and put these points in a $(|\vec{B}|^2, \nu_r)$ space.

The distribution of these points in the $(|\vec{B}|^2, \nu_r)$ space, the physical properties of ν_r lead us to approximate $\nu_r(|\vec{B}|^2)$ by a function belonging to the family defined by

$$\tilde{\nu}_{\varepsilon,\alpha,c,T}(x) = \varepsilon + (c-\varepsilon)\frac{x^\alpha}{x^\alpha+T} \qquad (3.6)$$

(with constraints of positiveness on parameters ε,α,c,T).
The approximation is made by a least-square method. A typical set of value (ε,α,c,T) obtained for stator characteristic approximation is

$$\varepsilon = 5.163619\ 10^{-4}$$
$$c = 0.175775$$
$$\alpha = 5.419241$$
$$T = 8.758756\ 10^{3}$$

The mean relative error when comparing to the experimental data is 3,5% (see fig. 4 and 5).

Remark 3.1 : ψ defined in (3.4) will be in fact the primitive function of $\tilde{\nu}_{\varepsilon,\alpha,c,T}$.

IV. THEORETICAL RESULTS

IV.1. Rigorous formulation

Let $H_o^1(\Omega)$ be the classical SOBOLEV space defined by :

$$H_o^1(\Omega) = \{v \mid v \in L^2(\Omega),\ \frac{\partial v}{\partial x_i} \in L^2(\Omega)\ ,\ v|_\Gamma = 0\} \qquad (4.1)$$

with Hilberts' norm

$$\|v\|^2_{H_o^1(\Omega)} = \int_\Omega |\text{grad } v|^2 \, dx. \qquad (4.2)$$

The precise formulation of our optimization problem is :

Find a function A such that $A \in H_o^1(\Omega)$, and

$$\mathcal{F}(A) \le \mathcal{F}(v) \text{ for every } v \in H_o^1(\Omega), \qquad (4.3)$$

where $\mathcal{F}$ is given by

$$\mathcal{F}(v) = \frac{1}{2}\int_\Omega \psi(x, |\text{grad } v|^2)\ dx - \int_\Omega \mu_o\ j \cdot v\ dx.$$

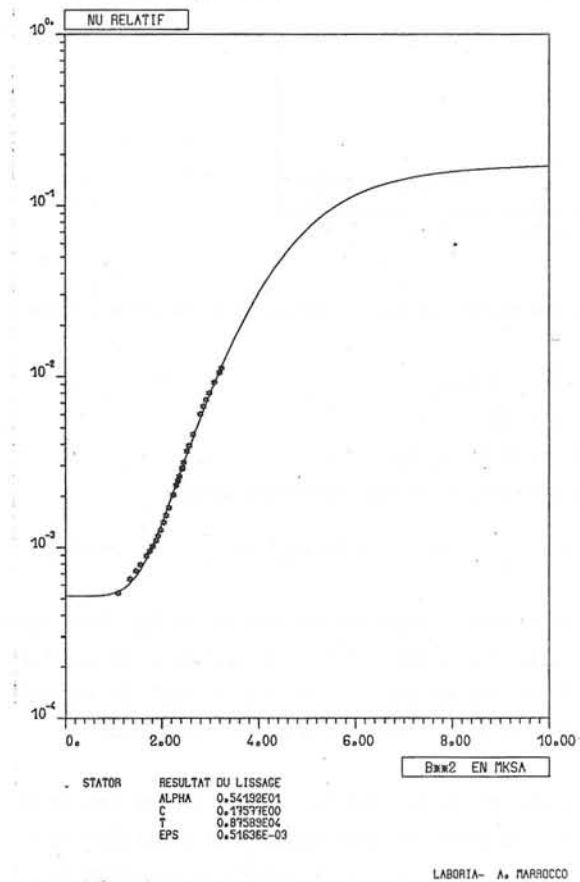

Figure 4

Reluctivity approximation (stator)

IV.2. Existence and uniqueness results for the problem (4.3)

Theorem : The optimization problem (4.3) has a solution and this solution is unique

Very briefly this result comes directly from the following properties

a) $\mathcal{F}$ is strongly continuous on $H_o^1(\Omega)$,

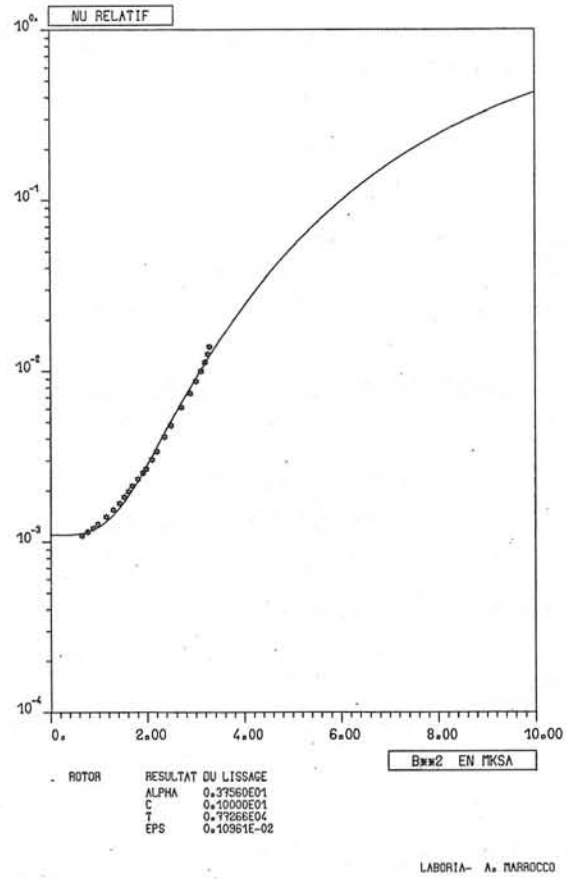

Figure 5

Reluctivity approximation (rotor)

b) $\mathcal{F}$ is strictly convex,

c) $\mathcal{F}(v) \to +\infty$ when $\|v\|_{H_o^1(\Omega)} \to +\infty$.

IV.3. Relations between the non linear partial differential equation formulation (3.2) and the optimization (or variational) formulation (4.3)

Theorem. - A, solution of (4.3) is the unique solution of (3.2) in $H_o^1(\Omega)$.

Proof : $\mathcal{F}$ is gateaux-differentiable, i.e.

$\forall u \in H_o^1(\Omega)$, here exists $\mathcal{F}'(u) \in H^{-1}(\Omega)$ such that

$$\lim_{\substack{t\to 0 \\ t\neq 0}} \frac{\mathcal{F}(u+tv)-\mathcal{F}(u)}{t} = (\mathcal{F}'(u),v)$$

for each $v \in H_o^1(\Omega)$

If A is solution of (4.3) we have

$$\frac{\mathcal{F}(A+tv)-\mathcal{F}(A)}{t} \geq 0 \quad \forall t > 0 \ , \ \forall v \in H_o^1(\Omega)$$

At the limit we have

$$(\mathcal{F}'(A),v) \geq 0 \qquad \forall v \in H_o^1(\Omega)$$

In the same way for $t < 0$, we have

$$(\mathcal{F}'(A),v) \leq 0 \qquad \forall v \in H_o^1(\Omega)$$

It follows that

$$(\mathcal{F}'(A),v) = 0 \quad \forall v \in H_o^1(\Omega) \tag{4.4}$$

so that we have :

$$\mathcal{F}'(A) = 0 \qquad \text{(equality in } H^{-1}(\Omega)). \tag{4.5}$$

The explicit form of (4.4) and (4.5) are respectively given by (4.6) and (4.7)

$$\int_\Omega \nu_r(x,|\text{grad } A|^2)\ \text{grad } A \cdot \text{grad } V\ dx - \int_\Omega \mu_o j.v\ dx = 0 \tag{4.6}$$

$$\forall v \in H_o^1(\Omega),$$

$$\left.\begin{aligned} &-\sum_{i=1}^{2} \frac{\partial}{\partial x_i}\left(\tilde{\nu}_r(x,|\text{grad } A|^2)\ \frac{\partial A}{\partial x_i}\right) - \mu_o j = 0 \\ &A|_\Gamma = 0. \end{aligned}\right\} \tag{4.7}$$

Actually A is completely characterized by (4.4), because $\mathcal{F}$ is strictly convex.

V. FINITE ELEMENT APPROXIMATION

V.1. Triangulation of Ω and notations (see fig. 6)

The triangulation $\mathcal{C}_h$ will be a set of triangles T such that

$$\bigcup_{T\in \mathcal{C}_h} T \subset \bar{\Omega} \tag{5.1}$$

If T_1 and $T_2 \in \mathcal{C}_h$ we have

$$\left.\begin{aligned} &T_1 \cap T_2 = \emptyset \\ &\text{or } T_1 \text{ and } T_2 \text{ have a common edge} \\ &\text{either } T_1 \text{ and } T_2 \text{ have a common vertex.} \end{aligned}\right\} \tag{5.2}$$

As usual, h will be the largest edges' lenght of $\mathcal{C}_h$.

We define

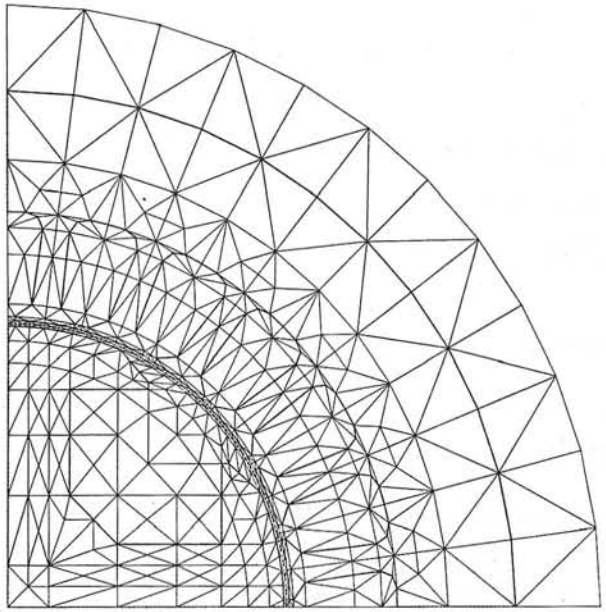

Figure 6

Triangulation of the domain

$$\Omega_h = \overline{\bigcup_{T \in \mathcal{C}_h} T} \ , \ \Gamma_h = \partial\Omega_h \tag{5.3}$$

$$\omega_h = \{P_l \,|\, P \in \Omega_h, \ P \text{ vertex of } T, \ T \in \mathcal{C}_h\} \tag{5.4}$$

$$\gamma_h = \{P \,|\, P \in \Gamma_h, \ P \text{ vertex of } T \in \mathcal{C}_h\} \tag{5.5}$$

$$\bar{\omega}_h = \omega_h + \gamma_h \tag{5.6}$$

Remark.

With the triangulation used, the boundaries between air and iron, air and cooper, never cross a triangle and are unions of edges of triangles which belong to $\mathcal{C}_h$.

V.2. Approximation of $H_o^1(\Omega)$

$H_o^1(\Omega)$ is approximated by

$$V_{oh} = \{v_h \,|\, v_h \in C^o(\bar{\Omega}_h), \ d^\circ v_h \leq 1 \text{ on } T, \ T \in \mathcal{C}_h, \ v_h = 0 \text{ on } \Gamma_h\} \tag{5.7}$$

Remarks

. dim V_{oh} = Card(ω_h) and $v_h \in V_{oh}$ is completely determined by the values it takes on ω_h ; we shall denote

$$v_i = v_h(M_i) \ , \ \forall M_i \in \omega_h \tag{5.8}$$

. As classical, V_{oh} may be considered as a subspace of $H_o^1(\Omega)$ obtained by extending $v_h \subset V_{oh}$ by 0 on $\Omega - \Omega_h$

. grad v_h is constant on each element $T \in \mathcal{C}_h$, so that ν_r which is a function of $|\text{grad } v_h|^2$ is also constant on each triangle.

V.3. Formulation and solvability of the approximated problem

Problem (4.3) will be approximated by

$$\left.\begin{array}{l} \text{Find } A_h \text{ such that} \\ \mathcal{J}(A_h) \leq \mathcal{J}(v_h) \quad \forall v_h \in V_{oh} \\ A_h \in V_{oh} \end{array}\right\} \tag{5.9}$$

where $\mathcal{J}$ is given by (3.5).

Theorem

The problem (5.9) has one and only one solution characterised by:

$$\frac{\partial \mathcal{J}}{\partial v_i}(A_h) = 0 \tag{5.10}$$

V.4. Convergence of A_h when $h \to 0$

Theorem

If :

i) $\Omega - \Omega_h \to 0$ when $h \to 0$ (i.e. $\forall K \subset \Omega$, K compact, we have $K \subset \Omega_h$ for h small enough).

ii) The angles of all $T \in \mathcal{C}_h$ are bounded below by some $\theta_o > 0$, θ_o independent of h, then

$$A_h \to A \text{ strongly in } H_o^1(\Omega) \text{ when } h \to 0. \tag{5.11}$$

VI. NUMERICAL SOLUTION OF THE APPROXIMATED PROBLEM

VI.1. Solution by linearization

A variational formulation of the approximated problem is

$$\left.\begin{array}{l}\displaystyle\int_\Omega \tilde{\nu}_r(x,|\text{grad } A_h|^2)\ \text{grad } A_h \cdot \text{grad } v_h\ dx = \int_\Omega \mu_o\ j \cdot v_h\ dx\ \forall v_h \in V_{oh} \\ A_h \in V_{oh}.\end{array}\right\} \quad (6.1)$$

Then it is natural to use the following algorithm

$$A_h^o \text{ given in } V_{oh} \qquad (A_h \equiv 0 \text{ for example}) \quad (6.2)$$

A_h^n know, A_h^{n+1} is computed by solving the linear problem

$$\left.\begin{array}{l}\displaystyle\int_\Omega \nu_r(x,|\text{grad } A_h^n|^2)\ \text{grad } A_h^{n+1} \cdot \text{grad } v_h = \int_\Omega \mu_o\ j \cdot v_h\ dx \quad \forall v_h \in V_{oh} \\ A_h^{n+1} \in V_{oh}\end{array}\right\} \quad (6.3)$$

If we make use of an iterative method for solving the linear system (6.3) (overrelaxation method for instance), an obvious variant is to make only one cycle to find A_h^{n+1}, using as initial value A_h^n. For both techniques, convergence is obtained only if j is small enough ($j \le j_o = 0.5$ A/mm^2). For these values of j we have not magnetic saturation in iron and the problem is only a practically linear problem with non constant coefficients. For small values of j we have small flux density B in the machine and the relative reluctivity ν is quasi-constant, and this lead to a linear problem. When we take greater j, the process does not converge any more and oscillations appear (the value of ν_r may change very much from one iteration to the following). A remedy for this oscillation is to under-relax the reluctivities, for example in (6.3) we replace

$$\tilde{\nu}_r(x,A_h^n) \text{ by } \nu_n \text{ evaluated by}$$

$$\nu^n(x) = \rho_n\ \nu^{n-1}(x) + (1-\rho_n)\ \nu_r^n(x,A_h^n) \quad , \quad 0 < \rho_n < 1 \quad (6.4)$$

or by

$$\nu^n(x) = \tilde{\nu}_r(x,\rho_n\ A_h^{n-1} + (1-\rho_n)\ A_h^n). \quad (6.5)$$

Such algorithms can be found for example in ERDELY and FUCHS [3] . The parameter ρ_n is chosen independent of n (value 0.1) and the overrelaxation factor is 1.3 for A_h, but theoretical results of convergence for such an algorithm are known.

VI.2. Newton-Raphson method

The explicit form of the Newton Raphson algorithm is the following :

$$A_h^o \text{ given in } V_{oh} \qquad (A_h^o \equiv 0 \text{ for example}),$$

we suppose A_h^n known and we compute A_h^{n+1} by solving the linear system

$$\left.\begin{array}{l}\displaystyle\int_\Omega \left[\tilde{\nu}_r(x,|\text{grad } A_h^n|^2)+2\tilde{\nu}_r'(x,|\text{grad } A_h^n|^2)\cdot|\text{grad } A_h^n|^2\right]\text{grad } A_h^{n+1}\cdot\text{grad } v_h\ dx \\ \displaystyle = \int_\Omega \mu_o\ j\cdot v_h\ dx + 2\int_\Omega \tilde{\nu}_r'(x,|\text{grad } A_h^n|^2)\cdot|\text{grad } A_h^n|^2\,\text{grad } A_h^n\cdot\text{grad } v_h\ dx \\ \forall v_h \in V_{oh},\ A_h^{n+1} \in V_{oh} \\ \displaystyle \tilde{\nu}_r'(x,|\text{grad } A|^2) = \frac{\partial}{\partial|\text{grad } A|^2}\nu_r(x,|\text{grad } A|^2).\end{array}\right\} \quad (6.6)$$

A variant of the Newton-Raphson method is to make only one cycle of point, overrelaxation to find A_h^{n+1}.

VI.3. Solution by non linear point over-relaxation

We denote $N = N_h = \dim V_{oh}$ and $v_h = (v_1, v_2, \ldots v_N)$, so we have to solve

$$\frac{\partial \mathfrak{F}}{\partial v_i}(A_1, A_2, \ldots A_N) = 0 \qquad i = 1,2\ldots N \quad (6.7)$$

Algorithm SNL1

$$A_h^o \text{ given in } V_{oh} \quad (A_h^o \equiv 0 \text{ for example}) \quad (6.8)$$

A_h^n known, A_h^{n+1} is computed, component by component by

$$\left.\begin{array}{l}\displaystyle\frac{\partial \mathfrak{F}}{\partial v_i}(A_1^{n+1}, A_2^{n+1} \ldots A_{i-1}^{n+1}, \bar{A}_i^{n+1}, A_{i+1}^n, \ldots A_N^n) = 0 \\ \displaystyle A_i^{n+1} = A_i^n + \omega(\bar{A}_i^{n+1} - A_i^n) \ , \ i=1,2\ldots N. \quad 0 < \omega < \omega_M \le 2\end{array}\right\} \quad (6.9)$$

The convergence of this algorithm can be proved using theoritical results obtained by SCHECHTER [4] .

Algorithm SNL2

$$A_h^o \text{ given in } V_{oh} \qquad (A_h^o \equiv 0) \quad (6.10)$$

A_h^n known, A_h^{n+1} is computed component by component by solving

$$\frac{\partial \mathfrak{F}}{\partial v_i}(A_1^{n+1}, \ldots A_{i-1}^{n+1}, A_i^{n+1}, A_{i+1}^n \ldots A_N^n) = (1-\omega)\ \frac{\partial \mathfrak{F}}{\partial v_i}(A_1^{n+1}, \ldots, A_{i-1}^{n+1}, A_i^n \ldots A_N^n) \quad (6.11)$$

$0 < \omega < 2$ $\qquad$ $i=1,2...N.$

The convergence of SNL2 is not proved (if $\omega \neq 1$), but practically it runs like SNL1. For problems completely non linear, SNL2 seems more robust than SNL1. In SNL1 we have a relaxation of the variables and in SNL2 a relaxation of the equations. This is the same for the linear case.

Some remarks on SNL1 and SNL2

The use of SNL1 or SNL2 leads to solve for each i, a non linear equation (non linear in only one variable $\bar{A}_i^{n+1}$ or A_i^{n+1}).

In this condition it is natural to use the well known Newton method (in only one variable). To solve

$$\left.\begin{aligned} &f(x) = 0 \text{ we use} \\ &x_o \text{ given} \\ &x_{m+1} = x_m - \frac{f(x_m)}{f'(x_m)} \end{aligned}\right\} \qquad (6.12)$$

The iterations are stopped when $\dfrac{|x_{n+1}-x_m|}{|x_{m+1}|} \leq 10^{-4}$ (if $x_{m+1} \neq 0$)

In our particular problem, the use of (6.12) gives the results in only 2 or 3 iterations for the starting point

$$x_o = A_i^n.$$

These remarks lead evidently to consider a variant of algorithms SNL1 and SNL2 :

we take for $\bar{A}_i^{n+1}$ or A_i^{n+1} the first iterate of Newton algorithm with an initialization by A_i^n, then we obtain the same algorithm, which will be denoted by EGSN (extrapolated Gauss Seidel Newton).

The explicit form of EGSN is given by

$$A_h^o \text{ given in } V_{oh} \qquad (A_h^o \equiv 0). \qquad (6.13)$$

$$A_i^{n+1} = A_i^n - \omega \frac{\dfrac{\partial \mathfrak{J}}{\partial v_i}(A_i^{n+1},\ldots A_{i-1}^{n+1}, A_i^n, A_{i+1}^n \ldots A_N^n)}{\dfrac{\partial^2 \mathfrak{J}}{\partial v_i^2}(A_i^{n+1},\ldots A_{i-1}^{n+1}, A_i^n, A_{i+1}^n \ldots A_N^n)}.$$

$$0 < \omega < \omega_M \leq 2 \ , \quad i=1,2...N.$$

The proof of the convergence of this algorithm can be obtained by using SCHECHTER [4].

The numerical results we obtained prove that EGSN is more efficient than SNL1 and SNL2.

VI.4. Penalty-duality algorithm.

We apply here a penalty-duality method which is proposed for example in R. GLOWINSKI-A. MARROCCO [5].

We have to minimize on V_{oh} the functional

$$\mathfrak{J}(v_h) = \frac{1}{2}\int_\Omega \psi(x, |\text{grad } v_h|^2)\, dx - \int_\Omega \mu_o\, j \cdot v_h\, dx \ ; \qquad (6.14)$$

grad v_h is constant on each $T \subset \mathcal{T}_h$, we denote by χ_T the characteristic function of T and define

$$L_h = \{z_h \mid z_h = \sum_{T \in \mathcal{T}_h} z_T\, \chi_T,\ z_T \in \mathbb{R}^2\}. \qquad (6.15)$$

We define the application $J : V_{oh} \times L_h \to \mathbb{R}$ by

$$J(v_h, z_h) = \frac{1}{2}\int_\Omega \psi(x, |z_h|^2)\, dx - \int_\Omega \mu_o\, j \cdot v_h\, dx \qquad (6.16)$$

The optimization problem on V_{oh} is equivalent to

$$\left.\begin{aligned} &J(A_h, y_h) \leq J(v_h, z_h) \quad \forall z_h \in L_h\ , \forall v_h \in V_{oh}, \\ &\text{grad } v_h - z_h = 0,\ (A_h, y_h) \in V_{oh} \times L_h,\ \text{grad } A_h - y_h = 0. \end{aligned}\right\} \qquad (6.17)$$

For the problem (6.17) we can introduce the Lagrangian

$$\mathcal{L}(v_h, z_h; \mu_h) = J(v_h, z_h) + \int_\Omega \mu_h\, (z_h - \text{grad } v_h)\, dx.$$

By dualization and penalisation of the constraint grad $v_h - z_h = 0$, we introduce, for $\varepsilon > 0$,

$$J_\varepsilon(v_h, z_h) = J(v_h, z_h) + \frac{1}{\varepsilon}\int_\Omega |z_h - \text{grad } v_h|^2\, dx, \qquad (6.18)$$

and then an augmented Lagrangian

$$\mathcal{L}_\varepsilon(v_h, z_h; \mu_h) = J_\varepsilon(v_h, z_h) + \int_\Omega \mu_h\, (z_h - \text{grad } v_h)\, dx. \qquad (6.19)$$

For the penalisation (6.18), it is in fact more convenient to define J_ε by

$$J_\varepsilon(v_h, z_h) = J(v_h, z_h) + \frac{1}{\varepsilon}\int_\Omega \eta(x)\,|z_h - \text{grad } v_h|^2\, dx \qquad (6.20)$$

with $\eta(x) > 0$ on Ω

In the numerical applications, $\eta(x)$ will be a function constant over each triangle and will permit a homogeneous penalisation. For the engineer this function $\eta(x)$ is more important, it has the same signification than the relative reluctivity ν_r, and could be estimated by him ; if this estimation is good, the following process of resolution converge very quickly.

Algorithm of penalty-duality method

$$A_h^o \equiv 0\ ,\ y_h^o \equiv 0\ ,\ \lambda_h^o \equiv 0 \qquad (6.21)$$

A_h^n , y_h^n , λ_h^n known

1°) A_h^{n+1} is solution of the linear problem.

$$\left.\begin{aligned} &\int_\Omega \eta(x)\ \text{grad } A_h^{n+1}\cdot\text{grad } v_h\, dx = \frac{\varepsilon}{2}\int_\Omega \mu_o j\cdot v_h\, dx + \int_\Omega \left(\frac{\varepsilon\lambda_h^n}{2} + \eta(x)\ y_h^n\right) \\ &\qquad\qquad \cdot\text{grad } v_h\, dx \\ &\forall v_h \in V_{oh}\ ,\ A_h^{n+1} \in V_{oh} \end{aligned}\right\} \qquad (6.22)$$

2°) We compute y_h^{n+1} by solving the non linear equations

$$\left.\begin{aligned} &\int_\Omega \tilde{\nu}_r(x, |y_h^{n+1}|)\, y_h^{n+1}\cdot z_h\, dx + \frac{2}{\varepsilon}\int_\Omega \eta(x)\cdot(y_h^{n+1} - \text{grad } A_h^{n+1})\cdot z_h\, dx \\ &\qquad\qquad + \int_\Omega \lambda_h^n\, z_h\, dx = 0 \\ &\forall z_h \in L_h\ ;\ y_h^{n+1} \in L_h \end{aligned}\right\} \qquad (6.23)$$

3°) We compute λ_h^{n+1}, triangle by triangle by

$$\lambda_{h,T}^{n+1} = \lambda_{h,T}^N + \rho\eta_T(y_{h,T}^{n+1} - \text{grad } A_{h_T}^{n+1}) \qquad (6.24)$$

If we take $\rho = \frac{2}{\varepsilon}$ in (6.24) we can prove the convergence of this algorithm as in MERCIER [6].

The non-linear problem (6.23) is in fact a system of Card $\mathcal{T}_h$ non linear equation, in only one variable, and these equations are independent.

If we denote by $|q_T|$ the modulus of a on $T \in \mathcal{T}_h$, the non linear equation we have to solve for each triangle is

$$|q_T|\cdot(\tilde{\nu}_r(x, |q_T|^2) + \frac{2\eta_T}{\varepsilon}) = \sqrt{\left[\frac{2\eta_T}{\varepsilon}\frac{\partial A_h^{n+1}}{\partial x_1}\Big|_T - \lambda_{1,T}^n\right]^2 + \left[\frac{2\eta_T}{\varepsilon}\frac{\partial A_h^{n+1}}{\partial x_2}\Big|_T - \lambda_{2,T}^n\right]^2} \qquad (6.25)$$

It is possible to use Newton's method to solve (6.25) but we have to handle this algorithm with care (because the function $q \rightsquigarrow q\cdot(\tilde{\nu}_r(x, q^2) + 2\alpha)$ has a derivative which is not monotone).

For this penalty-duality algorithm we have to solve a each step

- a linear problem (always the same)
- Card($\mathcal{T}_h$) n.l.-equation (only one variable)
- 2 Card $\mathcal{T}_h$ instruction

With this decomposition of the problem it is easy to implement this new algorithm on a parallel computer.

VII. NUMERICAL RESULTS

For a quarter of alternator, the triangulation has 812 triangles and 384 interior nodes.

The stopping test for all algorithm described in VI is

$$\left.\begin{aligned} &\text{Res}(n) = \frac{\sum_{i=1}^N |A_i^{n+1} - A_i|}{\sum_{i=1}^N |A_i^{n+1}|}\ , \\ &\text{Res}(n) \le \varepsilon. \end{aligned}\right\} \qquad (7.1)$$

We choose $\varepsilon = 10^{-5}$ in (7.1) ; this test is very strong. To obtain 10^{-6} of 10^{-7} it is necessary to compute with double precision.

The algorithm VI.1 (linearization) gives acceptable results for only $j \le 0.5$.

VII.1. Results for Newton-Raphson algorithm.

The linear system at each step is solved by a direct method (CHOLESKY BAND - a renumerotation of nodes is made to reduce the band width).

The computing time from A_h^n to A_h^{n+1} is 13 s. on CII IRIS 80 computer. See on table VII.1 the results obtained with Newton-Raphson algorithm. The algorithm is started with $A_h^o \equiv 0$.

For large values of the current density j, the starting point $A_h^o \equiv 0$ is a bad one, and we observe large oscillations of A_h^n.

RES / J	5.10^{-4}	10^{-4}	5.10^{-5}	10^{-5}
0.5			2 it	3 it
1	3 it		4 it	6 it
2	6 it	7 it	8 it and oscillation	
3	8 it	11 it	14 it	22 it
4	9 it	12 it	15 it	19 it
5	10 it	14 it	16 it	22 it
7.5	9 it	12 it	14 it	19 it
10	13 it	17 it	19 it	28 it
15	51 it	55 it	56 it	62 it
20	big oscillations			

TABLE VII.1. : Newton-Raphson results.

On fig. 7, we give the variation of RES(n) (7.1) when using Newton-Raphson algorithm.

For large values of j we can use the following process (interpolation or under-relaxation).

$$A_h^o \equiv 0 \text{ given}$$

A_h^n known, A_h^{n+1} is computed by

$$\left.\begin{array}{ll} 1°) & A_h^{n+1} \text{ solution of (6.6)} \\ 2°) & A_h^{n+1} = A_h^n + \omega(\bar{A}_h^{n+1} - A_h^n) \qquad 0 < \omega < 1 \end{array}\right\} \quad (7.2)$$

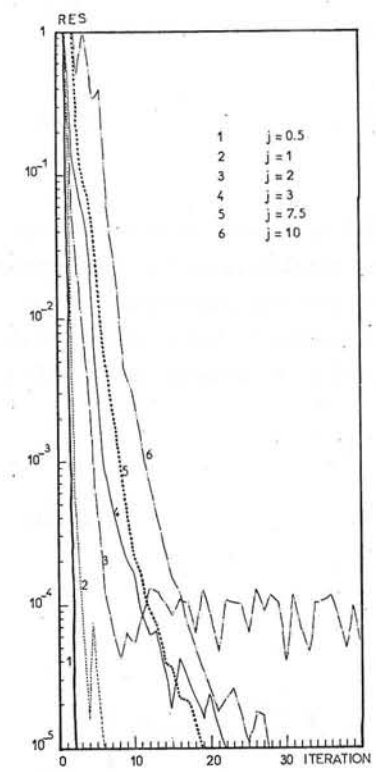

Fig. 7 - Newton Raphson algorithm

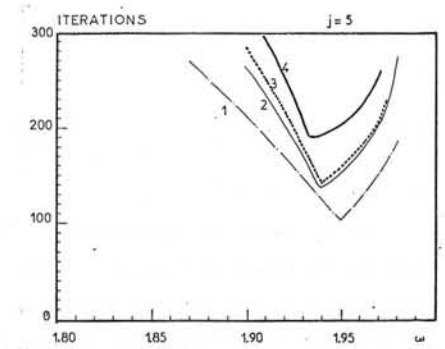

Fig. 8 - Iterative variant of Newton-Raphson

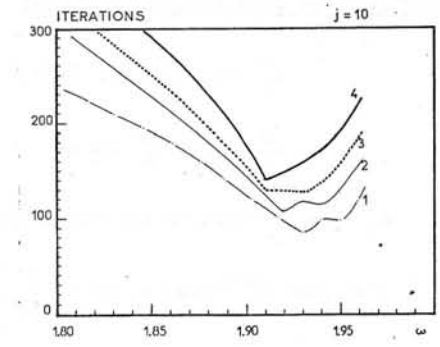

Fig. 9 - Iterative variant of Newton-Raphson

We choose $\omega = 0.5$ in (7.2), this is not optimal, and we obtain the results shown in table VII.2.

Another variant of the algorithm is the following : if we take the linear system (6.6), A_h^{n+1} is obtained from A_h^n by only one cycle of point over-relaxation process. The computing time from A_h^n to A_h^{n+1} is 0.9 s. on CII IRIS 80 computer. With the starting point $A_h^o \equiv 0$, this variant (iterative variant of Newton) is always more efficient than Newton-Raphson method for large values of the current density j (which leads to a strongly non-linear problem). We can see on fig. 8, 9, 10 the variation of the number of cycles needed for the convergence, for the current density j=5,10,20.

VII.2. Non-linear point over relaxation

For EGSN process the computer time from A_h^n to A_h^{n+1} is 0.65 s. on CII IRIS 80. For SNL1 and SNL2 this time is not constant and depends on the in-

J \ RES	5.10^{-4}	10^{-4}	5.10^{-5}	10^{-5}
0.5	11 it	14 it	15 it	16 it
2	11 it	14 it	15 it	18 it
7.5	13 it	19 it	23 it	31 it
15	17 it	22 it	25 it	34 it
20	16 it	21 it	24 it	34 it

TABLE VII.2. : Newton-Raphson with under-relaxation $\omega = 0.5$

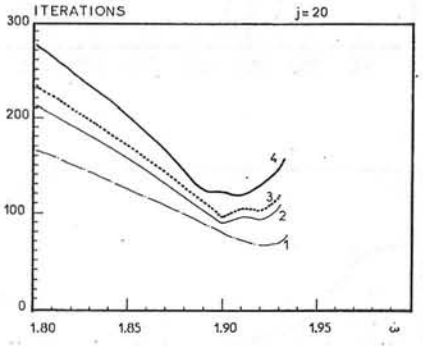

Fig. 10 - Iterative variant of Newton-Raphson

ternal Newton process. We can see on fig. 11, 12, 13, 14, 15, 16, 17, 18 results obtained with SNL2 and EGSN.

These algorithms, in particular EGSN, are very efficient and do not need very much storage on the computer. We have also solved the problem for the complete machine. The number of triangles is then 3240, the number of interior nodes is 1597. This algorithm was run on the middle size computer CII 10070 (128K words), without auxiliary memory . For j=10, ω=1.93 and $\varepsilon=10^{-5}$ in (7.1), EGSN needs 162 iterations and the computing time is about 16 mn. (less than 10 mn. on CII IRIS 80).

VII.3. Results obtained with penalty-duality algorithm

This method need more computer storage, but presents the following interesting particularities

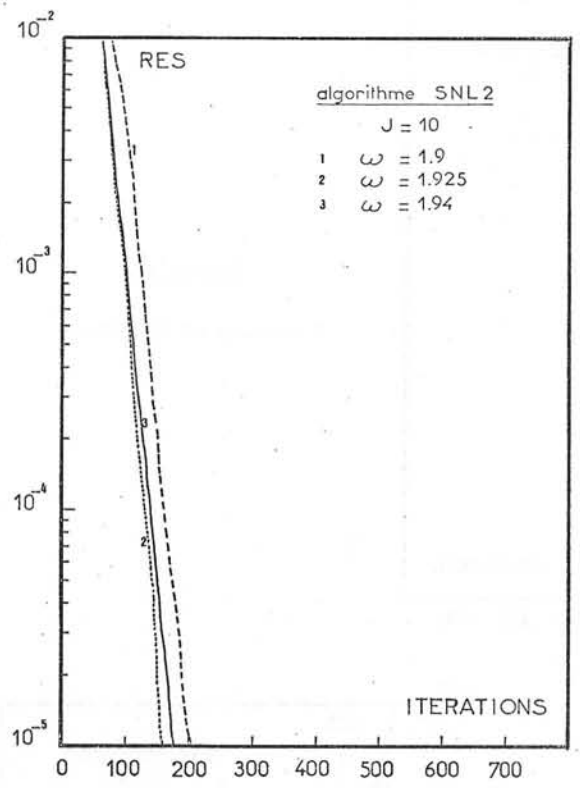

Figure 11

Variation of RES (7.1)

a) each step of the algorithm (6.22), (6.23), (6.24) is easy to solve, since we have to solve

- . a linear problem (with a fixed matrix)
- . a set of non linear independent equations
- . explicit calculation for λ^{n+1}

b) This algorithm is easy to implement on a parallel computer

c) The electrical engineer has the possibility of choosing the function $\eta(x)$ which has a concrete signification for him (he can estimate the solution of his problem in term of flux density repartition).

The results presented here are made with constant value of $\eta(x)$ in air (the value is 1) and in stator, and in rotor the value is [k* minimal value of ν_r] in respective material, with $k > 0$.

The number of iterations necessary to achieve the convergence is shown in fig. 19-29. We give the variation of the number of iterations in

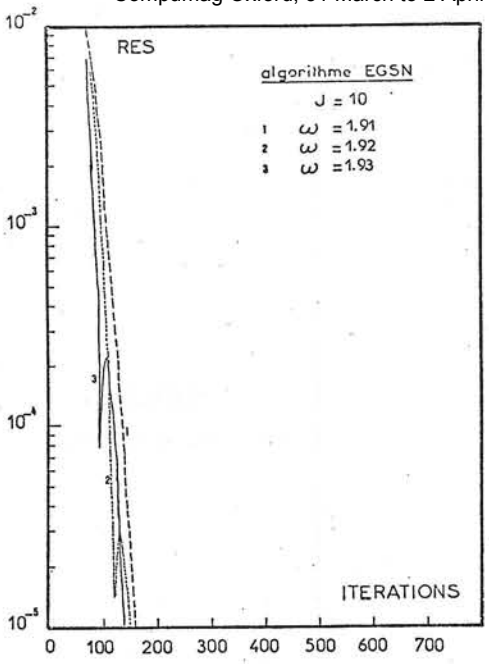

Figure 12

Variation of RES (7.1)

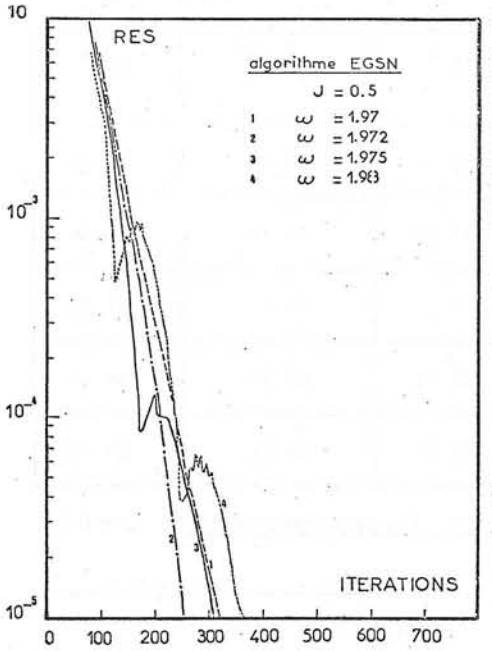

Figure 14

Variation of RES (7.1)

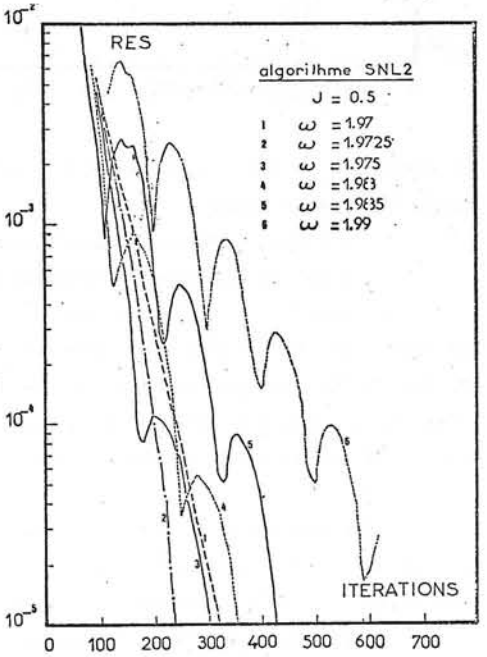

Figure 13

Variation of RES (7.1)

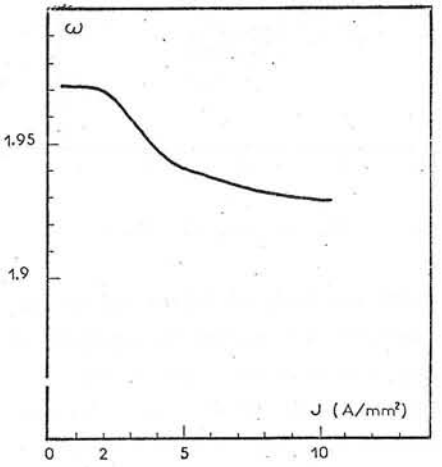

Figure 15

Optimal choice of relaxation parameter for EGSN algorithm.

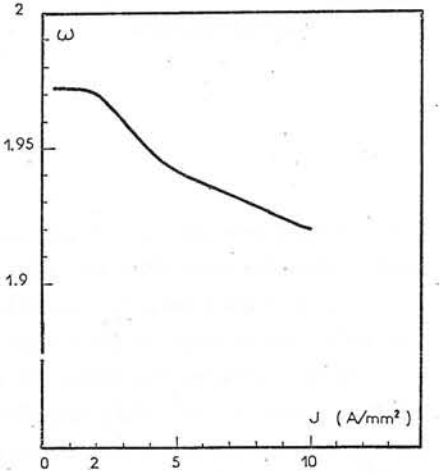

Figure 16

Optimal choice of relaxation parameter for SNL2 algorithm.

function of the penalisation parameter ε. We give in table VII.3, computing time on CII IRIS 80 for different values of parameters ε, k, j. The stopping test in (7.1) is 10^{-5}.

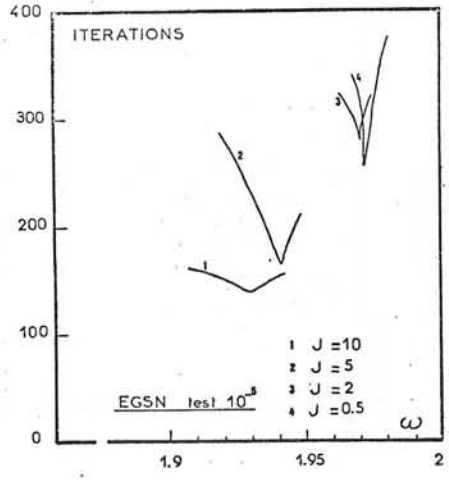

Figure 17

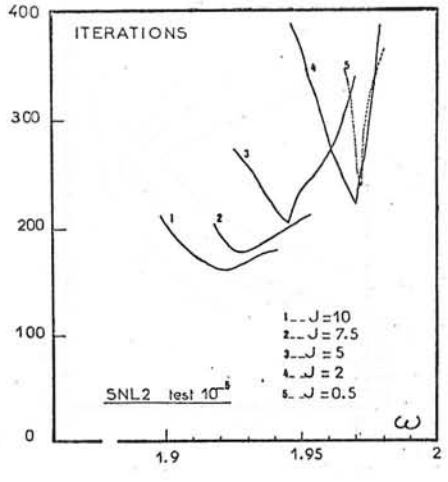

Figure 18

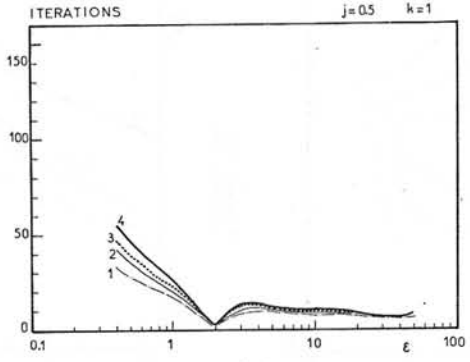

Figure 19

Current density: j = 0.5							
k=1		k=10		k=20		k=50	
ε = 2	2 it. 17s	ε = 3	20 it. 51s				
		ε = 4	18 it. 49s				
		ε = 5	23 it. 56s				
Current density : j = 2.							
ε =0.1	152it.363s	ε =0.75	60 it.126s	ε = 1	77 it. 176s	ε = 5	40 it. 95s
ε =0.2	90it.215s	ε =1	55 it.115s	ε = 2	53 it. 121s	ε =7.5	38 it. 91s
ε =0.3	111it.258s	ε =2	79 it.156s	ε = 3	63 it. 139s	ε =10	45 it.106s
Current density : j = 7.5							
ε =0.075	137it.329s	ε =0.4	59 it.126s	ε = 0.5	67 it. 142s	ε = 1	74 it.154s
ε =0.1	131it.265s	ε =0.5	49 it.105s	ε = 0.75	53it. 113s	ε = 2	54 it.113s
ε =0.2	133it.267s	ε =0.75	70 it.140s	ε = 1	56 it. 117s	ε = 3	65 it.142s
Current density : j = 20							
ε =0.1	114it.232s	ε =0.3	53 it.116s			ε = 1	57 it.123s
ε =0.2	93it.191s	ε =0.4	47 it.104s			ε = 2	43 it. 95s
ε =0.3	124it.248s	ε =0.5	53 it.115s			ε = 3	65 it.136s

TABLE VII.3. Results with duality-penalty algorithm.

We give in Figure 30 an example of repartition of flux lines, for current density j = 10.

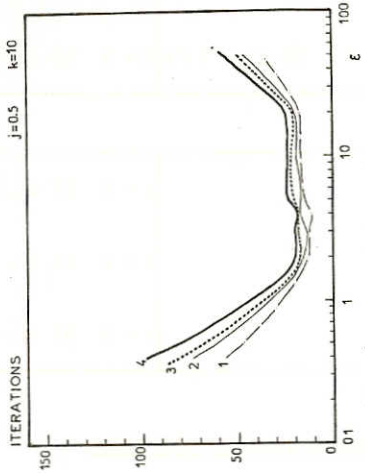

Figure 20

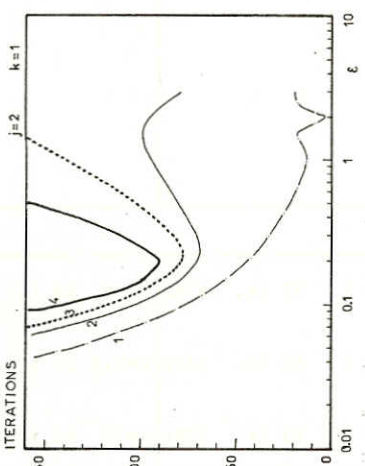

Figure 21

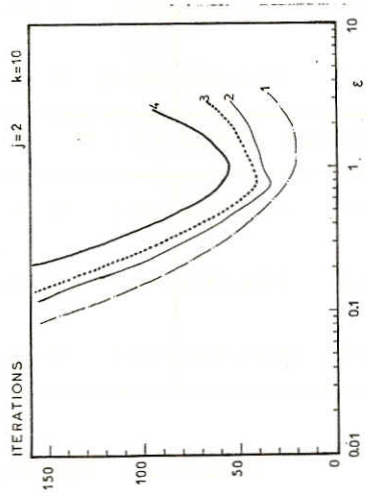

Figure 22

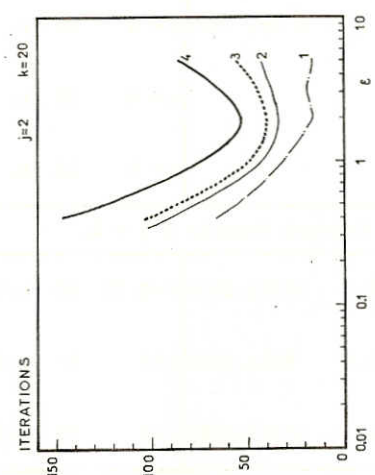

Figure 23

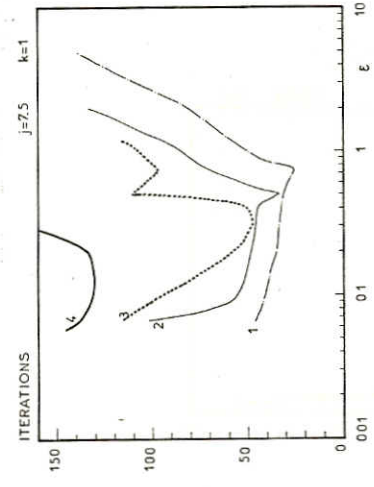

Figure 24

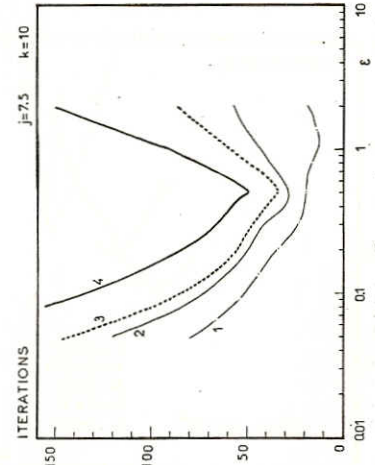

Figure 25

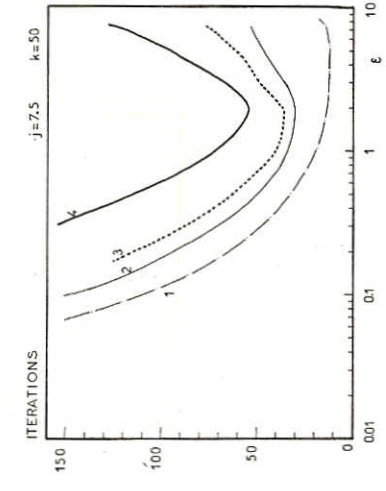

Figure 26

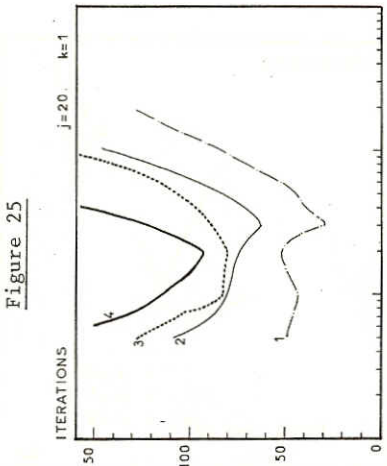

Figure 27

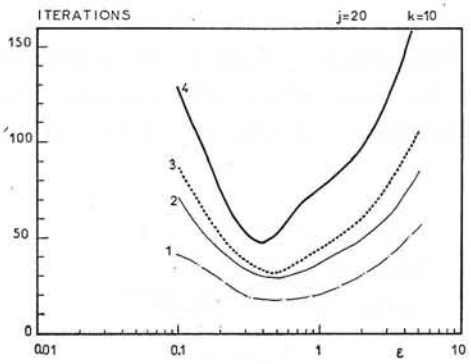

Figure 28

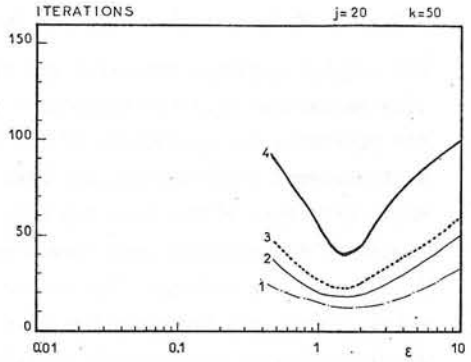

Figure 29

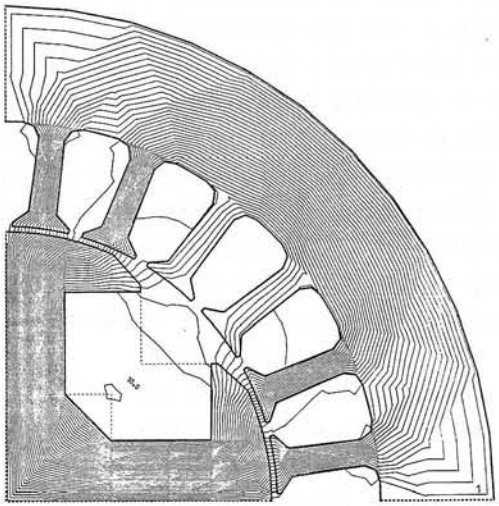

Figure 30

Flux line for j=10 A/mm^2

REFERENCES

0 - R. GLOWINSKI - A. MARROCCO - Analyse numérique du champ magnétique d'un alternateur par éléments finis et surrelaxation ponctuelle non linéaire. Computer methods in applied mechanics and engineering, 3, 1, (1974)

1 - E. DURAND - Magnétostatique. Masson & Cie, Paris 1968.

2 - P. SILVESTER - MVK CHARI - Analysis of turbo-alternator magnetic fields by finite elements. IEEE PAS, 90, 2, (1971).

3 - E.A. ERDELY - E.F. FUCHS - Non linear field analysis of D.C. machines. IEEE PAS, 80, N° 7 (1546-1583), 1970.

4 - S. SCHECHTER - Minimisation of convex functions by relaxation. Ch. 7 of Interger and non linear programming. J. ABADIE, North-Holland, 1970.

5 - R. GLOWINSKI - A. MARROCCO - Sur l'approximation par éléments finis d'ordre 1 et la résolution par pénalisation dualité d'une classe de problèmes de Dirichlet non linéaires. C.R.A.S. Paris, T. 278, 26 Juin 1974, Série A, 1949-1652. RAIRO , R-2, Août 1975.

6 - B. MERCIER - On the finite element approximation and the solution by a penalty duality algorithm of an elasto-plastic problem. Rapport Laboria, N° 149, Janvier 1975.

R. Glowinski - Université Paris VI, U.E.R. 48, Laboratoire Analyse Numérique, Paris.

A. Marrocco - IRIA/LABORIA, Domaine de Voluceau, Rocquencourt, 78150 Le Chesnay.

MAGNETIC FIELD CALCULATION FOR A SALIENT-POLE HYSTERESIS COUPLING

M.J.Jevons

The University of Aston in Birmingham, Birmingham B4 7PB, England

1 The hysteresis coupling

One form of salient-pole circumferential-flux hysteresis coupling is shown in fig. 1 [1]. The stator is made of soft magnetic material and each pole has an exciting coil supplied with dc. The rotor comprises a thin annular ring of hard magnetic material on a non-magnetic arbor.

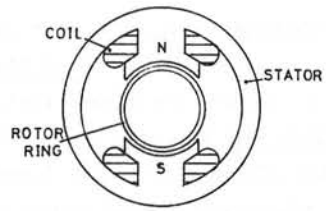

Fig. 1 Salient-pole hysteresis coupling

As the relative magnetic permeability of the ring is low, the airgap flux density waveforms - illustrated in fig. 2 for the outer surface of the rotor - are quite different from those of conventional salient-pole machines and the usual design procedures are not applicable.

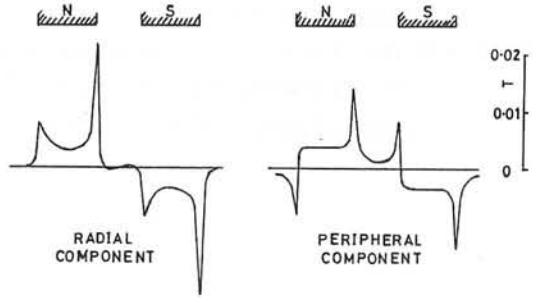

Fig. 2 Airgap flux density waveforms

The waveforms exhibit large peaks in the vicinity of the pole-tips, and the size of the peak in the radial component at the lagging pole-tip largely determines the torque/excitation characteristic of the coupling [2]. The size can be estimated from the values obtained from an actual machine without a rotor and the rotor saturation magnetization. The problem is to predict this value, and the total permeance as part of the design.

A qualitative theory has been based on a 2-pole idealized machine in which the stator is assumed to be infinitely permeable and the magnetic field to result from surface polarity and not current sources. End effects have been neglected to permit a 2-dimensional approach. Two mathematical models have been used to predict the airgap flux density waveform. The first simply consists of two equipotential circular arcs which represent the pole-faces (see fig. 3).

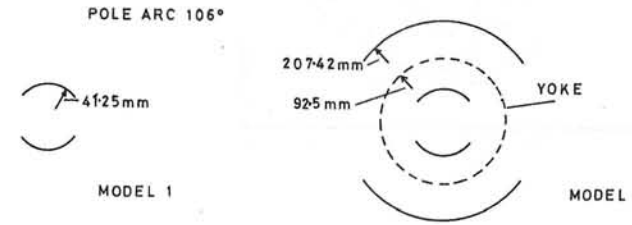

Fig. 3 Mathematical models for the idealized machine without a rotor

The complex magnetic potential and the vector magnetic field are evaluated from an inverse elliptic function transformation [3] (see App.7.1). Although the waveforms are apparently of the required shape, detailed comparison with observed results shows the need for an improved model. In the second model (see fig. 3) the yoke has been simulated by including another pair of equipotential circular arcs formed by the inversion of the first pair about the axis of the machine. The radius of inversion equals the radius of the yoke. There does not appear to be a tractable solution for the Laplace equation in this case and the magnetic field has been evaluated numerically. Differences still exist between the predicted and observed waveforms, but are to be expected in view of the initial assumptions.

In the numerical solution adopted - the method of sub-elements - the surface polarity is assumed to vary in a known manner over short lengths (sub-elements) of the replica pole-arcs. A finite number of simultaneous equations are then formed which relate the potentials of the several surfaces to the values of surface polarity. Once these are known, the magnetic field can be calculated at any point in the model. In particular, values of the radial magnetic field strength (or flux density) can be calculated along the circumference of a pitch circle corresponding to the outer surface of the rotor and the maximum value found.

Various aspects of the method of sub-elements are considered in this paper, all with reference to the models described above. Working formulae for two different representations of the surface distribution are derived and their relative merits discussed. Results for both models have been

included; for although the first is an oversimplification, numerical results can be checked against theoretical values, and comparison of the different field distributions enables the practical effect of the yoke to be assessed.

2 Basic theory

There is no simple expression for the distribution of surface polarity (m) over the pole-face (fig. 4a). The shape of the curve is predictable: away from the pole-tips m changes only slightly, it exhibits a minimum at the pole centre-line and is symmetrical about this line; at the pole-tips m is theoretically infinite.

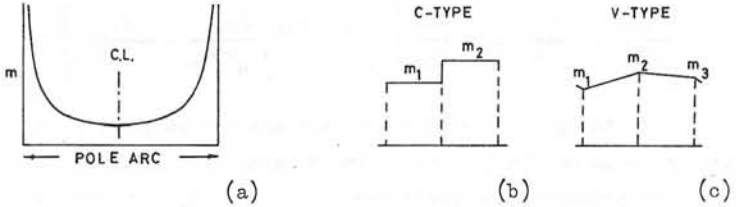

Fig. 4 Surface polarity on the pole-arc

To facilitate numerical evaluation of m, each pole-arc is divided into sections (sub-elements) over which m is assumed to have a known variation. For example; m could be constant - m_1, m_2, ..(fig. 4b); or vary linearly - $m_1 m_2, m_2 m_3$, ..(fig. 4c). These are the approximations considered here and are subsequently referred to as C- and V-type. Both are inadequate near to the pole-tips, because of the singularity, but this difficulty has been overcome by assuming m to vary as $x^{-\frac{1}{2}}$ (see App.7.2) in V-type sub-elements which include the pole-tips. The widths of the sections need not be the same and are chosen to anticipate a good fit.

2.1 Evaluation of potential

Each of the magnetized sub-elements contributes to the total potential of a given sub-element, but because of the discrete approximation of m, the potential is not constant over the width. If constant values of m have been assumed then the potential of a sub-element is taken as the value calculated at the mid-point of the width (see fig. 5a).

$$\phi_p = \sum - \frac{R_n m_n}{2\pi} \int_{-\frac{1}{2}A_n}^{\frac{1}{2}A_n} \ln(R_n^2+X^2-2R_n X\cos(f_n+f))^{\frac{1}{2}}\,df \qquad (2.1)$$

The summation includes all of the sub-elements on each arc of the model - ($2\,n_{actual} + 2\,n_{image}$), but because of symmetry the potentials are only determined at $\frac{1}{2}n$ (n even) or $\frac{1}{2}(n+1)$ (n odd) points as there are only these distinct values of m. The product $|R_n m_n|$ is the same for a sub-element and its image. Eq. (2.1) is integrated numerically using Bode's quadrature formula[4], except when $f_n=0$ and $R_n=X$. Then the integral is evaluated as

$$A_n\left[\ln(\tfrac{1}{2}R_n A_n) - 1 - \sum_{q=1}^{\infty} \frac{B_{2q-1}\,A_n^{2q}}{2^{2q+1}\,n\,(2q+1)!}\right] \qquad (2.2)$$

where B_{2q-1} is a Bernoulli number. Usually 2 terms of the series give sufficient accuracy.

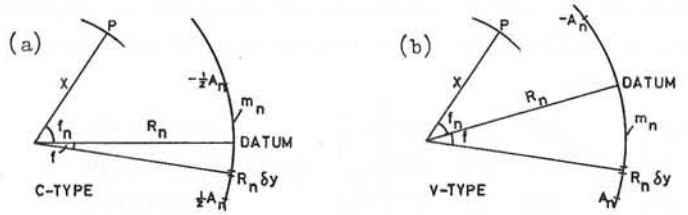

Fig. 5 Meaning of symbols used in equations (2.1) and (2.3)

When a linear variation of m is assumed, the potential is calculated at each end of the sub-element. If the mid-point were used then the solution of the equations for m_n would become unstable as the number of sub-elements is increased. Sub-elements which include the pole-tips are treated similarly except that the potential is calculated at the 'finite' end only. The potential equation corresponding to (2.1) is (see fig. 5b)

$$\phi_p = \sum - \frac{R_n m_n}{2\pi} \int_0^{A_n} (1-\frac{f}{A_n})^v \ln(R_n^2+X^2-2R_n X\cos(f_n \mp f))^{\frac{1}{2}}\,df \qquad (2.3)$$

$$= \sum - \frac{R_n m_n A_n}{2\pi}\left[\frac{1}{1+v}\ln(R_n^2+X^2)^{\frac{1}{2}} + \tfrac{1}{2}\int_0^1 (1-t)^v \ln(1-G_n\cos(f_n \mp tA_n))\,dt\right] \qquad (2.4)$$

where m_n is the value of m at one end of the sub-element, v is either 1 (linear) or $-\frac{1}{2}$ (pole-tip) and $G_n = 2R_n X/(R_n^2+X^2)$. The singularity which occurs with -ve v is removed by integrating by parts, when

$$\phi_p = \sum - \frac{R_n m_n A_n}{2\pi(1+v)}\left[\ln(R_n^2+X^2-2R_n X\cos(f_n)) \mp \tfrac{1}{2}A_n \int_0^1 \frac{(1-t)^v G_n \sin(f_n \mp tA_n)}{1-G_n\cos(f_n \mp tA_n)}\,dt\right] \qquad (2.5)$$

These equations are also integrated numerically using Bode's formula, except when $f_n=0$ and $R_n=X$. Then the integral in eq. (2.3) is evaluated as

$$-A_n\left[\frac{1}{1+v}\left[\ln(R_nA_n)+\psi(1)+\psi(2+v)\right]-\sum_{q=1}^{\infty}\tfrac{1}{2}B_{2q-1}A_n^{2q}\sum_{k=0}^{2q}\frac{(-1)^k}{(2n-k)!\,k!\,(1+k+v)}\right] \quad (2.6)$$

where $\psi(j)$ is the digamma function.

At distances large in comparison with the sub-element widths the surface polarity could be considered concentrated into magnetic poles at the ends of the sub-elements and the calculation simplified. This has not been done in the present work.

Because each of the discrete surface distributions contributes to the potential of every sub-element, the coefficient matrices are dense. The equations are poorly conditioned and ill-suited to iterative solution schemes, as eq. (2.7) for 3 sub-elements of equal width (over half of the pole-arc) shows.

$$\begin{bmatrix}1.0\\1.0\\1.0\end{bmatrix}=\frac{10^{-4}}{2\pi}\begin{bmatrix}917 & 346 & 148\\651 & 615 & 265\\577 & 531 & 467\end{bmatrix}\begin{bmatrix}m_1\\m_2\\m_3\end{bmatrix} \quad \text{whence} \quad \begin{matrix}m_1=58.2\ \text{A/m}\\m_2=48.6\ \text{A/m}\\m_3=46.9\ \text{A/m}\end{matrix} \quad (2.7)$$

This is for Model 1 – 120° pole-arc and V-type sub-elements. The coefficient matrix is unsymmetrical because the symmetry of the model has been used to reduce the number of equations. Multiplication by the transpose would make it symmetrical but would not improve its poor condition.

As there is no need for a large number of equations with the present simplified models, Gauss elimination has been used in the computer programs to evaluate the unknown surface polarities.

2.2 Evaluation of magnetic field strength

The radial component of the magnetic field strength at p (fig. 5b) is deduced from $\overline{H} = -\nabla\phi$ and eq. (2.3) as

$$H_r=\sum\frac{R_nm_n}{4\pi X}\int_0^{A_n}(1-\frac{f}{A_n})^v\left[1-\frac{R_n^2-X^2}{R_n^2+X^2-2R_nX\cos(f_n\mp f)}\right]df \quad (2.8)$$

Again the summation includes all of the sub-elements. The assumption of C-type sub-elements leads to poor results and is not pursued.

In the present application H_r is calculated close to the pole surface and this can cause loss of accuracy in the numerical evaluation of eq. (2.7), because $X\to R_n$ and $2R_nX\to(R_n^2+X^2)$. Simpson's $\frac{1}{3}$ formula is used in the computer program, with the panel width automatically halved[5] until the relative error between successive computations is less than a given value. This is based on a compromise between accuracy and fast running time – $|0.5|\times10^{-3}$ has been found suitable, together with a maximum of 7 halving cycles.

New variables $x_{1n}=(R_n^2-X^2)/2R_nX$, $x_{2n}=(R_n-X)^2/2R_nX$

$y_{1n}=1-\cos(f_n\mp f)$, $y_{2n}=1-\cos(f_n\mp A_n)$

are defined and the integral (eq. (2.8)) is evaluated in the form

(i) +ve v (e.g., v=1)

$$\frac{A_n}{1+v}\left[1-\frac{x_{1n}}{x_{2n}}\right]+\frac{x_{1n}}{x_{2n}}\int_0^{A_n}(1-\frac{f}{A_n})^v\left[\frac{y_{1n}}{y_{1n}+x_{2n}}\right]df \quad (2.9)$$

(ii) –ve v (e.g., v=$-\frac{1}{2}$)

$$\frac{A_n}{1+v}\left[1-\frac{x_{1n}}{y_{2n}+x_{2n}}\right]+\frac{x_{1n}}{x_{2n}}\int_0^{A_n}(1-\frac{f}{A_n})^v\left[\frac{y_{1n}}{y_{1n}+x_{2n}}-\frac{y_{2n}}{y_{2n}+x_{2n}}\right]df \quad (2.10)$$

At the pitch circle radius the maximum value of H_r occurs just under the pole-tip and is located in the program by testing the slope of the H_r curve at predetermined positions. Values of H_r are calculated at the pole-tip and at angular increments of 0.2° toward the pole centre-line. A change in the sign of the slope locates the maximum within the last two angular increments. This smaller section of the H_r curve is then examined using an increment of 0.1°. The process is repeated twice more.

3 Computer results

Details of the models reported on are given in Fig. 3 and the chief results are tabulated in App.7.3. The numbers of sub-elements referred to are for half of the pole-arc.

3.1 Surface polarity

The principal use of the first model was to assess the correlation between numerical and theoretical values. In this respect the permeance shape factor (S_p – App.7.3) is a useful concept, being numerically equal to half the total surface polarity on one pole. It does not provide a check on the correctness of the distribution.

Both methods of representing the surface distribution were used in the calculations. There was close agreement for the surface polarity on the centre-line of the pole even with 4 sub-elements. However considerable error was noted in the shape factor for the C-type distribution when used with equal width sub-elements. This was not so with the V-type, and the advantage of a simple computer program in the first case is diminished by the larger number of sub-elements necessary and the increased running time.

The distributions for Model 2 using 8 sub-elements are shown in Fig. 6.

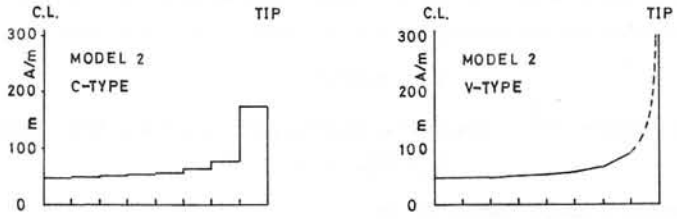

Fig. 6 Surface polarity using 8 equal width sub-elements

The almost constant value of polarity near the centre of the pole arc suggests that the widths of the sub-elements could be progressively increased from the pole-tip toward the pole centre-line. One example of this is shown in Fig. 7. The accuracy of the solution has been increased without increasing the number of equations, but there is a limit as the linear representation of the distribution just away from the pole-tip is inaccurate and introduces error. Further increase in accuracy then requires an increase in the number of equations.

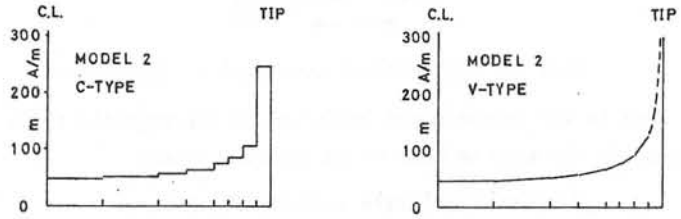

Fig. 7 Surface polarity using 8 variable width sub-elements

3.2 Magnetic field strength H_r

The variation of H_r along the rotor pitch circle is shown in Fig. 8 for Model 2, using eq. (2.9) and (2.10) with 8 equal width sub-elements. The shape is similar to that of the surface polarity because of the proximity of the pole-arc. In the interpole region H_r falls almost to zero, exhibiting a sign change with Model 2 but not Model 1. The position of the peak is slightly away from the pole-tip toward the pole centre-line. There is good correlation between the numerical and theoretical values of the peak obtained with Model 1 for a small number of sub-elements. The effect of the yoke, introduced in Model 2, is to increase the peak value by about 5% at this radius. The calculated position and size of the peak depend principally on the assumed variation of m near to the pole-tip, i.e., on the size of sub-elements and on the value of v (eq. (2.5)) for the sub-element at the pole-tip. A ln/ln graph of m_n and pole-arc measured from the pole-tip shows that as the number of sub-elements is increased the assumed variation $(v=-\frac{1}{2})$ is substantially correct up to 1^o of arc. A decreased value of v would slightly decrease the peak value. In practice the presence of pole-sides and a definite angle at the pole-tip will reduce the peak value.

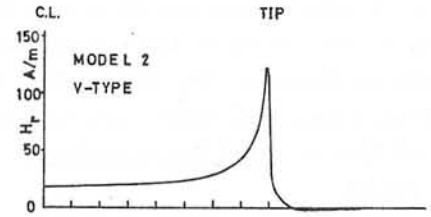

Fig. 8 Variation of H_r along the rotor pitch circle

4 Conclusion

The method of sub-elements is attractive because the surface polarity can be represented by simple functions; because the number of equations which have to be solved can be kept small by varying the widths of the sub-elements; and because the magnetic field strength can be calculated anywhere in the air region. It is clear from the present work that a better representation of the machine geometry would not lead to an unmanageable problem. The main disadvantage is that the coefficient matrices are ill-suited to iterative schemes and direct methods of solution must be used.

Certain improvements to the method are being examined. Representing the surface polarity over a sub-element by a polynomial may enable the number of equations to be further reduced, but at the expense of a more complicated computer program. A present weakness is that the potential is calculated only at points where the polarity is defined. Calculations based on the potential at the mid-points of V-type sub-elements were unstable, but the use of a weighting factor could give improved results. The extension of sub-elements to 3-dimensions - sub-areas - is well known[6] but the author is not aware of literature describing the use of V-type representations of surface polarity or charge density.

Even without these improvements the calculated peak value of H_r is sufficiently accurate for design purposes. The permeance shape factor for the improved model is high, but this can be modified empirically to allow for the pole-cores.

5 Acknowledgements

The author wishes to thank S.S.Gill and B.S.Jeer for verifying the sub-element formulae as part of an undergraduate project, and Dr.S.C.Bhargava for the waveforms in Fig. 2 and the analysis in App. (7.1).

6 References

1 S.C.Bhargava, "Non-Synchronous Operation of a Hysteresis Machine", Ph.D. Thesis, The University of Aston in Birmingham, 1972.

2 M.J.Jevons and S.C.Bhargava, "The Salient-Pole Hysteresis Coupling", IEEE Trans (Magnetics), Vol. Mag-11, pp. 1461-3, 1975.

3 P.Moon and D.E.Spencer, Field Theory Handbook, Springer-Verlag, 1961, pp. 51,54,73.

4 M.Abramowitz and I.A.Stegun, Handbook of Mathematical Functions, Dover, 1965, p. 886.

5 Modern Computing Methods, HMSO, 1961, p. 130.

6 R.F.Harrington, Field Computation by Moment Methods, Macmillan, 1968, Ch. 2.

7 Appendices

7.1 Analysis of Model 1

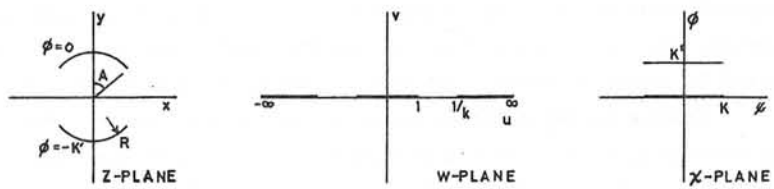

Fig. 9 Inverse sn transformation

The field due to two circular arcs on a pitch circle of radius R in the z-plane is transformed to a uniform field in the χ-plane (see fig. 9) by the transformation

$$\mathrm{sn}\chi = \frac{j}{k^{\frac{1}{2}}}\left[\frac{jR + z^*}{jR - z^*}\right] \qquad (7.1)$$

where $k = \tan^2(\frac{1}{2}A)$ = modulus of the Jacobian elliptic function
$K' = K(k')$ = associated complete elliptic integral of the first kind (see fig. 9).

Using $\overline{H} = -\nabla\phi$

$$H_r - jH_\theta = je^{-j\theta}\frac{\partial\chi}{\partial r} = je^{-j\theta}\frac{(1 - jk^{\frac{1}{2}}\mathrm{sn}\chi)^2}{2Rk^{\frac{1}{2}}\,\mathrm{sn}'\chi} \qquad (7.2)$$

This is readily evaluated at any point because $\mathrm{sn}\chi$ is given by eq. (7.1). In particular at the centre of the pole-arc, for potentials of 0,-K',

$$H_r = 1/2Rk^{\frac{1}{2}} \qquad (7.3)$$

For the model:- $k^{\frac{1}{2}} = \tan 26.5^\circ = 0.498..$, R = 41.5 mm , K'= 2.8066..

$$H_r = 24.311..$$

The permeance shape factor S_p is

$$S_p = \frac{4K}{K'} \doteq 2\pi/(\ln\frac{4}{k} - \frac{k^2}{4}) \qquad (7.4)$$

the approximation being sufficiently accurate when $k < 0.2$.

For the model $S_p = 2.274..$.

7.2 Surface polarity at the pole-tip

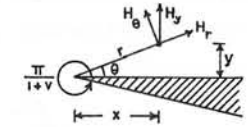

Fig. 10 Mathematical treatment of the pole-tip

Near to the pole-tip the variation of the magnetic field is approximately the same as that of an isolated corner

$$\phi = C r^{1+v}\sin(1+v)\theta + \text{constant terms} \qquad (7.5)$$

Using $\overline{H} = -\nabla\phi$ and noting that $H_y = H_r\sin\theta + H_\theta\cos\theta$

$$H_y = -(1+v)C r^v \cos v\theta \qquad (7.6)$$

If the pole-tip angle is 2π then $v=-\frac{1}{2}$ and $H_y \propto x^{-\frac{1}{2}}$.
Equating the derivative of H_y with respect to x, to zero shows that the peak occurs for

$$x_m = y\cot\frac{\pi}{2(1-v)} \quad (y \text{ constant}) \qquad (7.7)$$

or at an angular increment

$$\delta A = \frac{y}{R}\cot\frac{\pi}{2(1-v)} \qquad (7.8)$$

from the pole-tip.
For $v=-\frac{1}{2}$, $\delta A = 0.3207..$. This compares with a theoretical value of 0.3219 from eq. (7.2) and a practical value of 0.322.. for 8 sub-elements.

7.3 Results

The chief results are given below for the two models. The potentials are -1,+1 A, and the units of H_r are A/m.

Pole centre-line - H_r

(i) pole surface R=41.25 mm

number of sub-elements	4	8	16	(theory)
model 1	17.198	17.298	17.319	17.324

(ii) rotor pitch circle R=40.85 mm

number of sub-elements	8	(theory)
model 1	17.485	17.493
model 2	17.567	

Peak values of H_r

(i) pitch circle radius 40.85 mm

number of sub-elements	8	16	(theory)
model 1	114.563	115.092	116.135
model 2	123.94	122.67	

(ii) pitch circle radius 40.45 mm

number of sub-elements	16
model 2	86.259

Permeance shape factor - S_p

(i) C-type sub-elements

number of sub-elements	4	8	16	(theory)
model 1	2.191	2.232	2.253	2.274
model 2	2.683	2.731	2.761	

(ii) V-type sub-elements

number of sub-elements	4	8	16	(theory)
model 1	2.270	2.273	2.274	2.274
model 2	2.793	2.783	2.781	

The Use of Divided Differences in Finite Element Calculations

M.J. Long and K.W. Morton
Department of Mathematics, University of Reading

Summary

Divided differences are used to calculate gradients of functions computed by finite element methods. On regular elements the finite element equations can be interpreted as finite difference equations with local truncation errors. Examples of this are given together with the results of numerical trials for gradient approximations.

1. Introduction

The work presented in this paper was prompted by considering the relationships which exist between finite difference and finite element methods. The use of divided differences for calculating the gradients of functions which have been computed by finite element schemes provides an opportunity to pool the advantages of the two approaches. This is of great practical interest since in many cases it is the gradient of the calculated quantity which is most useful - e.g., electric and magnetic fields obtained from their scalar and vector potentials. With higher order finite element methods, these quantities are often carried as nodal parameters, but we are concerned here with lower order methods where they are normally obtained by actual or approximate differentiation.

In [3] we consider quite general boundary value problems and finite element methods on regular meshes: we shall in this paper, however, concentrate on specific second order problems in the plane - typically, Poisson's equation $(-\nabla^2 u = f)$ with homogeneous boundary conditions. In weak form this problem becomes

$$a(u, v) = \langle f, v \rangle \qquad (1.1)$$

where

$$a(u, v) = \int_\Omega \left(\frac{\partial u}{\partial x}\frac{\partial v}{\partial x} + \frac{\partial u}{\partial y}\frac{\partial v}{\partial y}\right) dx\, dy , \qquad (1.2)$$

$$\langle f, v \rangle = \int_\Omega fv\, dx\, dy \qquad (1.3)$$

and Ω is the region of interest (with boundary Γ). We limit our attention in the main to cases where Γ is a polygonal boundary such that Ω can be exactly subdivided into a regular mesh of finite elements and this can be done for a sequence of mesh sizes characterised by element diameter h, with $h \le h_0$ and tending to zero. We consider nodal finite element approximations to u of the form

$$u^h(x, y) = \sum_{(j)} u_j \phi_j(x, y) \qquad (1.4)$$

where the parameters u_j are function values or derivatives of u^h at nodes labelled by the index j. The basis functions ϕ_j are polynomial in each element, with support localised to the elements neighbouring the point j - they span a space of functions which includes all piecewise polynomials of degree less than k. The specific finite element approximation to the solution u of (1.1) is determined by the Galerkin equations

$$a(u^h, \phi_j) = \langle f, \phi_j \rangle, \quad \text{for all } \phi_j , \qquad (1.5)$$

and standard error analysis (see [4]) gives

$$\|u - u^h\|_0 = O(h^k) , \qquad [a(u - u^h, u - u^h)]^{\frac{1}{2}} = O(h^{k-1}) , \qquad (1.6), (1.7)$$

where $\|v\|_0 = \langle v, v \rangle$: (1.7) expresses the lower order of accuracy of the derivatives of u^h.

Now let us suppose we can define D_h, a difference operator approximating the differential operator $D(= \partial/\partial x$ or $\partial/\partial y)$ to formal order of accuracy k: then in [3] we have shown that

$$\|D_h u^h - Du\|_0 = O(h^k) . \qquad (1.8)$$

The proof of (1.8) develops after applying the triangle inequality to $\|D_h u^h - Du\|_0$ several times: if we firstly define the interpolant of a function $v(x, y)$ to be

$$v^I(x, y) = \sum_{(j)} \bar{v}_j \phi_j(x, y) , \qquad (1.9)$$

where $\bar{v}_j$ is the value of v (or one of its derivatives) at node j, then

$$\|D_h u^h - Du\|_0 \le \|D_h u^h - D_h u^I\|_0 + \|D_h u^I - (D_h u)^I\|_0 + \|(D_h u)^I - D_h u\|_0 + \|D_h u - Du\|_0 . \quad (1.10)$$

The third and fourth terms are $O(h^k)$ from the approximating properties of the basis functions and the local accuracy of D_h; the second term is $O(h^k)$ for suitable choices of D_h - examples of these are given in section 3; the first term is the most interesting: due to the ellipticity of the initial problem, this term is $O(h^k)$ if we can show that

$$a(u^I - u^h, u^I - u^h) = O(h^{2k}) . \quad (1.11)$$

Now $$a(u^I, \phi_j) - \langle f, \phi_j \rangle = h^2 T_j \quad (1.12)$$

where T_j is the truncation error of the finite difference scheme to which this Galerkin equation is equivalent. Thus

$$a(u^I - u^h, u^I - u^h) = h^2 \sum_{(j)} e_j T_j \quad (1.13)$$

where $e_j = \bar{u}_j - u_j$, the finite element error in $\bar{u}_j$. The proof of (1.8) therefore hinges on the structure of the Galerkin equations and their corresponding truncations errors. In section 2 we examine some important particular cases to illustrate certain special features of these equations. In section 3 we summarise the results of numerical trials for a simple model problem. Finally, some consideration is given in the last section to the use of divided differences when irregular elements are used. Few theoretical results are then possible but the difference technique is still almost as simple to apply and a practical test has shown encouraging results.

2. Explicit forms of the Galerkin Equations

We consider Poisson's equation defined on a region in the plane. A regular square mesh is superimposed on the domain - a typical 'patch' of elements is shown in figure 1. In this section we look at some examples of individual Galerkin equations obtained using a series of standard two dimensional elements; we shall ignore boundaries and examine typical internal nodes and their associated finite element equations.

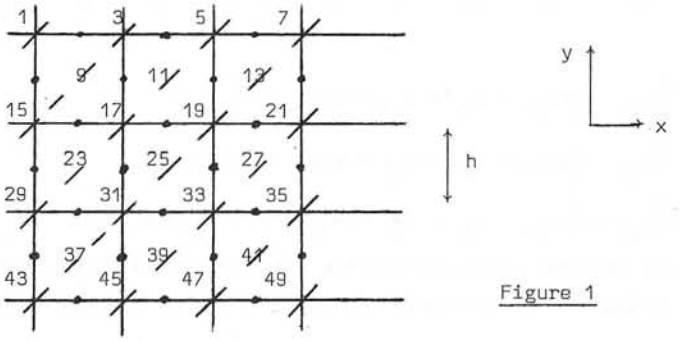

Figure 1

(a) Bilinear on a square:

The nodal parameters are the function values at the mesh points. There is only one type of node and corresponding Galerkin equation - typically node 31 of fig. 1; the equation here is

$$\frac{8}{3}u_{31} - \frac{1}{3}(u_{15} + u_{29} + u_{43} + u_{45} + u_{47} + u_{33} + u_{19} + u_{17}) = \langle f, \phi_{31} \rangle . \quad (2.1)$$

By expanding $a(u^I, \phi_{31}) - \langle f, \phi_{31} \rangle$ in a Taylor series expansion about node 31 we obtain

$$T_{31} = -\frac{h^2}{48}(3u_{xxxx} + 14u_{xxyy} + 3u_{yyyy})_{31} + O(h^4) \quad (2.2)$$

where $u_{xxxx} = \partial^4 u/\partial x^4$, etc. As the degree of approximation for this element is $k = 2$, the order of accuracy of T_{31} corresponds to the standard error estimate shown in (1.6).

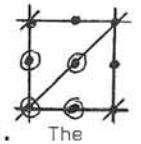

(b) Quadratic on a right triangle:

For this element the nodal parameters are again just function values but there are now four types of node - typically, points 31, 32, 24 and 25 in fig. 1. The corresponding Galerkin equations are respectively

$$4u_{31} - \frac{4}{3}(u_{30} + u_{38} + u_{32} + u_{24}) + \frac{1}{3}(u_{29} + u_{45} + u_{33} + u_{17}) = \langle f, \phi_{31} \rangle \quad (2.3)$$

$$\frac{16}{3}u_{32} - \frac{4}{3}(u_{31} + u_{39} + u_{33} + u_{25}) = \langle f, \phi_{32} \rangle \quad (2.4)$$

$$\frac{16}{3}u_{24} - \frac{4}{3}(u_{23} + u_{31} + u_{25} + u_{17}) = \langle f, \phi_{24} \rangle \quad (2.5)$$

$$\frac{16}{3}u_{25} - \frac{4}{3}(u_{24} + u_{32} + u_{26} + u_{18}) = \langle f, \phi_{25} \rangle \ . \quad (2.6)$$

Thus for mid-edge nodes one has the familiar second order, five-point scheme. The truncation errors of these difference schemes are

$$T_{31} = \frac{h^2}{48}(u_{xxxx} + u_{yyyy})_{31} + O(h^4) \quad (2.7)$$

$$T_j = -\frac{h^2}{144}(u_{xxxx} + u_{yyyy})_j + O(h^4) \ , \qquad j = 32, 24, 25 \ . \quad (2.8)$$

The order of accuracy of this element is ordinarily $k = 3$ but the truncation errors are one order lower. The Galerkin equations can however be combined into a reduced set relating the nodal parameters at points of type 25: by combining equation (2.7) with a linear combination of the surrounding equations of type (2.4), (2.5), (2.6), it is found that

$$\frac{10}{3}u_{25} - \frac{2}{3}(u_{23} + u_{39} + u_{27} + u_{11}) - \frac{1}{6}(u_9 + u_{37} + u_{41} + u_{13}) = \langle f, \Phi_{25} \rangle \quad (2.9)$$

where

$$\Phi_{25} = \phi_{25} + \frac{3}{8}(\phi_{24} + \phi_{32} + \phi_{26} + \phi_{18}) + \frac{1}{4}(\phi_{17} + \phi_{31} + \phi_{33} + \phi_{19}) + \frac{1}{16}(\phi_{10} + \phi_{16} + \phi_{30} + \phi_{38} + \phi_{40} + \phi_{34} + \phi_{20} + \phi_{12}) \ . \quad (2.10)$$

Equation (2.9) is the familiar nine-point difference scheme; its truncation error ($\overline{T}_{25}$) combines $3(=1 + 4\times\frac{3}{8} + 8\times\frac{1}{16})$ times (2.8) with $1(=4\times\frac{1}{4})$ times (2.7), and because of the symmetry we obtain $\overline{T}_{25} = O(h^4)$. Other combinations of the original equations (2.3)-(2.6) relate all the remaining nodal parameters to this reduced set. It follows that all the nodal errors are of the same order if those for the reduced system are of fourth order.

(c) Quadratic on a square:

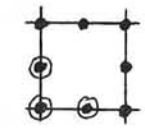

This element is at first glance very similar to the previous one except that there are only three types of node, that corresponding to the middle of the square being omitted. The Galerkin equations however take the more complicated form

$$208u_{31} - 74(u_{30} + u_{38} + u_{32} + u_{24}) + 45(u_{29} + u_{45} + u_{33} + u_{17}) - 23(u_{22} + u_{36} + u_{44} + u_{46} + u_{40} + u_{26} + u_{18} + u_{16} - u_{15} - u_{43} - u_{47} - u_{19}) = 45\langle f, \phi_{31} \rangle \quad (2.11)$$

$$208u_{32} - 74(u_{31} + u_{33}) + 16(u_{18} + u_{46}) - 23(u_{17} + u_{45} + u_{47} + u_{19}) = \langle f, \phi_{32} \rangle \quad (2.12)$$

with a similar equation using ϕ_{24}. The truncation errors are

$$T_{31} = \frac{h^2}{360}(25u_{xxxx} + 92u_{xxyy} + 25u_{yyyy}) + O(h^4) \quad (2.13)$$

$$T_{32} = -\frac{h^2}{360}(5u_{xxxx} + 46u_{xxyy} + 20u_{yyyy}) + O(h^4) \ . \quad (2.14)$$

Unlike the previous example, none of the nodal parameter sets can be eliminated, but combinations of the equations can yield a system where all the truncation errors are of fourth order.

(d) Hermite Cubic on a square:

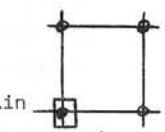

With this element there is only one type of node (typically node 31) but there are three types of Galerkin equation associated with each one of these points. The parameters at each node are the function value and the x- and y-derivatives. The Galerkin equations are

$$4416u_{31} - 696(u_{29} + u_{45} + u_{33} + u_{17}) - 408(u_{15} + u_{43} + u_{47} + u_{19}) + 6h(u^x_{33} - u^x_{29} + u^y_{17} - u^y_{45}) + 60h(u^x_{19} - u^x_{15} + u^x_{47} - u^x_{43} + u^y_{19} - u^y_{47} + u^y_{15} - u^y_{43}) = 1260\langle f, \phi_{31} \rangle \text{ [function value]} \quad (2.15)$$

$$h^2[272u^x_{31} - 46(u^x_{33} + u^x_{29}) + 32(u^x_{17} + u^x_{45}) + 2(u^x_{15} + u^x_{43} + u^x_{47} + u^x_{19})] - h[6(u_{33} - u_{29}) + 60(u_{19} - u_{15} + u_{47} - u_{43})] = 1260\langle f, \phi^x_{31}\rangle$$

[x-derivative] (2.16)

with a similar equation for ϕ^y_{31} — ϕ_{31}, ϕ^x_{31}, ϕ^y_{31} are the three types of basis function at node 31; u^x_j and u^y_j are the parameters associated with the x- and y-derivatives at node j. In all cases

$$a(u^I, \phi^*_{31}) - \langle f, \phi^*_{31}\rangle = O(h^6), \qquad \phi^*_{31} = \phi_{31}, \phi^x_{31}, \phi^y_{31} \quad . \tag{2.17}$$

However, only the first of these three equations is consistent with $-\nabla^2 u = f$; the other two are consistent with $-(u_{xxx} + u_{yyx}) = f_x$ and $-(u_{xxy} + u_{yyy}) = f_y$ respectively.

The first three examples given in this section are generalised in [3] to produce the theoretical arguments in proving (1.11). The last example is a case where we would not really expect to use divided differences, though in the next section this element provides a comparison with the accuracies achieved by differencing with lower order elements.

3. Numerical results for a simple model problem

Numerical experiments were conducted with Laplace's equation $\nabla^2 u = 0$ on the square $0 \le x, y \le 3$ with the natural or symmetry boundary condition $\frac{\partial u}{\partial y} = 0$ along $y = 0$ and u set equal to the solution $\ell n[(x - \frac{7}{2})^2 + y^2]$ on the other three sides of the square. Computations were carried out with $h^{-1} = 1, 2, 3, 4$ and 5 so that convergence tests could be made for overall and pointwise errors. We use the same elements as discussed in the previous section.

(a) Bilinear elements ($k = 2$):- we begin by checking whether (1.11) is approximately true for this element and compare the results with the error $a(u - u^h, u - u^h)$ [c.f. (1.7)]:

h^{-1}	1	2	3	4	5
$a(u^I - u^h, u^I - u^h)$	0.025	$0.0^2 49$	$0.0^2 13$	$0.0^3 47$	$0.0^3 20$

Convergence between last pair : $O(h^{3.8})$

$a(u - u^h, u - u^h)$	1.1	0.29	0.13	0.017	0.046

Convergence between last pair : $O(h^{2.0})$

This table confirms our expectations of the asymptotic behaviour of the error.

Three pairs of difference schemes were used for the gradients - these are all suitable for internal gradient approximations:

$$\left.\begin{aligned} D^{(1)}_x v &= [v(x + h, y) - v(x - h, y)]/2h \ , \\ D^{(1)}_y v &= [v(x, y + h) - v(x, y - h)]/2h \ , \end{aligned}\right\} \tag{3.1}$$

$$\left.\begin{aligned} D^{(2)}_x v &= [v(x + \tfrac{h}{2}, y) - v(x - \tfrac{h}{2}, y)]/h \ , \\ D^{(2)}_y v &= [v(x, y + \tfrac{h}{2}) - v(x, y - \tfrac{h}{2})]/h \ , \end{aligned}\right\} \tag{3.2}$$

$$D^{(3)}_x v = [v(x + \tfrac{h}{2}, y + \tfrac{h}{2}) + v(x + \tfrac{h}{2}, y - \tfrac{h}{2}) - v(x - \tfrac{h}{2}, y + \tfrac{h}{2}) - v(x - \tfrac{h}{2}, y - \tfrac{h}{2})]/2h \tag{3.3}$$

and similar expression for $D^{(3)}_y v(x, y)$; each is second order accurate to their respective derivatives. In table 1 we give the maximum error for $h^{-1} = 1, 3, 5$ over points which are the 'natural' centres for each scheme for all three values of h. Thus for $D^{(1)}_x$ and $D^{(1)}_y$ the points considered are (1, 1), (1, 2), (2, 1), (2, 2); for $D^{(2)}_x$ they are ($\frac{1}{2}$, 1), (1$\frac{1}{2}$, 1), (2$\frac{1}{2}$, 1), ($\frac{1}{2}$, 2), (1$\frac{1}{2}$, 2), (2$\frac{1}{2}$, 2), and for $D^{(2)}_y$, (1, $\frac{1}{2}$), (1, 1$\frac{1}{2}$), etc.; for $D^{(3)}_x$ and $D^{(3)}_y$ they are the centres of the nine unit squares which make up Ω. In the final columns of the tables are given the worst convergence rates over the same set of points, calculated from the errors for $h^{-1} = 3$ and 5.

Table 1 : Maximum errors for difference approximations to derivatives using bilinear elements.

	h^{-1} = 1	3	5	Conv Rate		h^{-1} = 1	3	5	Conv Rate
$D_x^{(1)}$	.046	$.0^2 44$	$.0^2 15$	2.0	$D_y^{(1)}$	.16	.020	$.0^2 72$	1.8
$D_x^{(2)}$	.080	$.0^2 41$	$.0^2 15$	2.0	$D_y^{(2)}$	.15	.020	$.0^2 74$	1.9
$D_x^{(3)}$	.041	$.0^2 82$	$.0^2 33$	1.6	$D_y^{(3)}$	.13	$.0^2 77$	$.0^2 30$	1.8

There would seem to be little to choose between the accuracies of the schemes, bearing in mind the differences between the points considered. However, by further comparison over the whole of Ω, the most compact schemes $D_x^{(2)}$ and $D_y^{(2)}$ appear to be the most reliable. It should be noted that the maximum error for the function values over the same set of points for $h^{-1} = 5$ is $0.0^3 74$. The differencing errors are somewhat larger than this, but at (1, 0) the function error does increase to $0.0^2 38$.

(b) Quadratic triangle elements (k = 3):- the Galerkin equations studied in the previous section suggested that the nodal errors for function values should converge like $O(h^4)$: this is in fact confirmed by the numerical experiments. One cannot expect this order of convergence between the nodal points where it drops to $O(h^3)$ - this is an example of the phenomenon of superconvergence (c.f. [1]). Similarly, we expect $a(u^I - u^h, u^I - u^h)$ to converge like $O(h^6)$ and not at an enhanced rate - the table below indicates the actual behaviour:

h^{-1}	1	2	3	4	5
$a(u^I - u^h, u^I - u^h)$	$0.0^2 38$	$0.0^3 27$	$0.0^4 46$	$0.0^4 12$	$0.0^5 37$
Convergence between last pair : $O(h^{5\cdot 3})$					
$a(u - u^h, u - u^h)$	0.073	$0.0^2 94$	$0.0^2 23$	$0.0^3 80$	$0.0^3 34$
Convergence between last pair : $O(h^{3\cdot 8})$					

The only difference schemes we have considered for the gradient are the usual fourth order approximations

$$D_x^{(4)} v(x, y) = [8v(x + \tfrac{h}{2}, y) - 8v(x - \tfrac{h}{2}, y) - v(x + h, y) + v(x - h, y)]/6h \qquad (3.4)$$

and a similar expression for $D_y^{(4)} v(x, y)$. In table 2 we give the errors obtained for $h^{-1} = 1, 3, 5$ at the central point $(1\frac{1}{2}, 1\frac{1}{2})$, which is one of the reduced set, and the maximum over the subsidiary points (1, 1), (1, 2), (2, 1), (2, 2). Except where noted convergence rates are calculated for the last pair of errors.

Table 2 : Maximum errors for difference approximations to derivatives using quadratic triangle elements.

		h^{-1} = 1	3	5	Conv Rate		h^{-1} = 1	3	5	Conv Rate
$(1\frac{1}{2}, 1\frac{1}{2})$	$D_x^{(4)}$	$.0^3 89$	$.0^5 29$	$.0^6 32$	4.3	$D_y^{(4)}$	$.0^3 89$	$.0^5 11$	$.0^6 12$	4.3
Subsid.	$D_x^{(4)}$	$.0^2 51$	$.0^4 74$	$.0^4 11$	3.7	$D_y^{(4)}$	$.0^2 28$	$.0^5 27$	$.0^5 18$	4.6

* between $h^{-1} = 1$ and 5

Clearly superconvergence also occurs for these gradient approximations, but the error increases between the nodes to give approximately the $O(h^3)$ convergence rate predicted by the analysis.

(c) Quadratic square elements (k = 3):- the results of numerical experiments were very similar to those for the previous element, all the function errors actually being $O(h^4)$. We give only the difference approximation errors, which were substantially larger, in table 3. The same difference schemes (3.4) were used.

Table 3 : Maximum errors for difference approximations to derivatives using quadratic square elements.

		h^{-1} = 1	3	5	Conv Rate		h^{-1} = 1	3	5	Conv Rate
$(1\frac{1}{2}, 1\frac{1}{2})$	$D_x^{(4)}$	$.0^2 36$	$.0^4 44$	$.0^5 57$	4.0	$D_y^{(4)}$	$.0^2 74$	$.0^6 23$	$.0^6 31$	6.2*
Subsid.	$D_x^{(4)}$	.031	$.0^3 35$	$.0^4 37$	4.4	$D_y^{(4)}$	$.0^2 68$	$.0^4 55$	$.0^5 73$	4.0

* between $h^{-1} = 1$ and 5

(d) Hermite Cubic elements (k = 4):- the numerical results showed that both function and derivative errors at nodes converged like $O(h^4)$. However, one important point arises: over the four points (1, 1), (1, 2), (2, 1), (2, 2), the divided difference results for quadratics were more accurate than the direct derivative approximations achieved with this element.

4. Concluding Remarks

To be of practical utility, the divided difference techniques described above must be applicable to a finite element solution obtained with irregular elements. Very few theoretical results are then possible, though in one-dimension certain hypotheses can be deduced. Basically, there are two general rules here: (1) there needs to be a smooth variation of the mesh over the domain; (2) the step length and difference scheme used at any point should be determined by the most closely approximating uniform mesh. Many automatic element generators start with a basic mesh which is regular over large regions and incorporate smoothing algorithms to be applied to irregularities introduced at boundaries, interfaces, etc.; in these cases the rules should be easy to apply. A simple practical example in the computation of surface velocities over an aerofoil has produced encouraging results (c.f. [2]). More computational experience is needed, however, before being too definite or attempting to obtain theoretical results.

References

[1] Douglas, J.H. and Dupont, T. : 1972, Proc. Conf. on Numerical Analysis, (ed. J.J.H. Miller) Royal Irish Academy, Dublin.

[2] Long, M.J. : 1975, Ph.D. thesis, University of Reading.

[3] Long, M.J. and Morton, K.W. : 1975, Numerical Analysis Report 2/75, Dept. of Maths., University of Reading.

[4] Strang, G. and Fix, G.J. : 1973, 'An anlysis of the finite element method', New York, Prentice-Hall.

DETERMINATION OF MAGNETIC FIELDS AT THE CONDUCTOR FOR SOLENOIDS AND TOROIDS

R. W. Moses, Jr. and R.L. Willig
University of Wisconsin, Madison, Wisconsin, U.S.A.

ABSTRACT

Superconducting magnets must have the magnetic field smaller than the critical field the conductor is designed for. For optimal use of material the maximum field should be known everywhere along the length of the conductor. Here large single layer solenoids with superconductive energy storage applications are considered. An analytic expression is given for the midplane field correction due to conductor separation. Similar expressions are presented for sectored toroidal tokamak coils. Numerical examples are given to demonstrate the large fields found at the ends of single layer solenoids. Optimization procedures are used to redistribute conductors to reduce the end fields to acceptable levels.

INTRODUCTION

In most discussions of the magnetic fields and forces for solenoids and toroids it is assumed that the current flows in a continuous sheet at the surface of the magnet. Although this simplifies many computations it does not account for field variations near individual conductors. Also large radial fields at the ends of a solenoid are often neglected. These effects and some means of compensating them will be examined in detail in this paper.

First let us consider a solenoid or toroid with current distributed uniformly over the surface in a thin sheet. There are N turns of conductor carrying a current I. For a solenoid of length ℓ and diameter D, the aspect ratio is defined as $\beta \equiv \ell/D$. When β is large the internal field away from the ends is $B \simeq \mu_o NI/\ell$. For smaller values of β the maximum field on the midplane, B_M, is at the inner surface of the wall and is expressed as follows

$$B_M = \mu_o NI\, K'(\beta)/\ell. \tag{1}$$

$K'(\beta)$ is a correction factor between 0.5 and 1 (Moses, 1975).

The field in a toroid with uniform surface currents is expressed in terms of the radius, as measured from the major axis, R. Once again taking N turns of current I one gets

$$B = \mu_o NI/2\pi R. \tag{2}$$

The purpose of this paper is to present corrections to Eqs. (1) and (2), accounting for the use of conductors of finite size and separation. We also discuss the reduction of the end fields of solenoids. These can be substantially greater than the expression given in Eq. (1) (Walstrom and Lubell, 1973). As an example it is commonplace to see field increases of more than 100% over Eqs. (1) for energy storage magnets. When the conductor critical field is exceeded anywhere in a superconducting magnet part, if not all, of the magnet goes normal. For this reason it is essential to know the maximum field at each segment of conductor and be able to design magnets free of unnecessarily high fields.

MIDPLANE CORRECTION

We now consider a single layer solenoid made of a circular cable of radius c. The number of conductors per unit length is $n = N/\ell$, then the center to center separation of the cables is $s = 1/n$. The fraction of magnet surface covered by conductor is defined as the ratio $\gamma \equiv 2c/s$.

To obtain the correction for the discrete conductor field, consider an infinite plane of straight parallel cables next to a conducting sheet, see Fig. 1. The maximum field, B_m, is on the leftmost edge of each conductor, and it is given by

$$B_m = \mu_o nI\left[\frac{1}{2} + \frac{\gamma}{\pi}\sum_{j=-\infty}^{\infty}\frac{1}{\gamma^2+4j^2}\right]$$

$$= \mu_o nI[1 + K''(\gamma)]. \tag{3}$$

Equation (3) can be solved for K"; the results are plotted in Fig. 2. An approximate expression of K" is also shown,

$$K'' = \frac{1}{\pi\gamma} + \frac{\pi\gamma}{12} - \frac{1}{2}\,. \tag{4}$$

This is accurate to 10% for $\gamma \leq 0.7$.

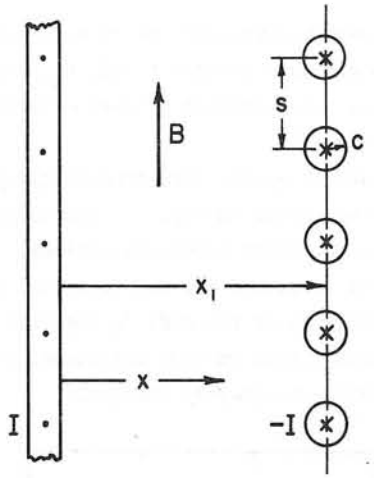

Fig. 1. Cross section of a set of straight conductors parallel to a uniform conducting sheet.

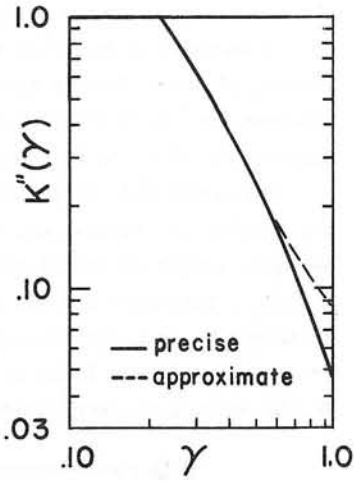

Fig. 2. Discrete coil correction factor as a function of γ.

Equation (3) is arranged to define K" as a correction to the field between two parallel conducting planes, $\mu_o nI$. Most of the value of K" is attributable to conductors close to the point where B_m is measured, thus the cables of Fig. 1 could be wrapped into a solenoid without changing the meaning of K". Now Eq. (1) is rewritten to give the maximum field at the conductor on the midplane of a solenoid

$$B_M = \mu_o nI[K'(\beta) + K''(\gamma)] \ . \qquad (5)$$

This and Fig. 2 make it clear that single layer solenoids with $\gamma < 1$ have maximum midplane fields substantially larger than those found in the continuous sheet model, Eq. (1). Throughout the paper B_m defines the maximum field on any segment of conductor while B_M defines the maximum midplane field.

END FIELD

If a thin walled solenoid is wound with turns evenly distributed along its length, very large radial fields are obtained at the ends of the magnet. A computer program was written to give the field on the inner side of the conductor at all points along the length of a solenoid.

Figure 3 illustrates these results for solenoids formed by continuous sheets of current. When a solenoid is infinitesimally thin there is a logarithmic singularity in the end field. This is shown for a variety of aspect ratios in Fig. 3.

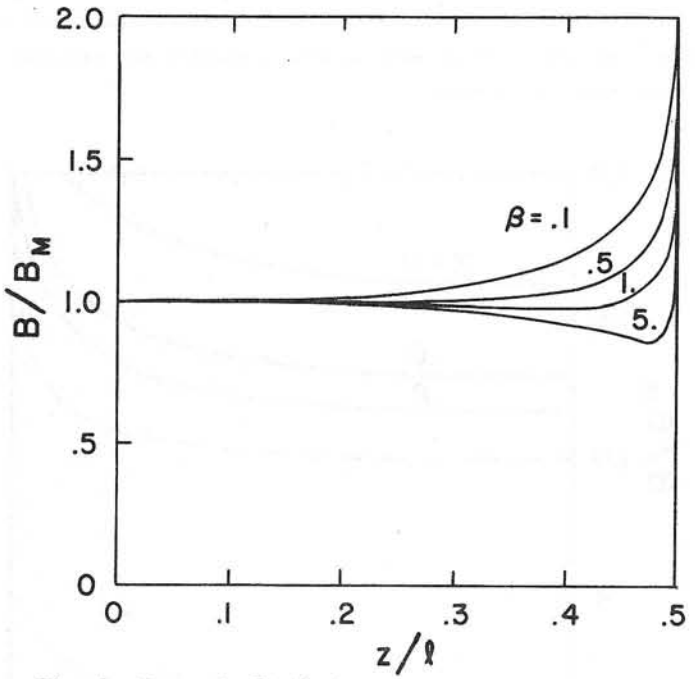

Fig. 3. Magnetic field along the inside surface of an infinitesimally thin solenoid with a uniform continuous current distribution.

As in the case of Eqs. (1) and (5) the conductor fields change for single layer solenoids made of discrete circular cables. Approximate values for the maximum field at each conductor are plotted for a $\beta = 0.3$ solenoid with several values of γ in Fig. 4.

The data in Figs. 3 and 4 make it clear that end fields can be very large in thin single layer solenoids. Such devices are particularly of interest for energy applications (Boom et al. 1974, 1976). Single layer magnets with nearly a thousand closely spaced turns are envisioned, certainly matching the severe field conditions shown in Fig. 4.

By varying the spacing of conductors along the length of a solenoid it is possible to manipulate the fields of Figs. 3 and 4 to

more desirable distributions. Since we are primarily concerned with energy storage, we want to store the maximum amount of energy with a given amount of conductor. In a solenoid one always maximizes the stored energy by placing the conductors as close together as possible. This is limited by the boundary condition that the critical field cannot be exceeded. Assuming there is one critical field, the stored energy is a maximum when the field at each conductor reaches the critical value (or a specified design limit).

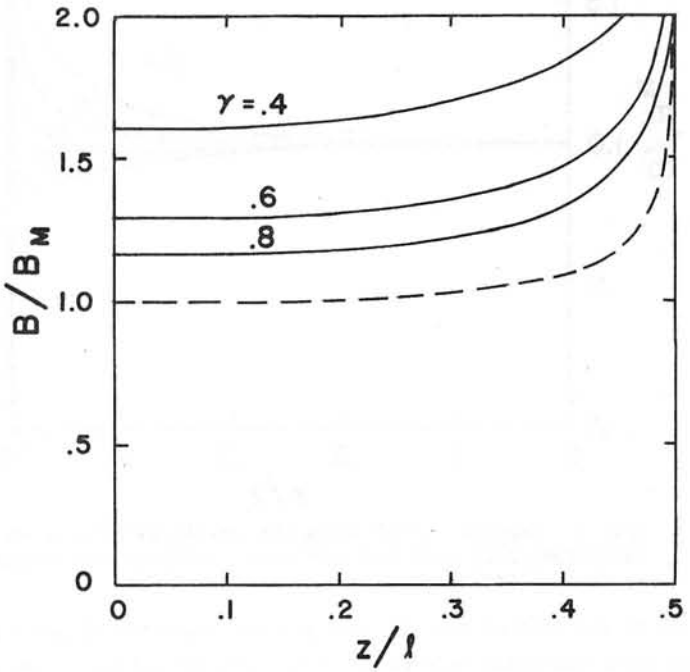

Fig. 4. Maximum field at the conductors of a single layer solenoid with current uniformly distributed in round conductor (N = 200). Here B_M in the midplane maximum for the current sheet model.

A smooth current distribution can be obtained by placing flat conductors close together. This gives a good mathematical model but is physically unrealistic. It is anticipated that large energy storage magnets would have a single layer of round superconducting cable embedded in a high purity aluminum stabilizer (Boom et al., 1975). Since the current is concentrated in the superconducting cable, we neglect the stabilizer. The variable current distribution is obtained by control of the conductor spacing s = 1/n.

A computer program was written which expresses the current per unit length, nI, as a Fourier series. A midplane maximum field, B_M, was selected and the Fourier coefficients were adjusted to make a least squares fit of B_m to B_M along the solenoid.

Solenoids made of continuous current sheets were studied first and the results for several values of β are given in Fig. 5. The current per unit length is normalized to the specified mid-field maximum, $\mu_o nI/B_M$. Typically the rms deviation is ≤0.03% for ten expansion coefficients. As expected, only a reshaping of the ends is required to bring the conductor field to a constant value in long solenoids, β = 5. On the other hand, very short solenoids are grossly reshaped.

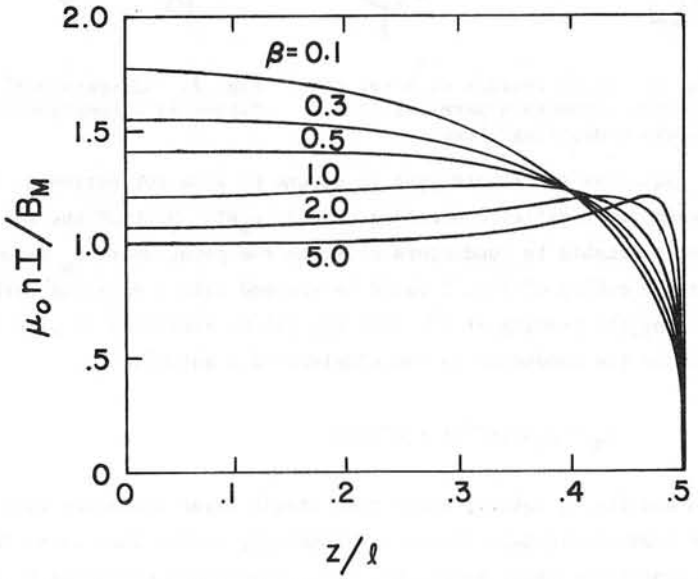

Fig. 5. Current distribution required to make the magnetic field constant along the inside surface of an infinitesimally thin solenoid.

The case of discrete round conductors was also studied and results are given for β = 0.3 and several values of γ_o in Fig. 6. Here $\gamma_o = 2c/s_o$ only represents the midplane value of γ. Each conductor carries the same current introducing a self field that is the same for all conductors. This leads to the radically different nI values in Fig. 6. Here

the end effects alter a much larger portion of the magnet than in the case of a continuous sheet conductor.

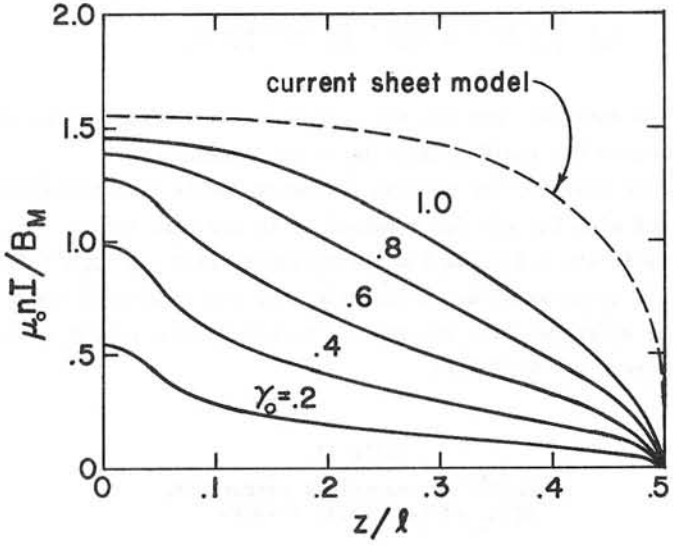

Fig. 6. Current distribution required to make the maximum magnetic field the same at every turn of a single layer solenoid.

Numerical computations for Fig. 6 were more difficult with rms errors of ≤1%. Detailed information on the numerical techniques will be published at a later date.

To quantify the above results we note that the ampere meters of conductor required to store a given amount of energy at a specific maximum field are (Moses, 1975)

$$IS = Q_{is} E^{2/3}/B_M^{1/3}. \quad (6)$$

Also the radius of a solenoid is given by the expression

$$r = GE^{1/3}/B_M^{2/3}. \quad (7)$$

The quality factor Q_{is} and the coefficient G are presented in Table I for the solenoids described in Figs. 3-6.

Table I

Conductor and radius factors for solenoids with constant field distributions as compared to those with constant current distribution

		Constant Current		Constant Field	
		Q_{is}	G	Q_{is}	G
	β	$AmT^{1/3}/J^{2/3}$	$mT^{2/3}/J^{1/3}$	$AmT^{1/3}/J^{2/3}$	$mT^{2/3}/J^{1/3}$
Continuous Current Sheet Model	0.1	604	0.0185	624	0.0205
	0.3	576	0.0112	582	0.0119
	0.5	592	0.00922	593	0.00954
	1.0	651	0.00731	646	0.00732
	2.0	759	0.00590	751	0.00578
	5.0	974	0.00437	966	0.00428
Discrete Conductor Model, β = 0.3	γ				
	0.2	806	0.0220	1009	0.0402
	0.4	675	0.0154	807	0.0255
	0.6	627	0.0133	706	0.0193
	0.8	606	0.0124	645	0.0159
	1.0	599	0.0121	622	0.0144

It must be emphasized that B_M represents the maximum midplane field in all cases. However, the end fields will be larger than B_M when the current distribution is uniform, Figs. 3 and 4. B_M for uniform current distributions is given by Eqs. (1) and (3). These formulae were used in earlier studies to establish values for Q_{is} and G. It was assumed that end fields would be compensated at a later date. Now Table I shows the minimum adjustments required to keep the field at all conductors within the limit of B_M.

It is very unlikely that a practical magnet would be built to the specifications outlined above. However, we have placed lower bounds on the conductor requirements, Q_{is}, and given an indication of the overall current distribution to strive for.

The problem of end fields may be partially solved by adding more superconductor in the ends of a magnet. That is, the field design limit of the composite superconductor is brought closer to the critical field

in the end turns. A tailored conductor design along with a compromise between the conductor and field distributions of Figs. 4 and 6 may give optimal results.

TOROIDAL FIELDS

Although toroidal magnets do not have the end field problems associated with solenoids, there can be a substantial field correction due to the discrete nature of a conductor. Equation (2) can be corrected in a manner similar to Eq. (1). A toroid can be treated as a solenoid with a component of toroidal curvature. Such a procedure gives very accurate expressions of the magnetic force on a sectored toroid (Moses and Young, 1975).

The midplane cross section of a toroidal field magnet is shown in Fig. 7, and a horizontal view is given in Fig. 8. Here ρ is the radius of curvature of the conductor which can vary along the coil, and the angle ϕ describes locations on the coil.

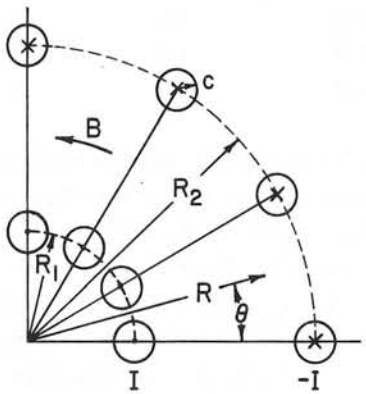

Fig. 7. Midplane cross section of a toroidal field magnet.

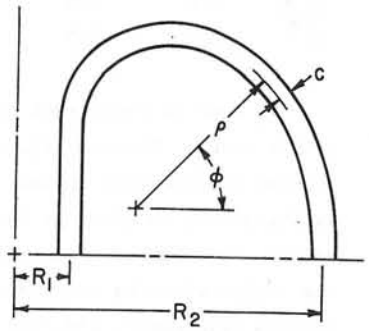

Fig. 8. Horizontal view of a toroidal field coil.

Equations (2) and (3) provide the basis for the expression of conductor field, but we add a correction for solenoidal curvature

$$\frac{\mu_o I}{2\pi\rho} \ln \frac{1.284R}{cN},$$

see Moses and Young (1975) Eq. (14). Incorporating the equations listed above one can approximate the field on the inner surface of a conductor as follows

$$B_m = \frac{\mu_o NI}{2\pi R}\left[1 + K''\left(\frac{Nc}{\pi R}\right) + \frac{R}{N\rho} \ln \frac{1.284R}{cN}\right]. \qquad (8)$$

Here R is measured from the major axis to the inside surface of the conductor where the field maximum is to be determined.

As an example, the maximum conductor fields were calculated numerically and with Eq. (8) for a toroid of 18 circular coils. The major and minor radii are 1.5 m and 1 m respectively while $c \equiv \pi\rho/N = 8.73$ cm. Here I is taken as 10^6A. A comparison of the results is shown in Table II. The numerical data are accurate to better than 0.01%; hence, Eq. (8) has an error of $\leq$ 2% here.

Table II

Analytic and numerical expressions of B_m on an 18 coil toroid.

ϕ	R/m	$N_c/\pi R$	K''	B_m/T	
				analytic	numerical
0	2.413	0.2072	1.090	3.25	3.31
$\pi/2$	1.500	0.333	0.540	3.74	3.80
π	0.573	0.851	0.0752	6.44	6.51

With the expression of Eq. (8) one now has a simple accurate formula for the maximum field on toroidal coils. This can serve as a replacement for many of the extensive computer field computations previously required to get the same data.

CONCLUSION

In this paper we have outlined semianalytical techniques for obtaining local fields in solenoids and toroids. A systematic reduction of the severe end fields of thin walled solenoids was presented. The results given here should enable the magnet designer to approach predetermined conductor field limits with greater precision and optimum use of material.

ACKNOWLEDGEMENTS

The authors would like to thank Professors R.W. Boom, H.A. Peterson and W.C. Young and Dr. M.A. Hilal for many helpful discussions of this work. We are also grateful to the Wisconsin Alumni Research Foundation, the National Science Foundation and the Wisconsin Electric Utilities Research Foundation for supporting this work.

REFERENCES

R.W. Boom, et al., "Wisconsin Superconductive Energy Storage Project," Feasibility Study Report, Volume 1, Madison, Wisconsin (July 1, 1974).

R.W. Boom, et al., "Magnet Design for Superconductive Energy Storage for Power Systems," 5th International Conference on Magnet Technology, Rome (April, 1975).

R.W. Boom, et al., "Wisconsin Superconductive Energy Storage Project," Feasibility Study Report, Volume 2, Madison, Wisconsin (1976).

R.W. Moses, "The Configurational Design of Superconductive Energy Storage Magnets," to be published in Advances in Cryogenic Engineering, Vol. 20, Plenum Press (1975).

R.W. Moses and W.C. Young, "Analytic Expressions for Magnetic Forces on Sectored Toroidal Coils," presented at the Sixth Symposium on Engineering Problems of Fusion Research, San Diego, Calif. (November 18-21, 1975).

P.L. Walstrom and M.S. Lubell, "Calculation of Radial Magnetic Fields for Axisymmetric Solenoids with Rectangular Cross-Section," ORNL-TM-4198, Oak Ridge National Laboratory (April, 1973).

A FORTRAN PACKAGE FOR SOLVING LINEAR ALGEBRAIC EQUATIONS WITH A LARGE DENSE MATRIX USING DIRECT ACCESS DISK STORAGE

M J Newman
Rutherford Laboratory, Chilton, Didcot, Oxon, OX11 0QX

1. INTRODUCTION

In solving the non-linear integral equation occurring in the GFUN[1,2,3,4] magnet design program, a requirement arose for solving large linear problems with a general dense matrix of coefficients. The matrix was too large to be held in main memory, and was stored on a direct access disk dataset. The method to be described uses Gaussian Elimination and Back Substitution. The matrix is partitioned so that only a fraction of the whole matrix need be in main memory at any time. The method has been optimised to minimise the total elapsed time required for solution. To solve a problem of order 1000 on an IBM 360/195 computer using 516k bytes of main memory and 4M bytes of a 3330 disk took 19 minutes, of which 5.6 minutes was central processor activity.

The computer package is coded in Fortran and all input and output is handled in a single routine. It should be a simple matter to implement the package on any computer.

An additional facility is provided whereby having solved a system $A\underline{x} = \underline{b}$, a similar system $A\underline{x} = \underline{c}$ can be solved very economically using the factorised matrix which is stored on the disk.

2. METHOD

Since, for the particular problem in hand, the matrix had no convenient properties such as symmetry or sparseness, the method used is Gaussian Elimination with Back Substitution. The complete matrix is partitioned into square sub-matrices. Each sub-matrix forms a single record on the disk. The order of the sub-matrix can be chosen by the user subject to a maximum of 32767 bytes (order = 90) imposed by the Fortran Direct Access system. At any time, four sub-matrices are present in main memory. It is convenient to consider the complete matrix A (of order n) being partitioned as follows:

$$A = \begin{vmatrix} a_{11} & a_{12} & a_{13} & \cdots & a_{1m} \\ a_{21} & a_{21} & a_{23} & \cdots & a_{2m} \\ \vdots & & & & \vdots \\ a_{m1} & a_{m2} & a_{m3} & & a_{mm} \end{vmatrix}$$

where a_{ij} is a square sub-matrix of order p. Then m = n/p. At a general stage in the elimination process the four sub-matrices in main memory will be:

1. A Pivotal sub-matrix a_{ii} $(1 \leqslant i \leqslant m-1)$
2. A Sub-Pivotal sub-matrix a_{ki} $(i < k \leqslant m)$
3. A Cross-Pivotal sub-matrix $a_{i\ell}$ $(i < \ell \leqslant m)$
4. A Cross Sub-Pivotal sub-matrix $a_{k\ell}$

Suffix i ranges from 1 to m-1. For every value of i, suffix k ranges from i+1 to m. For every value of k, suffix ℓ ranges from i + 1 to m. For each new value of i, when k = i + 1, the two sub-matrices a_{ii} and a_{ki} are searched to find the element in each column below the diagonal which has the largest modulus. The row number is stored in work space provided by the user and that row is exchanged to become the pivotal row. The search for largest element has been restricted to two sub-matrices in order to restrict the number of disk accesses. For the application in mind it was thought to be extremely unlikely that this limitation will be noticeable. As a precaution the package prints out the maximum multiplying factor used as an indication of how effective this restricted search has been. Values are typically between 1 and 2. In the event of no non-zero elements being found an error diagnostic is printed and the program stops. As elements which lie below the diagonal are eliminated they are over-written with the appropriate multiplying factor. As many operations as possible are performed on each sub-matrix before returning it to the disk. The complete algorithm can be best understood by referring to diagrams 1 to 4.

In order to reduce the accumulated rounding error, each sub-matrix is stored with double precision (64 bit) accuracy in main memory. However, to reduce the number of disk accesses, each sub-matrix is truncated to

single precision (32 bit) accuracy before storing it on the disk. The total number of disk accesses is:

$$\frac{1}{6}[8m^3 - 3m^2 + 13m - 6]$$

for an order of 1000, where m = 12, this is 2257. The average number of truncations is:

$$\frac{1}{6}[4m - 3 + \frac{5}{m} - \frac{6}{m^2}]$$

which for the same problem is 7.5 truncations. Since the number of numerical operations is approximately $\frac{1}{3} \times 10^9$, it will be seen that the saving in the number of disk accesses does not introduce an unacceptable decrease in accuracy. It should be noted, however, that troubles may be expected if the facility for resolving similar problems with the same matrix is used for iterative refinement.

Since on most machines the residuals could only be calculated with 64 bit accuracy, this may not be sufficiently greater than the overall accuracy of the factorisation,and the refinement procedure may not converge.

3. EFFICIENCY

The efficiency of the package is best illustrated by some statistics from sample runs.

Order of main matrix n	Order of sub-matrix p	Total No. of sub-mcs. m	Disk space (Mbytes)	Main memory (Kbytes)
200	20	100	0.16	70
500	50	100	1.0	194
1000	90	144	4.67	516

Order of main matrix	Solve $A\underline{x} = \underline{b}$			Resolve $A\underline{x} = \underline{c}$		
	CPU time (mins)	Lapsed time (mins)	Total No. of disk access	CPU time (mins)	Lapsed time (mins)	Total No. of disk access
200	0.0766	0.856	1304	0.00342	0.0737	110
500	0.801	5.25	1304	0.0136	0.55	110
1000	5.56	19.10	2257	0.0509	0.302	156

The elapsed time for a solution will depend on the number of disk accesses, the size of each record, and the intensity of activity from concurrent jobs on the shared channel to the disk.

4. USER INTERFACE

The matrix must first be stored on a disk dataset in the required format. First, p, the order of each sub-matrix should be chosen as large as the main memory allows. The maximum value which p can take is 90. This results in a record size of 32400 bytes. Next the value of m must be calculated. This is n/p rounded up to the nearest integer if necessary. The package allows for m not being a factor of n. The dataset is then created with code similar to the following:

```
      REAL*4 C4 (90,90)
      DO 1 J = 1, M
      DO 2 I = 1, M
[here fill C4 array with appropriate coefficients]
      NREC = (J - 1)*M + I
      WRITE (KSTR1'NREC) C4
    2 CONTINUE
    1 CONTINUE
      STOP
      END.
```

Next, in order to solve a system $A\underline{x} = \underline{b}$, the user must call subroutine DSKSOL. The argument list is as follows:

No.	Name	Type	Dimensions	Purpose
1	C11	Real*8 array	(MD,MD)	Work space for a sub-matrix
2	C21	"	"	" " " " " "
3	C12	"	"	" " " " " "
4	C22	"	"	" " " " " "
5	C4	Real*4 array	"	Work space for a record
6	MD	Integer variable	-	Dimension of above arrays
7	SOL	Real*8 array	(IORD)	Contains solution on return
8	B	"	"	Contains vector b on calling
9	USED	Integer*2 array	(MSQ)	Work space(see note 1 below)
10	IPIV	"	(IORD)	Work space
11	KSTR1	Integer variable	-	Stream No.of datset with matrix A
12	KSTR2	"	-	" " " "for factorised matrix
13	M	"	-	Order of sub-matrix
14	IORD	"		Order of complete matrix

Notes:

1. MSQ $\geqslant M^2$
2. MD $\geqslant$ M
3. B must contain the values of the vector b before DSKSOL is called. These values are destroyed by DSKSOL.
4. The dataset on KSTR2 must be identical in structure to that on KSTR1. If the original matrix A is not required after the solution is obtained, set KSTR2 = KSTR1 and only supply one dataset.

In order subsequently to solve a similar system $A\underline{x} = \underline{c}$, the user must call subroutine NEWRHS with a very similar argument list. This routine will destroy the values in the array c.

5. CONCLUSIONS

This package allows the solution of linear problems for which the coefficient matrix is larger than that which can be held in main memory. It is optimised towards minimising the total elapsed time for a solution. The accuracy obtained is close to that when the whole problem is solved in main memory with a word length of 64 bits.

6. REFERENCES

1. M J Newman, C W Trowbridge, L R Turner. GFUN: An Interactive Program as an aid to Magnet Design. RPP/A94. Also in Proc. 4th Int. Conf. on Magnet Technology, Brookhaven, 1972.

2. M J Newman, J Simkin, C W Trowbridge, L R Turner. GFUN Users Guide - A user guide to an Interactive Graphics Program for the Computer Aided Design of Magnets. RHEL/R244, 1972.

3. C J Collie, N J Diserens, M J Newman, C W Trowbridge. Progress in the Development of an Interactive Computer Program for Magnetic Field Design and Analysis in Two and Three Dimensions. RL-73-077. Also in Proc. Conf. on Analysis of Magnetic Fields, Nevada, 1973.

4. A G A M Armstrong, C J Collie, N J Diserens, M J Newman, J Simkin, C W Trowbridge. New Developments in the Magnet Design Computer Program GFUN. RL-75-066. Also in Proc. 5th Int. Conf. on Magnet Technology, Frascati, Rome, 1975.

7. ACKNOWLEDGEMENTS

The author wishes to thank Mr C W Trowbridge, Applied Physics Division, Rutherford Laboratory, for the motivation and encouragement to complete this work, and Dr J K Reid, Theoretical Physics, AERE Harwell, for the suggestion of the optimum algorithm.

MAIN FLOW DIAGRAM

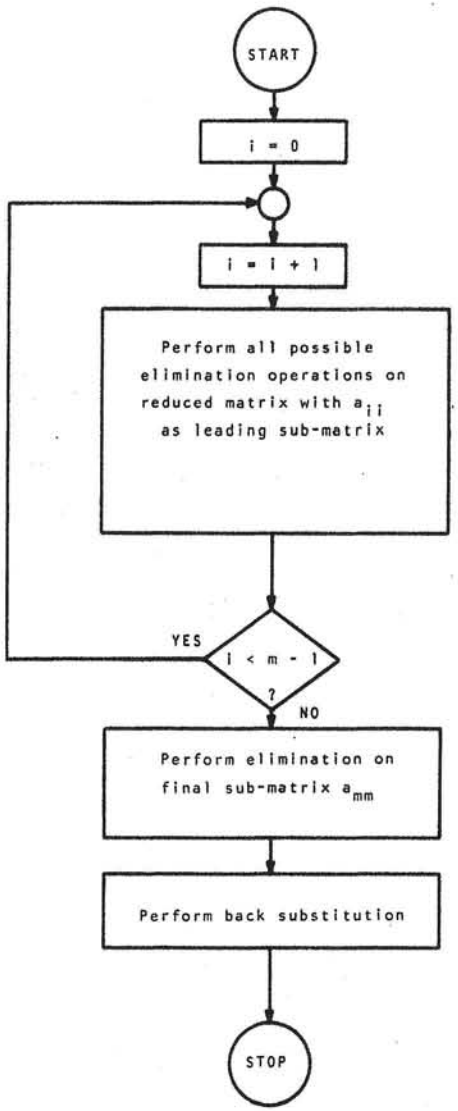

DIAGRAM 1

PERFORMING ALL POSSIBLE ELIMINATION OPERATIONS ON REDUCED MATRIX WITH a_{ii} AS LEADING SUB-MATRIX

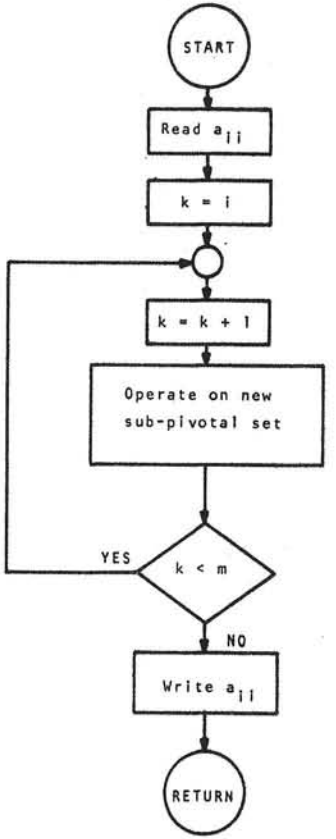

DIAGRAM 2

OPERATION ON NEW SUB-PIVOTAL SET

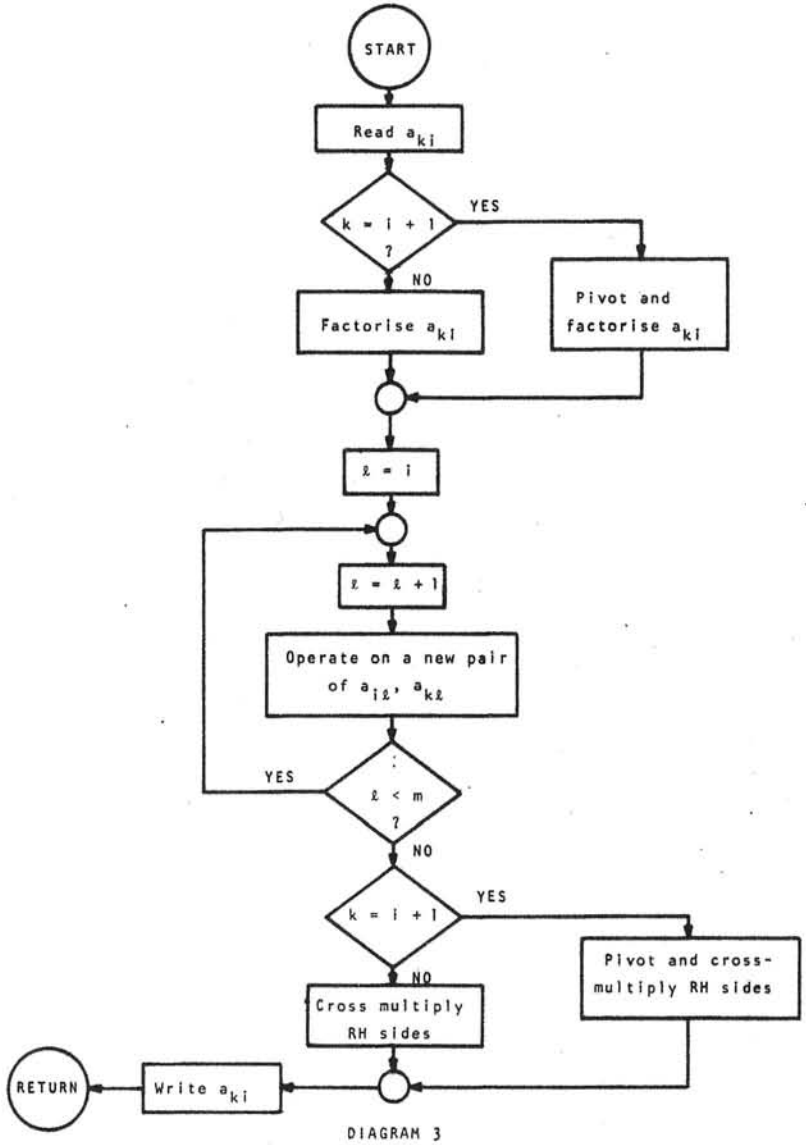

DIAGRAM 3

OPERATIONS ON A NEW PAIR $a_{iℓ}$ AND $a_{kℓ}$

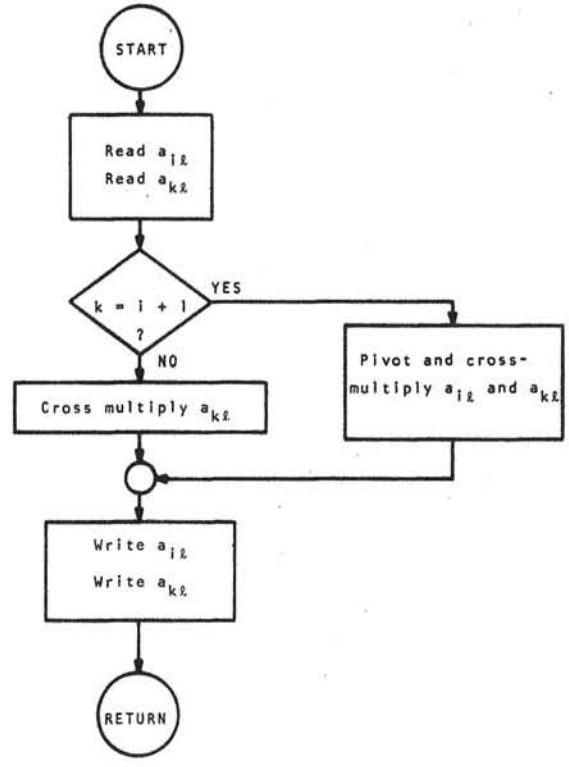

DIAGRAM 4

COMPUTATION OF THE INTEGRATED MULTIPOLE FIELD COMPONENTS IN A SUPERCONDUCTING QUADRUPOLE MAGNET WITH CONSTANT PERIMETER COIL ENDS

T. Tortschanoff
CERN
Geneva, Switzerland

INTRODUCTION

Several attempts have been made to calculate the multipole field components produced by a quadrupole geometry including the contribution of the ends of windings. In particular, at Saclay and Rutherford Laboratory the constant perimeter geometry has been extensively treated[1,2]. However, none of these calculations can be adapted to treat the geometry of the coil ends as they are actually manufactured at CERN and which represent a practical approximation of the ideal constant perimeter geometry.

For this reason, it was necessary to develop a special computer program to calculate the multipole components of the geometry which describes the quadrupole magnet in question. This calculation is especially important for the optimization of the space between each end of winding for the compensation of higher multipole components: by variation of the straight lengths, which determine the position of the ends of winding, one can eliminate a number of integrated multipole components which equals the number of coils per pole minus one. Thus, in the case of three windings per quadrant, the 12- and 20-pole components can be eliminated theoretically. In practice, however, this will not usually be feasible and other criteria for the optimization of the straight length have to be taken into account. In our case, the sum of the integrated gradient errors and the sum of their absolute values inside the useful region were taken as criteria.

1. METHOD OF CALCULATION

The method applied in these calculations is first to separate the straight part and the ends. The ends are treated as a series of very short straight parts by cutting them into a great number of thin slices perpendicular to the longitudinal axis of the magnet.

According to the complex variable method[3,4], for the two-dimensional case of a cylindrical geometry, the magnetic field produced by a sector winding can be written:

$$\vec{F} = B_y + i B_x = -\sum_{n=1}^{\infty} (a_n + b_n) z^{n-1} , \quad z = x + iy , \tag{1.1}$$

where, in the case of quadrupole windings, the contribution of each block of winding is (see Fig. 1)[5]:

$$a_n = \frac{4\mu_o}{\pi} \frac{j_o \left(r_2^{2-n} - r_1^{2-n}\right)}{n(2-n)} (\sin n\phi_2 - \sin n\phi_1)$$

$$n \neq 2, \; n = 6, 10, 14, \ldots$$

$$a_2 = \frac{2\mu_o}{\pi} j_o \ln \frac{r_2}{r_1} (\sin 2\phi_2 - \sin 2\phi_1) \tag{1.2}$$

$$b_n = \frac{4\mu_o}{\pi} \frac{j_o}{R^{2n}} \frac{\left(r_2^{n+2} - r_1^{n+2}\right)}{n(n+2)} (\sin n\phi_2 - \sin n\phi_1)$$

$$n = 2, 6, 10, 14, \ldots$$

j_o is the current density in the longitudinal direction
R is the inner radius of a $\mu = \infty$ cylindrical iron screen.

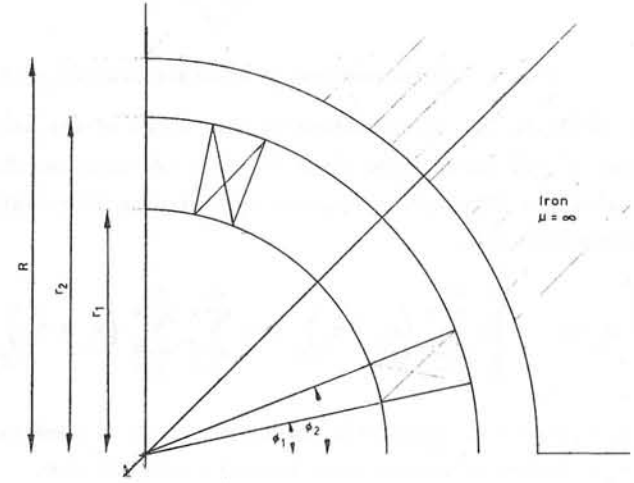

Fig. 1 Scheme for computation.

In order to extend these two-dimensional formulae to our three-dimensional problem, the a_n and b_n values have to be multiplied by the straight length, ℓ, and by the thickness of the thin slices, Δs, into which the ends are cut.

The geometry of the straight part of the coil is determined by the conductor which, in our case, is solid with rectangular cross-section. As shown in Fig. 2, the lateral sides of the blocks are parallel. Therefore, the blocks must be approximated by a suitable number of concentric layers which are treated as sectors. For each layer, the angles ϕ_1 and ϕ_2 can easily be determined from the design data (Fig. 2).

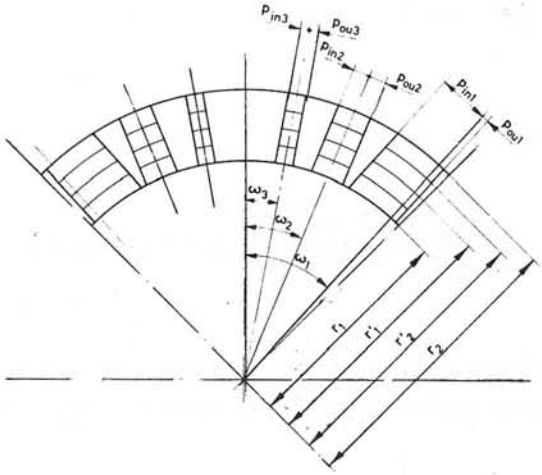

Fig. 2 Cross-section of straight part of coil.

By adding up the contributions of each layer of the straight part and each layer of all slices into which the ends are cut, one obtains the integrated multipole field components for each winding at a distance ρ from the longitudinal axis:

$$\int_{-\infty}^{\infty} B_n \, ds = -\left[\ell \sum_{i=1}^{n_\ell} \left(a_n + b_n \right)_i + \Delta s \sum_{j=1}^{n_s} \sum_{i=1}^{n_\ell} \left(a_n + b_n \right)_{ji} \right] \rho^{n-1} \quad , \quad (1.3)$$

where n_ℓ = number of concentric layers per block of winding, and
n_s = number of slices into which the ends are cut.

2. THE ENDS

The shape of the ends is determined by the condition that each turn of conductor must have the same circumference. It is obvious that in windings of considerable thickness this condition cannot be fulfilled for all wires in the block[1]. For the calculation of the constant perimeter it seems, therefore, advantageous to take the centre vertical layer as a reference, which in the straight part is at an angular position ω.

It is also obvious that this constant perimeter layer has an inclination at the end, which is pointing to the inside of the coil (Fig. 3).

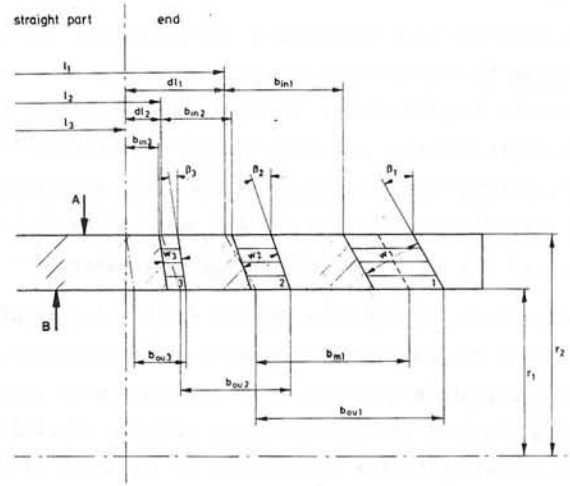

Fig. 3 Coil end cut along the 45° plane.

When making a constant perimeter end, one is free to decide at which cylinder radius of the coil the windings are describing an arc of circle. If it is intended to have the largest possible inclination to dilute the current density at the ends and thus decrease somewhat the magnetic field inside the winding, the arc of circle has to be at the outer surface of the cylinder (r_2).

For the layer which is on the inner cylinder (r_1), the end has the shape of a developed semi-ellipse with the centre displaced by the inclination β (Fig. 3). This end inclination, which produces the constant perimeter for the vertical layer of conductor, at the angular position ω in the straight part, is[6]:

$$\tan \beta = \frac{\pi}{4} \omega \quad . \quad (2.1)$$

The plane separating the straight part and the end (by definition) passes through the centre of the arc of circle describing the smallest

winding (No. 3 in Fig. 4) at the outer layer of the coil cylinder. Thus, if one starts to cut the end at a certain distance s from this separation plane, the cross-sections appear as shown in Fig. 5. If the cross-sections of the blocks of conductor at these cuts are subdivided into concentric layers, these cross-sections of blocks can also be approximated by a suitable number of circular sectors.

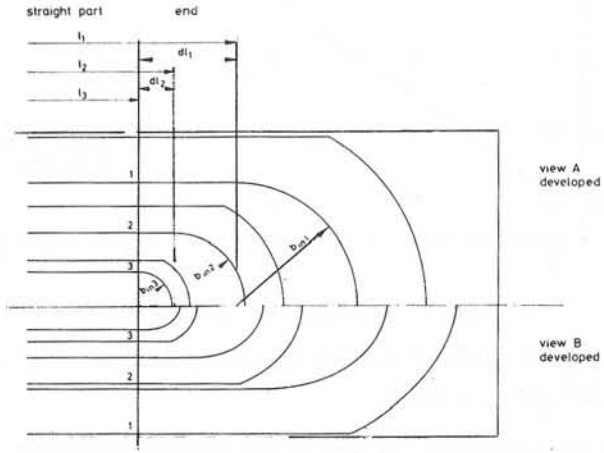

Fig. 4 Developed views of the coil end.

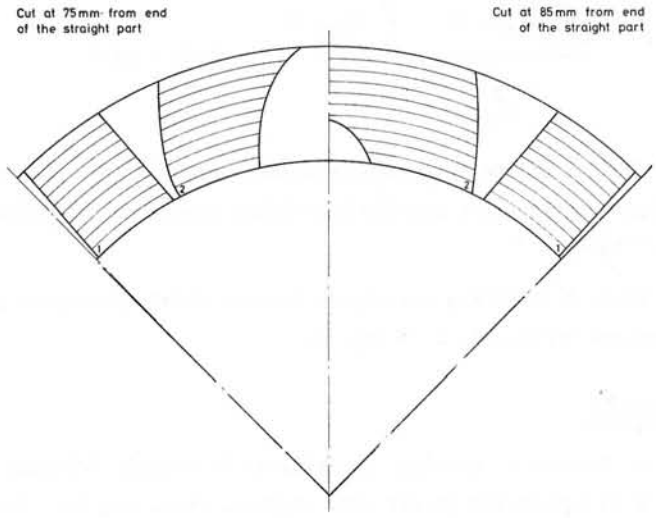

Fig. 5 Sections across the coil end.

Knowing the inner and outer radii of these sectors, the cut position, s, the parameters of the ellipses (on the developed surface of each concentric layer) and the displacement of the ellipse centres according to the end inclination β, one can easily calculate the approximated ϕ_1 and ϕ_2 angles for each circular sector.

Where the width of block is increased at the ends to a value w (by placing specially shaped spacers between the conductors), the parameters of the ellipses have to be corrected accordingly.

For each cut, one has to check:

- how many windings are concerned;
- whether the cut is performed in a straight or partially straight part of one winding;
- whether the peak of a winding is touched or partially touched ("tangential cut").

For each sector element, an average current density in longitudinal direction must be computed and applied in formula (1.2).

Now, the contributions of all sector elements have to be summed up according to formula (1.3).

4. COMPUTER PROGRAM ENDEF

A computer program was written to do the step-by-step integration along the quadrupole magnet. The input, consisting of 5 cards only per case, contains the basic geometric parameters of the coil as shown in Figs. 2 and 3, the current density for the straight part, the useful radius of aperture, the number of order (n) to which the multipole components will be calculated, the number of concentric layers (n_ℓ) into which each block of winding has to be divided and the distance between cuts (Δs) performed in the end region.

The computing time depends mainly on the last two data. With three windings per coil, 30 concentric layers per block of winding and 1 mm cut-distance, Δs, in the end region, the time needed is about 6 seconds for the CERN CDC-7600 computer.

The output of the program consists of the integrated field components at the radius of the useful aperture, of the relative multipole field components and the relative gradient errors. Further the sum of the gradient errors and that of the absolute values of the gradient errors are given. All these results are separately printed out for the straight part and for the total quadrupole magnet.

4. RESULTS

For the superconducting quadrupole for the CERN Intersecting Storage Rings (ISR), the optimization was performed by variation of the straight length l_1 and l_2, while the length of the smallest block, l_3, was kept constant. The sum of the gradient errors and the sum of their absolute values for different straight lengths l_1 and l_2 are shown in the diagrams of Figs. 6 and 7.

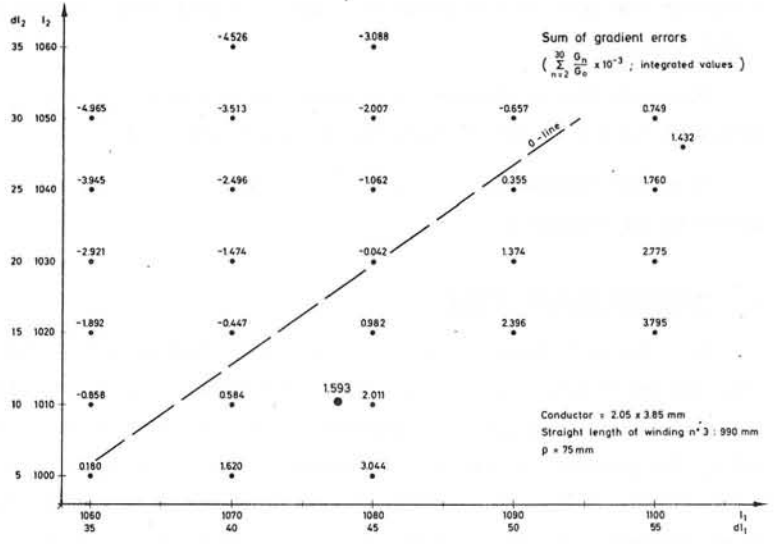

Fig. 6 Optimization of straight length

It can be seen that decreasing one length requires also a smaller length for the other block. A compromise had to be found which was compatible with the additional constraint that a certain free distance had to be kept for mechanical reasons between the ends of the blocks of windings. The straight length of the small blocks was kept at 990 mm, the other two blocks were finally chosen at 1010.6 mm and 1077.5 mm.

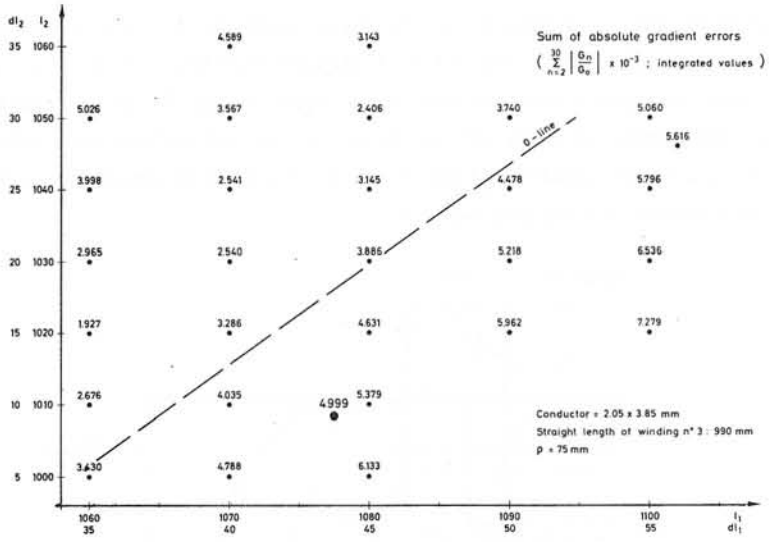

Fig. 7 Optimization of straight length

The inclinations of the end were calculated to be $\beta_1 = 29.17^{\circ}$, $\beta_2 = 18.54^{\circ}$ and $\beta_3 = 9.12^{\circ}$.

For this geometry, the sum of the integrated gradient error at a radial distance $\rho = 75$ mm is:

$$\frac{\int_{-\infty}^{\infty} G_{\rho=75}\, dz - \int_{-\infty}^{\infty} G_{\rho=0}\, dz}{\int_{-\infty}^{\infty} G_{\rho=0}\, dz} = 1.59 \times 10^{-3} . \qquad (4.1)$$

The sum of the integrated absolute values of the gradient errors (indicating the error outside the median plane) was calculated to be 5.00×10^{-3}.

Table 1 shows the parameters for the final quadrupole geometry (notations - Figs. 1, 2, 3 and 4).

REFERENCES

1) G. Bronca, J. Hamelin, S. Jaidane, M. Renard, Fringing fields and iron saturation in air core magnets, Proc. 3rd Int. Conf. on Magnet Technology, Hamburg, p. 64 (1970).

TABLE 1

Parameters for final quadrupole geometry

Parameter	Value	Parameter	Value
r_1	116.0 mm	Δs	1.0 mm
r_2	154.5 mm	j	195 A/mm^2
β_1	29.17°	l_1	1077.5 mm
β_2	18.41°	l_2	1010.6 mm
β_3	9.12°	l_3	990.0 mm
ω_1	42.0 °	w_1	43.24 mm
ω_2	25.0 °	w_2	26.92 mm
ω_3	10.5 °	w_3	12.64 mm
p_{in_1}	27.70 mm	R	176.0 mm
p_{ou_1}	5.10 mm	ρ	75 mm
p_{in_2}	14.70 mm	n	30
p_{ou_2}	3.75 mm	n_ℓ	30
p_{in_3}	4.10 mm		
p_{ou_3}	4.10 mm		

2) H.I. Rosten, The constant perimeter end, RL-73-096 (1973).

3) R.A. Beth, Evaluation of current-produced two-dimensional fields, J. Appl. Phys., Vol. 40, p. 4782 (1970).

4) K. Halbach, Fields and first order perturbation effects in two-dimensional conductor dominated magnets, Nucl. Instr. and Meth. 78, p. 185 (1970).

5) R. Perin, Private communication.

6) P. Pugin, Private communication.

A PRACTICAL METHOD FOR THE DETERMINATION OF STATIONARY TWO-DIMENSIONAL MAGNETIC FIELD

B. Zelenko

Poduzeće R.Končar, OOUR Elektrotehnički institut,
Zagreb, Yugoslavia

ABSTRACT

A method for the determination of magnetic field in a sector of an annulus with usual assumptions about magnetic properties of materials is described. The grid in a two dimensional polar coordinate system may be chosen according to the configuration of magnetic materials and each rectangular element of the grid may be divided in two triangular parts. A set of nonlinear equations is obtained by means of integral of the magnetic field strength along a closed curve around each node. This set is solved iteratively by the method of overrelaxation of potentials and underrelaxation of reluctivities.
Some node potentials may be corrected by the addition of an amount which is in accordance with the nonlinear equations.
The method is successfully applied to practical problems.

1. INTRODUCTION

The magnetic field in electrical machines is very often simplified and investigated in a two-dimensional region. The following equation

$$\frac{\partial \nu \frac{\partial A}{\partial x}}{\partial x} + \frac{\partial \nu \frac{\partial A}{\partial y}}{\partial y} = -J \qquad (1)$$

holds for a stationary two-dimensional magnetic field. The variable A is the magnetic potential, J is the current density. We neglect the hysteresis effect so that the reluctivity ν is determined by the flux density only.

In this paper we consider the magnetic field in a sector of an annulus. This region is chosen in accordance with many problems on electrical machines.
In a polar coordinate system (r,φ) the region (fig. 1) is covered with a net of circle arcs r = const and straight lines φ = const. The configuration of magnetic materials in this region can be irregular and therefore we suppose that a rectangular part of the net can be divided in two triangular parts (fig. 2). Of cause this division may be performed in two ways: from node (i, j) to (i+1, j+1) or from (i+1, j) to (i, j+1). We wish to determine the magnetic potentials belonging to the nodes. The potentials at other points of the region shall be interpolated linearly or bilinearly by means of its values at the nearest nodes.

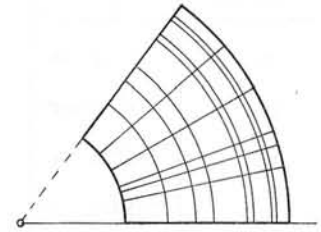

Figure 1. Sector of an annulus in a polar coordinate system

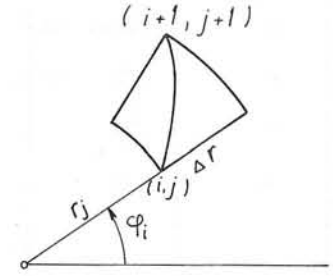

Figure 2. Division of a rectangular part (i, j) in two triangular ones

The equations between potentials at adjoining nodes are obtained by a line integral along a closed path. These equations are nonlinear if reluctivity depends on flux density and they can be solved by an iterative process only.

2. OBTAINING THE SET OF EQUATIONS

The value of the magnetic potential A is to be determined for each node of the net (fig. 1). Then the potential is approximately known at each point of the region by means of a bilinear interpolation:

$$A = a + b\varphi + c\,r + d\,r\varphi \,. \qquad (2)$$

In a rectangular part (fig. 3) the coefficients a, b, c and d are determined by four potentials A_{ij}, $A_{i+1,j}$, $A_{i+1,j+1}$ and $A_{i+1,j}$.

In a triangular part (fig. 2) d equals to zero and the values of a, b, and c are determined by the three potentials in the nodes of that part. Due to continuity of the potential at the boundary of two adjoining parts, the curve that divides a rectangular part in two triangular ones has to be an Archimedes's spirale i.e. $r = e + f\varphi$. By means of such a subdivision of the net in triangular parts a good representation of the magnetic material configuration can be obtained.

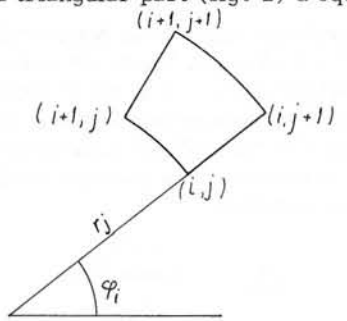

Figure 3. A rectangular part of the net

The equations which include the value of potentials at the nodes can be obtained by considering the adjoining parts of a node.

Figure 4 shows a node and a curve KLMN which goes by the middle of those parts. The points L and M lie on the dividing spirales. The curve KLMN is composed of arcs r = const and φ = const so that the following integral can be easily calculated:

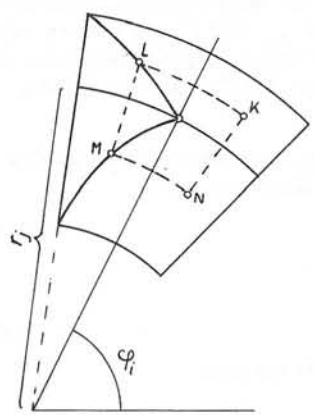

Figure 4. Node (i, j) and its adjoining parts

$$\int_{KLMN} \vec{H} \cdot d\vec{l} = I. \qquad (3)$$

Here I is the current surrounded by this curve, $\vec{H} = \nu \vec{B}$ is the magnetic strength, and the components of the flux densitu $\vec{B}$ are

$$B_r = \frac{\partial A}{r \partial \varphi} \quad \text{and} \quad B_\varphi = - \frac{\partial A}{\partial r} .$$

If the potentials at the boundary of the region are given, then equation (3) gives as many equations as unknown node potentials exist. These equations are nonlinear if in some parts there are ferromagnetic materials. The variable reluctivity in the inner of a certain part is approximated with a constant amount determined by the mean flux density in that part. The current density J for each part of the net is known and therefore it is easy to determine the right hand side of the equation (3). One equation connects 9 potentials of the neighbouring nodes (fig. 5) if all the four parts are nondivided. If some of them are divided in two triangular parts, the corresponding potentials at nodes 3, 5, 7 or 9 do not appear in the equation.

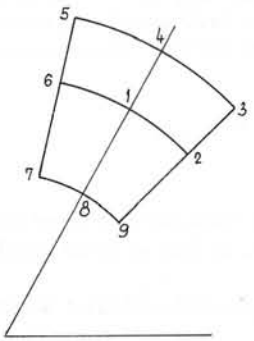

Figure 5. Neighbouring nodes in a net

Similar relations appear at the application of finite element method when the basis of the vector space, the set of functions w_{ij}, is chosen in the following manner. Each function $w = w_{ij}(r, \varphi)$ is equal to zero at all nodes exept at node (i, j) where $w_{i,j}$ is equal to 1. $w_{i,j}$ is interpolated linearly or bilinearly by means of the amounts at the neighbouring nodes in other points of the region. The equations obtained by means of the finite element method are somewhat different from (3). In the case of rectangular parts, a negative potential can be obtained at a node although the neighbouring potentials are not negative and J = O. This is not phisically acceptable. Similar results have been obtained with the method described in this paper, but because the equations (3) are physically clear and can be explained to every engineer, the finite element method has been avoided. An accurate comparision of these two methods is complicated. It is possible to prove the decrease of the difference between the equations obtained by these two methods if $\Delta\varphi$ and Δr tend to zero in the simplest case of triangular parts without current. Speaking more precisely, if the biggest coefficients of the two compared equations are equal to 1, then the differences of the corresponding coefficients tend to zero with the same order of magnitude as $\Delta\varphi$ and Δr.

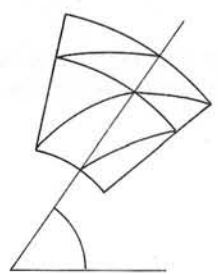

Figure 6. A simple triangular division

3. SOLVING THE EQUATIONS

The equations (3) are nonlinear and therefore they have to be solved iteratively. The well known method [1] with overrelaxation of potentials and underrelaxation of reluctivities has been applied. The overrelaxation factor ω :

$$(A_{ij})_{new} = (A_{ij})_{old} + \omega \cdot (A' - (A_{ij})_{old}) , \qquad (4)$$

(A' obtained from (3))

was determined by computing experiment at each particular problem. In large nets, e.g. with more than 2000 nodes, ω had to be as small as 1.5.

The reluctivity ν is stored for each part of the net and after a complete potential iteration (4) it is corrected to

$$(\nu_{ij})_{new} = (\nu_{ij})_{old} + (\nu' - (\nu_{ij})_{old})/F , \qquad (5)$$

(ν' corresponds to the mean calculated flux densities of that part).

The underrelaxation factor F was also experimentally determined. In large nets F is large, e.g. 30.

Beside the iterations (4) we also apply an additive correction of potentials in analogy to [3] for the net of rectangles. Namely, by adding some of equations (3) it is possible to obtain a new one which is very simple and which has a similar physical meaning as (3) :

$$\oint \vec{H} \cdot \vec{dl} = I . \qquad (6)$$

The convergence of the iterative process can be accelerated by means of this procedure, e.g. in cases that nonmagnetic materials are surrounded with magnetic ones.

According to figure 7 one determines

$$I_1 = \oint_{KLMN} \vec{H} \cdot \vec{dl} , \qquad (7)$$

$$I_0 = \oint_{KLMN} \vec{H}_0 \cdot \vec{dl} , \qquad (8)$$

The calculated magnetic field strength $\vec{H}$ is determined with the approximated values of A and ν after an iteration step (4), (5) for all the nodes. The fictitious magnetic force strength $\vec{H}_0$ is calculated with the same ν as before but with A = 1 at nodes inside the curve KLMN and A = 0 at other nodes. Then the potentials at nodes inside the curve KLMN have to be corrected with a common additive constant

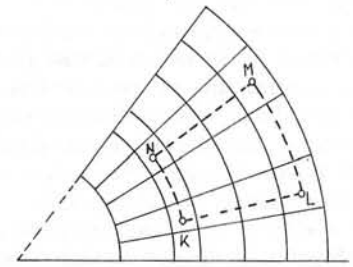

Figure 7. The integration path for additive correction fof potentials

$$\triangle = \frac{I - I_1}{I_0} , \qquad (9)$$

where I is the total current surrounded by KLMN.

This procedure corresponds to adding some of equations (3) as follows. Let

$$x = C x + b \qquad (10)$$

represent the linear system of equations (3) with constant reluctivities. x is the vector of unknown potentials A_{ij} and C is a matrix with diagonal elements equal to 0. We choose a vector z which has the components equal to 1 for nodes inside the curve KLMN, and the others equal to 0.

If an iteration vector $x^{(n)}$ is already known, by means of (9) we find the vector $d = \Delta z$ which is to be added to the vector x' :

$$x' = C x^{(n)} + b , \qquad (11)$$

so that a new iteration vector is obtained :

$$x^{(n+1)} = x' + d . \qquad (12)$$

Let z^T be the transpose of z. Then from (9) we have

$$= (z^T(x' - Cx^{(n)}) - z^T(x' - Cx'))/k, \; k = z^T(z - Cz).$$

The procedure (11), (12) is linear:

$$x^{(n+1)} = D x^{(n)} + E b \qquad (13)$$

where

$$Dx = Cx - (z^T(C - C^2)x)/k \cdot z , \; Eb = b + (z^T C b)/k \cdot z.$$

Hence the additive correction corresponds to adiong some of equations (3) .

Here z^T is the transpose of z and I is the unit matrix.

It would be advantageous if z were an eigenvector of C with an eigenvalue not equal to 1. Then z would be an eigenvector of D with eigenvalue o. But unfortunately we can choose z approximately equal to an eigenvector of C in some cases only. This is fulfilled in the above mentioned case of nonmagnetic material surrounded with magnetic one.

Some of such additive corrections can be tied together because of the proximity of the corresponding curves. If these curves are ill chosen, the additional corrections may even prevent the convergence of the iterative process. This may happen if we choose for example two additive corrections according to figure 8. If we first correct in the region KLMN and then in the region K'L'M'N' it may happen that the iterative process does not converge.

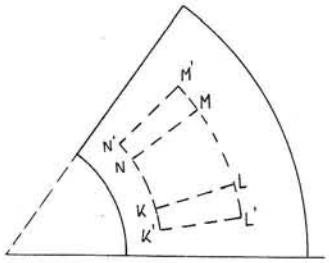

Figure 8. An example of ill chosen paths for additive corrections

4. CRITERIA FOR THE TERMINATION OF THE COMPUTATION

The magnetic field computation may serve for determinationing of flux densities locally or for global determination of the m.m. force. The very amounts of the magnetic potential is by no means important. Therefore any criterion for the termination of the computation should not be based on the amounts of the potential only.

According to our computations these criteria have been:
- small maximal correction of flux density
- small maximal correction of reluctivity
- the m.m. forces over various integration paths:

$$\Theta = \int \vec{H} \quad d\vec{l} \qquad (14)$$

have to be in mutual accordance. For example in regions without current the m.m.f. can depend only on two end points of a curve along which Θ is calculated.

We emphasize that the result Θ in (14) is calculated in full accordance with equations (3) and formulae (6) to (9).

In practical applications the correction of flux density may be decreased at about o.ol T. The correction of the reluctivity may be decreased so that the corresponding flux densities differ in amount of o.ool T only. The m.m.f. along various paths with the same end points may differ from 2 to 5%.

5. APPLICATIONS

The described method is used for the determination of the flux density and m.m.f. in core backs of rotating machines. The holes are bored for the cooling improvement in the core back and they influence the flux density distribution, the thermal losses and the m.m. force.

In practical problems the number of nodes varies up to more than 2ooo. The computed m.m.f. Θ_c differs in most cases from the m.m.f. Θ_o determined by usual calculations. Θ_c is sometimes much greater and sometimes much smaller than Θ_o. Up to now the measurements have conformed our computations, and the magnetizing current calculated by means of Θ_1 was greater than the measured one while the current calculated by means of Θ_o was much smaller than the measured one.
The computed maximal flux density in the core back was in accordance with the measured one.

Figure 9 shows the cross-section of a part of a stator core back with holes. For this core back it was computed Θ_1 = 1loo A and Θ_o = 5oo A.

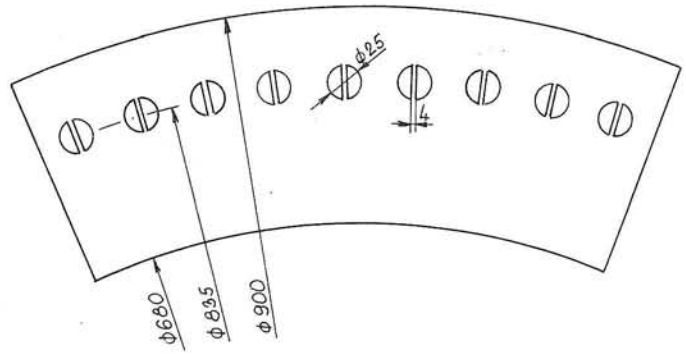

Figure 9. A part of a stator core back with holes

The calculating net for this example had looo nodes. The magnetic field computation lasted 6 minutes on Univac lllo computer. This time includes 32o iterations with all results, tables and figures.

6. CONCLUSIONS

A practical method for the determination of stationary two-dimensional magnetic field is described. This method is based on clear physical representation of used equations. The setting of the configuration is not complicated since the net in the sector of an annulus is based on circle arcs and straight lines. Practical applications give satisfactory results until now.

References

[1] S.V.Ahamed, E.A.Erdélyi : Flux distribution in dc machines at no-load and overloads, IEEE Trans. Power Apparatus and Systems, vol. PAS-85, pp. 960-967, September 1966.

[2] I. Mandić: Izrada programa za proračun magnetskog polja u zoni zuba za digitalno računalo C 9O-4O, elaborat E 32052, Poduzeće "R. Končar", Elektrotehnički institut, 1967.

[3] E. de la Vallée-Poussin, A. Lion: Calcul itératif de 1' induction magnétique dans les machines électriques, Revue générale de 1' électricité, 731-739, avril 1967.

[4] F. Melkes: Metoda konečnych prvků pri řešeni magnetickeho pole. Interni rad VUEST, Brno 1968.

A METHOD FOR COMPUTATION THE SUPERCONDUCTING MAGNETS WINDING CONFIGURATION TO CREATE A PRESCRIBED MAGNET FIELD DISTRIBUTION

B.N.Zhukov, V.N.Lebedev, I.A.Mozalevsky

D.V.Efremov Scientific Research Institute for Electrophysical Apparatus

A number of ways is known to generate a given magnet field distribution in a given aperture by choosing adequate winding configuration. We shall discuss briefly some of these ways.

I. HOMOGENOUS CURRENT DENSITY WINDINGS (IDEAL WINDINGS)

1. It is well known that homogenous and linear field distribution can be obtained in a system of intersecting circular or elliptical current blocks. In this case the region free of currents, where the specified field exists, is wider than the aperture, the later being commonly circular or elliptical. The stored energy and the superconductor weight are, therefore, greater than those in a winding lying close to the aperture boundary.

2. In the work [1] the computation method is described in which the set of parameters of the winding configuration is the solution of the system of nonlinear equations representing relation of the multipole field coefficients and these parameters. This method can be easily modified to enable the computation of the winding configuration for noncircular apertures and unsaturated circular iron shell. The approximate solution of the system is obtained by modified Newton method which takes a lot of computer time and is very sensitive to the choice of the initial approximation.

3. In the work [2] the configuration of the closely lying winding is the approximate solution of the system of equations derived from condition of continuity of the vector potential on the outer winding boundary.

The real magnet windings are wound of the conductor of rather large cross-section to satisfy various technology and economical demands, and hence the above discussed methods are not applicable to real magnets design, the field error going up to few per cent if the ideal winding is simply "stuffed" with conductor.

II. WINDINGS OF REAL CONDUCTOR

1. One of the possible real winding configurations is an approximation of a harmonic current distribution with the set of current blocks of constant radial thickness and varying angular width. Such windings do not fit from economical point of view; besides, in case of noncircular apertures the solution analogous to harmonic current distribution cannot be easily obtained.

2. A lot of methods for discrete closely lying winding computation is developed based on minimization of some functional of field. (For instance [3], the energy stored in the aperture, on condition that the field magnitude (or gradient) in the aperture center is kept fixed, has minimum, when the higher harmonics are equal to zero). The minimization is proceeded by one or another gradient method requiring big computers.

We have developed a group of methods for computation the real magnet winding configurations to create any specified field in arbitrary aperture, with or without unsaturated iron shell. All of these methods are various modifications of a simple and fast working algorythm of computation an ideal winding for the circular aperture.

Basic algorythm description

Let us consider the algorythm for calculating the outer boundary of the ideal winding lying close to the circular aperture of the ironless magnet. Let the required field be

$$H(Z) = H_y + i H_x = \sum_{\kappa \in K} a_\kappa Z^\kappa, \qquad (1)$$

where $\{a_\kappa\}_{\kappa \in K}$ is a finite set of given multipole coefficients. For instance, we want to create a homogeneous field $H(Z) \equiv H_0$, so we shall require $a_0 = H_0$, and $a_2 = a_4 = a_6 = a_8 = 0$ to obtain small enough field error. We add the condition $a_{-1} = 0$, if the required field symmetry differs from the aperture symmetry, and thus garantee the zero total current.

We choose the initial approximation for the outer boundary $r^{(0)}(\varphi) \equiv r_0$, r_0 being the aperture radius. The work of the algorythm is the successive approximate compensation of the field disturbing harmonics. Let the outer boundary be, after the n-th step of iterations, $r^{(n)}(\varphi) = r_0 + \left| \sum_{\kappa \in K} c_\kappa^{(n)} \cos(\kappa+1)\varphi \right|$, and the current density $j^{(n)}$ be $j^{(n)} = |j| \cdot sign\left(\sum_{\kappa \in K} c_\kappa^{(n)} \cos(\kappa+1)\varphi \right)$. The winding produces the field $H^{(n)}(Z) = \sum_{\kappa=0}^{\infty} a_\kappa^{(n)} Z^\kappa$, where

$$a_\kappa^{(n)} = -0.2 \int_0^{2\pi} j^{(n)} \cos(\kappa+1)\varphi \, d\varphi \int_{r_0}^{r^{(n)}(\varphi)} r^{-\kappa} dr, \quad \kappa \geq 0. \qquad (2)$$

Formula (2) can be derived by exanding the Poisson integral $H(Z) = -0.2 \iint_S j(\zeta) dS/(\zeta - Z)$, into Taylor series. As it is known [4], the field disturbances $\Delta a_\kappa^{(n)} = a_\kappa - a_\kappa^{(n)}$ would be compensated, if we put current with the surface density

$$\sigma^{(n)}(\varphi) = \sum_{\kappa \in K} \sigma_\kappa^{(n)} \cos(\kappa+1)\varphi,$$

$$\sigma_\kappa^{(n)} = \Delta a_\kappa^{(n)} r_0^\kappa / 0.2\pi \qquad (3)$$

onto aperture boundary. This compensation can be approximated by altering the winding outer boundary

$$r^{(n+1)}(\varphi) = r_0 + \left| \sum_{\kappa \in K} \left(c_\kappa^{(n)} + \frac{\sigma_\kappa^{(n)}}{|j|} \right) \cos(\kappa+1)\varphi \right| = r_0 + \left| \sum_{\kappa \in K} c_\kappa^{(n+1)} \cos(\kappa+1)\varphi \right| \qquad (4)$$

and this accomplishs the n-th step of iteration. We have distributed the current with the density $\sigma^{(n)}(\varphi)$ along the strip of width depending on φ and carrying constant current density $|j|$.

The iteration is repeated until the field deviation $\max_{|Z| < r_w} |\Delta H^{(n)}(Z)|$ becomes less than permitted. The field error of about 0.01% at $r_w = r_0$ is achieved in 1÷2 minutes with the BESM-4 computer ($2 \cdot 10^4$ op.per sec).

Noncircular aperture. Round iron shell

With the iron shell presence the field $H^{(n)}(Z)$ and the compensating current $\sigma^{(n)}(\varphi)$ are calculated with the shell contribution taken into account [5], and the iron inner radius $R_s^{(n)}$ is determined at each step by the condition $\max_\varphi |H^{(n)}(R_s^{(n)} e^{i\varphi})| = H_p$, where H_p is a given value less than iron saturation field.

If the aperture boundary is described by equation $r = r_g(\varphi)$ we have to substitute $r_g(\varphi)$ instead of r_0 into (2) and into the formula for $r^{(n)}(\varphi)$. The compensating current $\sigma^{(n)}(\varphi)$ in (3) is calculated for more or less arbitrary r_0, the later

becoming a parameter, having no geometrical significance.

The ideal winding configurations computed as discussed above for various types of field, aperture shapes and values of $|j|$ are shown in figs 1 and 2.

Real windings

The real superconducting windings are wound of cable of finite cross-section and, as a rule, are provided with some spacers and channels of cooling system. The commonest types of windings are pancake and shell windings. Both types are characterized by the number of layers N and the number of turns W_i in each i-th layer. To define these parameters we "fill" the ideal winding with the conductor at each step of iteration according the chosen winding structure. The coefficients $\alpha_\kappa^{(n)}$ are calculated following actual conductor position; it can be easily done for simple shapes of the conductor cross-section [5]. After that the iteration step is completed according formulae (2), (3); $|j|$ value in (3) should be taken equal to j_{av} - the average current density in winding.

The available field forming accuracy (i.e. the error magnitude does not decrease when one turn is added or removed) depends on conductor size and is about 0.1÷0.01% if the current in a single conductor is in the interval 500 to 5000 amps. The computer time is 1÷3 minutes for BESM-4 computer.

Fig.3 represents the real windings computed for both winding structures of a dipole magnet of the accelerator-storage unit [6].

Magnet field in current region

Such characteristics as forces in the winding, stored energy, residual field, etc., are of importance when the magnet is designed. These values can be easily obtained if the field distribution in winding is known. However, the direct summating of the elemental fields of each conductor for every point of winding takes too much computer time. Luckily, we can approximate the magnet field in real winding with the field in the ideal winding producing the same field in the aperture and carrying the current density $j = j_{av}$.

The field in the ideal winding can be easily found:

$$H(z,\bar{z}) = \tilde{H}(z) + 0.2\pi j(\bar{z} - f(z)). \qquad (5)$$

Here $f(z)$ is analytical in current region, $\bar{z} = f(z)$ being the aperture boundary equation; $\tilde{H}(z)$ is the analytic continuation of $H(z)$ into current region. The above mentioned continuation obviously exists if $H(z) = \sum_{\kappa=0}^{\infty} a_\kappa z^\kappa$, where all but a finite subset of a_κ are equal to zero. If the described $f(z)$ exists also, then formula (5) realy represents the magnet field in current region, for $H(z,\bar{z})$ satisfies there the Maxwell equation $\partial H(z,\bar{z})/\partial\bar{z} = 0.2\pi j$ and is continuous on the aperture boundary. The function $f(z)$ can be explicitly written down for simple shapes of the aperture. In case of the circular aperture we have $\bar{z} = r_0^2/z$, and for elliptical

$$\bar{z} = \frac{a^2+b^2}{a^2-b^2} z - \frac{2ab}{a^2-b^2}\sqrt{z^2 - a^2 + b^2},$$

a and b being major and minor radii of ellipse respectively.

So, for circular aperture the field in the winding is

$$H(Z,\bar{Z}) = \tilde{H}(Z) + 0.2\pi j\,(\bar{Z} - r_0^2/Z) \qquad (6)$$

and for elliptical aperture –

$$H(Z,\bar{Z}) = \tilde{H}(Z) + 0.2\pi j\,(\bar{Z} - \frac{a^2+b^2}{a^2-b^2}Z + \frac{2ab}{a^2-b^2}\sqrt{Z^2-a^2+b^2}).$$

REPERENCES

1. G.H.Morgan, IEEE Trans., 1969. Part.Accel.Conf.
2. V.G.Davidovsky, Preprint INP 40-70. SOAN USSR.
3. W.W.Lee and Snowdon. IEEE Trans. on Nucl.Sci., 1973, vol.NS-200, No.3, p.726.
4. R.A.Beth, Proc. of the Nat.Part.Accel.Conf., Washington D.C. March 1-3, 1967.
5. B.N.Zhukov, V.N.Lebedev, Preprint NIIEFA, 1972, B-0149 , B-0156 , Leningrad.
6. Y.M.Ado et al. Proc. of the IV all - Union Conf. on Charged Part.Accel. vol.1, p.44, Moskow, "Nauka", 1975.

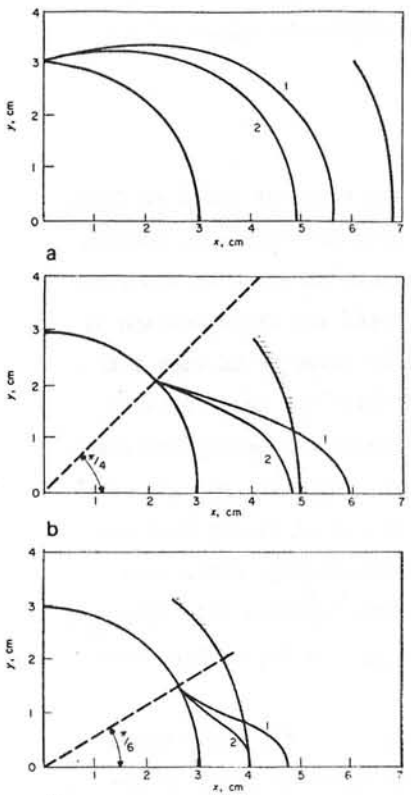

Fig.1 The effect of an iron shield
a – dipole magnet a_0 = 45 kOe, $(\Delta H(r_0)/a_0) < 10^{-4}$; b – quadrupole a_1 = 10 k Oe cm^{-1}, $(\Delta H(r_0)/a_1\, r_0) < 10^{-3}$; c – sextupole a_2 = 2 kOe cm^{-2}, $(\Delta H(r_0)/a r_0^2) < 10^{-4}$
1 – the configuration of an ideal winding of an iron-free magnet;
2 – the same with a shield, $j = 3 \times 10^4$ A cm^{-2}, r_0 = 3 cm

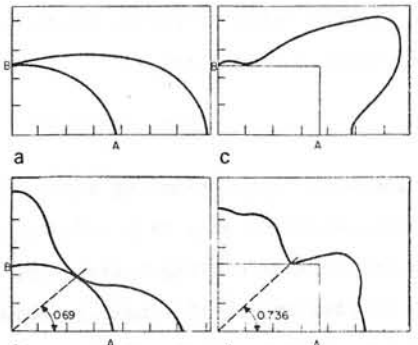

Fig.2 Ideal windings for an elliptical aperture A = 3.7 cm, B = 2.4 cm
a – dipole a_0 = 45 kOe, $(\Delta H/a_0)|_{r_{op}}$ = 3 cm $< 10^{-4}$; b – quadrupole a_1 = 10 kOe cm^{-1}, $(\Delta H/a_1 r)|_{r_{op}}$ = 3 cm $< 10^{-3}$. For a rectangular aperture: c – dipole a_0 = 45 kOe, $(\Delta H/a_0)|_{r_{op}}$=3cm $< 10^{-4}$; d – quadrupole a_1 = 10 kOe cm^{-1}, $(\Delta H/a_1 r)|_{r_{op}}$ = 3 cm $< 10^{-3}$

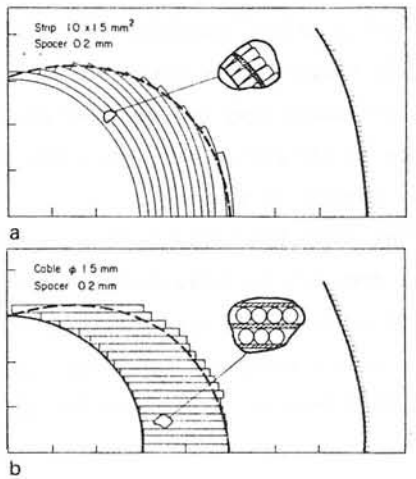

Fig.3 Real windings a_0 = 45 kOe, $(\Delta H/a_0)|_{r_{op}=2\text{ cm}} \approx 2.5 \times 10^{-4}$
a – shell; b – pancake. The mean current density in the winding $j = 3 \times 10^4$ A cm^{-2}; r_0 = 3 cm